ISSN 2222-0682 (online)

World Journal of *Methodology*

2013 Bound Volume 3 Issue 1-4: 1-69

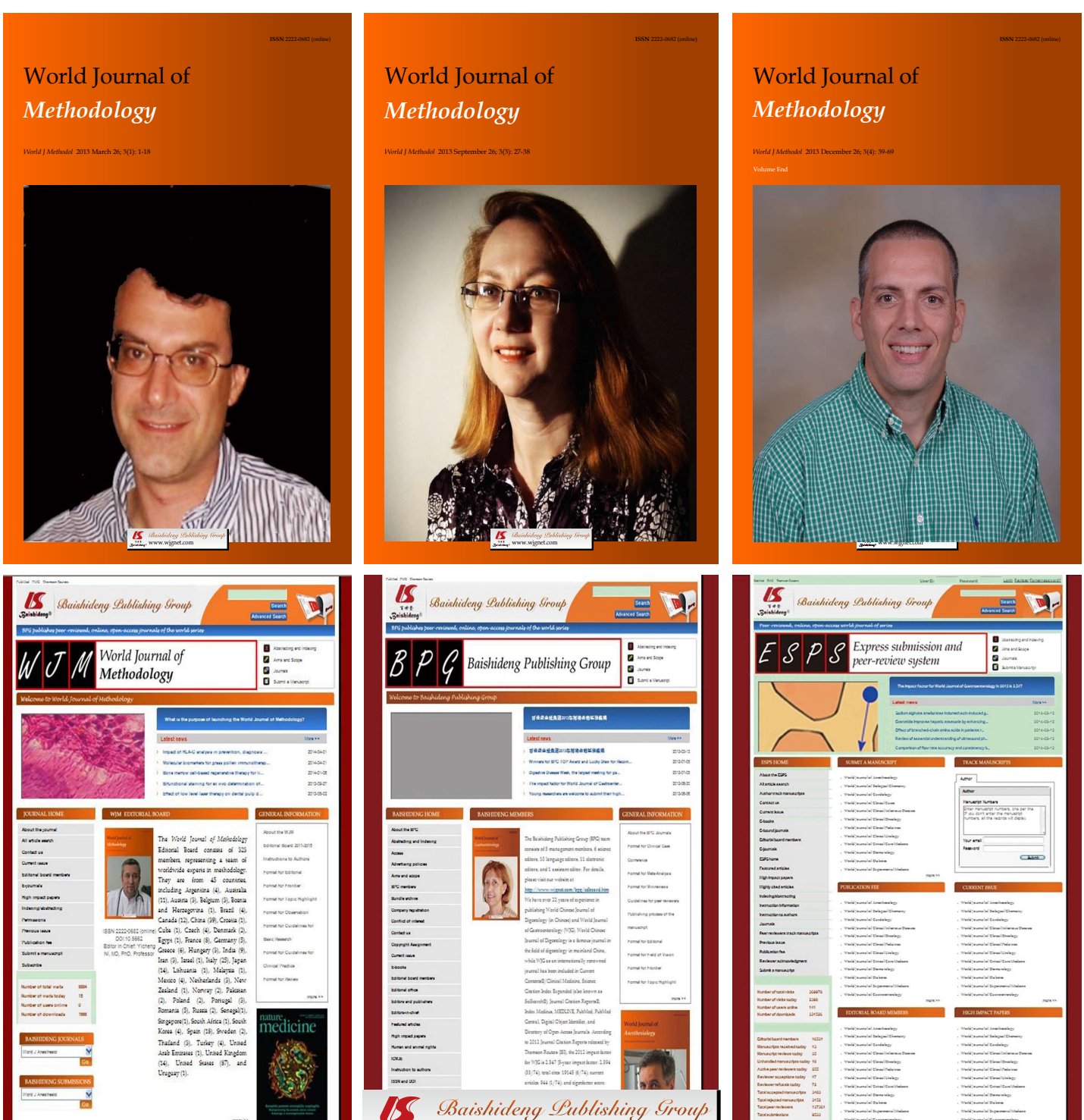

World Journal of Methodology

A peer-reviewed, online, open-access journal of methodology

Editorial Board

2011-2015

The *World Journal of Methodology* Editorial Board consists of 323 members, representing a team of worldwide experts in methodology. They are from 45 countries, including Argentina (4), Australia (11), Austria (3), Belgium (3), Bosnia and Herzegovina (1), Brazil (4), Canada (12), China (39), Croatia (1), Cuba (1), Czech Republic (4), Denmark (2), Egypt (1), France (8), Germany (5), Greece (6), Hungary (3), India (9), Iran (3), Israel (1), Italy (25), Japan (14), Lithuania (1), Malaysia (1), Mexico (4), Netherlands (3), New Zealand (1), Norway (2), Pakistan (2), Poland (2), Portugal (3), Romania (5), Russia (2), Senegal (1), Singapore (1), South Africa (1), South Korea (4), Spain (18), Sweden (2), Thailand (3), Turkey (4), United Arab Emirates (1), United Kingdom (14), United States (87), and Uruguay (1).

Tong-Wen Xu, *Hefei*
Shi-Ying Xuan, *Qingdao*
Xi-Lin Yang, *Hong Kong*
Bang-Ce Ye, *Shanghai*
Wen-Wu Yu, *Nanjing*
Yue-Hong Zhang, *Hangzhou*
Zhong-Ying Zhao, *Hong Kong*
Chun-Fu Zheng, *Wuhan*
Ma Zheng, *Beijing*
Jun-Jie Zhu, *Nanjing*

Croatia

Marijeta Kralj, *Zagreb*

Cuba

Mariano R Ricard, *Habana*

Czech Republic

Kamil Kuca, *Hradec Kralove*
Bozena Novotna, *Prague*
Jiri Sedy, *Prague*
Miroslav Sip, *Ceske Budejovice*

Denmark

Morten Mørup, *Lyngby*
Hans Sanderson, *Roskilde*

Egypt

Nervana S Bayoumi, *Cairo*

France

Marc Y Bardou, *Dijon*
Mohammed M Bettahar, *Nancy*
Olivier David, *Grenoble*
Guido Kroemer, *Paris*
Florian Lesage, *Sophia Antipolis*
Patrick Maison, *Creteil*
Sandrine Marquet, *Marseille*
Jean Yves Rotge, *Bordeaux*

Germany

Harald Hampel, *Frankfurt*
Frank Peinemann, *Cologne*
M Lienhard Schmitz, *Giessen*
Alfons Schnitzler, *Duesseldorf*
Frank Werner, *Magdeburg*

Greece

Konstantinos P Economopoulos, *Athens*
Georgios A Koumantakis, *Aegion*
Michael Koutsilieris, *Athens*
Demosthenes Panagiotakos, *Athens*
Issidora Papassideri, *Athens*
Falaras Polycarpos, *Pallini Attikis*

Hungary

Péter Halász, *Budapest*
András Komócsi, *Pécs*
László Vécsei, *Szeged*

India

Dipshikha Chakravortty, *Bangalore*
DK Dhawan, *Chandigarh*
R Jayakumar, *Cochin*
Abdul Viqar Khan, *Aligarh*
Geetha Manivasagam, *Vellore*
Jacob Peedicayil, *Vellore*
YS Prabhakar, *Lucknow*
Debasish Sarkar, *Orissa*
Rakesh Kumar Sinha, *Ranchi*

Iran

Mehran Javanbakht, *Tehran*
Enayat Kalantar, *Sanandaj*
Shekoufeh Nikfar, *Tehran*

Israel

Dan Frenkel, *Tel Aviv*

Italy

Giuseppe Biondi-Zoccai, *Latina*
Carlo Bonanno, *Vicenza*
Paolo Borrione, *Turin*
Filippo Cademartiri, *Monastier di Treviso*
Alberto Chiesa, *Bologna*
Annamaria Cimini, *L'Aquila*
Giovanni Di Leo, *San Donato Milanese*
Rosario Donato, *Via del Giochetto*
Alfio Ferlito, *Udine*
Giovanna Ferraioli, *Milan*
Irene Floriani, *Milan*
Landoni Giovanni, *Milano*
Stefano Girotti, *Bologna*
Paola Irato, *Padova*
Giovanni Martinotti, *Rome*
Mario Mascalchi, *Florence*
Patrizia Mecocci, *Perugia*
Germano Orrù, *Cagliari*
Maurizio Pompili, *Rome*
Carlo Riccardi, *Perugia*
Domenico Rubello, *Rovigo*
Gianfranco Spalletta, *Rome*
Gambardella Stefano, *Rome*
Mauro Valtieri, *Rome*

Japan

Kohei Akazawa, *Niigata*
Subash CB Gopinath, *Tsukuba*
Masafumi Goto, *Miyagi*
Koichi Hattori, *Tokyo*
Satoshi Hirohata, *Okayama*
Yukihiro Ikeda, *Osaka-sayama*
Masahiro Kohzuki, *Sendai*
Yoshinori Marunaka, *Kyoto*
Kenji Miura, *Tokorozawa*
Ryuichi Morishita, *Suita*
Mitsuhiko Noda, *Tokyo*
Yurai Okaji, *Tokyo*
Hirosato Seki, *Osaka*
Hisanori Umehara, *Kahoku-gun*

Lithuania

Giedrius Barauskas, *Kaunas*

Malaysia

Iis Sopyan, *Kuala Lumpur*

Mexico

Javier Camacho, *Mexico City*
Mejía Aranguré Juan Manuel, *Col Doctores*
Martha Rodríguez-Moran, *Durango*
Julio Sotelo, *Mexico City*

Netherlands

Kristien Hens, *Maastricht*
Bart J Polder, *Emmeloord*
Frank Twisk, *Limmen*

New Zealand

Valery Feigin, *Auckland*

Norway

David F Mota, *Oslo*
Tore Syversen, *Trondheim*

Pakistan

Muhammad A Noor, *Islamabad*
Yasir Waheed, *Islamabad*

Poland

Piotr Dziegiel, *Wroclaw*
Tadeusz Robak, *Lodz*

Portugal

Nuno Lunet, *Porto*
Hugo Sousa, *Porto*

Romania

Elena Moldoveanu, *Bucharest*
Monica Neagu, *Bucharest*
Florin-Dan Popescu, *Bucharest*

Eugen Rusu, *Galati*

Russia

Galina B Bolshakova, *Moscow*
Sergey V Dorozhkin, *Moscow*

Senegal

Badara Cissé, *Dakar*

Singapore

Zhang Yong, *Singapore*

South Africa

Robin Alexander Emsley, *Cape Town*

South Korea

Sang Soo Hah, *Seoul*
Chang-Yong Lee, *Kongju*
Kwan Sik Lee, *Seoul*

Spain

Salvador F Aliño, *Valencia*
Mohamed Farouk Allam, *Cordoba*
Alejandro Cifuentes, *Madrid*
Miren Lopez de Alda, *Barcelona*
Joaquin de Haro, *Madrid*
M de la Guardia, *Valencia*
Emma Garcia-Meca, *Cartagena*
Mónica H Giménez, *Zaragoza*
Josep M Guerrero, *Barcelona*
Fernando Marin, *Madrid*
José A Orosa, *A Coruña*
Jesús Osada, *Zaragoza*
Soledad Rubio, *Córdoba*
Helmut Schröder, *Barcelona*
Jesus Simal-Gandara, *Ourense*
Bahi Takkouche, *Santiago de Compostela*
Gabriela Topa, *Madrid*
Miguel A Vallejo, *Madrid*

Sweden

Stefan Karlsson, *Lund*
Jenny Selander, *Stockholm*

Thailand

Amporn Jariyapongskul, *Bangkok*
Apiwat Mutirangura, *Bangkok*
Bungorn Sripanidkulchai, *Khon Kaen*

Turkey

Mehmet Doğan, *Çağış-Balikesir*
Ferda E Percin, *Ankara*
Ahmet Yildirim, *Bornova-Izmir*
Aysegul Yildiz, *Izmir*

United Arab Emirates

Hassib Narchi, *Al Ain*

United Kingdom

Richard H Barton, *London*
Paul Evans, *London*
Giuseppe Garcea, *Leicester*
Marta I Garrido, *London*
Sinead Keeney, *Belfast*
Maurice J O'Kane, *Londonderry*
Abdullah Pandor, *Sheffield*
Susan Pang, *Teddington*
Pankaj Sharma, *London*
Andrew Harvey Sims, *Edinburgh*
David E Whitworth, *Aberystwyth*
Sorrel E Wolowacz, *Manchester*
Feng Wu, *Headington*
Shangming Zhou, *Swansea*

United States

Nasar U Ahmed, *Miami*
Mike Allen, *Milwaukee*
Srinivas Ayyadevara, *Little Rock*
Charles F Babbs, *West Lafayette*
Janet Barletta, *Baltimore*
Lawrence T Bish, *Philadelphia*
Richard W Bohannon, *Storrs*
Mark Bounthavong, *San Diego*
M Ahmad Chaudhry, *Burlington*
Pei Chen, *Beltsville*
Tao Chen, *Jefferson*
Yong Q Chen, *Winston-Salem*
Machado Christian, *Southfield*
Patricia Ann D'Amore, *Boston*
Undurti N Das, *Shaker Heights*
Feng Ding, *Chapel Hill*
Mary E Edgerton, *Houston*
D Mark Estes, *Athens*
Bingliang Fang, *Houston*
Ronnie Fass, *Tucson*
Vesna D Garovic, *Rochester*
Alexandros Georgakilas, *Greenville*
Ronald Gillam, *Logan*
Shannon S Glaser, *Temple*
Ga Nagana Gowda, *West Lafayette*
Anton B Guliaev, *San Francisco*
Zong Sheng Guo, *Pittsburgh*
James P Hardwick, *Rootstown*
Diane M Harper, *Kansas*
Odette A Harris, *Stanford*
Rod Havriluk, *Tallahassee*
Moonseong Heo, *Bronx*
Guoyuan Huang, *Evansville*
Michael Huncharek, *Columbia*
Reinhold J Hutz, *Milwaukee*
Bankole A Johnson, *Charlottesville*
Joseph M Kaminski, *Silver Spring*
Yong S Kim, *Bethesda*
Mark S Kindy, *Charleston*
Jennifer Kisamore, *Tulsa*
Georgios D Kitsios, *Boston*
Ronald Klein, *Shreveport*
Heidemarie Kremer, *Miami*
S Lakshmivarahan, *Norman*
Dawei Li, *New Haven*
Kenneth Maiese, *Newark*
Sameer Malhotra, *New York*
JL Mehta, *Little Rock*
Ray M Merrill, *Provo*
M Mimeault, *Nebraska*
Ron B Mitchell, *St Louis*
Anirban P Mitra, *Los Angeles*
Walter P Murphy, *Evanston*
Marja Tuuli Nevalainen, *Philadelphia*
Yan Peng, *Dallas*
George Perry, *San Antonio*
Ilona Petrikovics, *Huntsville*
Shengping Qin, *Davis*
Peter J Quesenberry, *Providence*
P Hemachandra Reddy, *Beaverton*
James V Rogers, *Columbus*
Troy Rohn, *Boise*
Paul R Sanberg, *Tampa*
Tor C Savidge, *Galveston*
Dong-Chul Seo, *Bloomington*
Igor Sevostianov, *Las Cruces*
Judy Y Tan, *Hillside*
Weihong Tan, *Gainesville*
Guangwen Tang, *Boston*
Paul D Terry, *Knoxville*
Guochuan Emil Tsai, *Torrance*
Catherine E Ulbricht, *Somerville*
Thomas TH Wan, *Orlando*
Xiao-Jing Wang, *Aurora*
Jang-Yen Wu, *Boca Raton*
Qing Wu, *Scottsdale*
Eleftherios S Xenos, *Lexington*
Lijun Xia, *Oklahoma City*
Xiong Xu, *New Orleans*
Li-Jun Yang, *Gainesville*
Wancai Yang, *Chicago*
Xinan Yang, *Chicago*
Fahd A Zarrouf, *Anderson*
Henry Zeringue, *Pittsburgh*
Jingbo Zhang, *New York*

Uruguay

Matias Victoria, *Salto*

ISSN 2222-0682 (online)

World Journal of *Methodology*

World J Methodol 2013 March 26; 3(1): 1-18

Baishideng Publishing Group
www.wjgnet.com

World Journal of Methodology

Contents

Quarterly Volume 3 Number 1 March 26, 2013

Contents

World Journal of Methodology
Volume 3 Number 1 March 26, 2013

AIM AND SCOPE

World Journal of Methodology (*World J Methodol*, *WJM*, online ISSN 2222-0682, DOI: 10.5662) is a peer-reviewed open access academic journal that aims to guide clinical practice and improve diagnostic and therapeutic skills of clinicians.

The primary task of *WJM* is to rapidly publish high-quality original articles, reviews, and commentaries that deal with the methodology to develop, validate, modify and promote diagnostic and therapeutic modalities and techniques in preclinical and clinical applications. *WJM* covers topics concerning the subspecialties including but not exclusively anesthesiology, cardiac medicine, clinical genetics, clinical neurology, critical care, dentistry, dermatology, emergency medicine, endocrinology, family medicine, gastroenterology and hepatology, geriatrics and gerontology, hematology, immunology, infectious diseases, internal medicine, obstetrics and gynecology, oncology, ophthalmology, orthopedics, otolaryngology, radiology, serology, pathology, pediatrics, peripheral vascular disease, psychiatry, radiology, rehabilitation, respiratory medicine, rheumatology, surgery, toxicology, transplantation, and urology and nephrology.

INDEXING/ABSTRACTING

World Journal of Methodology is now indexed in Digital Object Identifier.

NAME OF JOURNAL
World Journal of Methodology

ISSN
ISSN 2222-0682 (online)

LAUNCH DATE
September 26, 2011

FREQUENCY
Quarterly

EDITOR-IN-CHIEF
Yicheng Ni, MD, PhD, Professor, Department of Radiology, University Hospitals, KU, Leuven, Herestraat 49, B-3000, Leuven, Belgium

EDITORIAL OFFICE
Jin-Lei Wang, Director
Xiu-Xia Song, Vice Director

World Journal of Methodology
Room 903, Building D, Ocean International Center, No. 62 Dongsihuan Zhonglu, Chaoyang District, Beijing 100025, China
Telephone: +86-10-59080039
Fax: +86-10-85381893
E-mail: wjg@wjgnet.com
http://www.wjgnet.com

PUBLISHER
Baishideng Publishing Group Co., Limited
Flat C, 23/F., Lucky Plaza, 315-321 Lockhart Road, Wanchai, Hong Kong, China
Fax: +852-65557188
Telephone: +852-31779906
E-mail: bpgoffice@wjgnet.com
http://www.wjgnet.com

PUBLICATION DATE
March 26, 2013

INSTRUCTIONS TO AUTHORS
Full instructions are available online at http://www.wjgnet.com/2222-0682/g_info_20100722180909.htm

ONLINE SUBMISSION
http://www.wjgnet.com/esps/

World Journal of Methodology

Online Submissions: http://www.wjgnet.com/esps/
wjm@wjgnet.com
doi:10.4329/wjm.v3.i1.1

World J Methodol 2013 March 26; 3(1): 1-6
ISSN 2222-0682 (online)

EDITORIAL

Pre-participation screening for the prevention of sudden cardiac death in athletes

Paolo Borrione, Federico Quaranta, Emanuela Ciminelli

Paolo Borrione, Federico Quaranta, Emanuela Ciminelli, Department of Movement, Human and Health Sciences, University of Rome "Foro Italico", 00194 Rome, Italy
Author contributions: Quaranta F and Ciminelli E contributed equally in writing the article and in reviewing the literature; Borrione P contributed in the conception, design, writing and final approval of the article.
Correspondence to: Paolo Borrione, MD, Department of Movement, Human and Health Sciences, University of Rome "Foro Italico", Piazza Lauro de Bosis 15, 00194 Rome, Italy. paolo.borrione@uniroma4.it
Telephone: +39-6-36733569 Fax: +39-6-36733344
Received: February 23, 2013 Revised: March 9, 2013
Accepted: March 18, 2013
Published online: March 26, 2013

Abstract

Pre-partecipation screening is the systematic practice of medically evaluating large populations of athletes before participation in sport activities for the purpose of identifying abnormalities that could cause disease progression or sudden death. In order to prevent sudden cardiac death (SCD), cardiovascular screening should include a strategy for excluding high-risk subjects from athletic and vigorous exercise. There are two major screening programmes in the world. In the United States competitive athletes are screened by means of family and personal history and physical examination. In Italy there is a mandatory screening for competitive athletes, which includes a resting electrocardiogram (ECG) for the detection of cardiac abnormalities. The most important issue to be addressed is whether a screened subject is really guaranteed that she/he is not suffering from any cardiac disease or at risk for SCD. Conceivably, the introduction of echocardiogram during the pre-participation screening, could be reasonable, despite the discrete sensitivity of ECG, in raising clinical suspicions of severe cardiac alterations predisposing to SCD. It is clear that the cost-benefit ratio per saved lives of the ECG screening is a benchmark of the Public Health policy. On the contrary, the additional introduction of echocardiography in a large population screening programme seems to be too much expansive for the Public Health and for this reason not easily practicable, even if useful and not invasive. Even if we strongly believe that a saved life is more important than any cost-efficacy evaluation, the issue of the economical impact of this approach should be further assessed.

Key words: Sudden cardiac death; Prevention; Athletes; Pre-participation screening; Screening

Core tip: The review underlines the different incidence of sudden cardiac death (SCD) and the reason of this discrepancy as well as the different kind of approach to competitive athletes in Italy and United States. We emphasize the importance of electrocardiogram (ECG) as a simple and economical diagnostic tool, considering the opportunity of implementing the pre-participation screening (PPS) with echocardiogram, in order to detect mild structural cardiac diseases. After a cost-effectiveness analysis we finally suggest an innovative proposal in order to further prevent SCD: a rapid but focused echocardiogram assessment during the first PPS in addition to physical examination and ECG.

Borrione P, Quaranta F, Ciminelli E. Pre-participation screening for the prevention of sudden cardiac death in athletes. *World J Methodol* 2013; 3(1): 1-6 Available from: URL: http://www.wjgnet.com/2222-0682/full/v3/i1/1.htm DOI: http://dx.doi.org/10.4329/wjm.v3.i1.1

SUDDEN CARDIAC DEATH

The Framingham definition of sudden death (SD) is the most universally used among medical researchers: "SD

is a death that occurs within 1 h of the onset of symptoms". Other definitions are commonly used, for example Maron's one: "SD is defined as a witnessed or unwitnessed natural death occurring unexpectedly within 6 h of a previously normal state of health"[1].

Most of the sport related SDs (almost 90%) occur in subjects who have pre-existing and often clinically silent cardiac abnormalities[2]. In these circumstances the sudden cardiac death (SCD) is defined as "non traumatic, nonviolent, unexpected natural death of cardiac origin occurring within 1 h of the onset of symptoms in a person who does not have a previously recognized cardiovascular condition that would appear fatal"[1].

When considering athletes, sport related SCD occurs during or immediately after physical exercise. Hence, physical efforts are considered an important acute trigger factor (like emotional stress, environmental factors, sympathetic-vagal imbalance, myocardial ischemia, hemodynamic changes) able to interact with a substrate causing life threatening ventricular tachyarrhythmias[3]. The incidence of SCD during sports is quite low and variable among the different studies available in literature. Moreover, a distinction between older athletes (> 35 years) and young athletes (< 35 years) is mandatory when analyzing SCD events. Indeed, in the former group the most important cause of SCD is represented by premature coronary artery disease (CAD)[4,5]; less frequently by acquired valvular diseases and cardiomyopathies (*i.e.*, hypertrophic cardiomyopathy)[6]. The incidence of SCD in this age group ranges from 1:15000 to 1:50000[7-9]. When considering younger athletes, autopsy-based studies and epidemiologic observations often revealed structural cardiac abnormalities such as inheritable cardiomyopathies as well as congenital coronary artery anomalies[10]. Other relatively common causes of SCD in subjects under 35 years of age are represented by: myocarditis, Marfan syndrome, valvular heart diseases, dilated cardiomyopathy, CAD, and myocardial bridge[2,11].

In addition, there is a growing number (from 2% to 10%, up to 31% for Australian authors) of unexplained death, even after autopsy, plausibly due to ionic-channel disorders such as short and long QT syndrome, catecholaminergic polymorphic ventricular tachycardia, or Brugada syndrome[12-14]. Finally, Haïssaguerre *et al*[15] recently reported that "among patients with an history of idiopathic ventricular fibrillation, there is an increased prevalence of early repolarization", opening in this way a "new age"of SCD identification.

The incidence of SCD in young athletes ranges from 2.1/100000 (Italy)[8] to 0.4-0.6 per 100000 athletes per year in the United States[16]. This discrepancy is mainly explained by the different sources of information adopted. Indeed, in the United States available data have been obtained through the review of public media reports and other available electronic resources, which could, obviously, underestimate the true incidence of SCD. On the contrary, in Italy a prospective registry of juvenile SD is regularly updated. In addition, it is necessary to consider other differences that could further justify the observed discrepancies; namely differences of age (older athletes in the Italian series) and gender (larger proportion of females in the United States series). Smaller studies, performed as population based investigations, reported, also in the United States, an incidence of either SCD of young individuals and athletes similar to that reported by Shen *et al*[17] in Italy. Similarly, Maron *et al*[18] in 2009 reported an annual incidence of SCD among United States high-school and college athletes roughly similar to that observed in Italy.

In any case, differences between Italian and United States data, constitute the basis of the debate between two different approaches to pre-participation screening (PPS): (1) American Heart Association (AHA) consensus panel: (medical history and physical examination)[19]; and (2) European Society of Cardiology (ESC) consensus panel (based on Italian PPS): medical history and physical examination plus a 12-lead electrocardiogram (ECG) with interpretation[20].

PPS

Both AHA and ESC recommend and emphasize the weight of ECG screening, but the AHA 2007 update sustains the impracticability of PPS with ECG in the United States because of the lack of logistical and economical resources[21]. Actually, high schools athletes and Olympic athletes, usually undergo, in United States, a screening based on medical history and physical examination, which seems inadequate to prevent SD. This hypothesis is supported by a case record of Maron retrospectively analyzing 134 cases of SD. This study concluded that only 3% of the SD were suspected through medical history and physical examination[2].

The contradiction of this approach has been extensively discussed in the recent literature. The most important issue is that professional athletes, already evaluated during the years and most likely healthy, are more safeguarded when compared to young adolescents at the beginning of their sport activity, when congenital or genetic diseases typically arise[21]. This everlasting dispute, will hardly come to an end since it reflects two different philosophies as well as two different ways of considering Public Health. Notably, in Italy PPS, after the abolition of compulsory military service, is now the fundamental medical screening for apparently healthy youths. Indeed 5 million of athletes repeat the medical evaluation every year since it is compulsory for competitive sport.

PPS, in Italy, is a general medical screening and the cardiovascular system is deeply investigated, since most of the sport related SD is of cardiac origin[10]. It consists in medical history, physical examination, spirometry, urine analysis plus basal and after step test 12-lead ECG[22]. Second level investigations include: echocardiogram, stress test[23], 24 h ECG and ambulatory blood pressure monitoring; all requested in case of clinical and/or electrocardiographic abnormalities. In Italy, all

athletes are evaluated accordingly to the current Cardiologic Protocols for Competitive Sports Qualification. This document indicates guidelines for all the cardiovascular diseases, including high risk early repolarization patterns, isolated left ventricle non-compaction as well as many other doubtful conditions[24].

The huge experience obtained with PPS in Italy, clearly indicates that ECG, characterized by an excellent negative predictive value, when compared with only physical examination, is an essential tool to suspect or diagnose cardiac structural and electric channels pathologies[20,25]. The usefulness of ECG as a preventive tool during PPS, is underlined by one of the most significant studies of Corrado, showing how the annual incidence of SCD in competitive athletes decreased by 89% in Italy, after the introduction of PPS. In particular, SCD cases varied from 3.6/100000 athletes per year during the pre PPS period (1979-1981) to 0.4/100000 athletes per year during the PPS period (1993-2004)[26]. In particular, Corrado *et al*[27] confirmed the efficacy of ECG in the identification of hypertrophic cardiomyopathy. Indeed, in a large population-based study of screening outcomes, the diagnostic power of ECG was similar to that observed in a population-based study in the United States, using echocardiography[28]. Nevertheless, it's comprehensible how difficult it is to identify, despite instrumental evaluation, many mild structural cardiac abnormalities, eventually associated with short and long-time hemodynamic and arrhythmic sequels. This observation gains even more strength when considering children and adolescents since such cardiac abnormalities are still not complicated and for this reason usually clinically silent[28,29].

Unfortunately, even if ECG has to be considered the most reliable and feasible analysis to detect severe cardiomyopathies[10,30,31] as well as ionic channel disorders[32] many asymptomatic pathologies could remain unrecognized through standard PPS. For example, mitral valve prolapse (MVP) and bicuspid aortic valve (BAV), considered among the most common congenital cardiomiopathies in the adult population (0.6% up to 2.4%, in the Framingham heart study, for MVP[33,34] and 0.5%-0.6% for BAV[35]) remain often undiagnosed through PE and ECG. With this regard, it is known that these valvulopaties are frequently complicated by severe dysfunctions requiring cardio surgery[36-38], that more than 50% of BAV evolve to root or proximal ascending aorta dilatation caused by wall vessel structural alterations, with possible spontaneous rupture and dissection[39,40] and that, occasionally, MVP and BAV are the only pathological findings at the autopsy of athletes death suddenly[2,41]. For these reasons, it has been proposed to implement standard PPS with echocardiography in order to allow a risk stratification as well as an adequate follow up and recommendations[42,43]. With this regard, it has to be considered that the overall prevalence of mild cardiac pathologies in asymptomatic subjects has not been entirely investigated.

Steinberger *et al*[44] reported a prevalence of 3.6% of cardiomiopathies among 357 asymptomatic children. More recently, we evaluated, with the introduction of echocardiography during the PPS, a large population (3100 athletes) of active, asymptomatic, apparently healthy children and adolescents, finding a prevalence of 1.8% of previously unrecognized cardiomiopathies[45]. Taken together, these observations may suggest that the introduction of echocardiogram during the PPS, could be reasonable, despite the discrete sensitivity of ECG, in raising clinical suspicions of severe cardiac alterations predisposing to SCD. Obviously, a 2.7% (our study) and 3.6% (Steinberg' study) of prevalence of structural cardiac disease cannot justify the execution of echocardiogram every year in competitive athletes. Nonetheless, it has to be underlined the usefulness of echocardiogram in association with ECG in occasion of the first visit since the early diagnosis and subsequent reparation of congenital lesions, reduce the risk of future hemodynamic and arrhythmic complications.

It is well known that ECG abnormalities are commonly found both in patients affected by potentially life-threatening congenital cardiac disorders and healthy highly trained subjects as a result of the athletes' hearth modifications. In the latter situation, it is usually necessary to perform a differential diagnosis by means of an echocardiography study. Sometimes, this analytical approach is not enough to reach a precise diagnosis and further evaluations are commonly requested. This situation is surely depressing for the athletes since they have to suspend their competitive or training programmes with potential detrimental effects on their competitive season. However, sports physicians have the legal duty to reach a definitive and correct diagnosis with any diagnostic tool available in order to ensure that the subject does not run unjustified and excessive risks. In case of uncertainty, sports physicians have the duty of rejecting sports eligibility[10]. On the contrary, it has to be remembered that a normal ECG have an high predictive negative value (96%)[46].

The last issue to be analyzed is the cost-effectiveness of this approach. Despite the unquestionable usefulness of a wide scale screening performed with echocardiogram on a large healthy population, it is obviously necessary to analyze the costs for Public Health. Recent data from the "National Centre for Health Statistics"[47] sustained the efficacy and the feasibility of the PPS based on medical history, PE and basal ECG, both when considering the cost-benefit ratio and the saved lives. In literature, it has been described that ECG has a more favorable cost-effectiveness ratio per life saved among high school athletes when compared to the adoption of only medical history and PE[48]. The same conclusion was described by Wheeler *et al*[49] (cost effectiveness ratio of $ 42900 per life year). In conclusion, it is clear that the cost-benefit ratio per saved lives of the ECG screening is below $ 50000 which is a benchmark of the Public Health policy[48-51].

Despite these observations, some United States au-

Table 1 Italian and United States pre-participation screening strategy

Italian pre-participation screening		United States pre-participation screening	
Advantage	**Disadvantage**	**Advantage**	**Disadvantage**
Rest ECG screening power (ionic-channel disorders, arrhythmias and cardiomyopathies)	Higher cost	Lower cost	Low diagnostic power in the detection of silent cardiovascular diseases
Post exercise ECG diagnosis (arrhytmias, stress-induced myocardial ischemia)	More complicated logistic	Easy logistic	Impossibility to detect post exercise ECG alterations
Spyrometry (pulmonary diseases)	More false positive	Less false positive	Only clinical diagnosis of pulmonary diseases
Urine analysis (diabete, proteinuria, kidney, liver and urogenital infectious diseases)	Possible psychological ramification of the screening	Easy feasibility	Athletes can compete without permission (PPS is not mandatory)
In Italy athletes health is protected by law (PPS is mandatory)			Many cardiovascular disorders cannot be detected by physical examination

ECG: Electrocardiogram; PPS: Pre-participation.

Table 2 Cost-efficacy trials

Studies	Considerations
Cost effectiveness analysis of screening of high school athletes for risk of sudden cardiac death[48]	A more favourable cost-effectiveness ratio of ECG when compared to medical history collection and physical examination or 2D echocardiograph
Cost-effectiveness of preparticipation screening for prevention of sudden cardiac death in young athletes[49]	Screening young athletes with 12-lead ECG plus cardiovascular-focused history and physical examination may be cost-effective
Usefulness and cost effectiveness of cardiovascular screening of young adolescents[50]	The cost of this screening system was lower when compared to the United States model
An electrocardiogram should not be included in routine prepartecipation screening of young athletes[52]	Implementing PPS with ECG could be too much expansive in the United States, in consideration of the enormous number of competitive high school and college athletes
Preventing sudden death of athletes with electrocardiographic screening: What is the absolute benefit and how much will it cost?[53]	The Italian strategy of ECG screening in the United States would result in enormous costs per life saved

ECG: Electrocardiogram; PPS: Pre-participation.

thors still discourage the adoption of ECG in routine PPS of young athletes since its cost seems to be excessive for the public health[52,53] (Tables 1 and 2).

Another viewpoint has been provided by the Israeli experience. Indeed, Israeli Sport Law implemented PPS in 1997. As reported in literature, they did not find any difference in the incidence of SCD in athletes following the introduction of PPS. For this reason they concluded that PPS is neither useful nor cost effective[54]. This divergence could be explained by the result of a recent Asian study illustrating the main causes of SCD in Israel: Marfan's syndrome, anomalous coronary arteries, catecholamine related arrhythmias and commotion cordis. All these pathologies are much more difficult to be detected by resting ECG when compared ti hypertrophic cardiomyopathy, dilated cardiomyopathy, valvular heart disease, ARVD, long QT syndrome and Brugada's syndrome, all representing the most common cause of SCD in Europe and United States[55].

Undoubtedly, echocardiogram seems to be too much expansive for the Public Health and for this reason not easily practicable, even if useful and not invasive. Partial solutions of this issue have been proposed by Weidenbener *et al*[56] with the inclusion of a single-view parasternal long and short-axis two-dimensional screening echocardiogram at an average cost of $7.34 per examination. The effectiveness of this approach has been confirmed during PPS[57] as well as for the follow up of other cardiovascular diseases such as hypertension in order to evaluate left ventricular hypertrophy[58,59].

Even if we strongly believe that a saved life is more important of any cost-efficacy evaluation, the issue of the economical impact of this approach should be further assessed.

REFERENCES

1 **Maron BJ**, Epstein SE, Roberts WC. Causes of sudden death in competitive athletes. *J Am Coll Cardiol* 1986; **7**: 204-214 [PMID: 3510233 DOI: 10.1016/S0735-1097(86)80283-2]

2 **Maron BJ**, Shirani J, Poliac LC, Mathenge R, Roberts WC, Mueller FO. Sudden death in young competitive athletes. Clinical, demographic, and pathological profiles. *JAMA* 1996; **276**: 199-204 [PMID: 8667563 DOI: 10.1001/jama.1996.03540030033028]

3 **Maron BJ**, Chaitman BR, Ackerman MJ, Bayés de Luna A, Corrado D, Crosson JE, Deal BJ, Driscoll DJ, Estes NA, Araújo CG, Liang DH, Mitten MJ, Myerburg RJ, Pelliccia A, Thompson PD, Towbin JA, Van Camp SP. Recommendations for physical activity and recreational sports participation for young patients with genetic cardiovascular diseases. *Circulation* 2004; **109**: 2807-2816 [PMID: 15184297 DOI: 10.1161/01.CIR.0000128363.85581.E1]

4 **Waller BF**, Roberts WC. Sudden death while running in conditioned runners aged 40 years or over. *Am J Cardiol* 1980; **45**: 1292-1300 [PMID: 7377127 DOI: 10.1016/0002-9149(80)90491-9]

5 **Northcote RJ**, Evans AD, Ballantyne D. Sudden death in squash players. *Lancet* 1984; **1**: 148-150 [PMID: 6140452 DOI: 10.1016/S0140-6736(84)90073-4]

6 **Noakes TD**. Heart disease in marathon runners: a review. *Med Sci Sports Exerc* 1987; **19**: 187-194 [PMID: 3298928 DOI: 10.1249/00005768-198706000-00001]

7 **Thompson PD**, Funk EJ, Carleton RA, Sturner WQ. Incidence of death during jogging in Rhode Island from 1975 through 1980. *JAMA* 1982; **247**: 2535-2538 [PMID: 6978411 DOI: 10.1001/jama.1982.03320430039028]

8 **Corrado D**, Basso C, Rizzoli G, Schiavon M, Thiene G. Does sports activity enhance the risk of sudden death in adolescents and young adults? *J Am Coll Cardiol* 2003; **42**: 1959-1963 [PMID: 14662259 DOI: 10.1016/j.jacc.2003.03.002]

9 **Corrado D**, Migliore F, Basso C, Thiene G. Exercise and the risk of sudden cardiac death. *Herz* 2006; **31**: 553-558 [PMID: 17036186 DOI: 10.1007/s00059-006-2885-8]

10 **Pigozzi F**, Rizzo M. Sudden death in competitive athletes. *Clin Sports Med* 2008; **27**: 153-181, ix [PMID: 18206573 DOI: 10.1016/j.csm.2007.09.004]

11 **Van Camp SP**, Bloor CM, Mueller FO, Cantu RC, Olson HG. Nontraumatic sports death in high school and college athletes. *Med Sci Sports Exerc* 1995; **27**: 641-647 [PMID: 7674867]

12 **Schiavon M,** Zorzi A, Basso C, Pelliccia A, Thiene G, Corrado D. Arrhythmogenic cardiomiopathy and sports related sudden death Cardiac Electrophysiology. *Cardiac Electrophysiology Clinics* 2011; **3:** 323-331 [DOI: 10.1016/j.ccep.2011.02.010]

13 **Bowker TJ**, Wood DA, Davies MJ, Sheppard MN, Cary NR, Burton JD, Chambers DR, Dawling S, Hobson HL, Pyke SD, Riemersma RA, Thompson SG. Sudden, unexpected cardiac or unexplained death in England: a national survey. *QJM* 2003; **96**: 269-279 [PMID: 12651971]

14 **Doolan A**, Langlois N, Semsarian C. Causes of sudden cardiac death in young Australians. *Med J Aust* 2004; **180**: 110-112 [PMID: 14748671]

15 **Haïssaguerre M**, Derval N, Sacher F, Jesel L, Deisenhofer I, de Roy L, Pasquié JL, Nogami A, Babuty D, Yli-Mayry S, De Chillou C, Scanu P, Mabo P, Matsuo S, Probst V, Le Scouarnec S, Defaye P, Schlaepfer J, Rostock T, Lacroix D, Lamaison D, Lavergne T, Aizawa Y, Englund A, Anselme F, O'Neill M, Hocini M, Lim KT, Knecht S, Veenhuyzen GD, Bordachar P, Chauvin M, Jais P, Coureau G, Chene G, Klein GJ, Clémenty J. Sudden cardiac arrest associated with early repolarization. *N Engl J Med* 2008; **358**: 2016-2023 [PMID: 18463377 DOI: 10.1056/NEJMoa071968]

16 **Maron BJ**, Gohman TE, Aeppli D. Prevalence of sudden cardiac death during competitive sports activities in Minnesota high school athletes. *J Am Coll Cardiol* 1998; **32**: 1881-1884 [PMID: 9857867]

17 **Shen WK**, Edwards WD, Hammill SC, Bailey KR, Ballard DJ, Gersh BJ. Sudden unexpected nontraumatic death in 54 young adults: a 30-year population-based study. *Am J Cardiol* 1995; **76**: 148-152 [PMID: 7611149]

18 **Maron BJ**, Haas TS, Doerer JJ, Thompson PD, Hodges JS. Comparison of U.S. and Italian experiences with sudden cardiac deaths in young competitive athletes and implications for preparticipation screening strategies. *Am J Cardiol* 2009; **104**: 276-280 [PMID: 19576360 DOI: 10.1016/j.amjcard.2009.03.037]

19 **Maron BJ**, Thompson PD, Ackerman MJ, Balady G, Berger S, Cohen D, Dimeff R, Douglas PS, Glover DW, Hutter AM, Krauss MD, Maron MS, Mitten MJ, Roberts WO, Puffer JC. Recommendations and considerations related to preparticipation screening for cardiovascular abnormalities in competitive athletes: 2007 update: a scientific statement from the American Heart Association Council on Nutrition, Physical Activity, and Metabolism: endorsed by the American College of Cardiology Foundation. *Circulation* 2007; **115**: 1643-1455 [PMID: 17353433]

20 **Corrado D**, Pelliccia A, Bjørnstad HH, Vanhees L, Biffi A, Borjesson M, Panhuyzen-Goedkoop N, Deligiannis A, Solberg E, Dugmore D, Mellwig KP, Assanelli D, Delise P, van-Buuren F, Anastasakis A, Heidbuchel H, Hoffmann E, Fagard R, Priori SG, Basso C, Arbustini E, Blomstrom-Lundqvist C, McKenna WJ, Thiene G. Cardiovascular preparticipation screening of young competitive athletes for prevention of sudden death: proposal for a common European protocol. Consensus Statement of the Study Group of Sport Cardiology of the Working Group of Cardiac Rehabilitation and Exercise Physiology and the Working Group of Myocardial and Pericardial Diseases of the European Society of Cardiology. *Eur Heart J* 2005; **26**: 516-524 [PMID: 15689345]

21 **Myerburg RJ**, Vetter VL. Electrocardiograms should be included in preparticipation screening of athletes. *Circulation* 2007; **116**: 2616-226; discussion 2626 [PMID: 18040041]

22 **Italian Ministry of Health.** Norme per la tutela sanitaria dell'attività sportiva agonistica. Gazzetta: Serie generale, 1982: 1715-1719

23 **Pigozzi F**, Spataro A, Alabiso A, Parisi A, Rizzo M, Fagnani F, Di Salvo V, Massazza G, Maffulli N. Role of exercise stress test in master athletes. *Br J Sports Med* 2005; **39**: 527-531 [PMID: 16046336 DOI: 10.1136/bjsm.2004.014340]

24 **Brambilla G**, Cenci T, Franconi F, Galarini R, Macrì A, Rondoni F, Strozzi M, Loizzo A. Clinical and pharmacological profile in a clenbuterol epidemic poisoning of contaminated beef meat in Italy. *Toxicol Lett* 2000; **114**: 47-53 [PMID: 10713468]

25 **Napolitano C**, Bloise R, Monteforte N, Priori SG. Sudden cardiac death and genetic ion channelopathies: long QT, Brugada, short QT, catecholaminergic polymorphic ventricular tachycardia, and idiopathic ventricular fibrillation. *Circulation* 2012; **125**: 2027-2034 [PMID: 22529064 DOI: 10.1161/CIRCULATIONAHA.111.055947]

26 **Corrado D**, Basso C, Schiavon M, Pelliccia A, Thiene G. Preparticipation screening of young competitive athletes for prevention of sudden cardiac death. *J Am Coll Cardiol* 2008; **52**: 1981-1989 [PMID: 19055989 DOI: 10.1016/j.jacc.2008.06.053]

27 **Corrado D**, Basso C, Schiavon M, Thiene G. Screening for hypertrophic cardiomyopathy in young athletes. *N Engl J Med* 1998; **339**: 364-369 [PMID: 9691102 DOI: 10.1056/NEJM199808063390602]

28 **Maron BJ**, Gardin JM, Flack JM, Gidding SS, Kurosaki TT, Bild DE. Prevalence of hypertrophic cardiomyopathy in a general population of young adults. Echocardiographic analysis of 4111 subjects in the CARDIA Study. Coronary Artery Risk Development in (Young) Adults. *Circulation* 1995; **92**: 785-789 [PMID: 7641357]

29 **Uner A**, Doğan M, Bay A, Cakin C, Kaya A, Sal E. The ratio of congenital heart disease and innocent murmur in children in Van city, the Eastern Turkey. *Anadolu Kardiyol Derg* 2009; **9**: 29-34 [PMID: 19196570]

30 **Advani N**, Menahem S, Wilkinson JL. The diagnosis of innocent murmurs in childhood. *Cardiol Young* 2000; **10**: 340-342 [PMID: 10950330]

31 **O'Connor M**, McDaniel N, Brady WJ. The pediatric electrocardiogram. Part I: Age-related interpretation. *Am J Emerg Med* 2008; **26**: 221-228 [PMID: 18272106 DOI: 10.1016/j.ajem.2007.08.003]

32 **O'Connor M**, McDaniel N, Brady WJ. The pediatric electrocardiogram part III: Congenital heart disease and other cardiac syndromes. *Am J Emerg Med* 2008; **26**: 497-503 [PMID: 18410822 DOI: 10.1016/j.ajem.2007.08.004]

33 **Cheng TO**. Prevalence of mitral valve prolapse in the Framingham Heart Study. *Am J Cardiol* 2002; **90**: 1425; author reply 1425-1426 [PMID: 12480067]

34 **Hepner AD**, Ahmadi-Kashani M, Movahed MR. The prevalence of mitral valve prolapse in patients undergoing echocardiography for clinical reason. *Int J Cardiol* 2007; **123**: 55-57 [PMID: 17292985]

35 **Movahed MR**, Hepner AD, Ahmadi-Kashani M. Echocardiographic prevalence of bicuspid aortic valve in the popu-

lation. *Heart Lung Circ* 2006; **15**: 297-299 [PMID: 16914375]
36 **Spataro A**, Pelliccia A, Rizzo M, Biffi A, Masazza G, Pigozzi F. The natural course of bicuspid aortic valve in athletes. *Int J Sports Med* 2008; **29**: 81-85 [PMID: 17990219]
37 **Tzemos N**, Therrien J, Yip J, Thanassoulis G, Tremblay S, Jamorski MT, Webb GD, Siu SC. Outcomes in adults with bicuspid aortic valves. *JAMA* 2008; **300**: 1317-1325 [PMID: 18799444 DOI: 10.1001/jama.300.11.1317]
38 **Zuppiroli A**, Rinaldi M, Kramer-Fox R, Favilli S, Roman MJ, Devereux RB. Natural history of mitral valve prolapse. *Am J Cardiol* 1995; **75**: 1028-1032 [PMID: 7747683 DOI: 10.1016/S0002-9149(99)80718-8]
39 **Ward C**. Clinical significance of the bicuspid aortic valve. *Heart* 2000; **83**: 81-85 [PMID: 10618341 DOI: 10.1136/heart.83.1.81]
40 **Nistri S**, Sorbo MD, Marin M, Palisi M, Scognamiglio R, Thiene G. Aortic root dilatation in young men with normally functioning bicuspid aortic valves. *Heart* 1999; **82**: 19-22 [PMID: 10377302]
41 **Corrado D**, Basso C, Nava A, Rossi L, Thiene G. Sudden death in young people with apparently isolated mitral valve prolapse. *G Ital Cardiol* 1997; **27**: 1097-1105 [PMID: 9419819]
42 **Punnoose AR**, Lynm C, Golub RM. JAMA patient page. Antibiotics to prevent infective endocarditis. *JAMA* 2012; **308**: 935 [PMID: 22948707 DOI: 10.1001/jama.2012.6918]
43 **Di Filippo S**. Prophylaxis of infective endocarditis in patients with congenital heart disease in the context of recent modified guidelines. *Arch Cardiovasc Dis* 2012; **105**: 454-460 [PMID: 22958889 DOI: 10.1016/j.acvd.2012.02.011]
44 **Steinberger J**, Moller JH, Berry JM, Sinaiko AR. Echocardiographic diagnosis of heart disease in apparently healthy adolescents. *Pediatrics* 2000; **105**: 815-818 [PMID: 10742325 DOI: 10.1542/peds.105.4.815]
45 **Rizzo M**, Spataro A, Cecchetelli C, Quaranta F, Livrieri S, Sperandii F, Cifra B, Borrione P, Pigozzi F. Structural cardiac disease diagnosed by echocardiography in asymptomatic young male soccer players: implications for preparticipation screening. *Br J Sports Med* 2012; **46**: 371-373 [PMID: 21791458 DOI: 10.1136/bjsm.2011.085696]
46 **Pelliccia A**, Maron BJ, Culasso F, Di Paolo FM, Spataro A, Biffi A, Caselli G, Piovano P. Clinical significance of abnormal electrocardiographic patterns in trained athletes. *Circulation* 2000; **102**: 278-284 [PMID: 10899089 DOI: 10.1161/01.CIR.102.3.278]
47 Health, United States, 2007 with Chartbook on Trends in the Health of Americans. Hyattsville, MD: 2007. Available from: URL: http://www.cdc.gov/nchs/data/hus/hus07.pdf
48 **Fuller CM**. Cost effectiveness analysis of screening of high school athletes for risk of sudden cardiac death. *Med Sci Sports Exerc* 2000; **32**: 887-890 [PMID: 10795776 DOI: 10.1097/00005768-200005000-00002]
49 **Wheeler MT**, Heidenreich PA, Froelicher VF, Hlatky MA, Ashley EA. Cost-effectiveness of preparticipation screening for prevention of sudden cardiac death in young athletes. *Ann Intern Med* 2010; **152**: 276-286 [PMID: 20194233 DOI: 10.1059/0003-4819-152-5-201003020-00005]
50 **Tanaka Y**, Yoshinaga M, Anan R, Tanaka Y, Nomura Y, Oku S, Nishi S, Kawano Y, Tei C, Arima K. Usefulness and cost effectiveness of cardiovascular screening of young adolescents. *Med Sci Sports Exerc* 2006; **38**: 2-6 [PMID: 16394946 DOI: 10.1249/01.mss.0000183187.88000.53]
51 **Quaglini S**, Rognoni C, Spazzolini C, Priori SG, Mannarino S, Schwartz PJ. Cost-effectiveness of neonatal ECG screening for the long QT syndrome. *Eur Heart J* 2006; **27**: 1824-1832 [PMID: 16840497 DOI: 10.1093/eurheartj/ehl115]
52 **Chaitman BR**. An electrocardiogram should not be included in routine preparticipation screening of young athletes. *Circulation* 2007; **116**: 2610-2614; discussion 2615 [PMID: 18040040]
53 **Halkin A**, Steinvil A, Rosso R, Adler A, Rozovski U, Viskin S. Preventing sudden death of athletes with electrocardiographic screening: what is the absolute benefit and how much will it cost? *J Am Coll Cardiol* 2012; **60**: 2271-2276 [PMID: 23194938 DOI: 10.1016/j.jacc.2012.09.003]
54 **Steinvil A**, Chundadze T, Zeltser D, Rogowski O, Halkin A, Galily Y, Perluk H, Viskin S. Mandatory electrocardiographic screening of athletes to reduce their risk for sudden death proven fact or wishful thinking? *J Am Coll Cardiol* 2011; **57**: 1291-1296 [PMID: 21392644 DOI: 10.1016/j.jacc.2010.10.037]
55 **Uberoi A**, Froelicher V. Sudden cardiac death in athletes: big trouble, not so little Asia. *Asian J Sports Med* 2011; **2**: 275-276 [PMID: 22375249]
56 **Weidenbener EJ**, Krauss MD, Waller BF, Taliercio CP. Incorporation of screening echocardiography in the preparticipation exam. *Clin J Sport Med* 1995; **5**: 86-89 [PMID: 7882118 DOI: 10.1097/00042752-199504000-00003]
57 **Shry EA**, Leding CJ, Rubal BJ, Eisenhauer MD. The role of limited echocardiography and electrocardiography in screening physicals for amateur athletes. *Mil Med* 2002; **167**: 831-834 [PMID: 12392250]
58 **Sheps SG**, Frohlich ED. Limited echocardiography for hypertensive left ventricular hypertrophy. *Hypertension* 1997; **29**: 560-563 [PMID: 9040438 DOI: 10.1161/01.HYP.29.2.560]
59 **Black HR**, Weltin G, Jaffe CC. The limited echocardiogram: a modification of standard echocardiography for use in the routine evaluation of patients with systemic hypertension. *Am J Cardiol* 1991; **67**: 1027-1030 [PMID: 2018006 DOI: 10.1016/0002-9149(91)90178-N]

P- Reviewers Providência R, Steinberg JS
S- Editor Zhai HH **L- Editor** A **E- Editor** Xiong L

World Journal of Methodology

Online Submissions: http://www.wjgnet.com/esps/
wjm@wjgnet.com
doi:10.4329/wjm.v3.i1.7

World J Methodol 2013 March 26; 3(1): 7-10
ISSN 2222-0682 (online)

BRIEF ARTICLE

Confidence limit calculation for antidotal potency ratio derived from lethal dose 50

Ananda Manage, Ilona Petrikovics

Ananda Manage, Department of Mathematics and Statistics, Sam Houston State University, Huntsville, TX 77341, United States
Ilona Petrikovics, Department of Chemistry, Sam Houston State University, Huntsville, TX 77341, United States
Author contributions: Manage A derived the confidence interval; Petrikovics I came up with the application and the manuscript was written by both.
Correspondence to: Dr. Ilona Petrikovics, Department of Chemistry, Sam Houston State University, Huntsville, TX 77341, United States. ixp004@shsu.edu
Telephone: +1-936-2944389 Fax: +1-936-2944996
Received: July 25, 2012 Revised: November 5, 2012
Accepted: December 6, 2012
Published online: March 26, 2013

Abstract

AIM: To describe confidence interval calculation for antidotal potency ratios using bootstrap method.

METHODS: We can easily adapt the nonparametric bootstrap method which was invented by Efron to construct confidence intervals in such situations like this. The bootstrap method is a resampling method in which the bootstrap samples are obtained by resampling from the original sample.

RESULTS: The described confidence interval calculation using bootstrap method does not require the sampling distribution antidotal potency ratio. This can serve as a substantial help for toxicologists, who are directed to employ the Dixon up-and-down method with the application of lower number of animals to determine lethal dose 50 values for characterizing the investigated toxic molecules and eventually for characterizing the antidotal protections by the test antidotal systems.

CONCLUSION: The described method can serve as a useful tool in various other applications. Simplicity of the method makes it easier to do the calculation using most of the programming software packages.

Key words: Up-and-down method; Confidence limit; Potency ratio, Bootstrapping

Manage A, Petrikovics I. Confidence limit calculation for antidotal potency ratio derived from lethal dose 50. *World J Methodol* 2013; 3(1): 7-10 Available from: URL: http://www.wjgnet.com/2222-0682/full/v3/i1/7.htm DOI: http://dx.doi.org/10.4329/wjm.v3.i1.7

INTRODUCTION

To characterize toxic effects of poisons and overdosed drugs, acute toxicity testing methods were developed in the beginning of the 19th century. Trevan[1] first wrote up the concept of lethal dose 50 (LD_{50}) (medium lethal dose) in 1927. He also indicated that LD_{50} is not a biological constant, its precision depends on many factors (*e.g.*, number of animals used, sex, species, strain, age, diet, general health condition, route of administration, stress, formulation, intra and inter laboratory variations, *etc.*). To express acute toxicity, LD_{50} is a good tool, and many government agencies still rely on these data. Many methods have been developed to characterize the toxic effects (acute toxicity) of chemicals, and expressed as LD_{50} values and its 95% confidence limit and the slope of the probit line, *e.g.*, Litchfield and Wilcoxon[2], Bliss[3], Holland *et al*[4]. Up until the 90s, the Litchfield and Wilcoxon[2] method was one of the most frequently used tool for toxicologists to characterize acute toxicity, and the *in vivo* antidotal efficacy of various antidotal systems.

An example, Pei *et al*[5], analyzed data for LD_{50} values of paraoxon that is an organophosphorus (OP) type nerve agent, in the presence of various antidotal systems by the method of Litchfield and Wilcoxon, as adapted to

a computer program PHARM/PCS version 4.2. by Bergol'ts *et al*[6]. The antidotal potency ratios (APRs) derived from the dose-response curves of paraoxon were used to express the *in vivo* efficacy of various OP antidotal systems to antagonize the lethal effects of paraoxon (APR = LD_{50} of paraoxon antagonized/LD_{50} of paraoxon unantagonized). Tests for the parallelism of the dose-effect curves were done, and all statistical procedures were performed at the 95% confidence level. The authors used six groups of animals, 8 animals per groups (48 animals) for each LD_{50} value.

Since the Litchfield-Wilcoxon method requires a large number (40-50) of animals, efforts were done to introduce other LD_{50} determinations with a lesser number of animals. The up-and-down methods by Dixon[7], Bruce[8] can provide adequate estimation of LD_{50} and approximation of the 95% confidence interval by using as few as 6-9 animals. When this method was compared with the traditional Litchfield-Wilcoxon method, excellent agreement was obtained for all the 10 molecules tested.

Another example: Petrikovics *et al*[9], determined LD_{50} values for paraoxon by the method of Dixon[6], and 95% confidence limit was estimated by the method of Bruce[10]. For each experiment, 6-10 animals were used. The LD_{50} values were calculated from the equation of *Log (*LD_{50}*) = log (dose final) + k log (d)* where *dose final* is the final dose administered, *k* is the tabular value from the table, and *d* is the interval between doses. APRs were expressed as a simple number (without confidence limit). APR = mean LD_{50} of paraoxon antagonized/mean LD_{50} of paraoxon unantagonized.

Another example: Petrikovics *et al*[11], determined LD_{50} for cyanide by the up-and-down method of Dixon[7]. This method requires settings for the starting doses and the stage distances (dose difference between doses) for each test system. The software (based on "Implementation of Dixon and Massey UPD", Introduction to statistical Analysis, 1983, pp.434-438) provides information for the next dose for each stage, based on the mortality results for the given stage. The log dose difference of 0.1 was set up based on the earlier studies with cyanide (Petrikovics *et al*[12], where the LD_{50} values were determined by the classic Litchfield-Wilcoxon[2] method. For each LD_{50} values 10-18 were used. LD_{50} values were expressed as average ± 95% confidence limit by the software. APRs were expressed as a ratio of average LD_{50} of cyanide with antidotes and average LD_{50} of cyanide without antidotes. Again, confidence limits for APR were not expressed.

MATERIALS AND METHODS

In a situation like this where the distribution of the ratio is unknown, it is difficult to calculate the confidence intervals using classical methods. However, we can easily adapt the nonparametric bootstrap method which was invented by Efron[13] to construct confidence intervals in such situations like this. The bootstrap method is a resampling method in which the bootstrap samples are obtained by resampling from the original sample. A comprehensive coverage of the bootstrap method can be found in Efron and Tibshirani[14]. Chernick[15], Shao and Tu[16], Davison and Hinkley[17], Manly[18] and Hayden[19] are also useful references.

There are several ways of calculating bootstrap confidence intervals. Briefly, one way of calculating the bootstrap confidence interval for APR given below:

To assume that the data set is coming from two samples which we call sample 1 and sample 2 to calculate the APR.

(1) Obtain a bootstrap sample $X^* = (X_1^*, X_2^*,\ldots\ldots, X_{n1}^*)$ from the original sample 1 $X = (X_1, X_2,\ldots\ldots, X_{n1})$.

(2) Calculate logLD_{50} dose estimate using

$$LD_1^* = \frac{\Sigma X_i^*}{n_1} + \frac{d}{n_1}(A_1 + C_1)$$

[page 389 Dixon (1969)];

(3) Obtain a bootstrap sample $Y^* = (Y_1^*, Y_2^*,\ldots\ldots, Y_{n1}^*)$ from the original sample 2 $Y = (Y_1, Y_2,\ldots\ldots, Y_{n1})$;

(4) Calculate logLD_{50} dose estimate using,

$$LD_2^* = \frac{\Sigma Y_i^*}{n_2} + \frac{d}{n_2}(A_2 + C_2)$$

(5) Calculate the ratio,

$$APR^* = \frac{10^{LD_1^*}}{10^{LD_2^*}}.$$

(as the values are in log base 10);

(6) Repeat step 1 through step 5, a large number of times (B = 1000) to get a list of values;

(7) Find the quantiles $APR_{(\alpha/2)}$ and $APR_{(1-\alpha/2)}$ for the list of *B* ratio values. ($APR_{\alpha/2}$, $APR_{1-\alpha/2}$) is the 100 (1 - α)% confidence interval for the ratio. This confidence interval is usually called percentile bootstrap confidence interval.

RESULTS

We illustrate the method for LD_{50} ratio for the following two experiments (Figure 1). Figure 2 shows the histogram of the bootstrap distribution of the APR. Quantiles of this distribution are used to derive the relevant confidence limits. In our illustration here we use the 95% confidence limit. LD_{50} dose estimate for the first experiment is 7.834 and the LD_{50} dose estimate for the second experiment is 23.812. This gives the APR to be 0.32897. Therefore, the lower confidence limit, which is the 2.5th percentile of the bootstrap distribution is 0.25821 and the upper confidence limit which is the 97.5th percentile of the bootstrap distribution is 0.41714.

DISCUSSION

We used a simple method to construct the confidence interval for calculating APR derived from two LD_{50}. The described nonparametric bootstrap method to determine confidence intervals can easily be constructed even in situations where the distribution of the ratio is un-

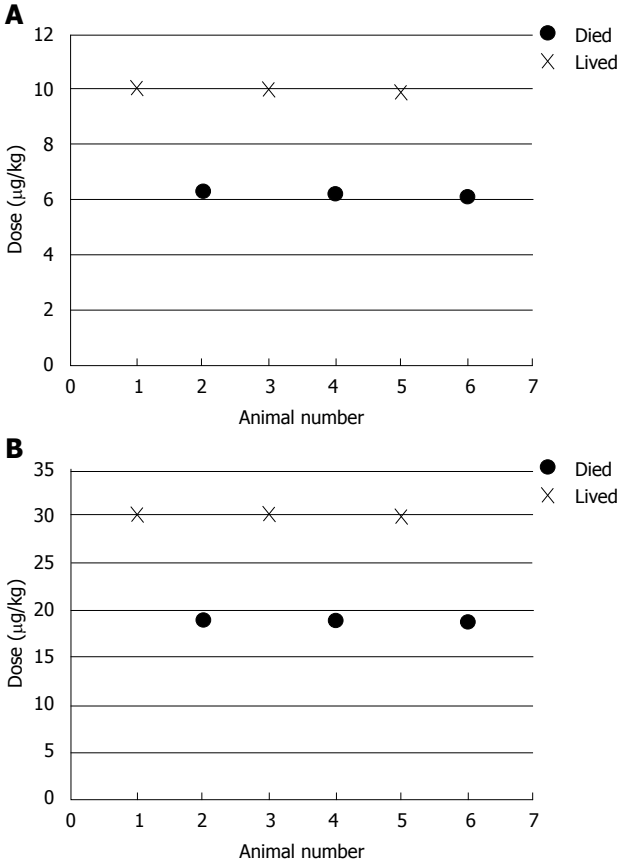

Figure 1 Graph of the dose and the outcome (lived or died) for the first (A) and second (B) experiment.

known. This presentation describes a calculation of the bootstrap confidence interval for APR. This can serve as a substantial improvement for toxicologists, who are directed to employ the Dixon up-and-down method with the application of lower number of animals to determine LD_{50} values for characterizing the investigated toxic molecules and eventually for characterizing the antidotal protections by the test antidotal systems. The described method can serve as a useful tool in various other applications. Simplicity of the method makes it easier to do the calculation using most of the programming software packages.

COMMENTS

Background

To characterize toxic effects of poisons and overdosed drugs, acute toxicity testing methods were developed in the beginning of the 19th century. To express acute toxicity, lethal dose 50 (LD_{50}) is a good tool, and many government agencies still rely on these data. Many methods have been developed to characterize the toxic effects (acute toxicity) of chemicals, and expressed as LD_{50} values and its 95% confidence limit and the slope of the probit line. To characterize antidotal efficacy of a given antidotal system, antidotal potency ratios (APRs) are calculated, that is the ratio of the LD_{50} of the toxic chemical with the test antidotal system and the LD_{50} of the toxic chemicals without any antidote(s) (control). The higher is the APR, the better is the antidotal system.

Research frontiers

When applying the classic Litchfield-Wilcoxon method for LD_{50} determination, a large number of animals (6-8 groups of animals, 6-8 animal/group = 36-64) are needed. To reduce the number of animals, new methods were developed, and the Dixon up-and-down method has become popular with its lower number of animal needed (8-18 animals/LD_{50}). However, when the Litchfield-Wilcoxon method was adapted to a computer program PHARM/PCS version 4.2. by Tallarida and Murray, the APR was automatically expressed with 95% confidence limits by the software. There is a need for the 95% confidence limit determination with the Dixon up-and-down method when expressing APR values. Although Bruce provided adequate estimation for it, this article introduces a more practical tool for filling this gap.

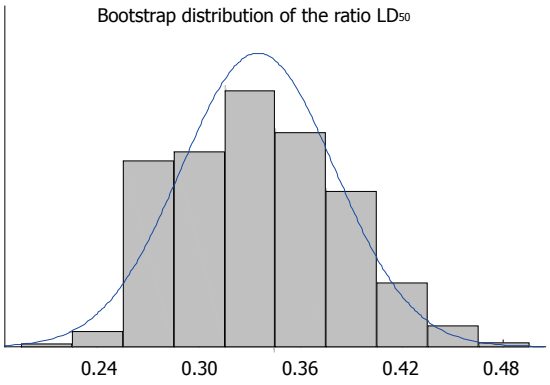

Figure 2 Bootstrap distribution of antidotal potency ratio. LD_{50}: Lethal dose 50.

Innovations and breakthroughs

Previous methods to characterize acute toxicity and/or determining antidotal efficacy for antidotal systems needed to be transformed in order to (1) reduce the number of animals used for LD_{50} determination (2) calculate 95% confidence limits for APR with lower number of animals used. This article can serve as a substantial help for toxicologists, who are directed to employ the Dixon up-and-down method with the application of lower number of animals to determine LD_{50} values for characterizing the investigated toxic molecules and eventually for characterizing the antidotal protections by the test antidotal systems.

Applications

The described method can serve as a useful tool in various other applications. Simplicity of the method makes it easier to do the calculation using most of the programming software packages. Authors used a simple MATLAB code to illustrate the confidence interval for the given example.

Terminology

LD_{50} is the dose that kills 50% of the tested animal population. APR = LD_{50} of the toxic chemicals in the presence of the test antidotal system(s)/LD_{50} of the toxic chemical without any antidote(s) (control). APR is use to express in vivo efficacy for antidotal systems. Bootstrap method is a standard technique in which we take simple random samples with replacement from the original sample. With this, overlapping samples is permissible in this technique. Strength of the paper is the application of the bootstrap method to calculate a confidence interval for the LD_{50} ratio. Validation of the method proven practically and theoretically in the literature.

Peer review

This is a good practical method to express 95% confidence limits for APR derived from the Dixon up-and-down method.

REFERENCES

1 **Trevan JW.** The error of determination of toxicity. *Proc R Soc Lond* 1927; **101:** 483-514 [DOI: 10.1098/rspb.1927.0030]
2 **Litchfield JT**, Wilcoxon F. A simplified method of evaluating dose-effect experiments. *J Pharmacol Exp Ther* 1949; **96**: 99-113 [PMID: 18152921]
3 **Bliss CL.** Some principles of bioassay. *Am Sci* 1957; **45:** 449-466
4 **Holland KD**, McKeon AC, Canney DJ, Covey DF, Ferrendelli JA. Relative anticonvulsant effects of GABAmimetic and GABA modulatory agents. *Epilepsia* 1992; **33**: 981-986

[PMID: 1334454]
5 **Pei L**, Petrikovics I, Way JL. Antagonism of the lethal effects of paraoxon by carrier erythrocytes containing phosphotriesterase. *Fundam Appl Toxicol* 1995; **28**: 209-214 [PMID: 8835230 DOI: 10.1006/faat.1995.1161]
6 **Bergol'ts VV**, Volodin IuIu. [A package of applied programs for pharmacological and biochemical calculations]. *Farmakol Toksikol* 1987; **50**: 70-73 [PMID: 3691785]
7 **Dixon WJ.** The up-and-down method for small animal samples. *Am Stat Assoc J* 1965; **12:** 967-978 [DOI: 10.2307/2283398]
8 **Bruce RD.** An Up-and-Down procedure for acute toxicity testing. *Fundam Appl Toxico* 1985; **5:** 15-157 [DOI: 10.1016/0272-0590(85)90059-4]
9 **Petrikovics I**, Hong K, Omburo G, Hu QZ, Pei L, McGuinn WD, Sylvester D, Tamulinas C, Papahadjopoulos D, Jaszberenyi JC, Way JL. Antagonism of paraoxon intoxication by recombinant phosphotriesterase encapsulated within sterically stabilized liposomes. *Toxicol Appl Pharmacol* 1999; **156**: 56-63 [PMID: 10101099]
10 **Bruce RD**. A confirmatory study of the up-and-down method for acute oral toxicity testing. *Fundam Appl Toxicol* 1987; **8**: 97-100 [PMID: 3556826]
11 **Petrikovics I**, Baskin SI, Beigel KM, Schapiro BJ, Rockwood GA, Manage AB, Budai M, Szilasi M. Nano-intercalated rhodanese in cyanide antagonism. *Nanotoxicology* 2010; **4**: 247-254 [PMID: 20795898]
12 **Petrikovics I,** Pei L, McGuinn WD, Cannon EP, Way JL. Cyanide antagonism with organic thiosulfonates and carrier red blood cells containing rhodanese. *Fund Appl Toxicol* 1995; **24:** 1-8 [DOI: 10.1006/taap.1998.8620]
13 **Efron B.** Bootstrap methods: another look at the jackknife. *Ann Statist* 1979; **7:** 1-26 [DOI: 10.1214/aos/1176344552]
14 **Efron B,** Tibshirani RJ. An Introduction to the Bootstrap. New York: Chapman and Hall, 1993
15 **Chernick M.** Bootstrap Methods: A practitioner's Guide. New York: Wiley, 2007
16 **Shao J,** Tu D. The Jackknife and Boostrap. New York: Springer, 1995 [DOI: 10.1007/978-1-4612-0795-5]
17 **Davidson A,** Hinkley D. Boostrap Method and Their Applications. Cambridge: Cambridge University Press, 1997
18 **Manly BFJ.** Randomization, Bootstrap and Monte Carlo Methods in Biology. Boca Raton, FL: Chapman and Hall/CRC Press, 2006
19 **Hayden RW.** A Review of: "Mathematical Statistics with Resampling and R, by L. M. Chihara and T. C. Hesterberg". *J Biopharm Stat* 2012; **22:** 1287-1288

P- Reviewers Hutz RJ, Dhawan DK, Wan TTH
S- Editor Zhai HH **L- Editor** A **E- Editor** Xiong L

World Journal of Methodology

Online Submissions: http://www.wjgnet.com/esps/
wjm@wjgnet.com
doi:10.4329/wjm.v3.i1.11

World J Methodol 2013 March 26; 3(1): 11-18
ISSN 2222-0682 (online)

BRIEF ARTICLE

Methods for the extraction and RNA profiling of exosomes

Emily Zeringer, Mu Li, Tim Barta, Jeoffrey Schageman, Ketil Winther Pedersen, Axl Neurauter, Susan Magdaleno, Robert Setterquist, Alexander V Vlassov

Emily Zeringer, Mu Li, Tim Barta, Jeoffrey Schageman, Ketil Winther Pedersen, Axl Neurauter, Susan Magdaleno, Robert Setterquist, Alexander V Vlassov, Life Technologies, Austin, TX 78744, United States
Author contributions: Zeringer E, Li M, Barta T, Schageman J, Pedersen KW and Neurauter A were involved in design of the study, data acquisition, analysis and interpretation of data; Magdaleno S, Setterquist R and Vlassov AV contributed to the conception and design of the study, and wrote the article.
Correspondence to: Alexander V Vlassov, PhD, Life Technologies, 2130 Woodward street, Austin, TX 78744, United States. sasha.vlassov@lifetech.com
Telephone: +1-512-7213843 Fax: +1-512-6510201
Received: February 27, 2013 Revised: March 8, 2013
Accepted: March 18, 2013
Published online: March 26, 2013

Abstract

AIM: To develop protocols for isolation of exosomes and characterization of their RNA content.

METHODS: Exosomes were extracted from HeLa cell culture media and human blood serum using the Total exosome isolation (from cell culture media) reagent, and Total exosome isolation (from serum) reagent respectively. Identity and purity of the exosomes was confirmed by Nanosight® analysis, electron microscopy, and Western blots for CD63 marker. Exosomal RNA cargo was recovered with the Total exosome RNA and protein isolation kit. Finally, RNA was profiled using Bioanalyzer and quantitative reverse transcription-polymerase chain reaction (qRT-PCR) methodology.

RESULTS: Here we describe a novel approach for robust and scalable isolation of exosomes from cell culture media and serum, with subsequent isolation and analysis of RNA residing within these vesicles. The isolation procedure is completed in a fraction of the time, compared to the current standard protocols utilizing ultracentrifugation, and allows to recover fully intact exosomes in higher yields. Exosomes were found to contain a very diverse RNA cargo, primarily short sequences 20-200 nt (such as miRNA and fragments of mRNA), however longer RNA species were detected as well, including full-length 18S and 28S rRNA.

CONCLUSION: We have successfully developed a set of reagents and a workflow allowing fast and efficient extraction of exosomes, followed by isolation of RNA and its analysis by qRT-PCR and other techniques.

Key words: Exosomes; Microvesicles; Cell culture media; Serum; RNA; Quantitative reverse transcription-polymerase chain reaction; Sequencing

Core tip: Exosomes are small vesicles (30-150 nm) perceived to be carriers of the unique effector or signaling macromolecules (miRNA, ncRNA, mRNA and protein) between very specific cells within our body. The spectrum of current scientific interests ranges from studying the functions and pathways of exosomes to utilizing them in diagnostics and therapeutics development. Here we describe a complete exosome workflow solution: fast and efficient isolation of exosomes; extraction of their cargo; characterization of exosomal RNA content using quantitative reverse transcription-polymerase chain reaction and other techniques.

Zeringer E, Li M, Barta T, Schageman J, Pedersen KW, Neurauter A, Magdaleno S, Setterquist R, Vlassov AV. Methods for the extraction and RNA profiling of exosomes. *World J Methodol* 2013; 3(1): 11-18 Available from: URL: http://www.wjgnet.com/2222-0682/full/v3/i1/11.htm DOI: http://dx.doi.org/10.4329/wjm.v3.i1.11

INTRODUCTION

Cells are known to secrete a large variety of vesicles, macromolecular complexes, and smaller molecules like

salts and cofactors, into the extracellular space. The types of vesicles secreted are diverse and depend on the origin of the cells and their current state, for example, transformed, differentiated, stimulated, or stressed. Exosomes are a type of microvesicle, 30-150 nm in size, that have received increased attention over the past decade[1-5]. Exosomes are secreted by all cell types in culture, and also found naturally in body fluids including blood, saliva, urine, and breast milk, in very high numbers (10^8-10^{11} per mL)[6,7]. Depending on the cell/tissue of origin, many different roles and functions have been attributed to exosomes: Facilitators of the immune response[8], antigen presentation[6], programmed cell death, angiogenesis, inflammation, coagulation[9], morphogen transporters in the creation of polarity during development and differentiation[4], and mediation of nontargeted effect of ionizing radiation[10]. Recent studies have demonstrated that exosomes are not only specifically targeted to recipient cells to exchange proteins and lipids or to trigger downstream signaling events, but also to deliver specific nucleic acid cargo for cell communication purposes. Valadi *et al*[11] demonstrated that MC/9 and human mast cell line-1 mast cells secrete exosomes that contain mRNA from approximately 1300 genes and small RNAs, including 121 unique microRNAs. The transfer of exosomes to a donor cell showed that at least some mRNAs were full-length, as they were translated in the recipient cell. Glioblastoma cells also secrete exosomes and microvesicles containing mRNA, miRNA and angiogenic proteins[12] - when taken up by host human brain microvascular endothelial cells, mRNA molecules were translated and tubule formation by the target endothelial cells was stimulated. The spread of oncogenes by exosomes and microvesicles secreted by tumor cells has also been reported[13]. Exosomes seem to play a crucial role in spreading pathogens such as prions and viruses from one cell to another[14-16]. Interest towards exosomes, from their function in the body to more practical applications, such as use in diagnostics and therapeutics development, has grown exponentially in the last few years[17-19].

Critical to further our understanding of exosomes, is the development of reagents, tools and protocols for their isolation, characterization and analysis of their RNA and protein contents. Several reports have been published to date, using quantitative reverse transcription-polymerase chain reaction (qRT-PCR) and next gen sequencing for initial characterization of the RNA content of exosomes derived from human acute monocytic leukemia cell line, human umbilical vein endothelial cells, dendritic cells and human embryonic stem cell-derived mesenchymal stroma cells, as well as serum, saliva, placenta and breast milk[14,20-22]. All these studies utilize ultracentrifugation protocols[23] which are proven methods, producing clean exosome preparations. However, the ultracentrifugation approach has numerous drawbacks: the method is highly labor intensive and time consuming (up to two days per preparation, for a protocol with sucrose gradient); one can not process more than 6 samples at a time (due to rotor limitation); it requires a large amount of starting material; exosome yields are typically low; extensive training for personnel is needed; and the method overall is not very reliable.

Here we describe a novel approach for fast and efficient isolation of exosomes from cell culture media and blood serum, followed by recovery of RNA cargo and its analysis by qRT-PCR. The procedure is completed in a fraction of the time, compared to the current standard protocols utilizing ultracentrifugation, and allows to recover fully intact exosomes in higher yields.

MATERIALS AND METHODS

Extraction of exosomes from serum and cell media using Total exosome isolation reagents

Cell culture media: Fresh cell media was harvested from HeLa cells, grown initially in the presence of 10% fetal bovine serum (FBS), and [after two phosphate buffered saline (PBS) washes] without FBS for the last 12 h. The cell media samples were then centrifuged at 2000 *g* for 30 min to remove cell debris. The supernatant containing the cell-free cell media was transferred to a fresh container and held on ice until use. Next, each sample was combined with 1/2th volume of Total exosome isolation (from cell culture media) reagent (Invitrogen) and mixed well by vortexing until a homogenous solution was formed. The samples were incubated at 4 ℃ overnight, then centrifuged at 4 ℃ at 10000 *g* for 1 h. The supernatant was aspirated and discarded, and the exosome pellet was resuspended in PBS buffer, then stored at 4 ℃ short term (1-7 d) and -20 ℃ long term.

Human blood serum: Frozen serum samples from different donors were thawed in a water bath at room temperature until samples were completely liquid, then centrifuged at 2000 *g* for 30 min to remove any cellular debris. The supernatant containing the cell-free serum was transferred to a fresh container and briefly held on ice until use. Next, each serum sample was combined with 1/5th volume of Total exosome isolation (from serum) reagent (Invitrogen) and then mixed well by vortexing until a homogenous solution was formed. The samples were incubated at 4 ℃ for 30 min, then centrifuged at room temperature at 10000 *g* for 10 min. The supernatant was aspirated and discarded, and the exosome pellet was resuspended in PBS buffer, then stored at 4 ℃ short term (1-7 d) and -20 ℃ for long term.

Isolation of exosomes from serum and cell media using ultracentrifugation protocols

Cell culture media: Using the same HeLa cell media that was prepared for the extraction of exosomes using the Total exosome isolation reagent, above, exosomes were isolated according to the differential ultracentrifugation Basic Protocol 1 as described by Théry *et al*[23]. Briefly, HeLa cell media was centrifuged at 4 ℃ at 2000 *g* for 10 min and then 10000 *g* for 30 min to produce a cell-

free conditioned medium. The pooled media was divided equally into each of 6 polyallomer tubes and centrifuged at 4 ℃ at 100000 *g* for 70 min. The subsequent pellet was re-suspended and washed with PBS followed by a second 100000 *g* centrifugation. A low volume of PBS was used to re-suspend the washed pellets and then they were combined in pairs to result in three concentrated exosomes samples. These samples were then processed by isopycnic centrifugation using continuous sucrose gradients. The gradients were prepared using solutions of 0.25 mol/L and 2 mol/L sucrose in 20 mmol/L 4-(2-hydroxyethyl)-1-piperazineethanesulfonic acid (HEPES), pH 7.3 as described by Abe *et al*[24].

Once prepared, the sucrose gradients were overlaid with one of the three concentrated exosome samples and then centrifuged at 4 ℃ at 110000 *g* for 16 h. Immediately after centrifugation, each of the gradients was fractionated using a peristaltic pump and fraction collector and each fraction was measured on a refractometer to identify those that contain exosomes based on the density range of 1.13-1.19 g/mL as defined by Record *et al*[25]. The resulting set of fractions were pooled within the respective sample and diluted 3-fold with 20 mmol/L HEPES, pH 7.3 then centrifuged in polyallomer konical™ tubes at 4 ℃ at 110000 *g* for 1 h to produce a final pellet consisting of purified exosome that was re-suspended in 200 μL PBS.

Human blood serum: Using the same human serum that was thawed for the extraction of exosomes using the Total exosome isolation reagent, above, exosomes were isolated according to the differential ultracentrifuge Basic Protocol 2 as described by Théry *et al*[23]. Briefly, serum was diluted with an equal volume of PBS and gently mixed until homogenous. Then the mixture was centrifuged at 4 ℃ at 2000 *g* for 30 min and 12000 *g* for 45 min to produce a cell-free serum. The pooled serum was divided equally into each of the 6 polyallomer tubes and centrifuged at 4 ℃ at 110000 g for 2 h. The subsequent pellet was re-suspended and washed twice with PBS followed each time by centrifugation at 4 ℃ at 110000 *g* for 70 min. A low volume of PBS was used to re-suspend the washed pellets, resulting in three concentrated exosomes samples.

Western blot analysis

Exosome samples isolated from cell media or blood serum (1-5 μL) were mixed with 2 × non-reducing Tris-glycine SDS sample buffer (Novex), then heated at 75 ℃ for 5 min and loaded onto a 1.5 mm × 15 mm well 4%-20% Tris-Glycine gel (Novex). Benchmark prestained protein ladder (Invitrogen) was added to one well as a control to monitor the molecular weight of the protein samples. The gel was run under denaturing conditions at 150 V for 1.5 h then transferred to a membrane using the iBlot instrument (Life Technologies). After transfer, the membranes were processed on the BenchPro 4100 (Life Technologies) with CD63 antibody diluted 100 μg × to 20 mL (Abcam). The WesternBreeze Chemiluminescence kit was utilized to label the membrane. Membranes were then exposed to X-ray film for 1-10 min and the film was analyzed.

RNA isolation

The Total exosome RNA and protein isolation kit (Invitrogen) was utilized for recovery of RNA from both the concentrated exosome samples (reagent and ultracentrifugation) and control samples for each sample type - HeLa cell pellets (1×10^6 cells/pellet) for the HeLa cell culture and cell-free serum for the serum samples. Two hundred microlitre of each sample (brought up to volume with PBS if necessary) was combined with 205 μL of 2× denaturing solution, vortexed to lyse, and then incubated on ice for 5 min. After incubation, 410 μL of Acid-Phenol: Chloroform was added to the mixture and vortexed for 30-60 s to mix. Samples were then centrifuged for 5 min at 10000 *g* at room temperature to separate the mixture into aqueous and organic phases. Once centrifugation was complete, the aqueous (upper) phase was carefully removed without disturbing the lower phase or the interphase, and transferred to a fresh tube. One point twenty-five volumes of 100% EtOH was added to the aqueous phase for each sample then vortexed to mix. About 700 μL of volume was placed onto spin column in a collection tube then spun at 10000 *g* for 15 s to move the sample through the filter cartridge. Samples were then washed once with 700 μL Wash Solution 1 × and 2 × with 500 μL wash solution 2/3 (centrifuged at 10000 *g* for 15 s for each wash). After washing, filter was dried by spinning for an additional 1 min at 10000 *g*. The filter cartridge was transferred into a fresh collection tube and 50 μL of preheated (95 ℃) nuclease-free water was applied to the center of the filter. Samples were centrifuged for 30 s at 10000 *g* to recover the RNA, then a second 50 μL volume of preheated (95 ℃) nuclease-free water was applied to the center of the filter and centrifuged for 30 s at 10000 *g*. After the second spin, the eluate containing the RNA was collected and stored at -20 ℃. A DNase treatment was performed on RNA extracted from the HeLa cell pellet using the DNase-free kit (Ambion) to remove any contaminating DNA. DNase treatment was not performed on other samples as they had a much smaller sample input. After treatment, the sample was diluted to 2 ng/μL and 1 μL of each RNA sample was analyzed on the Agilent 2100 Bioanalyzer using the Agilent RNA 6000 Pico kit (Series Ⅱ) to determine the mass of RNA going into downstream analysis.

Reverse transcription and quantitative real-time PCR analysis of the RNA sequences isolated from exosomes

Reverse Transcription (RT) Master Mixes were prepared for each sample using either the High Capacity cDNA Reverse Transcription kit and protocol with random primers for mRNA or the TaqMan® MicroRNA Reverse Transcription Kit reagents and protocol (Applied Biosystems) with gene specific RT primers for five miRNA

targets (let7e, miR26a, miR16, miR24 and miR451). Ten microlitre of the RT Master Mix was added to corresponding wells in a 96-well plate, and 5 μL of each sample was added to the master mix. Plates were covered with adhesive (non-optical) cover and spun down to remove air bubbles, and then placed into a 9700 thermocycler and incubated as follows: for mRNA - 25 ℃ for 10 min; 37 ℃ for 120 min; and 85 ℃ for 5 min; for miRNA - 4 ℃ for 5 min; 16 ℃ for 30 min; 42 ℃ for 30 min; and 85 ℃ for 5 min. Reactions were kept at 4 ℃ until use.

qPCR master mixes were prepared for each of five microRNAs (let7e, miR26a, miR16, miR24 and miR451) and two mRNAs [glyceraldehyde-3-phosphate dehydrogenase (GAPDH) and 18S] by combining 5 μL of AB Universal PCR Master Mix Ⅱ, 2.5 μL; of nuclease-free water, and 0.5 μL of the 20 × Taqman Assay. After mixing, 8 μL of each master mix was placed into wells in a 384-well plate (enough for triplicate reactions for each isolation replicate). Two microlitre of each RT reaction was added in triplicate to the master mix of each target and the plates were sealed with optical adhesive cover. Plates were spun down to remove air bubbles then placed into a 7900HT instrument and run using the following thermocycler protocol: 95 ℃ for 10 min; (95 ℃ for 15 s; 60 ℃ for 60 s) 40 cycles. Once the run was complete, automatic Ct analysis was performed with SDSv2.3 software and average and standard deviation was calculated for each set of isolations and qPCR reactions for each target.

RESULTS

Extraction of exosomes from cell media and serum

Isolation of exosomes from cell culture media and body fluids is presently a tedious, non-specific, and difficult process. The widely used approach is based on ultracentrifugation in combination with sucrose density gradients or sucrose cushions to float the relatively low-density exosomes away from other vesicles and particles[23]. The protocols range in time from 8 to 30 h and require an ultracentrifuge and extensive training to ensure successful isolation of exosomes.

As a way to simplify and shorten exosome isolation, we developed two Total exosome isolation reagents that enable straightforward and reliable concentration of intact exosomes from cell culture media and blood serum samples. By tying up water molecules, the reagents force less-soluble components, such as vesicles, out of solution. When the reagent is added to the biological sample, and solution is incubated at 4 ℃, the precipitated exosomes can be recovered by standard centrifugation at 10000 *g*. The pellet is then resuspended in PBS or similar buffer and exosomes are ready for downstream endpoint analysis or biological studies on their pathways, functions and trafficking.

We extracted exosomes from HeLa cell culture media and blood serum samples (derived from healthy human donors) using the Total exosome isolation reagents as well as the ultracentrifugation procedure[23], for comparison purposes. Sizing and quantification of exosomes was performed with the NanoSight® LM10 instrument, following the manufacturer's protocol. This instrument uses a laser light source to illuminate nano-scale particles (10-1000 nm) which are seen as individual point-scatters moving under Brownian motion. The paths of the point scatters, or particles, are calculated over time to determine their velocity which can be used to calculate their size independent of density. The image analysis NTA software compiles this information and allows one to automatically track the size and number of the nanoparticles. Results are shown in Figure 1A and B for HeLa cell culture media, and Figure 2A and B for serum. The reagent method recovered a significant number of nanovesicles, in comparable or higher yields *vs* the ultracentrifugation procedures; All nanovesicles were smaller than 300 nm, most of them being in the typical exosome size range of 30-150 nm. Similar results were obtained for cell media derived from THP-1 and Jurkat cell lines, 1-10 mL sample volume input (data not shown).

Samples were next analyzed by Western blots with antibody specific to CD63 - a well characterized exosomal marker[11,20,23]. Results are shown in Figure 1C for HeLa cell culture media and Figure 2C for serum - confirming that clean exosome populations were recovered with both protocols. CD9, TSG101, Annexin Ⅱ exosomal markers were also confirmed by Western blots (data not shown).

To further characterize samples obtained with the reagent, electron microscopy analysis was performed. Figure 3A shows a representative image of the unlabeled exosome, Figure 3B shows exosome immunolabeled with anti-CD63 antibodies followed by 10 nm protein A gold nanoparticles, and Figure 3C shows exosome immunolabeled with anti-CD81 antibodies followed by 10 nm protein A gold nanoparticles. The exosomes recovered with the reagent have typical appearance and size (about 100 nm[23]), and immunolabeling with anti-CD81 and anti-CD63 antibodies, which are well known exosomal markers[20,23], was very efficient confirming that the nanovesicles recovered with the reagent are exosomes.

RNA isolation and analysis by Agilent 2100 Bioanalyzer and qRT-PCR

Next, we proceeded with the isolation and analysis of the exosomal RNA cargo. The Total exosome RNA and protein isolation kit, developed specifically for this purpose, uses acid-phenol: Chloroform extraction to provide a robust, initial RNA purification step, followed by a final purification over a glass-fiber filter. Ethanol is added to samples that are passed through a filter cartridge containing the glass-fiber filter, which immobilizes the RNA. The filter is washed, and the RNA is eluted with a low ionic-strength solution.

We followed this protocol to isolate RNA from exosomes derived from HeLa cell culture media and blood serum samples using both the Total exosome isolation reagents and ultracentrifugation procedure[23]. Subsequent analysis with Qubit fluorometer has shown that for exo-

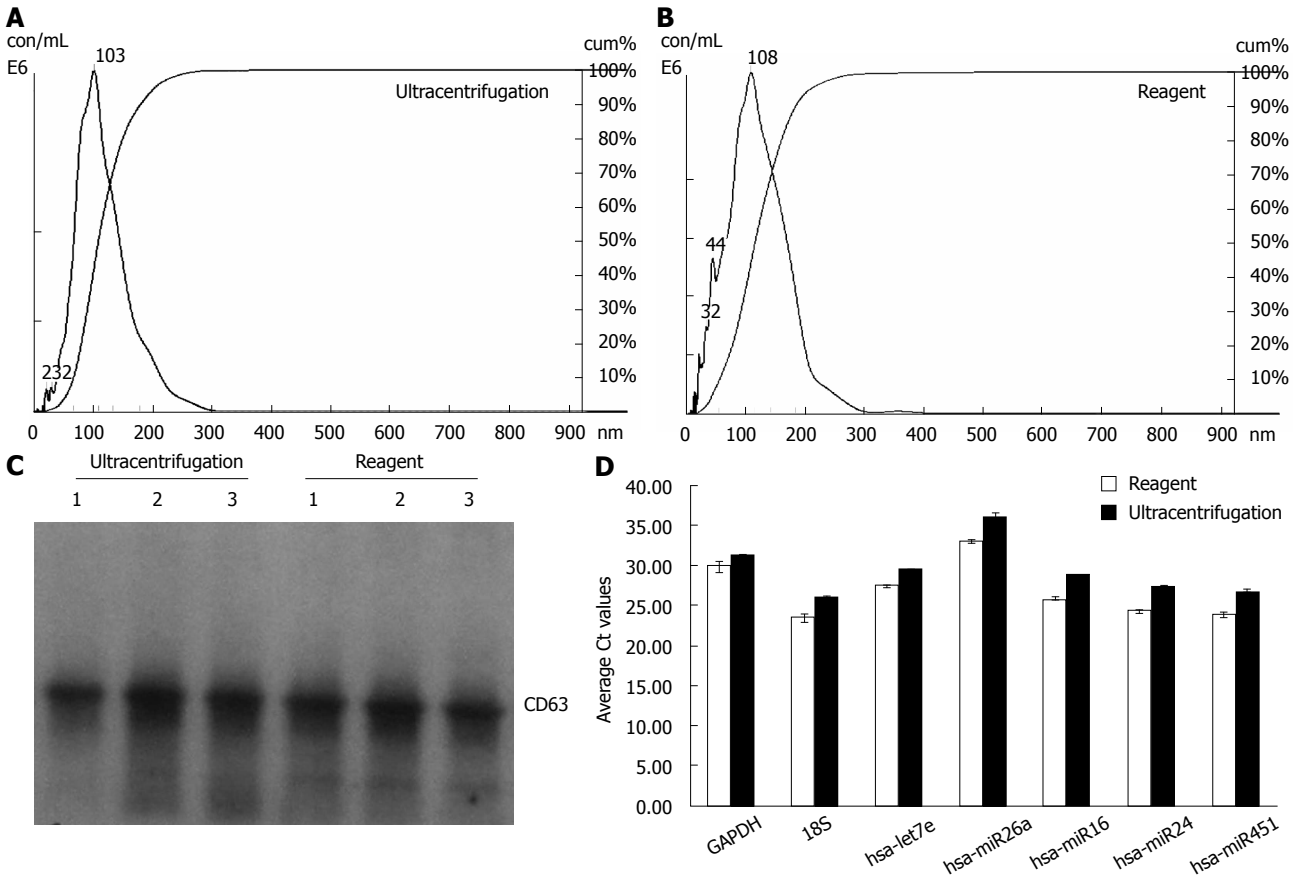

Figure 1 Exosomes isolated from cell media using the reagent are comparable to ultracentrifugation preparations. A, B: Analysis of exosomes recovered from HeLa cell culture media using the Total exosome isolation reagent (from cell culture media) and ultracentrifugation protocol-by Nanosight® LM10 instrument. The profiles are essentially very-finely segmented histograms, indicating the number of particles per mL (in millions) for each size in bins of 1 nm increment from 0 to 1000 nm; C: Western blot analysis for the presence of exosomal marker protein CD63 in cell culture media derived samples. Exosomes from three separate HeLa cell culture media preparations (isolated with either the Total exosome isolation reagent (from cell culture media) or ultracentrifugation) were separated on a Novex 4%-20% Tris-Glycine Gel under denaturing, non-reducing conditions. Standard Western blot procedures with anti-CD63 antibodies were used to detect cell media derived exosomal protein markers; D: Analysis of the exosomal miRNA and mRNA levels in HeLa cell culture media derived samples by quantitative reverse transcription-polymerase chain reaction (qRT-PCR). RNA was isolated using the Total exosome RNA and protein isolation kit from exosomes extracted using the Total exosome isolation reagent (from cell culture media) and the ultracentrifugation protocol. Levels of five microRNAs (let7e, miR26a, miR16, miR24 and miR451) and two mRNAs [glyceraldehyde-3-phosphate dehydrogenase (GAPDH) and 18S] were quantified by qRT-PCR using TaqMan assays and reagents.

somes isolated from 100 mL of HeLa cell culture media using the ultracentrifugation protocol, it is possible to recover approximately 380 pg RNA. The reagent method resulted in isolation of somewhat more exosomes from the same volume of HeLa cell culture media, containing approximately 520 pg RNA.

RNA recovered from exosomes with the reagent and ultracentrifugation was next characterized by capillary electrophoresis using the Agilent 2100 Bioanalyzer, and a RNA Pico chip. Results are shown in Figure 4. For both types of samples, profiles were similar: the majority of RNA content was small (< 200 nt), but there were some longer RNA species present including full-length 18S and 28S rRNA. This is in agreement with earlier studies[11,12,20], indicating that exosomes primarily contain short RNA (such as miRNA) and degraded mRNA, but also some full-length molecules including mRNA > 1 kb long. Overall, the amount of total RNA recovered, and specifically the small RNA fraction, is higher for the reagent method compared to ultracentrifugation protocol.

Finally, the levels of five microRNAs (let7e, miR26a, miR16, miR24 and miR451) and two mRNAs (GAPDH and 18S) earlier reported to be present in exosomes[11,20], were analyzed by qRT-PCR. Results are displayed in Figure 1D for HeLa cell culture media and Figure 2D for human blood serum. Based on Ct values, 25-33 for the majority of analytes, RNA isolation was efficient and the amount of material recovered is sufficient for standard PCR analysis - RNA recovered from exosomes derived from 3 μL serum or 30 μL cell media is sufficient for one qPCR reaction. The reagent method recovered somewhat higher levels of exosomes-compared to ultracentrifugation procedure, as indicated by 0.5-2 Ct shift up for different RNAs.

DISCUSSION

To conclude, we describe here a novel approach for fast and efficient isolation of exosomes from cell culture media and blood serum, that can be followed by

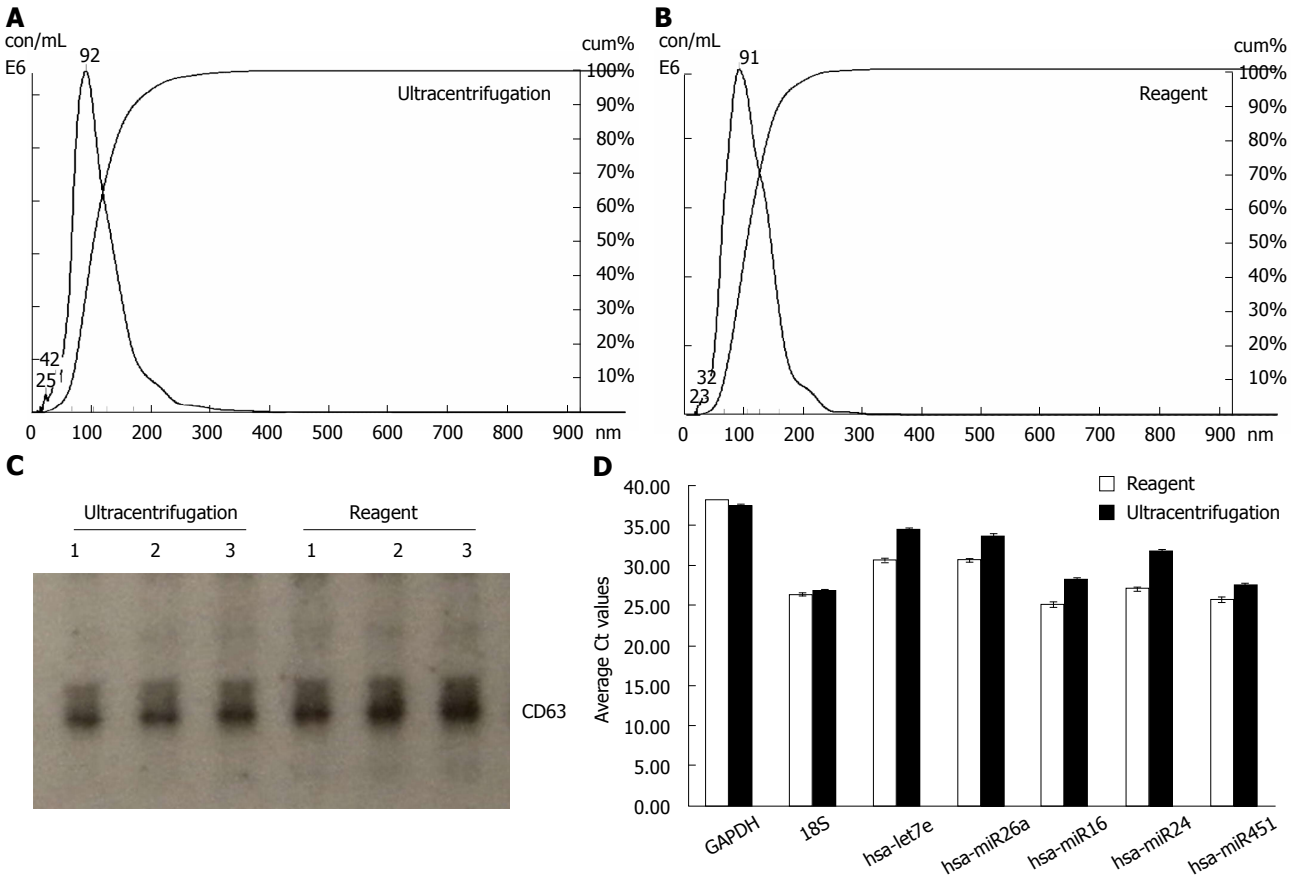

Figure 2 Exosomes isolated from serum using the reagent are comparable to ultracentrifugation preparations. A, B: Analysis of the exosomes recovered from human serum using the Total exosome isolation reagent (from serum) and the ultracentrifugation protocol-by Nanosight® LM10 instrument. The profiles are essentially very-finely segmented histograms, indicating the number of particles per mL (in millions) for each size in bins of 1 nm increment from 0 to 1000 nm; C: Western blot analysis for the presence of exosomal marker protein CD63 in blood serum derived samples. Exosomes from three separate serum preparations (isolated with either the Total exosome isolation reagent (from serum) or ultracentrifugation) were separated on a Novex 4%-20% Tris-Glycine Gel under denaturing, non-reducing conditions. Standard Western blot procedures with anti-CD63 antibodies were used to detect human blood serum derived exosomal protein markers; D: Analysis of the exosomal miRNA and mRNA levels in human blood serum by quantitative reverse transcription-polymerase chain reaction (qRT-PCR). RNA was isolated using the Total exosome RNA and Protein Isolation kit from exosomes extracted using the Total exosome isolation reagent (from serum) and the ultracentrifugation protocol. Levels of five microRNAs (let7e, miR26a, miR16, miR24 and miR451) and two mRNAs [glyceraldehyde-3-phosphate dehydrogenase (GAPDH) and 18S] were quantified by qRT-PCR using TaqMan assays and reagents.

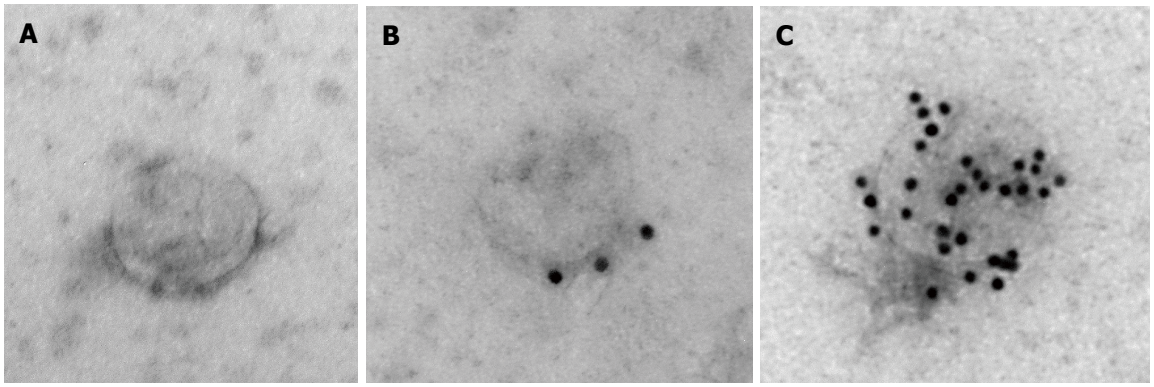

Figure 3 Electron microscopy analysis of exosomes isolated from HeLa cell culture media with the Total exosome isolation reagent. A: Representative image of the unlabeled exosome; B: Exosome immunolabeled with anti-CD63 followed by 10 nm protein A gold nanoparticles; C: Exosome immunolabeled with anti-CD81 followed by 10 nm protein A gold nanoparticles. For immunolabelling, exosome samples were precipitated undiluted at room temperature for 15 min to grids. Next, blocking with 0.5% bovine serum albumin was performed for 10 min. Labeling with anti-CD63 and anti-CD81 antibodies was carried out for 30 min. Following washing steps, Prot A Au were added and incubated for 15 min. After subsequent phosphate-buffered saline and water wash steps, embedding in 0.3% Uranyl acetate in methyl cellulose was finally performed, followed by electron microscop analysis of exosomes.

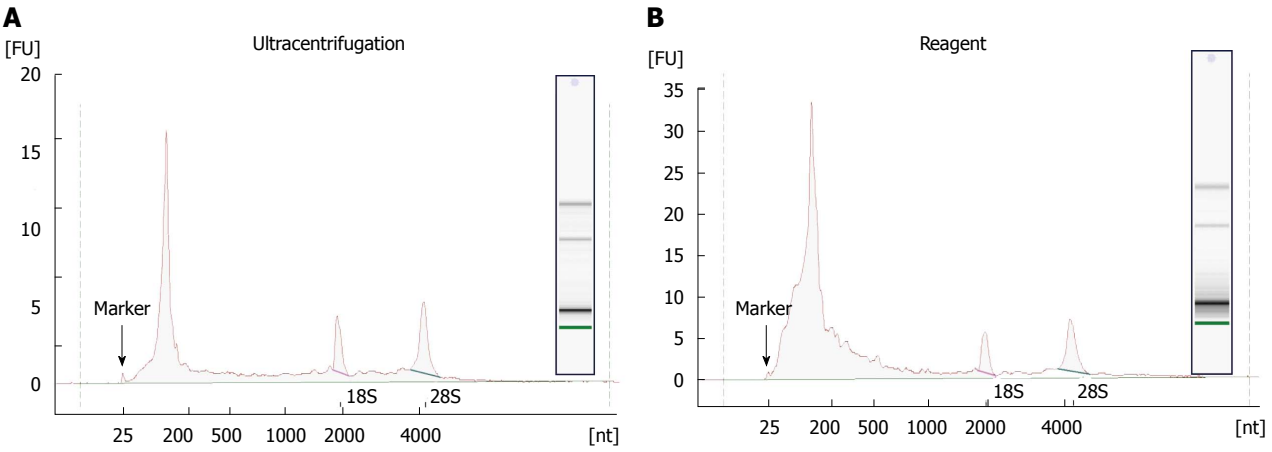

Figure 4 Analysis of RNA cargo of HeLa cell media exosomes by Agilent RNA pico chip. A: Exosomes isolated with ultracentrifugation protocol; B: Exosomes recovered with the Total exosome isolation reagent.

recovery of RNA cargo and its analysis by qRT-PCR or sequencing. The procedure is completed in a fraction of the time, compared to the current standard protocols utilizing ultracentrifugation, and allows recovery of fully intact exosomes in higher yields. This is the first step towards developing standardized techniques and protocols for fast, high throughput and robust isolation of exosomes from various sample types and downstream analysis of their constituents. We believe these reagents and workflows will be highly useful to scientists working on the edge of cellular and molecular biology and focusing on analysis of extracellular (circulating) RNA residing within the exosomes, microvesicles and protein complexes.

COMMENTS

Background

Exosomes are small (30-150 nm) vesicles containing unique RNA and protein cargo, secreted by all cell types in culture. They are also found in abundance in body fluids including blood, saliva, urine. At the moment, the mechanism of exosome formation, the makeup of the cargo, biological pathways and resulting functions are incompletely understood. One of their most intriguing roles is intercellular communication-exosomes function as the messengers, delivering various effector or signaling macromolecules between specific cells. There is an exponentially growing need to dissect structure and the function of exosomes and utilize them for development of minimally invasive diagnostics and therapeutics.

Research frontiers

Several reports have been published to date, using quantitative reverse transcription-polymerase chain reaction (qRT-PCR) and next gen sequencing for initial characterization of the RNA content of exosomes derived from severals cell lines, as well as serum, saliva, placenta and breast milk. All these studies utilize ultracentrifugation isolation protocols which allow to produce clean exosome preparations, however, suffer from numerous drawbacks. Critical to further our understanding of exosomes, is the development of reagents, tools and protocols for their simple and robust isolation, characterization and analysis of their RNA and protein contents.

Innovations and breakthroughs

The authors developed the workflow allowing fast and efficient extraction of exosomes, followed by isolation of RNA and its analysis by qRT-PCR. The procedure is completed in a fraction of the time, compared to the current standard protocols utilizing ultracentrifugation, and allows to recover fully intact exosomes in higher yields.

Applications

The workflow presented here allows fast isolation of exosomes and downstream analysis of their constituents, thus enabling basic exosome research as well as development of minimally invasive diagnostic alternative to biopsies.

Peer review

In this study, the authors describe a novel approach for fast and efficient extraction of exosomes from cell culture media and body fluids, and compare the effectiveness of isolation methods with ultracentrifigation protocol. This manuscript is well organized and the experiments are well conducted.

REFERENCES

1 **Mittelbrunn M,** Sanchez-Madrid F. Intercellular communication: diverse structures for exchange of genetic information. *Nature Reviews* 2012; **13:** 328-335
2 **Schorey JS**, Bhatnagar S. Exosome function: from tumor immunology to pathogen biology. *Traffic* 2008; **9**: 871-881 [PMID: 18331451 DOI: 10.1111/j.1600-0854.2008.00734.x]
3 **Smythies J**, Edelstein L. Transsynaptic modality codes in the brain: possible involvement of synchronized spike timing, microRNAs, exosomes and epigenetic processes. *Front Integr Neurosci* 2012; **6**: 126 [PMID: 23316146]
4 **Lakkaraju A**, Rodriguez-Boulan E. Itinerant exosomes: emerging roles in cell and tissue polarity. *Trends Cell Biol* 2008; **18**: 199-209 [PMID: 18396047 DOI: 10.1016/j.tcb.2008.03.002]
5 **Xu D,** Tahara H. The role of exosomes and microRNAs in senescence and aging. *Adv Drug Deliv Rev* 2012; **20:** 1
6 **Théry C**, Zitvogel L, Amigorena S. Exosomes: composition, biogenesis and function. *Nat Rev Immunol* 2002; **2**: 569-579 [PMID: 12154376]
7 **Vlassov AV,** Magdaleno S, Setterquist R, Conrad R. Exosomes: Current knowledge of their composition, biological functions, and diagnostic and therapeutic potentials. *Biochim Biophys Acta* 2012; **1820:** 940-948 [PMID: 22503788 DOI: 10.1016/j.bbagen.2012.03.017]
8 **Théry C**, Ostrowski M, Segura E. Membrane vesicles as conveyors of immune responses. *Nat Rev Immunol* 2009; **9**: 581-593 [PMID: 19498381 DOI: 10.1038/nri2567]
9 **Janowska-Wieczorek A**, Wysoczynski M, Kijowski J, Marquez-Curtis L, Machalinski B, Ratajczak J, Ratajczak MZ. Microvesicles derived from activated platelets induce metastasis and angiogenesis in lung cancer. *Int J Cancer* 2005; **113**: 752-760 [PMID: 15499615 DOI: 10.1002/ijc.20657]
10 **Al-Mayah AH**, Irons SL, Pink RC, Carter DR, Kadhim MA. Possible role of exosomes containing RNA in mediating nontargeted effect of ionizing radiation. *Radiat Res* 2012; **177**: 539-545 [PMID: 22612287 DOI: 10.1667/RR2868.1]

11 **Valadi H**, Ekström K, Bossios A, Sjöstrand M, Lee JJ, Lötvall JO. Exosome-mediated transfer of mRNAs and microRNAs is a novel mechanism of genetic exchange between cells. *Nat Cell Biol* 2007; **9**: 654-659 [PMID: 17486113 DOI: 10.1038/ncb1596]

12 **Skog J**, Würdinger T, van Rijn S, Meijer DH, Gainche L, Sena-Esteves M, Curry WT, Carter BS, Krichevsky AM, Breakefield XO. Glioblastoma microvesicles transport RNA and proteins that promote tumour growth and provide diagnostic biomarkers. *Nat Cell Biol* 2008; **10**: 1470-1476 [PMID: 19011622 DOI: 10.1038/ncb1800]

13 **Al-Nedawi K**, Meehan B, Micallef J, Lhotak V, May L, Guha A, Rak J. Intercellular transfer of the oncogenic receptor EGFRvIII by microvesicles derived from tumour cells. *Nat Cell Biol* 2008; **10**: 619-624 [PMID: 18425114 DOI: 10.1038/ncb1725]

14 **Bellingham SA**, Coleman BM, Hill AF. Small RNA deep sequencing reveals a distinct miRNA signature released in exosomes from prion-infected neuronal cells. *Nucleic Acids Res* 2012; **40**: 10937-10949 [PMID: 22965126 DOI: 10.1093/nar/gks832]

15 **Pegtel DM**, Cosmopoulos K, Thorley-Lawson DA, van Eijndhoven MA, Hopmans ES, Lindenberg JL, de Gruijl TD, Würdinger T, Middeldorp JM. Functional delivery of viral miRNAs via exosomes. *Proc Natl Acad Sci USA* 2010; **107**: 6328-6333 [PMID: 20304794 DOI: 10.1073/pnas.0914843107]

16 **Leblanc P**, Alais S, Porto-Carreiro I, Lehmann S, Grassi J, Raposo G, Darlix JL. Retrovirus infection strongly enhances scrapie infectivity release in cell culture. *EMBO J* 2006; **25**: 2674-2685 [PMID: 16724107 DOI: 10.1038/sj.emboj.7601162]

17 **Spielmann N**, Wong DT. Saliva: diagnostics and therapeutic perspectives. *Oral Dis* 2011; **17**: 345-354 [PMID: 21122035 DOI: 10.1111/j.1601-0825.2010.01773.x]

18 **Nilsson J**, Skog J, Nordstrand A, Baranov V, Mincheva-Nilsson L, Breakefield XO, Widmark A. Prostate cancer-derived urine exosomes: a novel approach to biomarkers for prostate cancer. *Br J Cancer* 2009; **100**: 1603-1607 [PMID: 19401683 DOI: 10.1038/sj.bjc.6605058]

19 **Taylor DD**, Gercel-Taylor C. MicroRNA signatures of tumor-derived exosomes as diagnostic biomarkers of ovarian cancer. *Gynecol Oncol* 2008; **110**: 13-21 [PMID: 18589210 DOI: 10.1016/j.ygyno.2008.04.033]

20 **Mathivanan S**, Fahner CJ, Reid GE, Simpson RJ. ExoCarta 2012: database of exosomal proteins, RNA and lipids. *Nucleic Acids Res* 2012; **40**: D1241-D1244 [PMID: 21989406 DOI: 10.1093/nar/gkr828]

21 **Nolte-'t Hoen EN**, Buermans HP, Waasdorp M, Stoorvogel W, Wauben MH, 't Hoen PA. Deep sequencing of RNA from immune cell-derived vesicles uncovers the selective incorporation of small non-coding RNA biotypes with potential regulatory functions. *Nucleic Acids Res* 2012; **40**: 9272-9285 [PMID: 22821563 DOI: 10.1093/nar/gks658]

22 **Wang K**, Zhang S, Weber J, Baxter D, Galas DJ. Export of microRNAs and microRNA-protective protein by mammalian cells. *Nucleic Acids Res* 2010; **38**: 7248-7259 [PMID: 20615901 DOI: 10.1093/nar/gkq601]

23 **Théry C,** Amigorena S, Raposo G, Clayton A. Isolation and characterization of exosomes from cell culture supernatants and biological fluids. *Curr Protoc Cell Biol* 2006; **Chapter 3:** Unit 3.22 [PMID: 18228490 DOI: 10.1002/0471143030.cb0322s30]

24 **Abe S,** Davies E. How to make sucrose density gradients. College of Agriculture, Ehime University, Japan. Available from: URL:http://web-mcb.agr.ehime-u.ac.jp/english/methods/gradient.htm

25 **Record M**, Subra C, Silvente-Poirot S, Poirot M. Exosomes as intercellular signalosomes and pharmacological effectors. *Biochem Pharmacol* 2011; **81**: 1171-1182 [PMID: 21371441 DOI: 10.1016/j.bcp.2011.02.011]

P- Reviewer Chang LS **S- Editor** Huang XZ
L- Editor A **E- Editor** Xiong L

World Journal of Methodology

Online Submissions: http://www.wjgnet.com/esps/
wjm@wjgnet.com
www.wjgnet.com

World J Methodol 2013 March 26; 3(1): I-V
ISSN 2222-0682 (online)

INSTRUCTIONS TO AUTHORS

GENERAL INFORMATION

World Journal of Methodology (*World J Methodol*, *WJM*, online ISSN 2222-0682, DOI: 10.5662) is a peer-reviewed open access (OA) academic journal that aims to guide clinical practice and improve diagnostic and therapeutic skills of clinicians.

Aims and scope

The primary task of *WJM* is to rapidly publish high-quality original articles, reviews, and commentaries that deal with the methodology to develop, validate, modify and promote diagnostic and therapeutic modalities and techniques in preclinical and clinical applications. *WJM* covers topics concerning the subspecialties including but not exclusively anesthesiology, cardiac medicine, clinical genetics, clinical neurology, critical care, dentistry, dermatology, emergency medicine, endocrinology, family medicine, gastroenterology and hepatology, geriatrics and gerontology, hematology, immunology, infectious diseases, internal medicine, obstetrics and gynecology, oncology, ophthalmology, orthopedics, otolaryngology, radiology, serology, pathology, pediatrics, peripheral vascular disease, psychiatry, radiology, rehabilitation, respiratory medicine, rheumatology, surgery, toxicology, transplantation, and urology and nephrology.

WJM is edited and published by Baishideng Publishing Group (BPG). BPG has a strong professional editorial team composed of science editors, language editors and electronic editors. BPG currently publishes 42 OA clinical medical journals, and is one of the leading medical publishers, with the first-class editing and publishing capacity and production.

Columns

The columns in the issues of *WJM* will include: (1) Editorial: The editorial board members are invited to make comments on an important topic in their field in terms of its current research status and future directions to lead the development of this discipline; (2) Frontier: The editorial board members are invited to select a highly cited cutting-edge original paper of his/her own to summarize major findings, the problems that have been resolved and remain to be resolved, and future research directions to help readers understand his/her important academic point of view and future research directions in the field; (3) Diagnostic Advances: The editorial board members are invited to write high-quality diagnostic advances in their field to improve the diagnostic skills of readers. The topic covers general clinical diagnosis, differential diagnosis, pathological diagnosis, laboratory diagnosis, imaging diagnosis, endoscopic diagnosis, biotechnological diagnosis, functional diagnosis, and physical diagnosis; (4) Therapeutics Advances: The editorial board members are invited to write high-quality therapeutic advances in their field to help improve the therapeutic skills of readers. The topic covers medication therapy, psychotherapy, physical therapy, replacement therapy, interventional therapy, minimally invasive therapy, endoscopic therapy, transplantation therapy, and surgical therapy; (5) Field of Vision: The editorial board members are invited to write commentaries on classic articles, hot topic articles, or latest articles to keep readers at the forefront of research and increase their levels of clinical research. Classic articles refer to papers that are included in Web of Knowledge and have received a large number of citations (ranking in the top 1%) after being published for more than years, reflecting the quality and impact of papers. Hot topic articles refer to papers that are included in Web of Knowledge and have received a large number of citations after being published for no more than 2 years, reflecting cutting-edge trends in scientific research. Latest articles refer to the latest published high-quality papers that are included in PubMed, reflecting the latest research trends. These commentary articles should focus on the status quo of research, the most important research topics, the problems that have now been resolved and remain to be resolved, and future research directions. Basic information about the article to be commented (including authors, article title, journal name, year, volume, and inclusive page numbers; (6) Minireviews: The editorial board members are invited to write short reviews on recent advances and trends in research of molecular biology, genomics, and related cutting-edge technologies to provide readers with the latest knowledge and help improve their diagnostic and therapeutic skills; (7) Review: To make a systematic review to focus on the status quo of research, the most important research topics, the problems that have now been resolved and remain to be resolved, and future research directions; (8) Topic Highlight: The editorial board members are invited to write a series of articles (7-10 articles) to comment and discuss a hot topic to help improve the diagnostic and therapeutic skills of readers; (9) Medical Ethics: The editorial board members are invited to write articles about medical ethics to increase readers' knowledge of medical ethics. The topic covers international ethics guidelines, animal studies, clinical trials, organ transplantation, *etc.*; (10) Clinical Case Conference or Clinicopathological Conference: The editorial board members are invited to contribute high-quality clinical case conference; (11) Original Articles: To report innovative and original findings in basic and clinical medical research methodolog; (12) Brief Articles: To briefly report the novel and innovative findings in basic and clinical medical research methodolog; (13) Meta-Analysis: To evaluate the clinical effectiveness in basic and clinical medical research methodolog by using data from two or more randomised control trials; (14) Case Report: To report a rare or typical case; (15) Letters to the Editor: To discuss and make reply to the contributions published in *WJM*, or to introduce and comment on a controversial issue of general interest; (16) Book Reviews: To introduce and comment on quality monographs of basic and clinical medical research methodolog; and (17) Autobiography: The editorial board members are invited to write their autobiography to provide readers with stories of success or failure in their scientific research career. The topic covers their basic personal information and information about when they started doing research work, where and how they did research work, what they have achieved, and their lessons from success or failure.

Name of journal

World Journal of Methodology

ISSN

ISSN 2222-0682 (online)

Launch date

September 26, 2011

Frequency

Quarterly

SPECIAL STATEMENT

All articles published in this journal represent the viewpoints of the authors except where indicated otherwise.

Biostatistical editing
Statistical review is performed after peer review. We invite an expert in Biomedical Statistics from to evaluate the statistical method used in the paper, including *t*-test (group or paired comparisons), chi-squared test, Ridit, probit, logit, regression (linear, curvilinear, or stepwise), correlation, analysis of variance, analysis of covariance, *etc*. The reviewing points include: (1) Statistical methods should be described when they are used to verify the results; (2) Whether the statistical techniques are suitable or correct; (3) Only homogeneous data can be averaged. Standard deviations are preferred to standard errors. Give the number of observations and subjects (*n*). Losses in observations, such as drop-outs from the study should be reported; (4) Values such as ED50, LD50, IC50 should have their 95% confidence limits calculated and compared by weighted probit analysis (Bliss and Finney); and (5) The word 'significantly' should be replaced by its synonyms (if it indicates extent) or the *P* value (if it indicates statistical significance).

Conflict-of-interest statement
In the interests of transparency and to help reviewers assess any potential bias, *WJM* requires authors of all papers to declare any competing commercial, personal, political, intellectual, or religious interests in relation to the submitted work. Referees are also asked to indicate any potential conflict they might have reviewing a particular paper. Before submitting, authors are suggested to read "Uniform Requirements for Manuscripts Submitted to Biomedical Journals: Ethical Considerations in the Conduct and Reporting of Research: Conflicts of Interest" from International Committee of Medical Journal Editors (ICMJE), which is available at: http://www.icmje.org/ethical_4conflicts.html.

Sample wording: [Name of individual] has received fees for serving as a speaker, a consultant and an advisory board member for [names of organizations], and has received research funding from [names of organization]. [Name of individual] is an employee of [name of organization]. [Name of individual] owns stocks and shares in [name of organization]. [Name of individual] owns patent [patent identification and brief description].

Statement of informed consent
Manuscripts should contain a statement to the effect that all human studies have been reviewed by the appropriate ethics committee or it should be stated clearly in the text that all persons gave their informed consent prior to their inclusion in the study. Details that might disclose the identity of the subjects under study should be omitted. Authors should also draw attention to the Code of Ethics of the World Medical Association (Declaration of Helsinki, 1964, as revised in 2004).

Statement of human and animal rights
When reporting the results from experiments, authors should follow the highest standards and the trial should conform to Good Clinical Practice (for example, US Food and Drug Administration Good Clinical Practice in FDA-Regulated Clinical Trials; UK Medicines Research Council Guidelines for Good Clinical Practice in Clinical Trials) and/or the World Medical Association Declaration of Helsinki. Generally, we suggest authors follow the lead investigator's national standard. If doubt exists whether the research was conducted in accordance with the above standards, the authors must explain the rationale for their approach and demonstrate that the institutional review body explicitly approved the doubtful aspects of the study.

Before submitting, authors should make their study approved by the relevant research ethics committee or institutional review board. If human participants were involved, manuscripts must be accompanied by a statement that the experiments were undertaken with the understanding and appropriate informed consent of each. Any personal item or information will not be published without explicit consents from the involved patients. If experimental animals were used, the materials and methods (experimental procedures) section must clearly indicate that appropriate measures were taken to minimize pain or discomfort, and details of animal care should be provided.

SUBMISSION OF MANUSCRIPTS

Manuscripts should be typed in 1.5 line spacing and 12 pt. Book Antiqua with ample margins. Number all pages consecutively, and start each of the following sections on a new page: Title Page, Abstract, Introduction, Materials and Methods, Results, Discussion, Acknowledgements, References, Tables, Figures, and Figure Legends. Neither the editors nor the publisher are responsible for the opinions expressed by contributors. Manuscripts formally accepted for publication become the permanent property of Baishideng Publishing Group Co., Limited, and may not be reproduced by any means, in whole or in part, without the written permission of both the authors and the publisher. We reserve the right to copy-edit and put onto our website accepted manuscripts. Authors should follow the relevant guidelines for the care and use of laboratory animals of their institution or national animal welfare committee. For the sake of transparency in regard to the performance and reporting of clinical trials, we endorse the policy of the ICMJE to refuse to publish papers on clinical trial results if the trial was not recorded in a publicly-accessible registry at its outset. The only register now available, to our knowledge, is http://www.clinicaltrials.gov sponsored

by the United States National Library of Medicine and we encourage all potential contributors to register with it. However, in the case that other registers become available you will be duly notified. A letter of recommendation from each author's organization should be provided with the contributed article to ensure the privacy and secrecy of research is protected.

Authors should retain one copy of the text, tables, photographs and illustrations because rejected manuscripts will not be returned to the author(s) and the editors will not be responsible for loss or damage to photographs and illustrations sustained during mailing.

Online submissions

Manuscripts should be submitted through the Online Submission System at: http://www.wjgnet.com/esps/. Authors are highly recommended to consult the ONLINE INSTRUCTIONS TO AUTHORS (http://www.wjgnet.com/2222-0682/g_info_20100722180909.htm) before attempting to submit online. For assistance, authors encountering problems with the Online Submission System may send an email describing the problem to wjm@wjgnet.com, or by telephone: +86-10-85381891. If you submit your manuscript online, do not make a postal contribution. Repeated online submission for the same manuscript is strictly prohibited.

MANUSCRIPT PREPARATION

All contributions should be written in English. All articles must be submitted using word-processing software. All submissions must be typed in 1.5 line spacing and 12 pt. Book Antiqua with ample margins. Style should conform to our house format. Required information for each of the manuscript sections is as follows:

Title page

Title: Title should be less than 12 words.

Running title: A short running title of less than 6 words should be provided.

Authorship: Authorship credit should be in accordance with the standard proposed by ICMJE, based on (1) substantial contributions to conception and design, acquisition of data, or analysis and interpretation of data; (2) drafting the article or revising it critically for important intellectual content; and (3) final approval of the version to be published. Authors should meet conditions 1, 2, and 3.

Institution: Author names should be given first, then the complete name of institution, city, province and postcode. For example, Xu-Chen Zhang, Li-Xin Mei, Department of Pathology, Chengde Medical College, Chengde 067000, Hebei Province, China. One author may be represented from two institutions, for example, George Sgourakis, Department of General, Visceral, and Transplantation Surgery, Essen 45122, Germany; George Sgourakis, 2nd Surgical Department, Korgialenio-Benakio Red Cross Hospital, Athens 15451, Greece

Author contributions: The format of this section should be: Author contributions: Wang CL and Liang L contributed equally to this work; Wang CL, Liang L, Fu JF, Zou CC, Hong F and Wu XM designed the research; Wang CL, Zou CC, Hong F and Wu XM performed the research; Xue JZ and Lu JR contributed new reagents/analytic tools; Wang CL, Liang L and Fu JF analyzed the data; and Wang CL, Liang L and Fu JF wrote the paper.

Supportive foundations: The complete name and number of supportive foundations should be provided, e.g. Supported by National Natural Science Foundation of China, No. 30224801

Correspondence to: Only one corresponding address should be provided. Author names should be given first, then author title, affiliation, the complete name of institution, city, postcode, province, country, and email. All the letters in the email should be in lower case. A space interval should be inserted between country name and email address. For example, Montgomery Bissell, MD, Professor of Medicine, Chief, Liver Center, Gastroenterology Division, University of California, Box 0538, San Francisco, CA 94143, United States. montgomery.bissell@ucsf.edu

Telephone and fax: Telephone and fax should consist of +, country number, district number and telephone or fax number, e.g. Telephone: +86-10-85381892 Fax: +86-10-85381893

Peer reviewers: All articles received are subject to peer review. Normally, three experts are invited for each article. Decision on acceptance is made only when at least two experts recommend publication of an article. All peer-reviewers are acknowledged on Express Submission and Peer-review System website.

Abstract

There are unstructured abstracts (no less than 200 words) and structured abstracts. The specific requirements for structured abstracts are as follows:

An informative, structured abstract should accompany each manuscript. Abstracts of original contributions should be structured into the following sections: AIM (no more than 20 words; Only the purpose of the study should be included. Please write the Aim in the form of "To investigate/study/…"), METHODS (no less than 140 words for Original Articles; and no less than 80 words for Brief Articles), RESULTS (no less than 150 words for Original Articles and no less than 120 words for Brief Articles; You should present *P* values where appropriate and must provide relevant data to illustrate how they were obtained, e.g. 6.92 ± 3.86 *vs* 3.61 ± 1.67, $P < 0.001$), and CONCLUSION (no more than 26 words).

Key words

Please list 5-10 key words, selected mainly from *Index Medicus*, which reflect the content of the study.

Core tip

Please write a summary of less than 100 words to outline the most innovative and important arguments and core contents in your paper to attract readers.

Text

For articles of these sections, original articles and brief articles, the main text should be structured into the following sections: INTRODUCTION, MATERIALS AND METHODS, RESULTS and DISCUSSION, and should include appropriate Figures and Tables. Data should be presented in the main text or in Figures and Tables, but not in both. The main text format of these sections, editorial, topic highlight, case report, letters to the editors, can be found at: http://www.wjgnet.com/2222-0682/g_info_20100725072755.htm.

Illustrations

Figures should be numbered as 1, 2, 3, *etc*., and mentioned clearly in the main text. Provide a brief title for each figure on a separate page. Detailed legends should not be provided under the figures. This part should be added into the text where the figures are applicable. Keeping all elements compiled is necessary in line-art image. Scale bars should be used rather than magnification factors, with the length of the bar defined in the legend rather than on the bar itself. File names should identify the figure and panel. Avoid layering type directly over shaded or textured areas. Please use uniform legends for the same subjects. For example: Figure 1 Pathological changes in atrophic gastritis after treatment. A: ...; B: ...; C: ...; D: ...; E: ...; F: ...; G: …*etc*. It is our principle to publish high resolution-figures for the E-versions.

Tables

Three-line tables should be numbered 1, 2, 3, *etc*., and mentioned clearly in the main text. Provide a brief title for each table. Detailed legends should not be included under tables, but rather added into the text where applicable. The information should complement,

but not duplicate the text. Use one horizontal line under the title, a second under column heads, and a third below the Table, above any footnotes. Vertical and italic lines should be omitted.

Notes in tables and illustrations

Data that are not statistically significant should not be noted. $^{a}P < 0.05$, $^{b}P < 0.01$ should be noted ($P > 0.05$ should not be noted). If there are other series of P values, $^{c}P < 0.05$ and $^{d}P < 0.01$ are used. A third series of P values can be expressed as $^{e}P < 0.05$ and $^{f}P < 0.01$. Other notes in tables or under illustrations should be expressed as ^{1}F, ^{2}F, ^{3}F; or sometimes as other symbols with a superscript (Arabic numerals) in the upper left corner. In a multi-curve illustration, each curve should be labeled with ●, ○, ■, □, ▲, △, *etc.*, in a certain sequence.

Acknowledgments

Brief acknowledgments of persons who have made genuine contributions to the manuscript and who endorse the data and conclusions should be included. Authors are responsible for obtaining written permission to use any copyrighted text and/or illustrations.

REFERENCES

Coding system

The author should number the references in Arabic numerals according to the citation order in the text. Put reference numbers in square brackets in superscript at the end of citation content or after the cited author's name. For citation content which is part of the narration, the coding number and square brackets should be typeset normally. For example, "Crohn's disease (CD) is associated with increased intestinal permeability[1,2]". If references are cited directly in the text, they should be put together within the text, for example, "From references[19,22-24], we know that..."

When the authors write the references, please ensure that the order in text is the same as in the references section, and also ensure the spelling accuracy of the first author's name. Do not list the same citation twice.

PMID and DOI

Pleased provide PubMed citation numbers to the reference list, e.g. PMID and DOI, which can be found at http://www.ncbi.nlm.nih.gov/sites/entrez?db=pubmed and http://www.crossref.org/SimpleTextQuery/, respectively. The numbers will be used in E-version of this journal.

Style for journal references

Authors: the name of the first author should be typed in bold-faced letters. The family name of all authors should be typed with the initial letter capitalized, followed by their abbreviated first and middle initials. (For example, Lian-Sheng Ma is abbreviated as Ma LS, Bo-Rong Pan as Pan BR). The title of the cited article and italicized journal title (journal title should be in its abbreviated form as shown in PubMed), publication date, volume number (in black), start page, and end page [PMID: 11819634 DOI: 10.3748/wjg.13.5396].

Style for book references

Authors: the name of the first author should be typed in bold-faced letters. The surname of all authors should be typed with the initial letter capitalized, followed by their abbreviated middle and first initials. (For example, Lian-Sheng Ma is abbreviated as Ma LS, Bo-Rong Pan as Pan BR) Book title. Publication number. Publication place: Publication press, Year: start page and end page.

Format

Journals

English journal article (list all authors and include the PMID where applicable)

1 **Jung EM**, Clevert DA, Schreyer AG, Schmitt S, Rennert J, Kubale R, Feuerbach S, Jung F. Evaluation of quantitative contrast harmonic imaging to assess malignancy of liver tumors: A prospective controlled two-center study. *World J Gastroenterol* 2007; **13**: 6356-6364 [PMID: 18081224 DOI: 10.3748/wjg.13.6356]

Chinese journal article (list all authors and include the PMID where applicable)

2 **Lin GZ**, Wang XZ, Wang P, Lin J, Yang FD. Immunologic effect of Jianpi Yishen decoction in treatment of Pixu-diarrhoea. *Shijie Huaren Xiaohua Zazhi* 1999; **7**: 285-287

In press

3 **Tian D**, Araki H, Stahl E, Bergelson J, Kreitman M. Signature of balancing selection in Arabidopsis. *Proc Natl Acad Sci USA* 2006; In press

Organization as author

4 **Diabetes Prevention Program Research Group**. Hypertension, insulin, and proinsulin in participants with impaired glucose tolerance. *Hypertension* 2002; **40**: 679-686 [PMID: 12411462 PMCID:2516377 DOI:10.1161/01.HYP.0000035706.28494.09]

Both personal authors and an organization as author

5 **Vallancien G**, Emberton M, Harving N, van Moorselaar RJ; Alf-One Study Group. Sexual dysfunction in 1, 274 European men suffering from lower urinary tract symptoms. *J Urol* 2003; **169**: 2257-2261 [PMID: 12771764 DOI:10.1097/01.ju.0000067940.76090.73]

No author given

6 21st century heart solution may have a sting in the tail. *BMJ* 2002; **325**: 184 [PMID: 12142303 DOI:10.1136/bmj.325.7357.184]

Volume with supplement

7 **Geraud G**, Spierings EL, Keywood C. Tolerability and safety of frovatriptan with short- and long-term use for treatment of migraine and in comparison with sumatriptan. *Headache* 2002; **42** Suppl 2: S93-99 [PMID: 12028325 DOI:10.1046/j.1526-4610.42.s2.7.x]

Issue with no volume

8 **Banit DM**, Kaufer H, Hartford JM. Intraoperative frozen section analysis in revision total joint arthroplasty. *Clin Orthop Relat Res* 2002; (**401**): 230-238 [PMID: 12151900 DOI:10.1097/00003086-200208000-00026]

No volume or issue

9 Outreach: Bringing HIV-positive individuals into care. *HRSA Careaction* 2002; 1-6 [PMID: 12154804]

Books

Personal author(s)

10 **Sherlock S**, Dooley J. Diseases of the liver and billiary system. 9th ed. Oxford: Blackwell Sci Pub, 1993: 258-296

Chapter in a book (list all authors)

11 **Lam SK**. Academic investigator's perspectives of medical treatment for peptic ulcer. In: Swabb EA, Azabo S. Ulcer disease: investigation and basis for therapy. New York: Marcel Dekker, 1991: 431-450

Author(s) and editor(s)

12 **Breedlove GK**, Schorfheide AM. Adolescent pregnancy. 2nd ed. Wieczorek RR, editor. White Plains (NY): March of Dimes Education Services, 2001: 20-34

Conference proceedings

13 **Harnden P**, Joffe JK, Jones WG, editors. Germ cell tumours V. Proceedings of the 5th Germ cell tumours Conference; 2001 Sep 13-15; Leeds, UK. New York: Springer, 2002: 30-56

Conference paper

14 **Christensen S**, Oppacher F. An analysis of Koza's computational effort statistic for genetic programming. In: Foster JA, Lutton E, Miller J, Ryan C, Tettamanzi AG, editors. Genetic programming. EuroGP 2002: Proceedings of the 5th European Conference on Genetic Programming; 2002 Apr 3-5; Kinsdale, Ireland. Berlin: Springer, 2002: 182-191

Electronic journal (list all authors)

15 Morse SS. Factors in the emergence of infectious diseases. Emerg Infect Dis serial online, 1995-01-03, cited 1996-06-05; 1(1): 24 screens. Available from: URL: http://www.cdc.gov/ncidod/eid/index.htm

Patent (list all authors)

16 **Pagedas AC**, inventor; Ancel Surgical R&D Inc., assignee.

Flexible endoscopic grasping and cutting device and positioning tool assembly. United States patent US 20020103498. 2002 Aug 1

Statistical data
Write as mean ± SD or mean ± SE.

Statistical expression
Express *t* test as *t* (in italics), *F* test as *F* (in italics), chi square test as χ^2 (in Greek), related coefficient as *r* (in italics), degree of freedom as υ (in Greek), sample number as *n* (in italics), and probability as *P* (in italics).

Units
Use SI units. For example: body mass, m (B) = 78 kg; blood pressure, p (B) = 16.2/12.3 kPa; incubation time, t (incubation) = 96 h, blood glucose concentration, c (glucose) 6.4 ± 2.1 mmol/L; blood CEA mass concentration, p (CEA) = 8.6 24.5 μg/L; CO_2 volume fraction, 50 mL/L CO_2, not 5% CO_2; likewise for 40 g/L formaldehyde, not 10% formalin; and mass fraction, 8 ng/g, *etc.* Arabic numerals such as 23, 243, 641 should be read 23 243 641.

The format for how to accurately write common units and quantums can be found at: http://www.wjgnet.com/2222-0682/g_info_20100725073806.htm.

Abbreviations
Standard abbreviations should be defined in the abstract and on first mention in the text. In general, terms should not be abbreviated unless they are used repeatedly and the abbreviation is helpful to the reader. Permissible abbreviations are listed in Units, Symbols and Abbreviations: A Guide for Biological and Medical Editors and Authors (Ed. Baron DN, 1988) published by The Royal Society of Medicine, London. Certain commonly used abbreviations, such as DNA, RNA, HIV, LD50, PCR, HBV, ECG, WBC, RBC, CT, ESR, CSF, IgG, ELISA, PBS, ATP, EDTA, mAb, can be used directly without further explanation.

Italics
Quantities: *t* time or temperature, *c* concentration, *A* area, *l* length, *m* mass, *V* volume.
Genotypes: *gyrA*, *arg* 1, *c myc*, *c fos*, *etc.*
Restriction enzymes: *Eco*RI, *Hin*dI, *Bam*HI, *Kbo* I, *Kpn* I, *etc.*
Biology: *H. pylori*, *E coli*, *etc.*

Examples for paper writing
All types of articles' writing style and requirement will be found in the link: http://www.wjgnet.com/esps/NavigationInfo.aspx?id=15.

SUBMISSION OF THE REVISED MANUSCRIPTS AFTER ACCEPTED
Authors must revise their manuscript carefully according to the revision policies of Baishideng Publishing Group Co., Limited. The revised version, along with the signed copyright transfer agreement, responses to the reviewers, and English language Grade A certificate (for non-native speakers of English), should be submitted to the online system *via* the link contained in the e-mail sent by the editor. If you have any questions about the revision, please send e-mail to esps@wjgnet.com.

Language evaluation
The language of a manuscript will be graded before it is sent for revision. (1) Grade A: priority publishing; (2) Grade B: minor language polishing; (3) Grade C: a great deal of language polishing needed; and (4) Grade D: rejected. Revised articles should reach Grade A.

Copyright assignment form
Please download a Copyright assignment form from http://www.wjgnet.com/2222-0682/g_info_20100725073726.htm.

Responses to reviewers
Please revise your article according to the comments/suggestions provided by the reviewers. The format for responses to the reviewers' comments can be found at: http://www.wjgnet.com/2222-0682/g_info_20100725073445.htm.

Proof of financial support
For papers supported by a foundation, authors should provide a copy of the approval document and serial number of the foundation.

Links to documents related to the manuscript
WJGO will be initiating a platform to promote dynamic interactions between the editors, peer reviewers, readers and authors. After a manuscript is published online, links to the PDF version of the submitted manuscript, the peer-reviewers' report and the revised manuscript will be put on-line. Readers can make comments on the peer reviewer's report, authors' responses to peer reviewers, and the revised manuscript. We hope that authors will benefit from this feedback and be able to revise the manuscript accordingly in a timely manner.

Publication fee
WJGO is an international, peer-reviewed, OA online journal. Articles published by this journal are distributed under the terms of the Creative Commons Attribution Non-commercial License, which permits use, distribution, and reproduction in any medium and format, provided the original work is properly cited. The use is non-commercial and is otherwise in compliance with the license. Authors of accepted articles must pay a publication fee. Publication fee: 600 USD per article. All invited articles are published free of charge.

ISSN 2222-0682 (online)

World Journal of *Methodology*

World J Methodol 2013 June 26; 3(2): 19-26

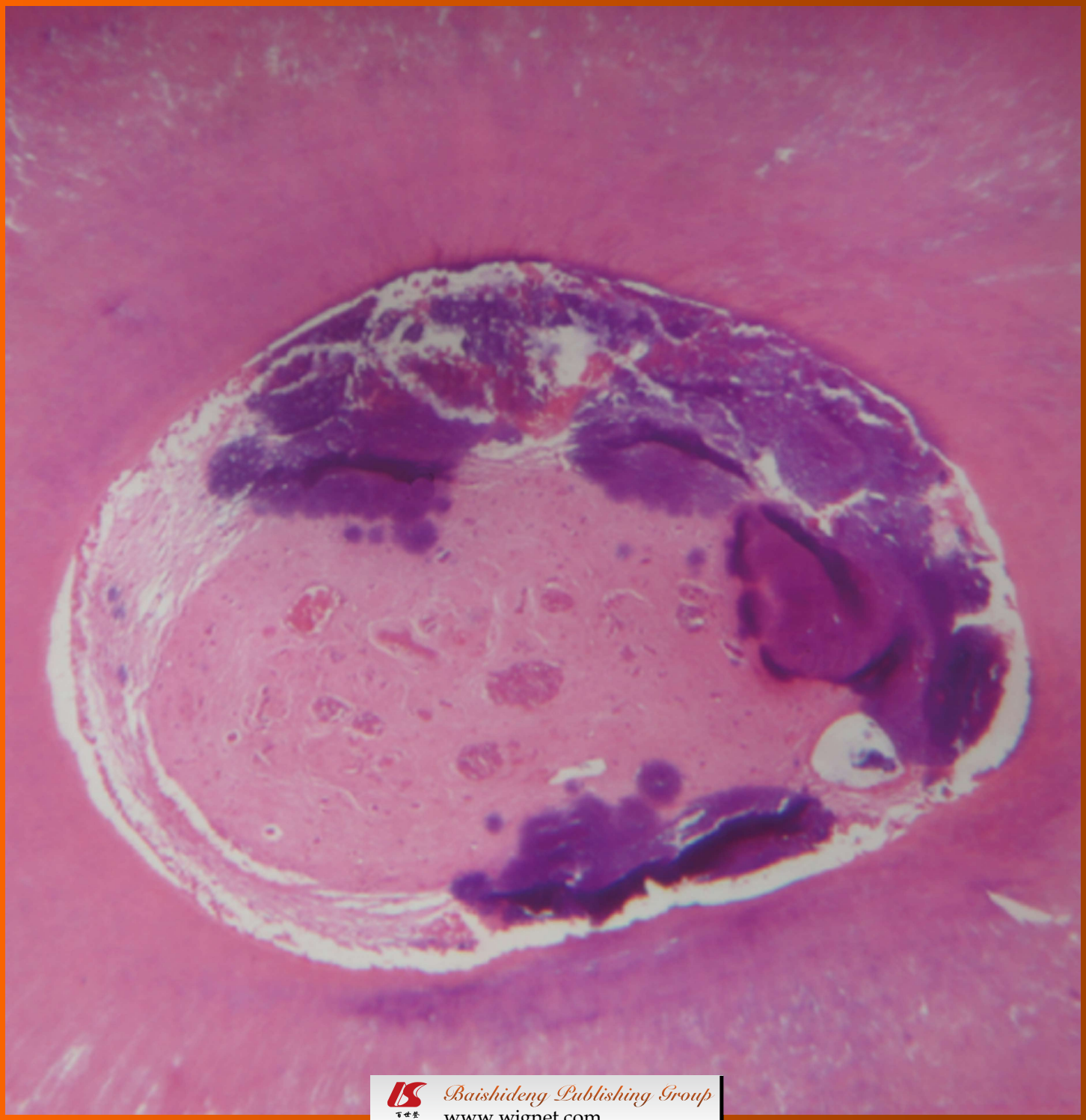

Baishideng Publishing Group
www.wjgnet.com

WJM World Journal of Methodology

Contents

Quarterly Volume 3 Number 2 June 26, 2013

Contents

World Journal of Methodology
Volume 3 Number 2 June 26, 2013

AIM AND SCOPE

World Journal of Methodology (*World J Methodol*, *WJM*, online ISSN 2222-0682, DOI: 10.5662) is a peer-reviewed open access academic journal that aims to guide clinical practice and improve diagnostic and therapeutic skills of clinicians.

The primary task of *WJM* is to rapidly publish high-quality original articles, reviews, and commentaries that deal with the methodology to develop, validate, modify and promote diagnostic and therapeutic modalities and techniques in preclinical and clinical applications. *WJM* covers topics concerning the subspecialties including but not exclusively anesthesiology, cardiac medicine, clinical genetics, clinical neurology, critical care, dentistry, dermatology, emergency medicine, endocrinology, family medicine, gastroenterology and hepatology, geriatrics and gerontology, hematology, immunology, infectious diseases, internal medicine, obstetrics and gynecology, oncology, ophthalmology, orthopedics, otolaryngology, radiology, serology, pathology, pediatrics, peripheral vascular disease, psychiatry, radiology, rehabilitation, respiratory medicine, rheumatology, surgery, toxicology, transplantation, and urology and nephrology.

INDEXING/ABSTRACTING

World Journal of Methodology is now indexed in Digital Object Identifier.

NAME OF JOURNAL
World Journal of Methodology

ISSN
ISSN 2222-0682 (online)

LAUNCH DATE
September 26, 2011

FREQUENCY
Quarterly

EDITOR-IN-CHIEF
Yicheng Ni, MD, PhD, Professor, Department of Radiology, University Hospitals, KU, Leuven, Herestraat 49, B-3000, Leuven, Belgium

EDITORIAL OFFICE
Jin-Lei Wang, Director
Xiu-Xia Song, Vice Director

World Journal of Methodology
Room 903, Building D, Ocean International Center, No. 62 Dongsihuan Zhonglu, Chaoyang District, Beijing 100025, China
Telephone: +86-10-59080039
Fax: +86-10-85381893
E-mail: wjg@wjgnet.com
http://www.wjgnet.com

PUBLISHER
Baishideng Publishing Group Co., Limited
Flat C, 23/F., Lucky Plaza, 315-321 Lockhart Road, Wanchai, Hong Kong, China
Fax: +852-65557188
Telephone: +852-31779906
E-mail: bpgoffice@wjgnet.com
http://www.wjgnet.com

PUBLICATION DATE
June 26, 2013

INSTRUCTIONS TO AUTHORS
Full instructions are available online at http://www.wjgnet.com/2222-0682/g_info_20100722180909.htm

ONLINE SUBMISSION
http://www.wjgnet.com/esps/

World Journal of Methodology

Online Submissions: http://www.wjgnet.com/esps/
wjm@wjgnet.com
doi:10.5662/wjm.v3.i2.19

World J Methodol 2013 June 26; 3(2): 19-26
ISSN 2222-0682 (online)

BRIEF ARTICLE

Effect of low level laser therapy on dental pulp during orthodontic movement

Ángela Domínguez, Rosa Emilia Ballesteros, Jairo Hernán Viáfara, Oscar Mario Tamayo

Ángela Domínguez, Rosa Emilia Ballesteros, Jairo Hernán Viáfara, Department of Orthodontics, Faculty of Dentistry, Universidad del Valle, Cali 76001000, Colombia
Oscar Mario Tamayo, Histology and Anatomy, Medicine Department, Universidad Santiago de Cali, Cali 76001000, Colombia
Author contributions: Domínguez Á designed the study, performed the majority of experiments and edited the manuscript; Tamayo OM, author of the decalcification process applied in this study, prepared and processed the histological specimens; Ballesteros RE and Viáfara JH contributed to data recollection, results analysis and writing of the manuscript.
Correspondence to: Ángela Domínguez, DDS, Orthodontist, Professor, Department of Orthodontics, Faculty of Dentistry, Universidad del Valle, Calle 4B No 36-00, Cali 76001000 Colombia. angela.dominguezc@gmail.com
Telephone: +57-2-3212100 Fax: +57-2-3169450
Received: May 2, 2013 Revised: June 4, 2013
Accepted: June 12, 2013
Published online: June 26, 2013

Abstract

AIM: To validate the protocol described here to be used in future clinical trials related to the effect of laser therapy on dental pulp.

METHODS: Histologically treated samples from eight human healthy premolar teeth obtained from the middle root level were distributed in four groups: group 1 (G1) absolute control; group 2 (G2) only laser irradiation; group 3 (G3) exposed only to orthodontics; and group 4 (G4) treated with orthodontics and laser. Laser treatment was performed at 830 nm wavelength, 100 mW (energy 80 J/cm^2, 2.2 J), for 22 s in the vestibular surface and 22 s in the palatal surface, 1 mm away from the dental root mucosa. Three staining methods were performed: hematoxylin-eosin (HE), Masson's Trichrome method and Gomori's method.

RESULTS: The pulp histology parameters were evaluated and the results classified in to 3 parts: an inflammatory response, soft tissue response (dental pulp) and hard tissue response (dentin and predentin). There was no inflammation (chronic or acute) in any of the evaluated groups. The zones of pulp necrosis were found in one premolar of G3 and in one of G4; in groups G2 and G4 there was higher angiogenesis than in the other two groups. G4 group presented the highest level of vascularization. A reduced nerve density was observed in G3. A G2 specimen showed increased nerve density. A higher rate of calcification was observed in G1 compared to G2. Denticles, either real or false, were observed in G1, G2 and G3. Sclerosis of dentin and focal dentin loss was observed among all the groups. Secondary dentin was present in one sample in G1 and G2. A necrosis zone was found in one sample of G3 and G4. No differences between groups were observed in the odontoblast irregularity layer but the layer was wider in the group treated with laser only. A notable difference was detected in reduction of the cell-free layer between the groups G1 and G4. The findings in pulp tissue favor its adaptative response against dental movement induced by orthodontics. No definitive conclusions may be derived as this is a pilot study.

CONCLUSION: The protocol described here was shown to be an effective method to evaluate changes in dental pulp submitted to low level laser in teeth under orthodontic movement.

Key words: Low level laser therapy; Pulpal; Orthodontic movement; Histological protocol; Dentin

Domínguez A, Ballesteros RE, Viáfara JH, Tamayo OM. Effect of low level laser therapy on dental pulp during orthodontic movement. *World J Methodol* 2013; 3(2): 19-26 Available from: URL: http://www.wjgnet.com/2222-0682/full/v3/i2/19.htm DOI: http://dx.doi.org/10.5662/wjm.v3.i2.19

INTRODUCTION

Low level laser therapy (LLLT) causes positive effects to physiological bone remodeling[1-6] and its effects are considered positive and not cytotoxic for cells participating in induced dental movement, such as fibroblasts[7-12] osteoblasts[13-18], osteoclasts and pre osteoclasts[19,20]. Laser application during orthodontic treatment accelerates orthodontic induced movement[21-25] and reduces pain symptoms during the different treatment stages[26-30].

The orthodontic dental movement has an inflammatory-like effect on pulp tissue, initially causing changes in blood flow[31-33], increasing the level of angiogenic growth factors[34], central and peripheral angiogenesis[35] and generating changes in the odontoblastic layer[36]. Early biochemical changes include a reduction in the activity of alkaline phosphatase[37] and increased activity of aspartate aminotransferase[38].

At the neuronal level, the expression of substance P (SP) in response to orthodontic movement in pulp has been described as well as its potent action in neurogenic inflammation which is directly related to the pain sensation during orthodontic treatment[39].

Some studies in orthodontically treated teeth showed injuries such as root canal calcification[40] and degeneration of the odontoblastic layer due to blood flow alteration, accompanied by edema with pulp vessel congestion and fibrotic changes in pulp tissue, including necrosis[41-43].

In vitro and animal model studies suggest that laser application during orthodontic movement may be able to accelerate pulp damage repair. Miyata *et al*[44] analyzed the effect of low level laser on pulp tissue from an extracted third molar, finding that this irradiation activated the phosphorylation of mitogen activated protein kinase (MAPK) and increased extracellular signals regulated by protein kinase (ERK). This MAPK/ERK activation is indicative of cell proliferation, differentiation and survival.

Abi-Ramia *et al*[45] published a study on the effect of LLLT on Wistar rats. They applied a 0.4 N force and laser (Ga-Al-As of 830 nm, 100 mW, 18 J) on the control group. In this group, the authors found increased pulp vascularization and concluded that laser application during orthodontic movement may help to repair pulp tissue.

The effect of low level laser therapy used to accelerate dental movement and reduce pain during orthodontic treatments on human dental pulp is not clear. The purpose of this pilot study is to first validate the modified protocol described here to be used in future clinical trials. Secondly, to describe the histological changes in human pulp tissue related to the effect of low level laser therapy as used during the alignment and leveling stage of orthodontic treatment.

MATERIALS AND METHODS

Ethical issues

This study protocol number 124-010 was approved by the Ethics Committee of the Universidad del Valle (Cali, Colombia), conforms to the principles of the declaration of Helsinki and all the patients signed informed consent before any intervention.

According to the Colombian Ministry of Health Resolution 8430 from 1993, this research study is classified in the category of minimum risk for the patients.

Two patients treated at the orthodontics department of dentistry of the Universidad del Valle (23 and 25 years old) provided the sample of eight first premolar teeth programmed to be extracted as part of the orthodontic treatment. Histological sections taken from the middle root zone were obtained from the freshly extracted premolar teeth.

The selected teeth should be completely healthy, without previous endodontic, orthodontic, whitening or restorative treatment, periodontally healthy and free of any trauma or fracture.

The premolar teeth were randomly assigned to four groups, as follows: (1) Control group (G1): Two healthy premolar teeth, without laser therapy and orthodontic treatment; (2) Laser treated group (G2): Two healthy premolar teeth treated with laser without orthodontic treatment; (3) Orthodontic group (G3): Two healthy premolar teeth submitted to orthodontic alignment with standard brackets but not laser treated. The extractions were carried out one month after initiating orthodontic treatment; and (4) Orthodontic and laser group (G4): Two healthy premolar teeth were submitted to the same orthodontic treatment as in G3. The laser treatment was performed after bracket bonding, following the protocol for therapeutic laser use. The extractions were carried out one month later and a second laser dose was applied before the procedure.

Orthodontic initial stage

The patients were treated using a straight-wire technique with Synthesis® brackets (Ormco, S.A. de C.V. Mexico). All the brackets were bonded with Transbond XT® resin (Unitek, Monrovia, CA). The initial arch wire was Cu-NiTi 0.014 inch.

Irradiation protocol

The healthy premolars in the corresponding groups to be laser treated were irradiated using a Photon II Laser (Equipamentos DMC, Sao Carlos, Brazil) at a wavelength of 830 nm, 100 mW (energy: 80 J/cm^2, 2.2 J) at a distance of 1mm away from the mucosa in the vestibular and palatal surface each one for 22 s. This protocol has been shown to be effective for therapeutic purposes in previous studies[24,30].

Histological protocol

All the extracted teeth were treated following the same histological protocol by the same operator and read by a previously standardized pathologist.

The histological protocol includes: (1) Immediately after extraction, the premolar is cross-sectioned in the middle part using a high speed hand piece and diamond

Table 1 Soft tissue response

Histological findings	G1	G2	G3	G4
Necrosis	0	0	1	1
	0	0	0	0
Central angiogenesis	1	_	1	_
Peripheral angiogenesis	1	1	_	1
Central and peripheral	_	3	1	2
Vascular density	1	1	1	2
	1	1	2	2
Nerve density	1	1	NC	1
	1	2	NC	NC
Calcifications	2	0	1	1
	2	1	3	3
False denticles	1	1	0	0
Real denticles	1	1	1	0

0: Absent; 1: Low; 2: Moderate; 3: Severe; NC: Not changed.

Table 2 Connective tissue histological findings

Staining	G1	G2	G3	G4
Hematoxylin-eosin	1	1	1	2
	1	2	3	2
Masson's Trichrome method	2	1	1	2
	2	1	2	2
Gomori's method for reticulum	2	1	1	2
	2	2	2	2

0: Absent; 1: Low; 2: Moderate; 3: Severe.

tronco-cone bur; (2) The two fragments obtained are immediately submerged in a recipient with a mixture of glutaraldehyde 2.5% and paraformaldehyde 3% in PBS (phosphate buffer saline) at 4 ℃. Each sample was fixed in a recipient with a key indicating the group number, specimen number, tooth number according to the international dental nomenclature and the histological treatment date; (3) After the first week of fixation, the specimens are decalcified with a mixture of citrate, EDTA and formate following a technique developed by Dr. Oscar Tamayo from the histology laboratory of the Universidad del Valle (patent under process); (4) The specimens are washed in PBS 0.01 M during two days (4 wash outs per day); (5) The specimens are dehydrated in ethanol (70%, 95%, 100%, plus Xylol) and then included in paraffin molds to be sectioned with microtome at the level of the cement-enamel junction in 5 micrometer slices; (6) The slices are extended in a water bath at 40 ℃ and dried out in a furnace for one hour at 56 ℃. The slide sheet are immersed in xylol and absolute ethanol (100%, 95%, 70% and water); (7) Staining for general cell contents and angiogenesis evaluation is performed using hematoxylin-eosin (HE); (8) The Masson's Trichrome method staining is used to observe type I collagen fibers; and (9) The Gomori's method for reticulum staining is used to visualize the reticulum fibers (Type Ⅲ collagen fibers).

RESULTS

Each descriptive parameter was classified in an ordinal scale as 0: absent, 1: low, 2: moderate, 3: severe, NC: not changed.

Pulp histological findings

The pulp histology parameters were evaluated and the results are summarized in Table 1, classified in to 3 parts: an inflammatory response, soft tissue response (dental pulp) and hard tissue response (dentin and predentin), as recommended by Sübay *et al*[46].

Inflammatory response: There was no inflammation (chronic or acute) in any of the evaluated groups, G1, G2, G3 and G4.

Soft tissue response: Connective tissue histological findings: The observations made under this three stain techniques applied to evaluate connective tissue fibrosis are summarized in Table 2. Figure 1A clearly shows pulp fibrosis. Zones of pulp necrosis: Zones of pulp necrosis were found in one premolar of G3 and G4 (Figure 1B). Vascularization: There was more angiogenesis in the G2 and G4 groups than in the other two groups. The group receiving orthodontic treatment plus laser presented with the highest level of vascularization. Angiogenesis is observed under HE staining where the vascular endothelium shows no muscular layer, a clear indication that it is only developing. Nerves: A reduced nerve density was observed in the orthodontic positive group (laser negative). A G2 specimen (laser treated) showed increased nerve density (Figure 1C). Presence of calcification and denticles: A higher calcification was observed in G1 than in G2. No difference was detected in the orthodontic positive groups. Denticles, either real or false, were observed in G1, G2 and G3 (Figure 1D, E). Fibroblast morphology: No descriptive alterations in histological findings were observed between groups in the morphology of fibroblasts.

Hard tissue response (dentin and predentin): Histological findings in hard tissues are summarized in Table 3. Sclerosis of dentin and focal dentin lost was observed in all the groups (Figure 1F, G). Secondary dentin was present in one sample of G1 and G2. A necrosis zone was found in one sample of G3 and G4. Odontoblast layer: No relevant differences between groups were observed in odontoblast irregularities but the layer was wider in the group treated with laser only. No differences were detected regarding odontoblast vacuolization (Figure 1H, I). Acellular zone (Weil zone): A notable difference was detected in a reduction of the cell-free layer between the groups G1 and G4. Cell-rich zone: Fibroblast proliferation was minimal in G1 group.

DISCUSSION

The present study performed in human premolar healthy teeth explored possible histological changes in the pulp, related to orthodontics and/or LLLT during the initial

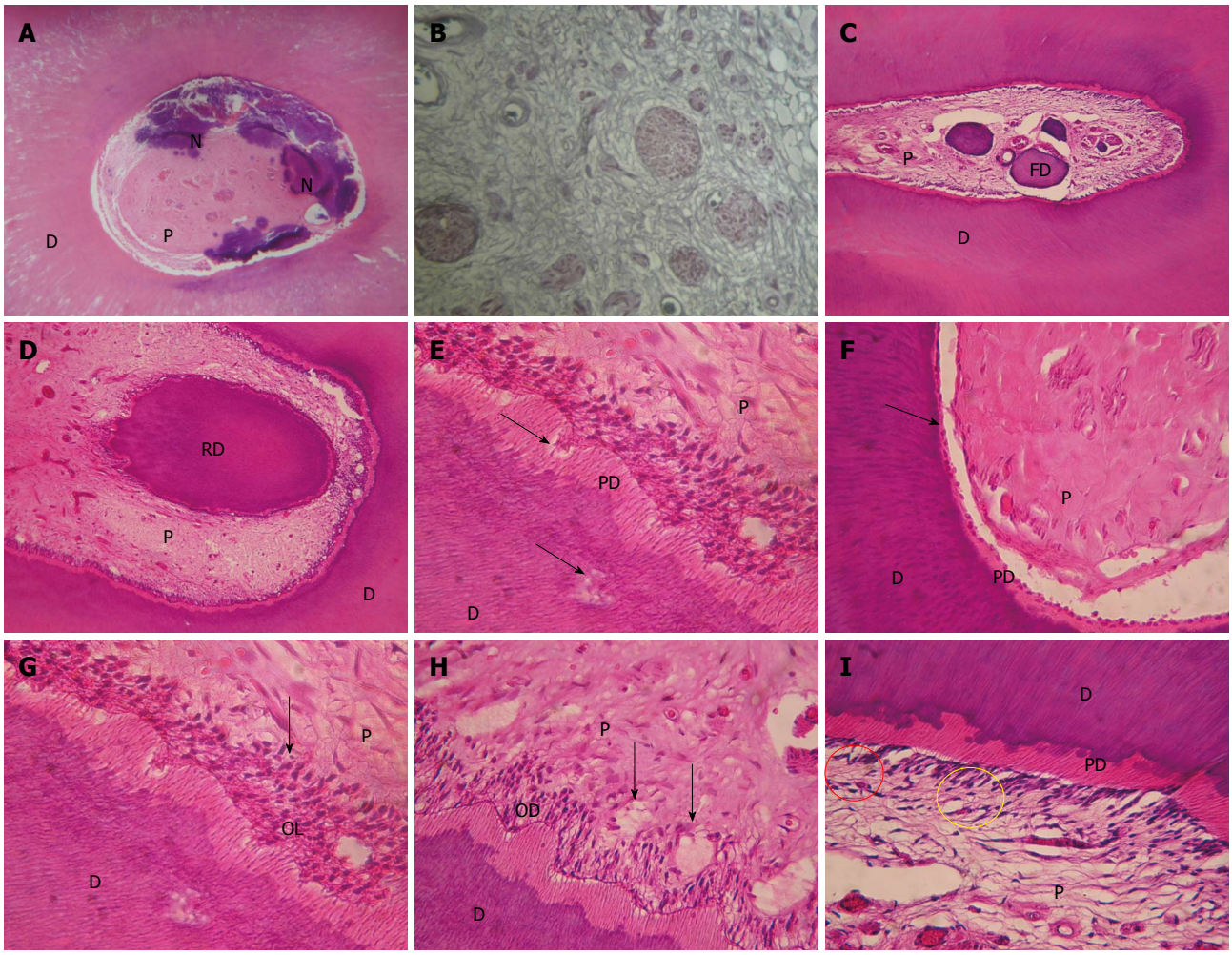

Figure 1 Photography. A: Showing necrotic areas in a slice of the group treated with orthodontics without laser (magnification × 10); B: Showing increased nerve density in the pulp of a laser irradiated specimen (magnification × 40); C: A control group premolar that shows a false denticle - denticle without epithelium (magnification × 10); D: A premolar from G3 group presenting a real denticle - with epithelium (magnification × 10); E: The arrows signal dentin and predentin sclerosis in a G2 specimen (magnification × 20); F: The arrows indicate focal predentin lost in a G1 premolar (magnification × 20); G: Irregularities in odontoblast layer. The thickness of odontoblast layer is indicated with the arrow in this G2 premolar slice (magnification × 20); H: The arrows indicate the presence of odontoblast vacuolization in a specimen treated both with orthodontics and laser (magnification × 20); I: The red circle shows a normal Weil cell-free zone and the yellow circle marks a zone invaded by cells and blood vessels in a G4 premolar (magnification × 20). D: Dentine; P: Pulp; N: Necrosis; FD: False denticle; RD: Real denticle; PD: Predentin; OL: Odontoblast layer.

phases or orthodontic treatment.

In their study, Villa *et al*[34] evaluated pulp-dentinal reactions after the application of a 4 ounce intrusive orthodontic force to human maxillary first premolars in patients given the NSAID nabumetone. The root surface histological slides were stained with hematoxylin-eosin, Masson's Trichrome method and Gomori's method for reticulum. Masson's Trichrome method was used to visualize fibrin, fibrosis and type I collagen fibers. Gomori' s method for reticulum was used to visualize reticulum fibers (Type Ⅲ collagen fibers). Even although there was this difference, similar findings are described for the pulp tissue.

The most relevant results are those related to pulp vascularization; the scientific literature indicates that orthodontic dental movement affects pulp vascularization. Taking into account that the pulp is surrounded by rigid structures and the blood supply comes from the apical foramen, any change in blood flow or tissue pressure may affect the pulp integrity[39,47,48].

Vascular alterations have a direct impact upon pulp metabolism, especially changes in blood supply and angiogenesis, as the research line of Derringer has proved[49-51].

Angiogenesis is the formation of new capillary structures through neovascularization. Angiogenesis stages include a breakdown of vascular membrane, endothelial cell mitosis and migration to form new capillaries, as well as cell folding to preserve the vessel lumen[35].

The importance of the increased vascularization found in the present study is that it accelerates the pulp repair, as described by Abi-Ramia *et al*[45] in 2010 in a report about the effect of LLLT in an animal model. The study was performed in 45 Wistar rats. The control group (n = 20 rats) received a 0.4 N stress for mesial movement

Table 3 Hard tissue (dentin and predentin) response

Histological findings	G1	G2	G3	G4
Sclerosis of dentin	2	1	1	1
	0	0	0	0
Secondary dentin	2	2	0	0
	0	0	0	0
Necrosis in dentin	0	0	1	1
	0	0	0	0
Focal dentin lost	2	0	0	0
	0	0	0	0
Focal predentin lost	2	2	1	1
	0	0	0	0
Irregularities in odontoblast layer	1	2	1	1
	1	3	1	1
Thickening of odontoblasts	1	2	3	2
	1	3	1	0
Odontoblast vacuolization	1	2	1	1
	2	2	2	2
Reduction of Weil zone	1	2	1	3
	1	2	3	3
Cell-rich zone	1	2	1	2
	1	2	3	2

0: Absent; 1: Low; 2: Moderate; 3: Severe.

and laser irradiation from Ga-Al-As laser at 830 nm, 100 mW, 18 J/cm^2 4 s per point in the vestibular, mesial and palatal surfaces, perpendicular to the molar axis. The authors found transitory hyperemia in the pulp in this group and suggested that the application of laser during orthodontic movement may accelerate pulp injury repair.

The same hypothesis is supported by the study of McDonald and Pitt Ford[52] made in maxillary permanent canine teeth; it suggests that the increment of pulp blood flow is a consequence of the inflammatory process triggered by the force applied for dental movement. During this process, the increased blood supply and the presence of inflammatory cells in the zone aim to repair the tissue.

The results of the present study show necrosis zones in G3 and G4. These zones can be the result of the orthodontic induced movement, as suggested by Woloshyn *et al*[42], Perinetti *et al*[37] and Bauss *et al*[53]. It should also be considered that the result is a consequence of the use of a high speed cutting bur when the teeth were cut into 2 fragments. The possibilities of a previous pulp necrosis related to dental trauma or leveling an alignment are ruled out due to a close verification process during experimentation time. The alterations observed in the odontoblastic layer are consistent with those described in previous studies. Santamaria *et al*[54], after applying 0.4 N to produce mesial tipping in maxillary molar teeth of rats, found hypertrophy of odontoblasts, especially at the mesial area of the coronal pulp.

There are also previous reports about the proliferative effect of LLLT on different cell lines, including odontoblasts[55-57]. In the present study, an irregular distribution of the odontoblast layer in all groups was observed, compared to the absolute control group. The widening of the odontoblast layer appears under LLLT stimulation compared to the control group.

Reports presented by Stenvik *et al*[58] in teeth with a closed apex submitted to dental movement indicate few or no vacuolization of the odontoblastic layer, indicating that the inflammatory changes generated by the orthodontic force are made without causing important degenerative breakdown in the odontoblasts. However, in the present study, vacuolization of odontoblasts in all the groups studied was observed, including the control group.

The reduction of the cell-free zone (Weil) was notorious when the control group G1 was compared to G4, especially in areas where more alterations were found in the odontoblast layer, agreeing with findings in previous reports[46,55,58].

In teeth under orthodontic movement with or without LLLT, it is usual to observe a cell-rich zone inside the cell-free layer that is differentiated from the central pulp portion by the high number of cells per area unit, mainly fibroblasts and undifferentiated mesenchymal cells, due to its proliferative effects on fibroblasts and collagen fibers. It is also known that this cell-rich zone is more abundant on irradiated teeth than in the control group[45]. In the present study, the difference was not relevant when the control group was compared to the experimental groups or among the experimental groups, probably due to the sample size.

It is not possible to compare the present study results with other human studies as there are only reports from animal models[45] that show some evidence that orthodontic movement associated with LLLT enhances vascularization and therefore could accelerate pulp tissue repair. On the other hand, there are reports in human subjects indicating that LLLT has deleterious effects when the energy released is high enough to increase the temperature in the pulp camera above the threshold of 5.5 ℃[59]. The present investigation suggests that the pulp tissue reacts in a way that tends to favor repair from the initial injury produced by the orthodontic force.

The most relevant contribution of the present study is the number of histological findings not previously shown in high quality slices in human pulp after application of LLLT in teeth under orthodontic movement. It is also relevant that this design and protocol might be applied to further studies using a sample of at least 12 dental specimens per group.

In conclusion, the protocol described here was shown to be an effective method to evaluate changes in human dental pulp tissue submitted to low level laser therapy on teeth under orthodontic movement. The findings made in pulp tissue favor its adaptative response against dental movement injury induced by orthodontics and this data should be validated in future randomized clinical trials.

ACKNOWLEDGEMENTS

The authors wish to thank the following methodological

and technical advisors: Dr. Adriana Jaramillo, Magister in Microbiology, Universidad del Valle, Dr. Herney Rengifo, Magister in Public Health and Epidemiology, Universidad del Valle and Dr Roberto Jaramillo, pathologist, Universidad del Valle. We also thank Dr. Luis Rogelio Hernández, Master of Science from the University of Southampton, and Dr. Sergio Velasquez, orthodontist, Universidad del Valle, for their assistance in the writing and translation of this article.

COMMENTS

Background

Laser application during orthodontic treatment accelerates orthodontic movement and reduces pain symptoms during the different treatment stages; however, the effect of low level laser therapy on human dental pulp is not clear.

Research frontiers

Some studies in orthodontically treated teeth showed injuries such as root canal calcification and degeneration of the odontoblastic layer due to blood flow alteration, accompanied by edema with pulp vessel congestion and fibrotic changes in pulp tissue, including necrosis. *In vitro* and animal model studies suggest that laser application during orthodontic movement may be able to accelerate pulp damage repair.

Innovations and breakthroughs

It is not possible to compare the present study results with other human studies as there are only reports from animal models that show some evidence that orthodontic movement associated with low level laser therapy (LLLT) enhances vascularization and therefore could accelerate pulp tissue repair. The present investigation suggests that the pulp tissue reacts in a way that tends to favor repair from the initial injury produced by the orthodontic force.

Applications

The most relevant contribution of the present study is the number of histological findings not previously shown in high quality slices in human pulp after application of LLLT in teeth under orthodontic movement. It is also relevant that this design and protocol might be applied to further studies with a higher number of specimens.

Terminology

LLLT has been advocated as a collateral-free therapy and its application has shown considerable reduction in pain caused by orthodontic appliance placement. Furthermore, LLLT has also shown biostimulatory effects; the energy output of the device is low enough not to exceed an irradiated tissue temperature of 36.5 ℃.

Peer review

This is an interesting study revealing the histological response of human dental pulp to the application of LLLT in teeth under orthodontic tooth movement.

REFERENCES

1 **Chung H**, Dai T, Sharma SK, Huang YY, Carroll JD, Hamblin MR. The nuts and bolts of low-level laser (light) therapy. *Ann Biomed Eng* 2012; **40**: 516-533 [PMID: 22045511 DOI: 10.5051/jpis.2010.40.3.105]

2 **Saito S**, Shimizu N. Stimulatory effects of low-power laser irradiation on bone regeneration in midpalatal suture during expansion in the rat. *Am J Orthod Dentofacial Orthop* 1997; **111**: 525-532 [PMID: 9155812 DOI: 10.1016/S0889-5406(97)70152-5]

3 **Habib FA**, Gama SK, Ramalho LM, Cangussú MC, Santos Neto FP, Lacerda JA, Araújo TM, Pinheiro AL. Laser-induced alveolar bone changes during orthodontic movement: a histological study on rodents. *Photomed Laser Surg* 2010; **28**: 823-830 [PMID: 21142724 DOI: 10.1089/pho.2009.2732]

4 **Fujita S**, Yamaguchi M, Utsunomiya T, Yamamoto H, Kasai K. Low-energy laser stimulates tooth movement velocity via expression of RANK and RANKL. *Orthod Craniofac Res* 2008; **11**: 143-155 [PMID: 18713151 DOI: 10.1111/j.1601-6343.2008.00423.x]

5 **Yamaguchi M**, Hayashi M, Fujita S, Yoshida T, Utsunomiya T, Yamamoto H, Kasai K. Low-energy laser irradiation facilitates the velocity of tooth movement and the expressions of matrix metalloproteinase-9, cathepsin K, and alpha(v) beta(3) integrin in rats. *Eur J Orthod* 2010; **32**: 131-139 [PMID: 20159792 DOI: 10.1093/ejo/cjp078]

6 **Almeida-Lopes L**, Rigau J, Zângaro RA, Guidugli-Neto J, Jaeger MM. Comparison of the low level laser therapy effects on cultured human gingival fibroblasts proliferation using different irradiance and same fluence. *Lasers Surg Med* 2001; **29**: 179-184 [PMID: 11553908 DOI: 10.1002/lsm.1107]

7 **Pereira AN**, Eduardo Cde P, Matson E, Marques MM. Effect of low-power laser irradiation on cell growth and procollagen synthesis of cultured fibroblasts. *Lasers Surg Med* 2002; **31**: 263-267 [PMID: 12355572 DOI: 10.1002/lsm.10107]

8 **Kreisler M**, Christoffers AB, Willershausen B, d'Hoedt B. Effect of low-level GaAlAs laser irradiation on the proliferation rate of human periodontal ligament fibroblasts: an in vitro study. *J Clin Periodontol* 2003; **30**: 353-358 [PMID: 12694435 DOI: 10.1034/j.1600-051X.2003.00001.x]

9 **Choi EJ**, Yim JY, Koo KT, Seol YJ, Lee YM, Ku Y, Rhyu IC, Chung CP, Kim TI. Biological effects of a semiconductor diode laser on human periodontal ligament fibroblasts. *J Periodontal Implant Sci* 2010; **40**: 105-110 [PMID: 20607054 DOI: 10.5051/jpis.2010.40.3.105]

10 **Saygun I**, Karacay S, Serdar M, Ural AU, Sencimen M, Kurtis B. Effects of laser irradiation on the release of basic fibroblast growth factor (bFGF), insulin like growth factor-1 (IGF-1), and receptor of IGF-1 (IGFBP3) from gingival fibroblasts. *Lasers Med Sci* 2008; **23**: 211-215 [PMID: 17619941 DOI: 10.1007/s10103-007-0477-3]

11 **Domínguez A,** Clarkson A, López R. An in vitro study of the reaction of periodontal and gingival fibroblasts to low- level laser irradiation: A pilot study. *J Oral Laser Applications* 2008; **8**: 235-244

12 **Ozawa Y**, Shimizu N, Kariya G, Abiko Y. Low-energy laser irradiation stimulates bone nodule formation at early stages of cell culture in rat calvarial cells. *Bone* 1998; **22**: 347-354 [PMID: 9556134 DOI: 10.1016/S8756-3282(97)00294-9]

13 **Coombe AR**, Ho CT, Darendeliler MA, Hunter N, Philips JR, Chapple CC, Yum LW. The effects of low level laser irradiation on osteoblastic cells. *Clin Orthod Res* 2001; **4**: 3-14 [PMID: 11553080 DOI: 10.1034/j.1600-0544.2001.040102.x]

14 **Fujihara NA**, Hiraki KR, Marques MM. Irradiation at 780 nm increases proliferation rate of osteoblasts independently of dexamethasone presence. *Lasers Surg Med* 2006; **38**: 332-336 [PMID: 16526043 DOI: 10.1002/lsm.20298]

15 **Soleimani M**, Abbasnia E, Fathi M, Sahraei H, Fathi Y, Kaka G. The effects of low-level laser irradiation on differentiation and proliferation of human bone marrow mesenchymal stem cells into neurons and osteoblasts--an in vitro study. *Lasers Med Sci* 2012; **27**: 423-430 [PMID: 21597948 DOI: 10.1007/s10103-011-0930-1]

16 **Dominguez A,** Castro P, Morales M. An In Vitro Study of the Reaction of Human Osteoblasts to Low-level Laser Irradiation. *J Oral Laser Appl* 2009; **9**: 21-28

17 **Dominguez AC,** Castro PZ, Morales MC. Cellular Effects related to the clinical uses of laser in orthodontics. *J Oral Laser Appl* 2009; **9**: 199-203

18 **Aihara N**, Yamaguchi M, Kasai K. Low-energy irradiation stimulates formation of osteoclast-like cells via RANK expression in vitro. *Lasers Med Sci* 2006; **21**: 24-33 [PMID: 16568210 DOI: 10.1007/s10103-005-0368-4]

19 **Domínguez A,** Bayona G, Casas A. In vitro response of Human Pre-Osteoclasts to low intensity Laser irradiation. *J Res Biol* 2012; **2**: 733-741

20 **Cruz DR**, Kohara EK, Ribeiro MS, Wetter NU. Effects of low-intensity laser therapy on the orthodontic movement ve-

locity of human teeth: a preliminary study. *Lasers Surg Med* 2004; **35**: 117-120 [PMID: 15334614]
21 **Limpanichkul W**, Godfrey K, Srisuk N, Rattanayatikul C. Effects of low-level laser therapy on the rate of orthodontic tooth movement. *Orthod Craniofac Res* 2006; **9**: 38-43 [PMID: 16420273 DOI: 10.1111/j.1601-6343.2006.00338.x]
22 **Youssef M**, Ashkar S, Hamade E, Gutknecht N, Lampert F, Mir M. The effect of low-level laser therapy during orthodontic movement: a preliminary study. *Lasers Med Sci* 2008; **23**: 27-33 [PMID: 17361391 DOI: 10.1007/s10103-007-0449-7]
23 **Domínguez A,** Velásquez SA. Acceleration Effect of Orthodontic Movement by Application of Low-intensity Laser. *J Oral Laser Appl* 2010; **10**: 99-105
24 **Sousa MV**, Scanavini MA, Sannomiya EK, Velasco LG, Angelieri F. Influence of low-level laser on the speed of orthodontic movement. *Photomed Laser Surg* 2011; **29**: 191-196 [PMID: 21254890 DOI: 10.1089/pho.2009.2652]
25 **Lim HM**, Lew KK, Tay DK. A clinical investigation of the efficacy of low level laser therapy in reducing orthodontic postadjustment pain. *Am J Orthod Dentofacial Orthop* 1995; **108**: 614-622 [PMID: 7503039 DOI: 10.1016/S0889-5406(95)70007-2]
26 **Harazaki M**, Takahashi H, Ito A, Isshiki Y. Soft laser irradiation induced pain reduction in orthodontic treatment. *Bull Tokyo Dent Coll* 1998; **39**: 95-101 [PMID: 9667142]
27 **Tortamano A**, Lenzi DC, Haddad AC, Bottino MC, Dominguez GC, Vigorito JW. Low-level laser therapy for pain caused by placement of the first orthodontic archwire: a randomized clinical trial. *Am J Orthod Dentofacial Orthop* 2009; **136**: 662-667 [PMID: 19892282 DOI: 10.1016/j.ajodo.2008.06.028]
28 **Xiaoting L**, Yin T, Yangxi C. Interventions for pain during fixed orthodontic appliance therapy. A systematic review. *Angle Orthod* 2010; **80**: 925-932 [PMID: 20578865 DOI: 10.2319/010410-10.1]
29 **Domínguez A,** Velásquez SA. Effect of low-level laser therapy on pain following activation of orthodontic final archwires: a randomized controlled clinical trial. *Photomed Laser Surg* 2013; **31**: 36-40 [DOI: 10.1089/pho.2012.3360]
30 **Barwick PJ**, Ramsay DS. Effect of brief intrusive force on human pulpal blood flow. *Am J Orthod Dentofacial Orthop* 1996; **110**: 273-279 [PMID: 8814028 DOI: 10.1016/S0889-5406(96)80011-4]
31 **Ikawa M**, Fujiwara M, Horiuchi H, Shimauchi H. The effect of short-term tooth intrusion on human pulpal blood flow measured by laser Doppler flowmetry. *Arch Oral Biol* 2001; **46**: 781-787 [PMID: 11420050 DOI: 10.1016/S0003-9969(01)00049-8]
32 **Sano Y**, Ikawa M, Sugawara J, Horiuchi H, Mitani H. The effect of continuous intrusive force on human pulpal blood flow. *Eur J Orthod* 2002; **24**: 159-166 [PMID: 12001552 DOI: 10.1093/ejo/24.2.159]
33 **Derringer KA**, Jaggers DC, Linden RW. Angiogenesis in human dental pulp following orthodontic tooth movement. *J Dent Res* 1996; **75**: 1761-1766 [PMID: 8955671 DOI: 10.1177/00220345960750100901]
34 **Villa PA**, Oberti G, Moncada CA, Vasseur O, Jaramillo A, Tobón D, Agudelo JA. Pulp-dentine complex changes and root resorption during intrusive orthodontic tooth movement in patients prescribed nabumetone. *J Endod* 2005; **31**: 61-66 [PMID: 15614010 DOI: 10.1097/01.DON.0000134212.20525.74]
35 **Hamilton RS**, Gutmann JL. Endodontic-orthodontic relationships: a review of integrated treatment planning challenges. *Int Endod J* 1999; **32**: 343-360 [PMID: 10551108 DOI: 10.1046/j.1365-2591.1999.00252.x]
36 **Perinetti G**, Varvara G, Salini L, Tetè S. Alkaline phosphatase activity in dental pulp of orthodontically treated teeth. *Am J Orthod Dentofacial Orthop* 2005; **128**: 492-496 [PMID: 16214632 DOI: 10.1016/j.ajodo.2004.07.042]
37 **Perinetti G**, Varvara G, Festa F, Esposito P. Aspartate aminotransferase activity in pulp of orthodontically treated teeth. *Am J Orthod Dentofacial Orthop* 2004; **125**: 88-92 [PMID: 14718884 DOI: 10.1016/j.ajodo.2003.02.006]
38 **Kim S**. Neurovascular interactions in the dental pulp in health and inflammation. *J Endod* 1990; **16**: 48-53 [PMID: 2201743 DOI: 10.1016/S0099-2399(06)81563-3]
39 **Parris WG**, Tanzer FS, Fridland GH, Harris EF, Killmar J, Desiderio DM. Effects of orthodontic force on methionine enkephalin and substance P concentrations in human pulpal tissue. *Am J Orthod Dentofacial Orthop* 1989; **95**: 479-489 [PMID: 2471405 DOI: 10.1016/0889-5406(89)90411-3]
40 **Delivanis HP**, Sauer GJ. Incidence of canal calcification in the orthodontic patient. *Am J Orthod* 1982; **82**: 58-61 [PMID: 6961778 DOI: 10.1016/0002-9416(82)90547-4]
41 **Mostafa YA**, Iskander KG, El-Mangoury NH. Iatrogenic pulpal reactions to orthodontic extrusion. *Am J Orthod Dentofacial Orthop* 1991; **99**: 30-34 [PMID: 1986523 DOI: 10.1016/S0889-5406(05)81677-4]
42 **Woloshyn H**, Artun J, Kennedy DB, Joondeph DR. Pulpal and periodontal reactions to orthodontic alignment of palatally impacted canines. *Angle Orthod* 1994; **64**: 257-264 [PMID: 7978520]
43 **Yamaguchi M,** Kasai K. The Effects of Orthodontic Mechanics on the Dental Pulp. *Seminars in orthodontics* 2007; **13**: 272-280 [DOI: 10.1053/j.sodo.2007.08.008]
44 **Miyata H**, Genma T, Ohshima M, Yamaguchi Y, Hayashi M, Takeichi O, Ogiso B, Otsuka K. Mitogen-activated protein kinase/extracellular signal-regulated protein kinase activation of cultured human dental pulp cells by low-power gallium-aluminium-arsenic laser irradiation. *Int Endod J* 2006; **39**: 238-244 [PMID: 16507078 DOI: 10.1111/j.1365-2591.2006.01080.x]
45 **Abi-Ramia LB**, Stuani AS, Stuani AS, Stuani MB, Mendes Ade M. Effects of low-level laser therapy and orthodontic tooth movement on dental pulps in rats. *Angle Orthod* 2010; **80**: 116-122 [PMID: 19852650 DOI: 10.2319/120808-619.1]
46 **Sübay RK**, Kaya H, Tarim B, Sübay A, Cox CF. Response of human pulpal tissue to orthodontic extrusive applications. *J Endod* 2001; **27**: 508-511 [PMID: 11501587 DOI: 10.1097/00004770-200108000-00003]
47 **Hamersky PA**, Weimer AD, Taintor JF. The effect of orthodontic force application on the pulpal tissue respiration rate in the human premolar. *Am J Orthod* 1980; **77**: 368-378 [PMID: 6928739 DOI: 10.1016/0002-9416(80)90103-7]
48 **Kim S**, Dörscher-Kim J. Hemodynamic regulation of the dental pulp in a low compliance environment. *J Endod* 1989; **15**: 404-408 [PMID: 2637333 DOI: 10.1016/S0099-2399(89)80172-4]
49 **Derringer KA**, Linden RW. Enhanced angiogenesis induced by diffusible angiogenic growth factors released from human dental pulp explants of orthodontically moved teeth. *Eur J Orthod* 1998; **20**: 357-367 [PMID: 9753817 DOI: 10.1093/ejo/20.4.357]
50 **Derringer KA**, Linden RW. Angiogenic growth factors released in human dental pulp following orthodontic force. *Arch Oral Biol* 2003; **48**: 285-291 [PMID: 12663073 DOI: 10.1016/S0003-9969(03)00008-6]
51 **Derringer KA**, Linden RW. Vascular endothelial growth factor, fibroblast growth factor 2, platelet derived growth factor and transforming growth factor beta released in human dental pulp following orthodontic force. *Arch Oral Biol* 2004; **49**: 631-641 [PMID: 15196981 DOI: 10.1016/j.archoralbio.2004.02.011]
52 **McDonald F**, Pitt Ford TR. Blood flow changes in permanent maxillary canines during retraction. *Eur J Orthod* 1994; **16**: 1-9 [PMID: 8181544 DOI: 10.1093/ejo/16.1.1]
53 **Bauss O**, Schäfer W, Sadat-Khonsari R, Knösel M. Influence of orthodontic extrusion on pulpal vitality of traumatized maxillary incisors. *J Endod* 2010; **36**: 203-207 [PMID: 20113775 DOI: 10.1016/j.joen.2009.10.025]

54 **Santamaria M**, Milagres D, Iyomasa MM, Stuani MB, Ruellas AC. Initial pulp changes during orthodontic movement: histomorphological evaluation. *Braz Dent J* 2007; **18**: 34-39 [PMID: 17639198]
55 **Shigetani Y**, Sasa N, Suzuki H, Okiji T, Ohshima H. GaAlAs laser irradiation induces active tertiary dentin formation after pulpal apoptosis and cell proliferation in rat molars. *J Endod* 2011; **37**: 1086-1091 [PMID: 21763899 DOI: 10.1016/j.joen.2011.05.020]
56 **Pereira LB**, Chimello DT, Ferreira MR, Bachmann L, Rosa AL, Bombonato-Prado KF. Low-level laser therapy influences mouse odontoblast-like cell response in vitro. *Photomed Laser Surg* 2012; **30**: 206-213 [PMID: 22375953 DOI: 10.1089/pho.2011.3087]
57 **Santamaria M**, Milagres D, Stuani AS, Stuani MB, Ruellas AC. Initial changes in pulpal microvasculature during orthodontic tooth movement: a stereological study. *Eur J Orthod* 2006; **28**: 217-220 [PMID: 16675546]
58 **Stenvik A**, Mjör IA. Pulp and dentine reactions to experimental tooth intrusion. A histologic study of the initial changes. *Am J Orthod* 1970; **57**: 370-385 [PMID: 5265007]
59 **de Alencar Mollo M**, Frigo L, Favero GM, Lopes-Martins RA, Brugnera Junior A. In vitro analysis of human tooth pulp chamber temperature after low-intensity laser therapy at different power outputs. *Lasers Med Sci* 2011; **26**: 143-147 [PMID: 20148278 DOI: 10.1007/s10103-009-0752-6]

P- Reviewers Ajcharanukul O, do Prado M
L- Editor Roemmele A **S- Editor** Wen LL **E- Editor** Lu YJ

ISSN 2222-0682 (online)

World Journal of *Methodology*

World J Methodol 2013 September 26; 3(3): 27-38

Baishideng Publishing Group
www.wjgnet.com

WJM

World Journal of Methodology

Contents

Quarterly Volume 3 Number 3 September 26, 2013

AIM AND SCOPE

World Journal of Methodology (*World J Methodol*, *WJM*, online ISSN 2222-0682, DOI: 10.5662) is a peer-reviewed open access academic journal that aims to guide clinical practice and improve diagnostic and therapeutic skills of clinicians.

The primary task of *WJM* is to rapidly publish high-quality original articles, reviews, and commentaries that deal with the methodology to develop, validate, modify and promote diagnostic and therapeutic modalities and techniques in preclinical and clinical applications. *WJM* covers topics concerning the subspecialties including but not exclusively anesthesiology, cardiac medicine, clinical genetics, clinical neurology, critical care, dentistry, dermatology, emergency medicine, endocrinology, family medicine, gastroenterology and hepatology, geriatrics and gerontology, hematology, immunology, infectious diseases, internal medicine, obstetrics and gynecology, oncology, ophthalmology, orthopedics, otolaryngology, radiology, serology, pathology, pediatrics, peripheral vascular disease, psychiatry, radiology, rehabilitation, respiratory medicine, rheumatology, surgery, toxicology, transplantation, and urology and nephrology.

NAME OF JOURNAL
World Journal of Methodology

ISSN
ISSN 2222-0682 (online)

LAUNCH DATE
September 26, 2011

FREQUENCY
Quarterly

EDITOR-IN-CHIEF
Yicheng Ni, MD, PhD, Professor, Department of Radiology, University Hospitals, KU, Leuven, Herestraat 49, B-3000, Leuven, Belgium

EDITORIAL OFFICE
Jin-Lei Wang, Director
Xiu-Xia Song, Vice Director

World Journal of Methodology
Room 903, Building D, Ocean International Center, No. 62 Dongsihuan Zhonglu, Chaoyang District, Beijing 100025, China
Telephone: +86-10-59080039
Fax: +86-10-85381893
E-mail: wjg@wjgnet.com
http://www.wjgnet.com

PUBLISHER
Baishideng Publishing Group Co., Limited
Flat C, 23/F., Lucky Plaza, 315-321 Lockhart Road, Wanchai, Hong Kong, China
Fax: +852-65557188
Telephone: +852-31779906
E-mail: bpgoffice@wjgnet.com
http://www.wjgnet.com

PUBLICATION DATE
September 26, 2013

INSTRUCTIONS TO AUTHORS
Full instructions are available online at http://www.wjgnet.com/2222-0682/g_info_20100722180909.htm

ONLINE SUBMISSION
http://www.wjgnet.com/esps/

World Journal of Methodology

Online Submissions: http://www.wjgnet.com/esps/
wjm@wjgnet.com
doi:10.5662/wjm.v3.i3.27

World J Methodol 2013 September 26; 3(3): 27-38
ISSN 2222-0682 (online)

ORIGINAL ARTICLE

Bifunctional staining for *ex vivo* determination of area at risk in rabbits with reperfused myocardial infarction

Yuanbo Feng, Zhan-Long Ma, Feng Chen, Jie Yu, Marlein Miranda Cona, Yi Xie, Yue Li, Yicheng Ni

Yuanbo Feng, Feng Chen, Jie Yu, Marlein Miranda Cona, Yicheng Ni, Theragnostic Laboratory, Department of Imaging and Pathology, Biomedical Sciences Group, 3000 KU Leuven, Belgium
Zhan-Long Ma, Departments of Radiology, the First Affiliated Hospital, Nanjing Medical University, Nanjing 210029, Jiangsu Province, China
Yi Xie, Departments of Electronics and Information System (ELIS), Ghent University, Sint-Pietersnieuwstraat 25, 9000 Gent, Belgium
Yue Li, Lab of Translational Medicine, Jiangsu Academy of Traditional Chinese Medicine, nanjing 210028, Jiangsu Province, China
Yicheng Ni, Radiology Section, University Hospitals, 3000 Leuven, Belgium
Author contributions: All authors made a substantial contribution to the conception and design of the manuscript, drafting the article or revising it.
Supported by The awarded grants of the KU Leuven Molecular Small Animal Imaging Center MoSAIC (KUL EF/05/08); the Center of Excellence *in vivo* Molecular Imaging Research (IMIR) of KU Leuven; a EU Project Asia-Link CfP 2006-Europe Aid/123738/C/ACT/Multi-Proposal, No. 128-498/111; and Jiangsu Province Natural Science Foundation, China, No. BK2010594
Correspondence to: Yicheng Ni, MD, PhD, Professor, Radiology Section, University Hospitals, KU Leuven Herestraat 49, 3000 Leuven, Belgium. yicheng.ni@med.kuleuven.be
Telephone: +32-16-330165 Fax: +32-16-343765
Received: July 12, 2013 Revised: July 16, 2013
Accepted: August 16, 2013
Published online: September 26, 2013

Abstract

AIM: To develop a method for studying myocardial area at risk (AAR) in ischemic heart disease in correlation with cardiac magnetic resonance imaging (cMRI).

METHODS: Nine rabbits were anesthetized, intubated and subjected to occlusion and reperfusion of the left circumflex coronary artery (LCx) to induce myocardial infarction (MI). ECG-triggered cMRI with delayed enhancement was performed at 3.0 T. After euthanasia, the heart was excised with the LCx re-ligated. Bifunctional staining was performed by perfusing the aorta with a homemade red-iodized-oil (RIO) dye. The heart was then agar-embedded for *ex vivo* magnetic resonance imaging and sliced into 3 mm-sections. The AAR was defined by RIO-staining and digital radiography (DR). The perfusion density rate (PDR) was derived from DR for the AAR and normal myocardium. The MI was measured by *in vivo* delayed enhancement (iDE) and *ex vivo* delayed enhancement (eDE) cMRI. The AAR and MI were compared to validate the bifunctional straining for cardiac imaging research. Linear regression with Bland-Altman agreement, one way-ANOVA with Bonferroni's multiple comparison, and paired t tests were applied for statistics.

RESULTS: All rabbits tolerated well the surgical procedure and subsequent cMRI sessions. The open-chest occlusion and close-chest reperfusion of the LCx, double suture method and bifunctional staining were successfully applied in all animals. The percentage MI volumes globally (n = 6) and by slice (n = 25) were 36.59% ± 13.68% and 32.88% ± 12.38% on iDE, and 35.41% ± 12.25% and 32.40% ± 12.34% on eDE. There were no significant differences for MI determination with excellent linear regression correspondence (r_{global} = 0.89; r_{slice} = 0.9) between iDE and eDE. The percentage AAR volumes globally (n = 6) and by slice (n = 25) were 44.82% ± 15.18% and 40.04% ± 13.64% with RIO-staining, and 44.74% ± 15.98% and 40.48% ± 13.26% by DR showing high correlation in linear regression analysis (r_{global} = 0.99; r_{slice} = 1.0). The mean differences of the two AAR measurements on Bland-Altman were almost zero, indicating RIO-staining and DR were essentially equivalent or inter-replaceable. The AAR was significantly larger than MI both globally and slice-by-slice (P < 0.01). After correction with the background and the blank heart without bifunctional staining (n = 3), the PDR for the AAR and normal myocardium was 32% ± 15% and 35.5% ± 35%, respectively,

which is significantly different ($P < 0.001$), suggesting that blood perfusion to the AAR probably by collateral circulation was only less than 10% of that in the normal myocardium.

CONCLUSION: The myocardial area at risk in ischemic heart disease could be accurately determined postmortem by this novel bifunctional staining, which may substantially contribute to translational cardiac imaging research.

Key words: Reperfused; Acute myocardial infarction; Rabbit model; Cardiac magnetic resonance imaging; Oil-red-o dye; Iodized oil

Core tip: For developing therapeutic procedures/drugs aimed at modulating infarct size after coronary artery disease, it is important not only to measure myocardial infarction but also to know the extent of area at risk (AAR). However, determination of the AAR both *in vivo* and *ex vivo* can be challenging, and controversial. In this experiment we sought to develop a reliable method to accurately localize the culprit coronary occlusion for postmortem verification after *in vivo* cardiac magnetic resonance imaging and to establish a new bifunctional staining as a standard reference for *ex vivo* area at risk identification, which may substantially contribute to translational cardiac imaging research.

Feng Y, Ma ZL, Chen F, Yu J, Cona MM, Xie Y, Li Y, Ni Y. Bifunctional staining for *ex vivo* determination of area at risk in rabbits with reperfused myocardial infarction. *World J Methodol* 2013; 3(3): 27-38 Available from: URL: http://www.wjgnet.com/2222-0682/full/v3/i3/27.htm DOI: http://dx.doi.org/10.5662/wjm.v3.i3.27

INTRODUCTION

Acute occlusion of a coronary artery initiates an expanding process of myocardial infarction (MI) and this process ends in complete necrosis of the myocardial tissue within the perfusion bed if without a prompt therapeutic intervention. To develop therapeutic procedures and/or drugs aimed at modulating infarct size, it is very important not only to measure the MI size but also to know the extent of perfusion defect zone after coronary occlusion, which is also known as the area at risk (AAR) of myocardium[1]. Since the AAR includes both infracted/nonviable and viable/salvageable myocardium, detection of the AAR may provide an accurate index in clinical practice and preclinical research for diagnostic, therapeutic and prognostic assessment of ischemic heart disease[2,3]. To define the AAR by both *in vivo* and *ex vivo* imaging can be challenging. Currently, the most widely used methods for *in vivo* AAR identification are contrast enhanced computed tomography[4] or cardiac magnetic resonance imaging (cMRI)[5], radionuclide perfusion imaging[6], and contrasted echocardiography[7]. However, determination of the AAR proves difficult and controversial in clinical cardiology[8]. The T2-weighted cMRI may highlight myocardial edema and therefore often overestimate infarct size, and sestamibi single photon emission computed tomography is limited by its low spatial resolution and radioactive nature. Compared to the AAR, MI can be evaluated *in vivo* by delayed enhancement (DE) cMRI, an established technique that is widely accepted in clinic to reveal acute and chronic MI in patients[9]. This technique has been validated in animal models with reperfused MI using extracellular contrast agents[10,11].

Experimentally, to validate *in vivo* imaging observations, a variety of *ex vivo* methods have been developed and attempted to directly visualize and quantify the AAR and MI in animal experiments, because exact postmortem detection of myocardial AAR and MI is deemed necessary as the gold reference. A few decades ago, some investigators tried to assess the AAR through postmortem intracoronary injections of colored industrial dyes[12] or barium gels[13], which stained the normal myocardium but left the AAR unstained. However, highly viscous injectants and undetermined pressure could lead to inaccurate AAR delineation. Nowadays, widespread techniques used for determination of coronary perfusion or AAR are blue dyes (typically Evans blue) and radiolabeled or colored microspheres, with which the heart is perfused at the end of experiments after re-occlusion of the coronary artery[1,14,15]. Triphenyltetrazolium chloride (TTC) histochemical staining is usually combined with a blue dye for simultaneous visualization of normal myocardium, AAR and MI[16]. These methods have their limitations. For instance, the most commonly used water-soluble blue dye Evans-blue may precipitate out of solution and affect the subsequent TTC staining[17]. These dyes are also prone to smearing during slicing, resulting in an ambiguous border definition[17]. The radiolabeled microspheres need the complex procedures and operators have to be exposed to radiation, in addition to the difficulty in some institutions due to unavailable nuclear facilities. The colored microspheres require tissue lyses for counting without morphometry. Therefore, such analyses still remain technically challenging.

To precisely recognize the location of previously occluded coronary branch is crucial for subsequent *ex vivo* calculation of AAR size. Few study detailed the technical information for accurate coronary re-ligation[18].

Given the suboptimal features of above-mentioned dyes and microspheres for visualizing the AAR in preclinical study, we sought to: (1) develop a reliable method to accurately localize the previous coronary occlusion site for postmortem re-ligation; (2) establish a new bifunctional staining as standard reference for *ex vivo* AAR evaluation; (3) validate the method by quantitative measurement and morphometry; and (4) compare the AAR defined by the new staining to the cMRI findings at a 3.0

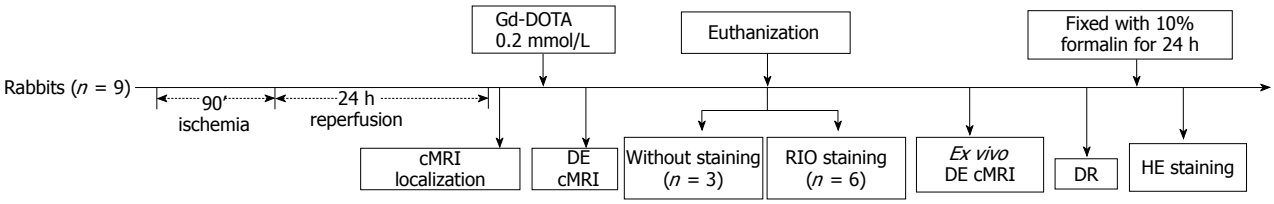

Figure 1 Flow chart of experimental protocol. cMRI: Cardiac magnetic resonance imaging; DE: Delayed enhancement; RIO: Red-iodized-oil; DR: Digital radiography; HE: Hematoxylin-eosin.

T clinic magnet with histological verifications.

The above goals could have been realized only when has a prior-established methodology, *i.e.*, an occlusion/reperfusion based rabbit model of acute MI and a technical platform for pre- and postmortem imaging co-localization now become available[19,20]. The rabbit as a mediate size experimental animal can be easily handled, with favorable cost-effectiveness and compatibility to clinically available MRI facilities with the entire heart section includable in a standard histological glass slide. The resulted outcomes are deemed pertinent to human patients[19,21].

MATERIALS AND METHODS

This experimental study was carried out according to a protocol (Figure 1) that was approved by the Animal Care and Use Committee of KU Leuven, Belgium.

Preparation of red iodized oil dye

The custom-made bifunctional dye of red iodized oil (RIO) was formulated by diluting 20 mg oil-red-O dye (Sigma-Aldrich) in 100 mL of any brand of commercially available iodized oil such as Lipiodol ultra fluid (Guerbet, France), which is also known as ethiodized oil consisting of about 30%-40% iodine and poppyseed oil originally used as a radio-opaque contrast agent to outline structures in radiological investigations or in combination for transarterial chemoembolization of malignant tumors[22,23].

Animal model of acute reperfused myocardial infarction

A total of 9 male New Zealand white rabbits (Animal House, KU Leuven, Belgium), weighing 3.2-4.0 kg, were included in this study. Animals were housed under standard laboratory conditions.

The model of acute reperfused MI was prepared by slight modification on a previously introduced method[19]. After sedation, endotracheal intubation and mechanical ventilation, the rabbit received intravenous (IV) injection of pentobarbital (Nembutal, Sanofi Sante Animale, Brussels, Belgium) at 40 mg/kg per hour to maintain anesthesia during the open-chest operation to dissect the paricardium and expose the left circumflex coronary branch (LCx). For making a removable coronary ligation *in vivo* and precise re-ligation *ex vivo*, we used a 1/2 circle shape triangular needle (Sutura, Inc. Fountain Valley, CA, United States) with spring eyes at the end (Figure 2A). Two silk sutures could be easily placed through the separate eyes (Figure 2B): the thicker one (2-0) was used for the LCx ligation that could be removed for reperfusion and the thinner one (5-0) was spared for later *ex vivo* LCx re-occlusion in order to perform postmortem bifunctional staining (Figure 2C). The acute reperfused MI was induced by tying the thicker suture with a detachable single knot for 90 min, and LCx reperfusion was achieved by pulling the exteriorized end of suture in the closed-chest condition as detailed previously[19]. The ECG (Accusync® 71, Milford, Connecticut, Unites States) was monitored to confirm the formation of MI and to detect the occurrence of arrhythmia, which was treated by IV dose of Xylocaine (AstraZeneca SA, Brussels, Belgium) at 2-4 mg/kg if needed. Buprenorfine hydrochloride (Temgesic; Schering-Plough, Brussels, Belgium) of 0.216 mg was intramuscularly injected to relieve pain. All rabbits were allowed to recover and kept alive until cMRI scanning 24 h after LCx reperfusion.

Cardiac magnetic resonance imaging

The rabbit was gas-anesthetized through a mask with 2% isoflurane in the mixture of 20% oxygen and 80% room air and placed supinely in a plastic holder. Using a commercial 8-channel phased array knee coil, the rabbit was subjected to cMRI at a 3.0 T clinical MRI scanner (Trio, Siemens, Erlangen, Germany) with a maximum gradient capability of 45 mT/m. The ECG and respiration were triggered and gated by a Small Animal Monitoring System (SA Instruments, Inc. Stony Brook, New York, United States). Two ECG surface electrodes were attached to the shaved thorax skin with apparently apical pulse and the left leg. The respiration control sensor was attached on the middle of the rabbit abdomen. All data were acquired during free breathing of the animal. After determining the cardiac axes with localizers, the DE cMRI using T1-weighted 3-dimensional segmented k-space inversion recovery turbo fast low angle shot sequence was performed 20 min after intravenous administration of 0.2 mmol/kg Gd-DOTA (Dotarem, Guerbet, France). Short-axis DE cMRI was acquired to depict the presence, location, and extent of the MI. The imaging parameters were: TR: 396 ms; TE: 1.54 ms; TI: 360 ms; FOV: 240 × 180 mm^2; FA: 15°; and in-plane resolution: 1.1 × 0.8 mm^2. The *ex vivo* higher resolution DE-cMRI was also obtained immediately after animal sacrifice using the same MRI unit with a wrist coil as previously described[19]. The DE cMRI using an extracellular nonspecific contrast agent has been ap-

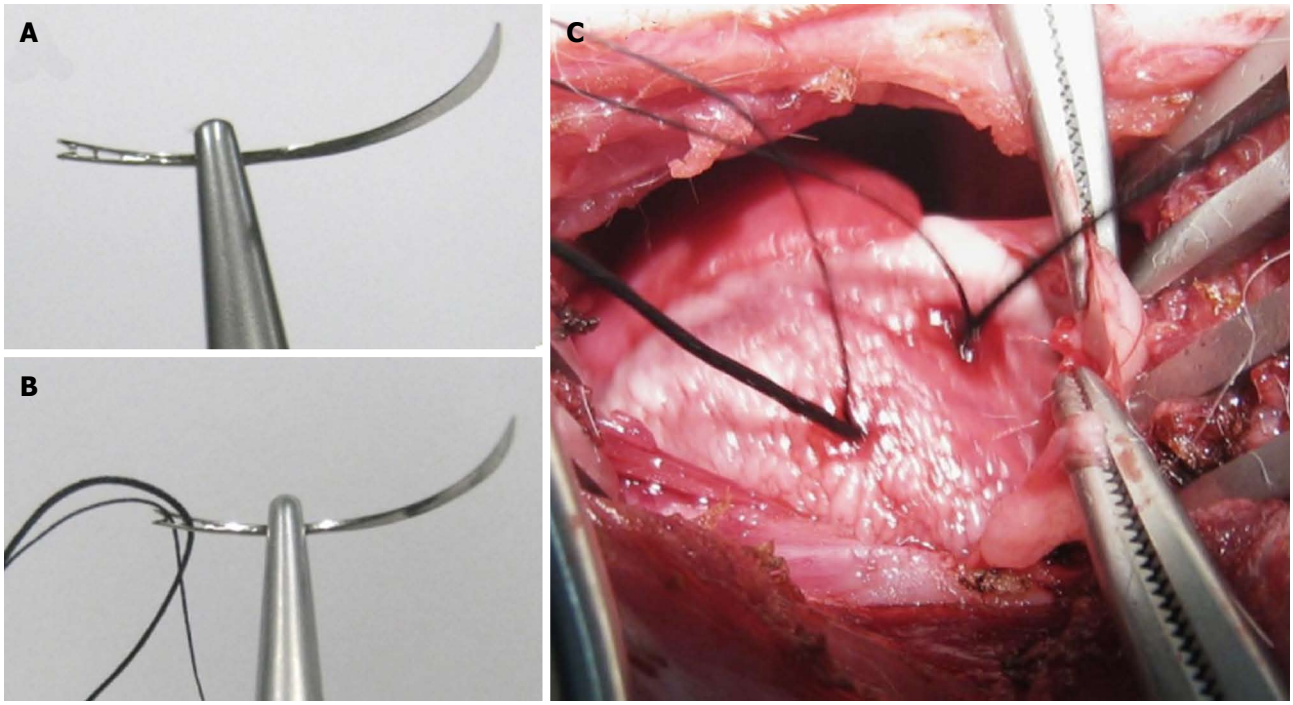

Figure 2 Double suture method in rabbit model of reperfused myocardial infarction. A: A 1/2 circle shape triangular needle has spring eyes at the end; B: Two silk sutures were placed through separate eyes; C: The thicker suture (2-0) was used for the left circumflex coronary artery (LCx) ligation, which would be removed for reperfusion, and the thinner one (5-0) was spared for later *ex vivo* LCx re-occlusion in order to perform postmortem bifunctional staining.

plied in both animal MI models and clinical patients as a gold standard technique for identification and quantification of the MI[10,11]. Therefore, the final MI size was also defined by *in vivo* and *ex vivo* DE-cMRI in this study.

Postmortem bifunctional staining

Bifunctional staining of the RIO dye refers to: (1) visualization, location and delineation of the AAR by using its red staining function for further morphometric quantification; and (2) microangiographic examination of the AAR by using the digital radiography (DR) function to compare the perfusion density rate (PDR) between the AAR and normal myocardium. This staining served as a postmortem index for regional myocardial blood flow. Briefly, after the last *in vivo* cMRI, the rabbit was IV injected with Heparin at 300 IU/kg to prevent coagulation. Under deep anesthesia and thoracotomy, the heart was excised with a section of the aortic arch isolated and pericardial tissue trimmed. As shown in Figure 3A, a plastic catheter filled with 0.9% saline was inserted into the aorta and anchored with its tip 1 cm above the aortic valves. Care was taken to avoid air bubbles entering the catheter that was connected to a 10 mL syringe fixed on the injection bump (BD PILOT, Becton Dickinson Infusion System, France). Under a perfusion pressure of 100 mmHg, 10 mL saline was infused until the eluate from the coronary sinus became clear. The heart was rinsed to wash out remaining blood. Then, the 5-0 suture spared at the coronary occlusion site during open-chest operation was tightened for causing re-occlusion, and 4 mL of RIO dye (Figure 3B) was infused through the aortic catheter for 15 min under the same pressure by using the same pump as mentioned above. The infusion was stopped when the normal myocardium was completely stained red by the RIO dye (Figure 3C). Upon this perfusion staining technique with the LCx re-ligated, the normal myocardium stained brick red and the AAR remained uncolored. Afterwards, the heart was imbedded in agar solution for *ex vivo* cMRI, followed by serial sectioning into 6-8 slices of 3.0 mm thickness to match with the corresponding short axis cMRI images. Such stained heart sections were exposed by DR with a mammographic unit (Embrace; Agfa-Ge-vaert, Mortsel, Belgium) at 25 KV and 18 mA, and photographed by a digital camera before and after 24 h of fixation with 10% formalin. The fixed heart sections were imbedded into paraffin and processed for histology with 5 micron thick hematoxylin-eosin (HE) stained slices for microscopic inspection.

Imaging analysis

The MI size on cMRI was determined in consensus by three authors with the built-in software of Siemens workstation (SyngoMR A30). To facilitate cardiac morphometric comparisons with different imaging methods, the dimension was calculated as a value relative to the entire left ventricular myocardium. The MI size (%) on DE cMRI was derived semi-automatically by computer to count all enhanced pixels with the signal intensity higher than two standard deviations above the mean of image intensities in the remote NM, which were divided by all ventricular pixels on the same short-axis image. Digital photographs of RIO-staining sections and DR images

Figure 3 Bifunctional staining methods. A: A plastic catheter filled with saline was inserted into the aorta and anchored with its tip 1 cm above the aortic valves, which was connected to a 10 mL syringe fixed in the injection bump. The heart was gently rinsed to wash out remaining blood, then the left circumflex coronary artery was re-ligated, and 2-4 mL of red iodized oil (RIO) dye was infused; B: Homemade RIO dye; C: Lateral view of the RIO perfused heart. The perfusion of RIO dye was stopped when the normal myocardium was stained completely scarlet red, while the area at risk remained unstained.

were transferred to a personal computer for planimetric analysis by using Image J 1.38x software (Research Services Branch, NIH, Bethesda, MD, United States). The AAR defined as non-stained area by RIO-dye and non-opaque area by DR was contoured with consensus on the computer screen. Due to partial volume effect and fatty tissue interference on DE cMRI, the apical and basal slices were excluded and the remaining slices (n = 25) obtained from 6 rabbits were used for the comparisons of the corresponding bifunctional staining sections.

Perfusion density rate measurement

The measurement of perfusion density rate (PDR%) measurement was performed on DR images of the heart sections using the same Image J 1.38x software. The blank myocardial density refers to the DR density of the heart tissues from control group (n = 3) without RIO dye staining. The AAR of low density and the normal myocardium of high density were delineated in all sections (n = 25) with an operator-defined region of interest. The mean gray value (GV) of all sections were automatically generated and normalized by the background GV. PDR% refers to the increased perfusion density relative to background, which was calculated by the following formula: $PDR\% = (GV_{\text{region of interest}}\text{-}GV_{\text{blank myocardial density}})/GV_{\text{background}} \times 100$.

Statistical analysis

Numerical data were expressed as mean ± SD. Comparisons among multiple factors were performed using one way ANOVA, followed by the Bonferroni's test to identify any differences between each two techniques. All tests were two tailed. The correlations were tested by Spearman's method. The linear regression and the means of Bland-Altman analysis were used for correlation and agreement, respectively. Correlations were described by the correlation coefficient with 95%CIs. A difference was considered statistically significant if the P value was less than 0.05. The paired student t test was used for comparison of the PDR between the AAR and MI. The statistical analyses were performed with Analyse-it® 2.14 for Excel and GraphPad Prism® 5.0.

RESULTS

General outcomes

All animals survived the anesthesia, surgical procedures for inducing acute reperfused MI and subsequent cMRI. As one of the critical steps, the double suture method was successfully applied in all animals, which ensured later bifunctional staining. The normal myocardium from all rabbits was well perfused by the RIO dye. Figure 4 demonstrated a case with a large reperfused MI by different techniques. The hyperenhanced transmural MI appeared similarly on both iDE and eDE (Figure 4A, B), which was somewhat smaller than the AAR as an unstained region by RIO (Figure 4C) and non-opacified region on DR (Figure 4D). With this bifunctional staining, the large haemorrhagic MI appeared brown greyish (Figure 4C) after overnight Formalin fixation. The myocardial necrosis

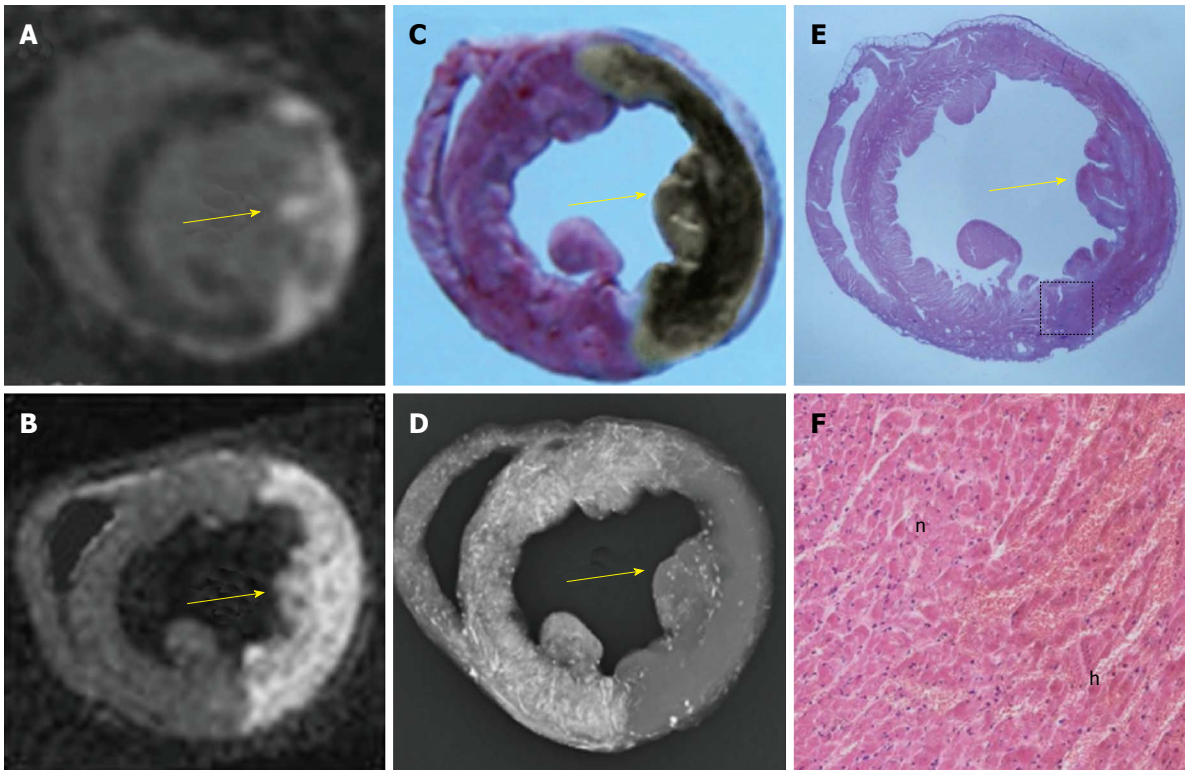

Figure 4 An example of a reperfused hemorrhagic myocardial infarction (arrow) shown by cardiac magnetic resonance imaging and the area at risk demonstrated with bifunctional staining method. A: The hyperenhanced transmural myocardial infarction (MI) was seen at the lateral wall on *in vivo* delay enhancement (DE) cardiac magnetic resonance imaging (cMRI); B: The *ex vivo* DE cMRI was highly correspondent with A; C: In contrast to the normal myocardium with red staining, the area at risk (AAR) was shown as an unstained region, on which the brown grayish area indicates a large intramural hemorrhagic infarction after the fixation by Formalin; D: On digital radiography (DR), the AAR was shown as non-opacified region in contrast to the opacified normal myocardium. Notice that the AAR defined by red iodized oil-staining (RIO-staining) in C and DR in D was somewhat larger than the MI defined by *in vivo* DE cMRI in A and *ex vivo* DE cMRI in B; E: The hematoxylin-eosin (HE) stained macroscopic view was obtained from the corresponding histological section of A, B, C, and D; F: Photomicroscopic view of the HE stained slice (magnification, × 100) confirmed the presence of myocardial necrosis with hemorrhage and tissue reaction. h: Hemorrhagic infarction; n: Adjacent normal myocardium with inflammatory infiltration.

with haemorrhage was finally confirmed by macro- and microscopic views of HE stained slice (Figure 4E, F).

Magnetic resonance imaging findings

The location and extent of the MI were clearly shown as the hyperenhanced region on DE cMRI in all cases. The percentage MI sizes globally (n = 6) and slice-by-slice (n = 25) were 36.59% and 35.41% on *in vivo* DEcMRI (iDE), and 32.88% and 32.40% on *ex vivo* DEcMRI (eDE). There was no significant difference between iDE and eDE. Linear regression analyses showed an excellent correlation both globally and slice-by-slice between MI volumes on iDE and eDE (r = 0.89, 0.98) (Figure 5A, B). By Bland-Altman analysis, there was a 1.2% bias with 95%CIs of 2.4% to 4.7% in global heart (Figure 5C) and 0.5% bias with 95%CIs of 2.6% to 3.6% by slice (Figure 5D), indicating high agreement of the two measurement methods.

Bifunctional staining findings with red-iodized-oil dye

The RIO dye was successfully formulated (Figure 3B). It showed homogenous distribution into the accessible cardiac tissues. After staining, the normal myocardium appeared scarlet red (Figure 3C) and rose red (Figure 4C) before and after formalin fixation and as more opacified region on DR images (Figure 4D), whereas the AAR showed as non-RIO-stained region on heart slices (Figure 4C) and the less opacified region on DR image (Figure 4D). By bifunctional staining, the percentage AAR_{global} was 44.8% ± 15.18% and 44.74% ± 15.98%, and percentage AAR_{slice} was 40.04% ± 13.64% and 40.48% ± 13.26% by RIO-staining and DR, respectively. There was no significant difference between RIO-staining and DR (P = 0.9). Linear regression analyses showed an excellent correlation both globally and slice-by-slice between AAR volumes defined by RIO-staining and DR (r = 0.99, 1.0) (Figure 6A, B). The limits of Bland-Altman agreement were 3.2%-3.0% (Figure 6C) by slice and 2.3%-1.8% (Figure 6D) in global measurements with RIO-staining and DR respectively. The mean difference was almost zero, indicating a very high agreement between RIO-staining and DR techniques.

Comparing different techniques

The MI quantified from both iDE and eDE cMRI were significantly smaller than the $AAR_{RIO\text{-}staining}$ and AAR_{DR} with bifunctional staining (P < 0.01; Figure 7), confirming that the final MI was smaller than ischemic region.

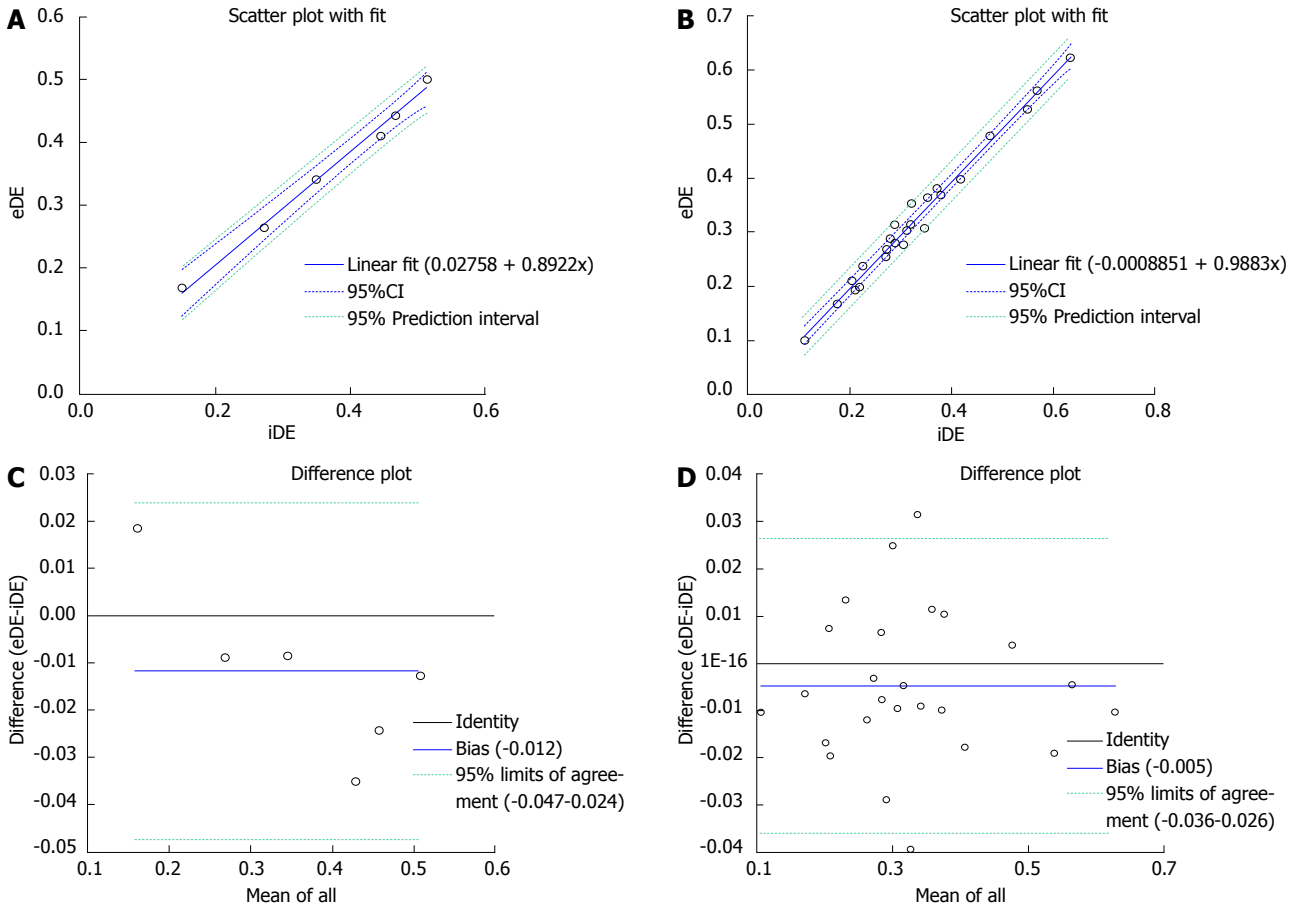

Figure 5 The linear correlation (above) and Bland-Altman analyses (bottom) plots comparing the myocardial infarction on *in vivo* and *ex vivo* delayed enhancement magnetic resonance imaging. The plots graph displayed a good correlation between MI measured with *in vivo* delayed enhancement (iDE) and *ex vivo* delayed enhancement (eDE) on global (A) and slices (B). Plots of differences in myocardial infarction on global (C) and slices (D) were indicative of high agreement between iDE and eDE.

However, the MI on eDE-cMRI correlated well with $AAR_{RIO\text{-}staining}$ and AAR_{DR} (Figure 8), suggesting that the bifunctional staining with RIO dye could successfully delineate and characterize the AAR.

Perfusion density rate

After aortic infusion with the RIO dye while the LCx was re-ligated, the PDR of the normal myocardium and AAR became 354.89% ± 35.18% and 32.28% ± 15.06% relative to the equipment background. The PDR was significantly lower in the AAR, *i.e.*, only about 9.10% ± 3.93% of the PDR in the normal myocardium ($P < 0.001$) (Figure 9), suggesting insufficient collateral coronary blood supply during the 90 min occlusion, leading to the rabbit model of reperfused MI.

DISCUSSION

We studied myocardial AAR in the rabbit heart after 90 min of LCx occlusion followed by reperfusion. The AAR refers to the myocardium without blood supply during coronary artery occlusion. The final MI was detected by *in vivo* and *ex vivo* DE cMRI. The main outcomes of the present study are: (1) the newly developed method of bifunctional staining enabled reliable high-quality images; (2) both *in vivo* and *ex vivo* DE cMRI allowed visualization and quantification of the MI; (3) though measured with different methods, the dimension of the AAR was significantly larger than that of the MI, suggesting the potential of this method to help discriminate the well perfused normal myocardium from the non-perfused nonviable and/or less perfused by viable probably salvageable myocardium; and (4) the PDR was 10 times lower in the AAR compared to the normal myocardium, suggesting that the bifunctional RIO dye may facilitate not only morphometry but also perfusion quantification.

The animal models of reperfused MI have been extensively applied for cardiovascular research both in large and small animals. How to accurately re-ligate coronary artery branch to replicate the exact occlusion site prior to reperfusion appears crucial. The majority of the authors used the snare-loop method for coronary artery occlusion-reperfusion on the open-chest MI model with later postmortem vessel re-ligation[24]. Other studies described re-occlusion of coronary branches with a balloon catheter under the close-chest conditions[25]. However, there is a lack of detailed information about how to imitate postmortem the exact *in vivo* artery occlusion, which

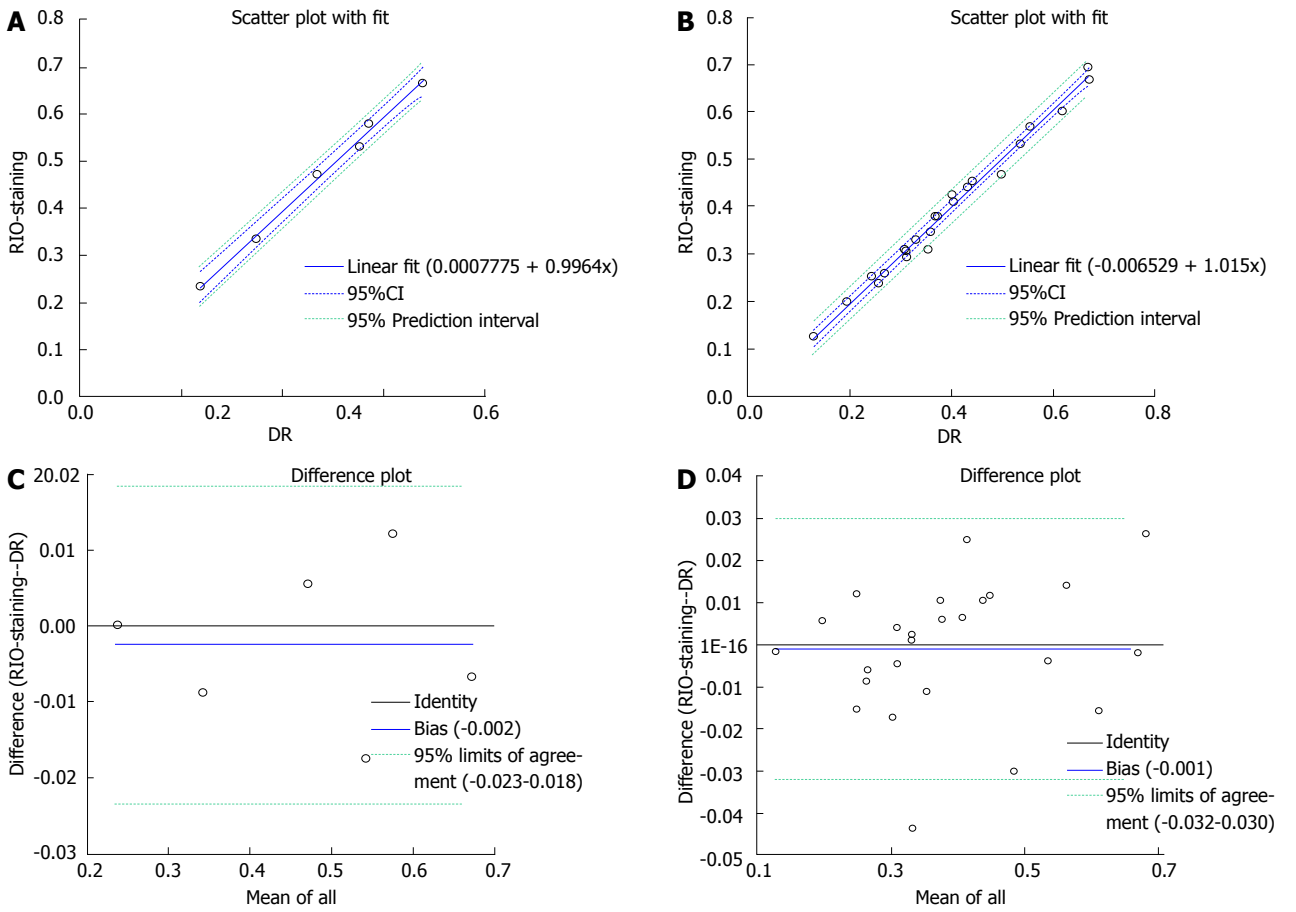

Figure 6 The linear correlations (above) and Bland-Altman analyses (bottom) to compare the area at risk by red iodized oil-staining and digital radiography of the bifunctional staining. The plots showed a good correlation between the area at risk (AAR) measured with red iodized oil (RIO)-staining and digital radiography (DR) on global (A) and slices (B). Plots of the differences in AAR on global (C) and slices (D) were almost zero, indicating that RIO-staining and DR are essentially equivalent.

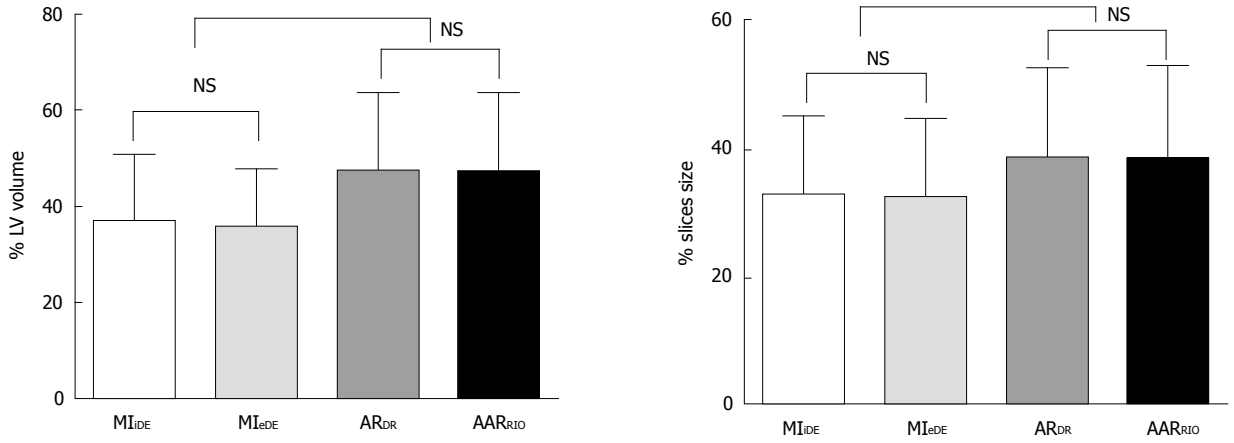

Figure 7 Comparisons between myocardial infarction and area at risk by different techniques. There were no significant differences between myocardial infarction *in vivo* delayed enhancement (MI iDE) and myocardial infarction *ex vivo* delayed enhancement (MI eDE) measured from cardiac magnetic resonance imaging in global (left) and slices (right). There were no significant differences between area at risk digital radiography (AAR_{DR}) and area at risk red iodized oil-staining ($AAR_{RIO\text{-}staining}$) in global (left) and slices (right).The significant differences were observed on AAR_{DR} *vs* MI iDE ($P < 0.01$); AAR_{DR} *vs* MI eDE ($P < 0.01$); $AAR_{RIO\text{-}staining}$ *vs* MI iDE ($P < 0.01$); $AAR_{RIO\text{-}staining}$ *vs* MI eDE ($P < 0.01$). NS: Not significant.

is though a prerequisite for defining the AAR or ischemic area. We have previously introduced an effective method for *in vivo* LCx occlusion and reperfusion[19]. In this study we modified that method by using the double sutures to precisely co-localize LCx obstruction both *in vivo* and *ex vivo*. Within the same puncture, one suture was for *in vivo* coronary occlusion and reperfusion, and the other suture was left spared *in vivo* but tightened with a knot to re-

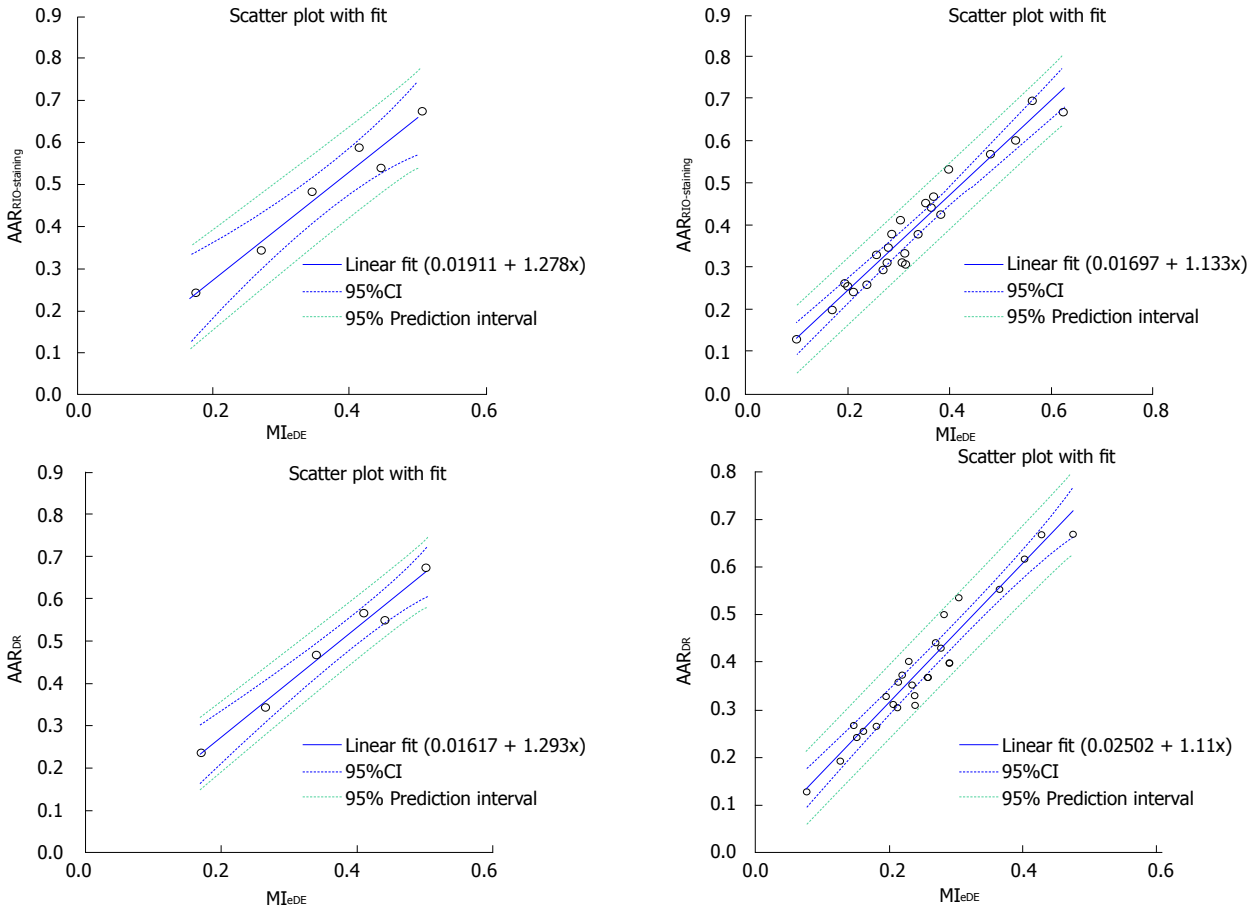

Figure 8 The linear correlations between *ex vivo* cardiac magnetic resonance imaging and bifunctional staining. The myocardial infarction (MI) measured by global (left) and slices (right) on *ex vivo* delayed enhancement cardiac magnetic resonance imaging corresponded well with area at risk by red iodized oil-staining (above) and digital radiography (bottom), confirming the bifunctional staining with RIO dye could successfully delineate and characterize the AAR. MI_{eDE}: Myocardial infarction *ex vivo* delayed enhancement; $AAR_{RIO\text{-}staining}$: Area at risk on red-iodized oil-staining; AAR_{DR}: Area at risk on digital radiography.

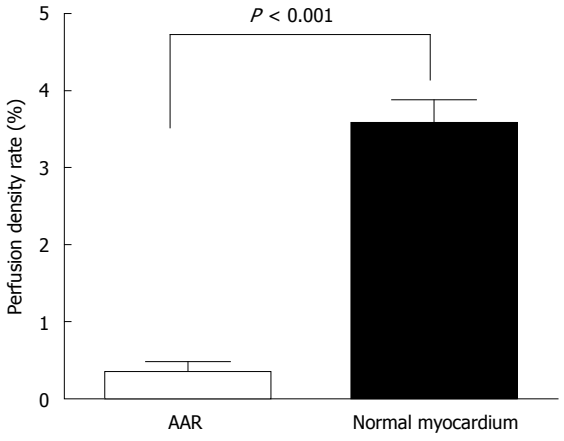

Figure 9 Comparison of perfusion density rate between area at risk and normal myocardium. Coronary artery occlusion caused a significant decrease of blood perfusion in ischemic region compared to non-ischemic region ($P < 0.001$), resulted in a difference over 10 times in-between. AAR: Area at risk.

occlude the coronary branch *ex vivo*. This double suture method was successfully validated in all animals, which is a critical step to ensure later bifunctional staining to obtain the desired results as presented.

In the cardiac imaging research on the ischemic heart disease using animal hearts, a most crucial issue is adequate staining of the AAR and discrimination between risk and non-risk zones, because a correctly defined borderline between the ischemic and necrotic zones will have a direct impact on MI diagnosis and therapeutic interventions. In this article we described a new bifunctional staining method to define the AAR, which, to our best knowledge, has not been reported in the literature. Function 1 is to visualize the normal myocardium in red color but the AAR uncolored utilizing the oil-red-o component of the custom-made RIO dye, which facilitates morphometric delineation, quantification and comparison; whereas function 2 is to enable visualization and volumetric density measurement of the non-opacified normal myocardium and the opacified AAR by utilizing the iodized oil component of the RIO dye for making DR to extrapolate, quantify and evaluate the difference in hemodynamic features such as coronary vessel density, interstitial distribution space and/or regional myocardial blood flow/volume between the normal and ischemic myocardium.

There have been some methods reported in the literature for postmortem delineation of the AAR. Coronary infusion of hydrophilic Evans-blue solution is the most

common technique to stain the remote myocardium while the insulted coronary branch is re-ligated[25-27]. Evans-blue is a water-soluble intravital dye with strong albumin binding capacity and has been used in hemodynamic studies for decades[28,29]. More recently Evans-blue has been found with high necrosis avidity and used to clearly mark the well-reperfused necrotic tissues[30-32]. Therefore, there is a risk of underestimation of the AAR due to contamination of the inwards diffused Evans-blue to the ischemic necrosis[15]. Some other groups tried to use TTC for demarcating the AAR, however TTC perfusion induced severe tissue contraction, which may affect the geometry of heart and might prevent subsequent successful dye perfusion[17]. Other studies used fluorescein dyes under dark background or radio- and color-labeled microspheres to define or quantify the AAR[33-35]. However, all these methods are only unifunctional and/or lacking required accuracy. The custom-made bifunctional RIO dye as introduced in this study appears a much better alternative to Evans blue. The first component of RIO dye is oil-red-O, which is a stable lipophilic pigment and can be easily diluted in any lipid media such as the iodized oil as the second component of this dye. The distribution of the RIO dye in the cardiac tissue after intracoronary infusion seems only pressure dependent rather than being diffusible afterwards driven by its concentration gradient due to the fact that a hydrophobic dye exists in the hydrophilic environment of myocardium, resulting in a more accurate delineation of the borders of the AAR without infiltration of the dye into the adjacent ischemic region.

Suspension of barium sulphate has also been used for postmortem coronary angiography[13,36]. However, the heavy particles tended to precipitate in its water media, leading to suboptimal perfusion to vascular bed with smaller vessels. As shown in this study, the second component of iodized oil in the RIO dye solved the problem well in DR and its quantification. Thus, the golden combination of the two dye components facilitated successfully the bifunctional staining and enabled comprehensive AAR study.

We have gained the following experiences: (1) heparinizing the animal prior to sacrifice and rinsing the coronary bed with normal saline beforehand proved beneficial for the next bifunctional staining of the AAR by RIO dye perfusion; (2) controlling adequate pressure and observing epicardial red coloration during dye infusion were crucial for the success of procedure; and (3) fixing the heart sections with formalin overnight helped color differentiation between the normal myocardium (rose red) and AAR (gray or brown grayish depending on the degree of hemorrhage) and later planimetric quantification due to a clear borderline.

Myocardial blood volume (capillary bed) and myocardial blood flow can be determined by microsphere methods in animals after excision of the heart[33,35]. Such methods, however, require cutting the myocardium into discrete samples, which may be a combination of normal tissue, border zone, hyperemic tissue, and severely ischemic tissue. Thus, the processing of selected tissue samples can bias the results as well as blur the exact relation to overall myocardial morphology. Although the degree of resolution for flow measurement could possibly be improved by cutting myocardium into smaller samples, this becomes tedious and impractical for studying flow throughout the heart. Besides, it is more difficult to get topographic information.

Using the PDR derived from microangiography on DR to indirectly evaluate vascular blood perfusion to viable and necrotic tissues has been reported[37]. In our experiment, The PDR was significantly lower in AAR, which was about 9% of the normal myocardium. This finding is close to the results of Connelly's group on myocardium blood flow measured by radioactive microspheres on the similar animal setting[38]. The other group showed that in the reperfusion MI dog model, myocardial samples with only mild (about 20%-30%) reductions in myocardial blood flow compared to non-ischemic regions[39], which appears higher than our results probably due to the richer collaterals of coronary artery in dogs than in rabbit[40]. The application of this new staining method on our rabbit model was successful and can be translated to other species.

Accurate quantitative measurement of MI size is an important aspect of cardiovascular research. The *in vivo* cMRI for accurate evaluation of MI has been described previously in rabbit models[19]. In this study we have performed the high resolution *ex vivo* cMRI with extensive postmortem evaluations on rabbit hearts, which were supported by histological staining and consistent to *in vivo* cMRI. The bifunctional staining could be incorporated into the study using clinically available MRI facilities to acquire outcomes that are more pertinent to human patients.

Study limitations

First, the AAR was demarcated by intracoronarily infusing the heart with the RIO dye after local re-occlusion. Such a procedure was time-consuming with possible technical failure to obtain homogeneous staining of all accessible normal myocardium. Secondly, the postmortem dye distribution may differ from *in vivo* blood perfusion of the normal myocardium when the related artery is occluded, because normal coronary flow is influenced by the intraventricular pressure so the flow in postmortem infusion may not exactly simulate the *in vivo* flow pattern. Furthermore, in this experiment by using RIO dye, we could achieve accurate delineation of the AAR postmortem, but we could hardly discriminate the MI from any ischemic but still viable tissues within the AAR. Considering these drawbacks, we have to further optimize this experimental setting for determination of both AAR and MI under both *in vivo* and *ex vivo* conditions.

In conclusion, this article introduced a novel bifunctional staining method to accurately visualize and quantify AAR postmortem, which was successfully applied in rab-

bit models with ischemia-reperfusion MI. The key advantages include a newly developed bifunctional RIO dye, a new *ex vivo* staining method with greater color intensity in the remote normal myocardium and improved contrast for border delineation to obtain both morphometric and functional information for reliable AAR measurement. This methodology is deemed of high research values and to substantially contribute to the translational research in cardiovascular sciences.

ACKNOWLEDGMENTS

The corresponding author Yicheng Ni is currently a Bayer Lecture Chair holder.

COMMENTS

Background

For developing therapeutic procedures/drugs aimed at modulating infarct size after coronary artery disease, it is important not only to measure myocardial infarction but also to know the extent of area at risk (AAR). However, determination of the AAR both *in vivo* and *ex vivo* can be challenging, and controversial.

Innovations and breakthroughs

In this experiment the authors sought to develop a reliable method to accurately localize the culprit coronary occlusion for postmortem verification after *in vivo* cardiac magnetic resonance imaging and to establish a new bifunctional staining as a standard reference for *ex vivo* area at risk identification, which may substantially contribute to translational cardiac imaging research.

Applications

The myocardial area at risk in ischemic heart disease could be accurately determined postmortem by this novel bifunctional staining, which may substantially contribute to translational cardiac imaging research.

Peer review

This is a conscientious and carefully written preclinical paper.

REFERENCES

1 **Aletras AH**, Tilak GS, Natanzon A, Hsu LY, Gonzalez FM, Hoyt RF, Arai AE. Retrospective determination of the area at risk for reperfused acute myocardial infarction with T2-weighted cardiac magnetic resonance imaging: histopathological and displacement encoding with stimulated echoes (DENSE) functional validations. *Circulation* 2006; **113**: 1865-1870 [PMID: 16606793 DOI: 10.1161/Circulationaha.105.576025]

2 **Berry C**, Kellman P, Mancini C, Chen MY, Bandettini WP, Lowrey T, Hsu LY, Aletras AH, Arai AE. Magnetic resonance imaging delineates the ischemic area at risk and myocardial salvage in patients with acute myocardial infarction. *Circ Cardiovasc Imaging* 2010; **3**: 527-535 [PMID: 20631034 DOI: 10.1161/Circimaging.109.900761]

3 **Darsee JR**, Kloner RA, Braunwald E. Demonstration of lateral and epicardial border zone salvage by flurbiprofen using an in vivo method for assessing myocardium at risk. *Circulation* 1981; **63**: 29-35 [PMID: 7002363 DOI: 10.1161/01.CIR.63.1.29]

4 **Mewton N**, Rapacchi S, Augeul L, Ferrera R, Loufouat J, Boussel L, Micolich A, Rioufol G, Revel D, Ovize M, Croisille P. Determination of the myocardial area at risk with pre- versus post-reperfusion imaging techniques in the pig model. *Basic Res Cardiol* 2011; **106**: 1247-1257 [PMID: 21874556 DOI: 10.1007/s00395-011-0214-8]

5 **Friedrich MG**, Abdel-Aty H, Taylor A, Schulz-Menger J, Messroghli D, Dietz R. The salvaged area at risk in reperfused acute myocardial infarction as visualized by cardiovascular magnetic resonance. *J Am Coll Cardiol* 2008; **51**: 1581-1587 [PMID: 18420102 DOI: 10.1016/j.jacc.2008.01.019]

6 **Ceriani L**, Verna E, Giovanella L, Bianchi L, Roncari G, Tarolo GL. Assessment of myocardial area at risk by technetium-99m sestamibi during coronary artery occlusion: comparison between three tomographic methods of quantification. *Eur J Nucl Med* 1996; **23**: 31-39 [PMID: 8586099]

7 **Villanueva FS**, Glasheen WP, Sklenar J, Kaul S. Characterization of spatial patterns of flow within the reperfused myocardium by myocardial contrast echocardiography. Implications in determining extent of myocardial salvage. *Circulation* 1993; **88**: 2596-2606 [PMID: 8252670 DOI: 10.1161/01.CIR.88.6.2596]

8 **Arai AE**, Leung S, Kellman P. Controversies in cardiovascular MR imaging: reasons why imaging myocardial T2 has clinical and pathophysiologic value in acute myocardial infarction. *Radiology* 2012; **265**: 23-32 [PMID: 22993218 DOI: 10.1148/radiol.12112491]

9 **Bondarenko O**, Beek AM, Hofman MB, Kühl HP, Twisk JW, van Dockum WG, Visser CA, van Rossum AC. Standardizing the definition of hyperenhancement in the quantitative assessment of infarct size and myocardial viability using delayed contrast-enhanced CMR. *J Cardiovasc Magn Reson* 2005; **7**: 481-485 [PMID: 15881532]

10 **Oshinski JN**, Yang Z, Jones JR, Mata JF, French BA. Imaging time after Gd-DTPA injection is critical in using delayed enhancement to determine infarct size accurately with magnetic resonance imaging. *Circulation* 2001; **104**: 2838-2842 [PMID: 11733404 DOI: 10.1161/hc4801.100351]

11 **Kim RJ**, Fieno DS, Parrish TB, Harris K, Chen EL, Simonetti O, Bundy J, Finn JP, Klocke FJ, Judd RM. Relationship of MRI delayed contrast enhancement to irreversible injury, infarct age, and contractile function. *Circulation* 1999; **100**: 1992-2002 [PMID: 10556226 DOI: 10.1161/01.CIR.100.19.1992]

12 **Lowe JE**, Reimer KA, Jennings RB. Experimental infarct size as a function of the amount of myocardium at risk. *Am J Pathol* 1978; **90**: 363-379 [PMID: 623206]

13 **Ohzono K**, Koyanagi S, Urabe Y, Harasawa Y, Tomoike H, Nakamura M. Transmural distribution of myocardial infarction: difference between the right and left ventricles in a canine model. *Circ Res* 1986; **59**: 63-73 [PMID: 3731411 DOI: 10.1161/01.RES.59.1.63]

14 **Hale SL**, Alker KJ, Kloner RA. Evaluation of nonradioactive, colored microspheres for measurement of regional myocardial blood flow in dogs. *Circulation* 1988; **78**: 428-434 [PMID: 3396179]

15 **Redel A**, Jazbutyte V, Smul TM, Lange M, Eckle T, Eltzschig H, Roewer N, Kehl F. Impact of ischemia and reperfusion times on myocardial infarct size in mice in vivo. *Exp Biol Med* (Maywood) 2008; **233**: 84-93 [PMID: 18156310 DOI: 10.3181/0612-RM-308]

16 **Khalil PN**, Siebeck M, Huss R, Pollhammer M, Khalil MN, Neuhof C, Fritz H. Histochemical assessment of early myocardial infarction using 2,3,5-triphenyltetrazolium chloride in blood-perfused porcine hearts. *J Pharmacol Toxicol Methods* 2006; **54**: 307-312 [PMID: 16580232 DOI: 10.1016/j.vascn.2006.02.010]

17 **Bohl S**, Medway DJ, Schulz-Menger J, Schneider JE, Neubauer S, Lygate CA. Refined approach for quantification of in vivo ischemia-reperfusion injury in the mouse heart. *Am J Physiol Heart Circ Physiol* 2009; **297**: H2054-H2058 [PMID: 19820193 DOI: 10.1152/ajpheart.00836]

18 **Rodrigues AC**, Hataishi R, Ichinose F, Bloch KD, Derumeaux G, Picard MH, Scherrer-Crosbie M. Relationship of systolic dysfunction to area at risk and infarction size after ischemia-reperfusion in mice. *J Am Soc Echocardiogr* 2004; **17**: 948-953 [PMID: 15337959 DOI: 10.1016/j.echo.2004.05.014]

19 **Feng Y**, Xie Y, Wang H, Chen F, Ye Y, Jin L, Marchal G, Ni Y. A modified rabbit model of reperfused myocardial infarction for cardiac MR imaging research. *Int J Cardiovasc*

Imaging 2009; **25**: 289-298 [PMID: 19043805 DOI: 10.1007/s10554-008-9393-2]
20 **Feng Y,** Chen F, Xie Y, Wang H, Cona MM, Yu J, Li J, Bogaert J, Janssens S, Oyen R, Ni Y. Lipomatous metaplasia identified in rabbits with reperfused myocardial infarction by 3.0 T magnetic resonance imaging and histopathology. *BMC Med Imaging* 2013; **13**: 18 [PMID: 23815556 DOI: 10.1186/1471-2342-13-18]
21 **van der Laarse A**, van der Wall EE. Rabbit models: ideal for imaging purposes? *Int J Cardiovasc Imaging* 2009; **25**: 299-301 [PMID: 19085084 DOI: 10.1007/s10554-008-9401-6]
22 **Eurvilaichit C**. Lipiodol enhanced CT scanning of malignant hepatic tumors. *J Med Assoc Thai* 2000; **83**: 398-406 [PMID: 10808700]
23 **Kurokohchi K**, Deguchi A, Masaki T, Himoto T, Yoneyama H, Kobayashi M, Maeta T, Kiuchi T, Kohi F, Miyoshi H, Taminato T, Kuriyama S. Successful treatment of hypovascular advanced hepatocellular carcinoma with lipiodol-targetting intervention radiology. *World J Gastroenterol* 2007; **13**: 4398-4400 [PMID: 17708619]
24 **Higuchi T**, Taki J, Nakajima K, Kinuya S, Namura M, Tonami N. Time course of discordant BMIPP and thallium uptake after ischemia and reperfusion in a rat model. *J Nucl Med* 2005; **46**: 172-175 [PMID: 15632049 DOI: 46/1/172]
25 **Dębiński M**, Buszman PP, Milewski K, Wojakowski W, Jackiewicz W, Pająk J, Szurlej D, Fryc-Stanek J, Wiernek S, Jelonek M, Spurlock ME, Martin J, Bochenek A, Buszman PE. Intracoronary adiponectin at reperfusion reduces infarct size in a porcine myocardial infarction model. *Int J Mol Med* 2011; **27**: 775-781 [PMID: 21399860 DOI: 10.3892/ijmm.2011.643]
26 **Michael LH**, Entman ML, Hartley CJ, Youker KA, Zhu J, Hall SR, Hawkins HK, Berens K, Ballantyne CM. Myocardial ischemia and reperfusion: a murine model. *Am J Physiol* 1995; **269**: H2147-H2154 [PMID: 8594926]
27 **Poulsen RH**, Bøtker HE, Rehling M. Postreperfusion myocardial technetium-99m-sestamibi defect corresponds to area at risk: experimental results from an ischemia-reperfusion porcine model. *Nucl Med Biol* 2011; **38**: 819-825 [PMID: 21843777 DOI: 10.1016/j.nucmedbio.2011.02.008]
28 **Heltne JK**, Farstad M, Lund T, Koller ME, Matre K, Rynning SE, Husby P. Determination of plasma volume in anaesthetized piglets using the carbon monoxide (CO) method. *Lab Anim* 2002; **36**: 344-350 [PMID: 12144744 DOI: 10.1258/002367702320162333]
29 **Fry DL**. Certain histological and chemical responses of the vascular interface to acutely induced mechanical stress in the aorta of the dog. *Circ Res* 1969; **24**: 93-108 [PMID: 5763742]
30 **Ni Y.** Metalloporphyrins and functional analogues as MRI contrast agents. *Curr Med Imaging Rev* 2008; **4**: 96-112 [DOI: 10.2174/157340508784356789]
31 **Li J**, Cona MM, Chen F, Feng Y, Zhou L, Yu J, Nuyts J, de Witte P, Zhang J, Himmelreich U, Verbruggen A, Ni Y. Exploring theranostic potentials of radioiodinated hypericin in rodent necrosis models. *Theranostics* 2012; **2**: 1010-1019 [PMID: 23139728 DOI: 10.7150/thno.4924]
32 **Wang H**, Miranda Cona M, Chen F, Li J, Yu J, Feng Y, Peeters R, De Keyzer F, Marchal G, Ni Y. Comparison between nonspecific and necrosis-avid gadolinium contrast agents in vascular disrupting agent-induced necrosis of rodent tumors at 3.0T. *Invest Radiol* 2011; **46**: 531-538 [PMID: 21577133 DOI: 10.1097/Rli.0b013e31821a2116]
33 **Malik AB**, Kaplan JE, Saba TM. Reference sample method for cardiac output and regional blood flow determinations in the rat. *J Appl Physiol* 1976; **40**: 472-475 [PMID: 931866]
34 **Deveci D**, Egginton S. Development of the fluorescent microsphere technique for quantifying regional blood flow in small mammals. *Exp Physiol* 1999; **84**: 615-630 [PMID: 10481220]
35 **Chien GL**, Anselone CG, Davis RF, Van Winkle DM. Fluorescent vs. radioactive microsphere measurement of regional myocardial blood flow. *Cardiovasc Res* 1995; **30**: 405-412 [PMID: 7585832 DOI: 0008-6363(95)00060-7]
36 **Jugdutt BI**, Hutchins GM, Bulkley BH, Pitt B, Becker LC. Effect of indomethacin on collateral blood flow and infarct size in the conscious dog. *Circulation* 1979; **59**: 734-743 [PMID: 421313]
37 **Wang H**, Sun X, Chen F, De Keyzer F, Yu J, Landuyt W, Vandecaveye V, Peeters R, Bosmans H, Hermans R, Marchal G, Ni Y. Treatment of rodent liver tumor with combretastatin a4 phosphate: noninvasive therapeutic evaluation using multiparametric magnetic resonance imaging in correlation with microangiography and histology. *Invest Radiol* 2009; **44**: 44-53 [PMID: 19034028 DOI: 10.1097/RLI.0b013e31818e5Ace]
38 **Connelly CM**, Leppo JA, Weitzman PW, Vogel WM, Apstein CS. Effect of coronary occlusion and reperfusion on myocardial blood flow during infarct healing. *Am J Physiol* 1989; **257**: H365-H374 [PMID: 2764125]
39 **Chu A**, Cobb FR. Reperfusion alters the relation between blood flow and the remaining myocardial infarction. *Circulation* 1989; **79**: 884-889 [PMID: 2924418]
40 **Feng Y,** Xie Y, Wang H, Chen F, Marchal G, Ni Y. Animal models of ischemic heart disease for cardiac MR imaging research. *Int J MIC* 2010; **9**: 288-310 [DOI: 10.1504/IJMIC.2010.032809]

P- Reviewer Chang ST **S- Editor** Song XX **L- Editor** A
E- Editor Lu YJ

ISSN 2222-0682 (online)

World Journal of *Methodology*

World J Methodol 2013 December 26; 3(4): 39-69

Volume End

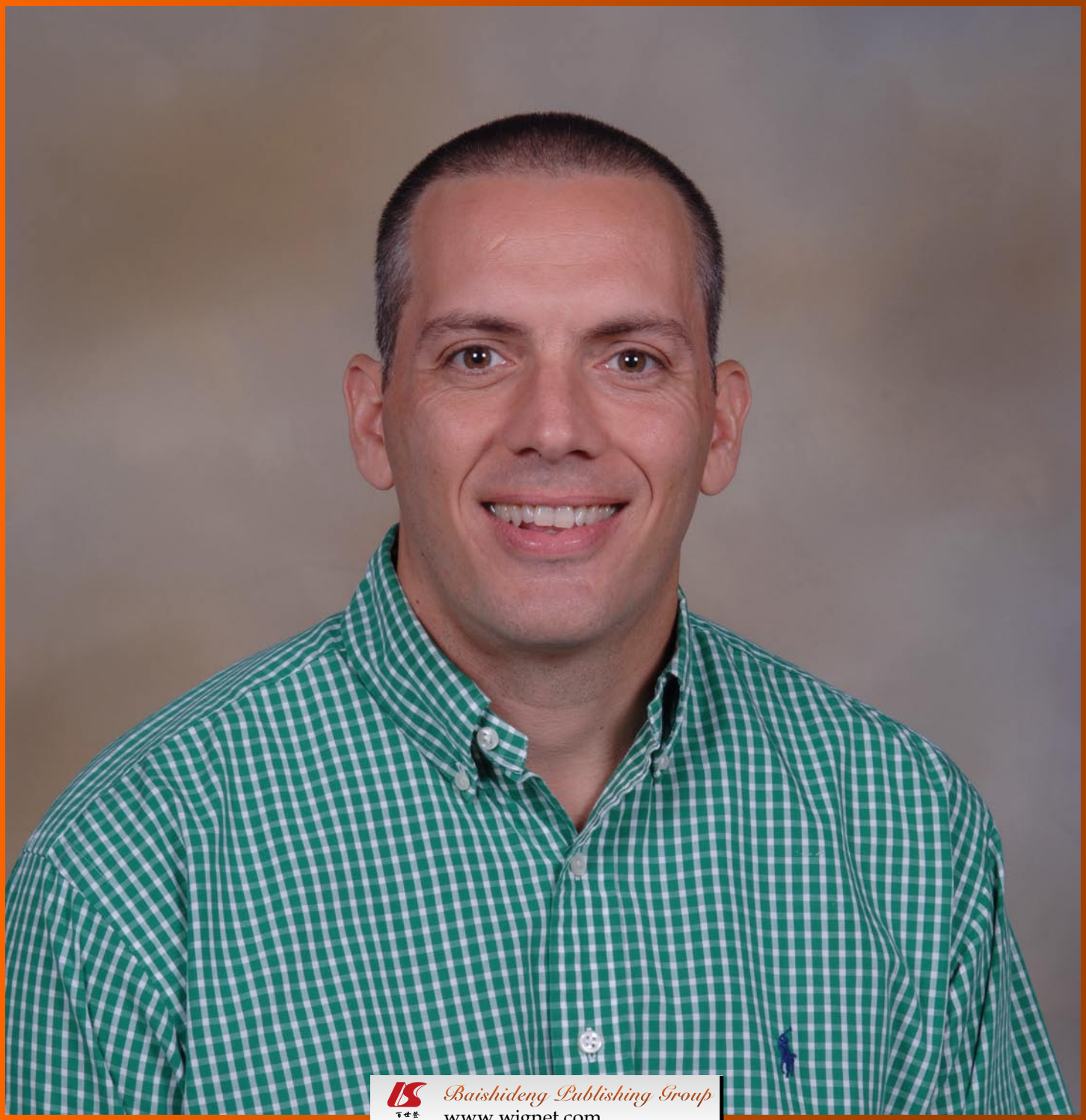

Baishideng Publishing Group
www.wjgnet.com

World Journal of Methodology

Contents

Quarterly Volume 3 Number 4 December 26, 2013

AIM AND SCOPE

World Journal of Methodology (*World J Methodol*, *WJM*, online ISSN 2222-0682, DOI: 10.5662) is a peer-reviewed open access academic journal that aims to guide clinical practice and improve diagnostic and therapeutic skills of clinicians.

The primary task of *WJM* is to rapidly publish high-quality original articles, reviews, and commentaries that deal with the methodology to develop, validate, modify and promote diagnostic and therapeutic modalities and techniques in preclinical and clinical applications. *WJM* covers topics concerning the subspecialties including but not exclusively anesthesiology, cardiac medicine, clinical genetics, clinical neurology, critical care, dentistry, dermatology, emergency medicine, endocrinology, family medicine, gastroenterology and hepatology, geriatrics and gerontology, hematology, immunology, infectious diseases, internal medicine, obstetrics and gynecology, oncology, ophthalmology, orthopedics, otolaryngology, radiology, serology, pathology, pediatrics, peripheral vascular disease, psychiatry, radiology, rehabilitation, respiratory medicine, rheumatology, surgery, toxicology, transplantation, and urology and nephrology.

INDEXING/ABSTRACTING

World Journal of Methodology is now indexed in Digital Object Identifier.

NAME OF JOURNAL
World Journal of Methodology

ISSN
ISSN 2222-0682 (online)

LAUNCH DATE
September 26, 2011

FREQUENCY
Quarterly

EDITOR-IN-CHIEF
Yicheng Ni, MD, PhD, Professor, Department of Radiology, University Hospitals, KU, Leuven, Herestraat 49, B-3000, Leuven, Belgium

EDITORIAL OFFICE
Jin-Lei Wang, Director
Xiu-Xia Song, Vice Director

World Journal of Methodology
Room 903, Building D, Ocean International Center, No. 62 Dongsihuan Zhonglu, Chaoyang District, Beijing 100025, China
Telephone: +86-10-59080039
Fax: +86-10-85381893
E-mail: bpgoffice@wjgnet.com
http://www.wjgnet.com

PUBLISHER
Baishideng Publishing Group Co., Limited
Flat C, 23/F., Lucky Plaza, 315-321 Lockhart Road, Wanchai, Hong Kong, China
Fax: +852-65557188
Telephone: +852-31779906
E-mail: bpgoffice@wjgnet.com
http://www.wjgnet.com

PUBLICATION DATE
December 26, 2013

INSTRUCTIONS TO AUTHORS
Full instructions are available online at http://www.wjgnet.com/2222-0682/g_info_20100722180909.htm

ONLINE SUBMISSION
http://www.wjgnet.com/esps/

World Journal of Methodology

Online Submissions: http://www.wjgnet.com/esps/
bpgoffice@wjgnet.com
doi:10.5662/wjm.v3.i4.39

World J Methodol 2013 December 26; 3(4): 39-44
ISSN 2222-0682 (online)

REVIEW

Sonoporation: Gene transfer using ultrasound

Minoru Tomizawa, Fuminobu Shinozaki, Yasufumi Motoyoshi, Takao Sugiyama, Shigenori Yamamoto, Makoto Sueishi

Minoru Tomizawa, Department of Gastroenterology, National Hospital Organization Shimoshizu Hospital, 934-5 Shikawatashi, Yotsukaido City, Chiba 284-0003, Japan
Fuminobu Shinozaki, Department of Radiology, National Hospital Organization Shimoshizu Hospital, 934-5 Shikawatashi, Yotsukaido City, Chiba 284-0003, Japan
Yasufumi Motoyoshi, Department of Neurology, National Hospital Organization Shimoshizu Hospital, 934-5 Shikawatashi, Yotsukaido City, Chiba 284-0003, Japan
Takao Sugiyama, Makoto Sueishi, Department of Rheumatology, National Hospital Organization Shimoshizu Hospital, 934-5 Shikawatashi, Yotsukaido City, Chiba 284-0003, Japan
Shigenori Yamamoto, Department of Pediatrics, National Hospital Organization Shimoshizu Hospital, 934-5 Shikawatashi, Yotsukaido City, Chiba 284-0003, Japan
Author contributions: Tomizawa M wrote the manuscript; Shinozaki F described the figures; Motoyoshi Y, Yamamoto S, Sugiyama T and Sueishi M supervised the manuscript.
Correspondence to: Minoru Tomizawa, MD, PhD, Department of Gastroenterology, National Hospital Organization Shimoshizu Hospital, 934-5 Shikawatashi, Yotsukaido City, Chiba 284-0003, Japan. nihminor-cib@umin.ac.jp
Telephone: +81-43-4222511 Fax: +81-43-4213007
Received: October 10, 2013 Revised: December 4, 2013
Accepted: December 12, 2013
Published online: December 26, 2013

Abstract

Genes can be transferred using viral or non-viral vectors. Non-viral methods that use plasmid DNA and short interference RNA (siRNA) have advantages, such as low immunogenicity and low likelihood of genomic integration in the host, when compared to viral methods. Non-viral methods have potential merit, but their gene transfer efficiency is not satisfactory. Therefore, new methods should be developed. Low-frequency ultrasound irradiation causes mechanical perturbation of the cell membrane, allowing the uptake of large molecules in the vicinity of the cavitation bubbles. The collapse of these bubbles generates small transient holes in the cell membrane and induces transient membrane permeabilization. This formation of small pores in the cell membrane using ultrasound allows the transfer of DNA/RNA into the cell. This phenomenon is known as sonoporation and is a gene delivery method that shows great promise as a potential new approach in gene therapy. Microbubbles lower the threshold of cavity formation. Complexes of therapeutic genes and microbubbles improve the transfer efficiency of genes. Diagnostic ultrasound is potentially a suitable sonoporator because it allows the real-time monitoring of irradiated fields.

Key words: Gene therapy; Cavity; Microbubbles; Contrast agent; Diagnostic ultrasound

Core tip: Ultrasound causes cavitation bubbles to form cell membrane pores through which DNA/RNA are transferred. This phenomenon is known as sonoporation. Microbubbles lower the threshold of cavity formation. Sonoporation is less toxic and not associated with tumorigenicity as compared with retroviral and adenoviral vectors. Sonoporation does not require surgical procedure and enhances gene transfer with lipofection. Current limitations of sonoporation are low efficiency of gene transfer and damage of target cells are The use of complexes with chemicals and diagnostic ultrasound are promising approaches to overcome these limitations.

Tomizawa M, Shinozaki F, Motoyoshi Y, Sugiyama T, Yamamoto S, Sueishi M. Sonoporation: Gene transfer using ultrasound. *World J Methodol* 2013; 3(4): 39-44 Available from: URL: http://www.wjgnet.com/2222-0682/full/v3/i4/39.htm DOI: http://dx.doi.org/10.4329/wjm.v3.i4.39

INTRODUCTION

Gene therapy is a promising approach to treat diseases

and is applicable to tissue engineering controlling differentiation of cells to form tissues[1,2]. Therapeutic genes are transferred using viral or non-viral vectors. Viral vectors are mainly retroviral vectors, adenoviral vectors and adeno-associated vectors. Retroviral vectors are the cause of tumorigenicity[3]. Adenoviral vectors provoke a severe systemic immune response[4]. Adeno-associated vectors do not cause major immune response, but they are not permissive to some types of cells[5]. On the other hand, plasmid DNA does not induce host immune responses because exogenous proteins such as viral capsid proteins are not produced[6]. Moreover, plasmid DNA rarely integrates with the host genome upon introduction into target cells and not associated with tumorigenicity[3,7]. Plasmid DNA is safe for gene transfer therapy, but its transfer efficiency is low. Methods should therefore be developed to improve transfection efficiency of plasmid DNA. Irradiation with low-output intensity ultrasound causes mechanical perturbation in the vicinity of cavitation bubbles. Collapse of the bubbles generates small transient holes in the cell membrane and induces cell membrane permeabilization. The membrane poration (cavitation) increases the efficiency of drug and gene delivery. This phenomenon, sonoporation, is a gene delivery technique that could potentially be used for gene therapy. Sonoporation, a method for targeted drug delivery and non-viral gene transfection, has new and advantageous possibilities. Sonoporation stimulates endocytosis of adno-associated virus and enhances efficiency of gene transfer[8,9]. However, no clinical trials using sonoporation have been reported to date because it is not yet a satisfactory technique for efficient and reliable gene transfer. In this chapter, we will review the potential application of sonoporation in gene therapy, with a focus on mircobubbles as a drug delivery agent. We will also discuss other non-viral delivery methods. Finally, we will outline the future direction of ultrasound-assisted gene delivery aiming at improvement of sonoporation and enhancement of gene expression for clinical applications.

NON-VIRAL GENE DELIVERY

In this section, we review non-viral gene delivery methods. Gene therapy requires the delivery of nucleic acid material to target tissues and its entry into target cells. Given that DNA and the cell membrane are both negatively charged, electrostatic forces result in the repulsion of DNA by the cell membrane. To overcome this limitation, a physical or chemical approach needs to be applied. Another restriction of gene transfer is the rapid degradation of DNA by nucleases in the plasma after systemic administration.

Electroporation

Electroporation is useful for gene transfer to primary cells. Primary cells are not introduced with genes with lipofection. Electroporation is the only method to introduce genes to cells, auch as normal human dermal fibroblasts[10]. Electroporation, in which high-voltage electrical currents create transient pores on the cell membranes, allows the transport of nucleic acid material into the cell[11]. Therapeutic genes are successfully transferred *in vivo*[12]. The electroporation method, however, has limitations such as short range of gene transfer, necessity of a surgical procedure, and tissue damage. Distance between electrodes normally requires 1 cm and is not suitable for a large area. Placement of internal electrodes requires a surgical procedure, and high voltage can damage tissue when applied. Therefore, less invasive methods are desirable.

Lipofection

Chemical non-viral vectors have been studied because they are generally considered safer than viral vectors. In addition to safety, liposomes can transfer larger genes with less toxicity and are relatively easy to prepare. Cationic lipids and polymers form complexes with negatively charged DNA. The complexes protect the DNA from nucleases and increase the effectiveness of transfection through the cell membrane. One major problem with lipofection is low efficiency of gene transfer. Transfection efficiency of lipofection is improved by condensing DNA with a double chain monovalent quaternary ammonium lipid[13]. Still genes are not introduced to target cells efficiently. More efficient methods have been waited.

Sonoporation

Sonoporation refers to the formation of small pores in cell membranes by using ultrasound for the transfer of nucleic acid materials (Figure 1). The biological effects of ultrasound are categorized as thermal and non-thermal. Non-thermal effects are composed of mechanical perturbation in the vicinity of bubbles. Cavitation bubbles cause membrane poration[14]. High speed camera images reveal that the cell membrane is fractionated, and cavitation bubbles are formed[15]. The cavitation bubbles induce cell death or permeability to allow the entry of a drug or genes into the cells. Sonoporation is similar to electroporation, wherein DNA is driven by an electrical force along the electric field. Sonoporation is mediated by passive diffusion. The transfer efficiency depends on ultrasound frequency and intensity[16]. The major advantages of sonoporation are its non-invasiveness and ability to transfer genes to internal organs without a surgical procedure[17]. Targeted gene transfer can be facilitated by ultrasound irradiation of selected tissues after systemic administration[18].

SONOPORATION

Emergence of sonoporation

Drug delivery with ultrasound was first reported by Tachibana *et al*[16]. The delivery of insulin on the skin surface when exposed to ultrasound energy in the range of 3000-5000 Pa or 5000-8000 Pa at 48 kHz for 5 min decreased blood glucose levels to 22.4% of the control

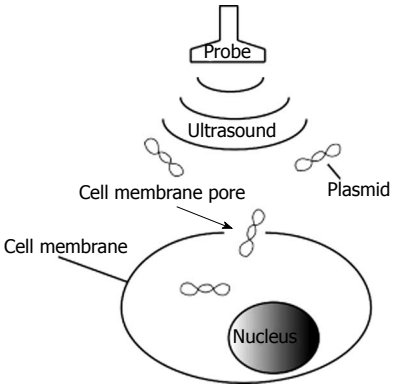

Figure 1 Formation of cell membrane pores after ultrasound irradiation. Nucleic acid such as plasmids enters the cells through the membrane pores that are formed with ultrasound.

in 120 min. It was postulated that insulin absorption increased with ultrasound vibration after intradermal injection. This report is interesting because it demonstrates the potential of ultrasound as a method to improve absorption of therapeutic materials. With ultrasound, chemotherapeutic agents are more efficiently absorbed in the mouse xenograft model of cancer[19].

In vitro experiments are simplified models to investigate the mechanisms of sonoporation *in vivo*. Fechheimer *et al*[20] transferred plasmid DNA encoding the G418 resistance gene to cultured mouse fibroblasts by sonoporation. Colonies were observed after G418 was added to the media. This was the first report demonstrating that plasmid DNA can be transferred to cells *in vitro* by using ultrasound. Kim *et al*[21] also reported that rat joint cells can be successfully transfected with plasmid DNA. Plasmid DNA encoding green fluorescent protein (GFP) was injected as a reporter of expression into the left ventricle of mice percutaneously[22]. Mice were irradiated with transthoracic ultrasound at 1 MHz for 1 min. Histological examination showed GFP expression in the subendocardial myocardium. Intraventricular co-injection of siRNA and GFP exhibited reduced expression of GFP in the coronary artery. These data indicate that plasmid DNA and siRNA can be introduced into cells *in vivo* by sonoporation.

Mechanism of sonoporation

Biophysical effects of ultrasound include cavitation, radiation pressure, and microstreaming[23]. Cavitation refers to the growth and collapse of microbubbles. Radiation pressure is the force in the irradiation field. Microstreaming is the shear forces that exist near the microbubbles. Formation of cavitation increases with a rising ultrasound intensity while the frequency decreases[24]. Mechanical index (MI) is defined as PRP/$\sqrt{F0}$ (PRP: peak rarefactional pressure; $\sqrt{F0}$: transmission center frequency)[25]. MI should be lower than 1.9 for clinical use of ultrasound. Forsberg *et al*[26] reported that cavitation is unlikely to occur at an MI of less than 0.7. Cavitation has been well investigated with ultrasound contrast agents because microbubbles lower the threshold of cavitation[27]. Zhou *et al*[28] developed a device to observe the behavior of a single bubble near the cell membrane. The motion of a single bubble was monitored with a high-speed camera. Cell membrane disruption was assessed by monitoring the transmembrane current. This study showed that a single microbubble expands and contracts with ultrasound irradiation. When the bubble collapses, the cell membrane is ruptured and a pore is generated. Changes in membrane permeability are directly correlated with the formation of pores. Carugo *et al*[29] reported that a standing wave is involved in sonoporation in the absence of microbubbles.

Microbubbles

The presence of microbubbles reduces the threshold of cavitation. Microbubble contrast agents are spheres filled with gas and stabilized with shells. Their size ranges between 1 and 10 μm[30]. They are small enough to circulate in blood vessels, but do not exit from the vessels. The contrast agents scatter ultrasound stronger than the surrounding blood and tissue. Thus, they are used as contrast agents for daily clinical practice. Tachibana *et al*[31] reported that albumin microbubbles (Albumex) accelerate thrombolysis by ultrasound. This was the first report that microbubbles improve the effects of ultrasound in tissues for purposes other than diagnostic imaging. Transfection of plasmid DNA into rat joint cells was improved in the presence of Albumex[21]. This report paved the way for the utilization of ultrasound contrast agents in sonoporation. Microbubbles expand and contract in response to compression and rarefaction of ultrasound (Figure 2). The microbubbles collapse at the high-pressure phase, emitting shock waves that perturb the cell membrane and increase permeability. Qiu *et al*[32] reported that pores on the cell membrane, generated by sonoporation with microbubbles, ranged from 100 nm to 1.25 μm in size. Their experiments used 1 MHz ultrasound at low acoustic pressures from 0.05 to 0.3 MPa. The pores generated with sonoporation were examined by scanning electron microscopy. The size of the pores enlarged with increased acoustic pressure or longer treatment. They concluded that the pores formed with shear stress. Liquid microjet, visualized with a high-speed camera in cultured cells exposed to single-shot short-pulsed ultrasound has been demonstrated[33]. Contrast agents are shells containing gas. Ultrasound scatters on the surface of contrast agents, and are visible as high echo on the display of diagnostic ultrasound. Physical and biological characteristics of contrast agents are basically the same as those of microbubbles. When a contrast agent (Levovist) was added to the media, the jet caused cell membrane damage. Interestingly, the cell membrane repair process suggests that the Ca^{2+}-independent and Ca^{2+}-trigger mechanisms are involved in rapid resealing. Positively charged microbubbles are more efficient in gene transfer than neutral ones[34]. It is hypothesized that positively charged microbubbles are more close to the cell membrane to enable more efficient gene transfer. Plasmids are

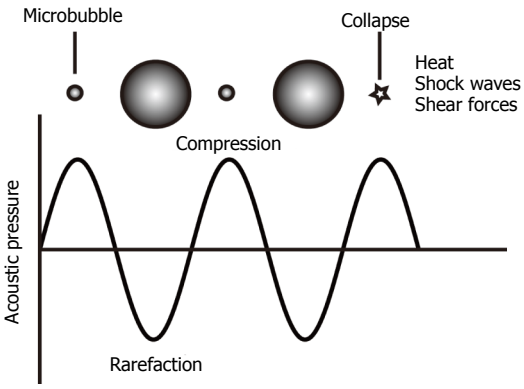

Figure 2 Microbubble response to an ultrasonic pressure wave. Microbubbles expand and contract when exposed to ultrasound at rarefaction and compression, respectively. At high pressure, microbubbles collapse and a shock wave is emitted.

introduced into cells *in vitro* and *in vivo* with sonoporation with microbubbles more efficiently than liposome that is commonly used for transfection[35,36].

Clinical trials

To date, no clinical trials have been reported using sonoporation. There are several reasons for this, including low transfer efficiency and difficulty in monitoring irradiated fields using sonoporators.

Limitations

Sonoporation harbors complicated aspects. Gene transfer efficiency is low with sonoporation. 37.5-50 μg of plasmid should be applied to a single rat with sonoporation *in vivo*[34]. This limitation is one of the reasons that sonoporation has not been applied clinically as mentioned above. Another limitation is cell damage caused with sonoporation. Miller *et al*[37] irradiated cells with 2.25 MHz continuous ultrasound for 1 min. When an ultrasound contrast agent (Definity, a perflutren lipid microsphere injectable suspension; Bristol Myers Squibb Medical Imaging, N. Billerica, MA) was added to the culture media, the irradiated cells underwent apoptosis. Enzymatic activity and mitochondrial membrane are changed after sonoporation[38]. Stresses to endoplasmic reticulum and mitochondria trigger apoptosis[39,40]. Sonoporation delays DNA synthesis to arrest cell cycle[41]. It should be noted that sonoporation itself may cause apoptosis when it is applied to cancer with therapeutic genes[37].

FUTURE PROSPECTS

Microbubbles are expected to improve gene transfer at lower MI for the safety of patients; therefore, microbubbles may be suitable for sonoporation in human trials. Microbubbles are destroyed more efficiently with decreased pulse frequency and increased acoustic pressure and pulse length[42]. Care should be taken when applying *in vitro* data to *in vivo* studies because the effects of MI on microbubble destruction might not be similar[43]. Standing wave may be another option to improve sonoporation. Real-time monitoring of the irradiated field is desirable to introduce therapeutic genes to target tissues. Diagnostic ultrasound could therefore be used as a sonoporator.

Cationic microbubbles

Wang *et al*[27] analyzed the protection of plasmid DNA xenograft tumors in mouse hind limb after intravenous administration of a complex of plasmid DNA (luciferase) with cationic or neutral microbubbles. Luciferase activity was 3.8-fold stronger in complexes with cationic microbubbles than in those with neutral microbubbles. Factors influencing the transfection efficiency were analyzed, and the superiority of cationic microbubbles was more evident at lower doses of microbubbles and plasmid DNA[34]. This strategy appears suitable for this application because nucleic acids are negatively charged. It is expected that plasmid DNA or siRNA will interact and form better complexes with cationic microbubbles than with neutral microbubbles.

Liposomal bubbles

It is difficult to modify surfaces of microbubbles with functional molecules for targeting. On the other hand, liposomes are easy to modify for targeting. Suzuki *et al*[44] developed polyethylene glycol-modified liposomes containing perfluoropropane, a contrast agent for ultrasound imaging. These so-called "bubble liposomes", significantly improved the transfection efficiency of plasmid DNA encoding luciferase into cultured cells. The luciferase reporter plasmid was injected into the femoral artery of mice. Two days after ultrasound irradiation, a signal was detected along the artery. These data suggest that the bubble liposome is a candidate for gene delivery both *in vitro* and *in vivo*. Bubble liposomes were transferred with the interleukin-12 gene in xenograft ovarian cancer mice, and the tumor sizes were reduced[45]. These animal experiments demonstrate that bubble liposomes may be applicable to clinical studies.

Diagnostic ultrasound

Sonoporators are typically used for sonoporation. One of the problems with sonoporators is that the irradiation field cannot be monitored. Diagnostic ultrasound is widely used in daily clinical practice. Diagnostic ultrasound is equipped with a display for image diagnosis. If diagnostic ultrasound could be utilized for sonoporation, therapeutic genes can be accurately introduced into the target fields. Miller and Quddus transfected cultured cells with plasmid DNA using diagnostic ultrasound[46]. They used a 3.5 MHz curved linear transducer of diagnostic ultrasound. A contrast agent of ultrasound (Optison) was added to the media. Although Optison may improve transfection efficiency, even without contrast agents, plasmid DNA was successfully introduced into cultured cells by using diagnostic ultrasound[47]. SiRNA of frizzled (Fz)-9, a receptor of the Wnt signaling pathway, transferred into cultured cells using diagnostic ultrasound sup-

presses cell proliferation[48]. SiRNA of Fz-9 transferred into cultured cells using lipofection also suppresses cell proliferation[49]. These 2 papers indicate that transfection efficiency of siRNA with diagnostic ultrasound is comparable with that of lipofection. Wang *et al*[27] investigated cell permeability of Evans Blue *in vivo* with diagnostic ultrasound. They observed the dye in xenograft hepatoma. Interestingly, they reported that efficiency of Evans Blue transfer was affected by MI sonication duration and dye dose. These data clearly demonstrate that ultrasound causes sonoporation, a biological process that is a promising new approach for the delivery of DNA/RNA for gene therapy.

CONCLUSION

Sonoporation is able to introduce plasmids to cells. Sonoporation is less toxic method of gene transfer as compared with retro viral vectors and adenoviral vectors because plasmids hardly causes immune response and are not associated with tumorigenicity. Sonoporation does not require surgical procedure and enhances gene transfer with lipofection. Current limitations of sonoporation are low efficiency of gene transfer and damage of target cells are the use of complexes with chemicals and diagnostic ultrasound are promising approaches to overcome these limitations.

REFERENCES

1 **Mellott AJ**, Forrest ML, Detamore MS. Physical non-viral gene delivery methods for tissue engineering. *Ann Biomed Eng* 2013; **41**: 446-468 [PMID: 23099792 DOI: 10.1007/s10439-012-0678-1]

2 **Feichtinger GA,** Hofmann AT, Slezak P, Schuetzenberger S, Kaipel M, Schwartz E, Neef A, Nomikou N, Nau T, van Griensven M, McHale AP, Redl H. Sonoporation Increases Therapeutic Efficacy of Inducible and Constitutive BMP2/7 In Vivo Gene Delivery. *Hum Gene Ther Methods* 2013 Nov 27; *Epub ahead of print* [PMID: 24164605]

3 **Miura K**, Okada Y, Aoi T, Okada A, Takahashi K, Okita K, Nakagawa M, Koyanagi M, Tanabe K, Ohnuki M, Ogawa D, Ikeda E, Okano H, Yamanaka S. Variation in the safety of induced pluripotent stem cell lines. *Nat Biotechnol* 2009; **27**: 743-745 [PMID: 19590502 DOI: 10.1038/nbt.1554]

4 **Raper SE**, Chirmule N, Lee FS, Wivel NA, Bagg A, Gao GP, Wilson JM, Batshaw ML. Fatal systemic inflammatory response syndrome in a ornithine transcarbamylase deficient patient following adenoviral gene transfer. *Mol Genet Metab* 2003; **80**: 148-158 [PMID: 14567964 DOI: 10.1016/j.ymgme.2003.08.016]

5 **Jin L**, Li F, Wang H, Li Y, Wei F, Du L. Ultrasound-targeted microbubble destruction enhances gene transduction of adeno-associated virus in a less-permissive cell type, NIH/3T3. *Mol Med Rep* 2013; **8**: 320-326 [PMID: 23817930]

6 **Wells DJ**. Electroporation and ultrasound enhanced non-viral gene delivery in vitro and in vivo. *Cell Biol Toxicol* 2010; **26**: 21-28 [PMID: 19949971 DOI: 10.1007/s10565-009-9144-8]

7 **Ledwith BJ**, Manam S, Troilo PJ, Barnum AB, Pauley CJ, Griffiths TG, Harper LB, Beare CM, Bagdon WJ, Nichols WW. Plasmid DNA vaccines: investigation of integration into host cellular DNA following intramuscular injection in mice. *Intervirology* 2000; **43**: 258-272 [PMID: 11251381 DOI: 10.1159/000053993]

8 **Geers B**, Lentacker I, Alonso A, Sanders NN, Demeester J, Meairs S, De Smedt SC. Elucidating the mechanisms behind sonoporation with adeno-associated virus-loaded microbubbles. *Mol Pharm* 2011; **8**: 2244-2251 [PMID: 22014166 DOI: 10.1021/mp200112y]

9 **Jin LF**, Li F, Wang HP, Wei F, Qin P, Du LF. Ultrasound targeted microbubble destruction stimulates cellular endocytosis in facilitation of adeno-associated virus delivery. *Int J Mol Sci* 2013; **14**: 9737-9750 [PMID: 23652832 DOI: 10.3390/ijms14059737]

10 **Takahashi K**, Tanabe K, Ohnuki M, Narita M, Ichisaka T, Tomoda K, Yamanaka S. Induction of pluripotent stem cells from adult human fibroblasts by defined factors. *Cell* 2007; **131**: 861-872 [PMID: 18035408 DOI: 10.1016/j.cell.2007.11.019]

11 **Neumann E**, Schaefer-Ridder M, Wang Y, Hofschneider PH. Gene transfer into mouse lyoma cells by electroporation in high electric fields. *EMBO J* 1982; **1**: 841-845 [PMID: 6329708]

12 **Daud AI**, DeConti RC, Andrews S, Urbas P, Riker AI, Sondak VK, Munster PN, Sullivan DM, Ugen KE, Messina JL, Heller R. Phase I trial of interleukin-12 plasmid electroporation in patients with metastatic melanoma. *J Clin Oncol* 2008; **26**: 5896-5903 [PMID: 19029422]

13 **Felgner PL**, Gadek TR, Holm M, Roman R, Chan HW, Wenz M, Northrop JP, Ringold GM, Danielsen M. Lipofection: a highly efficient, lipid-mediated DNA-transfection procedure. *Proc Natl Acad Sci USA* 1987; **84**: 7413-7417 [PMID: 2823261 DOI: 10.1073/pnas.84.21.7413]

14 **Miller DL**, Pislaru SV, Greenleaf JE. Sonoporation: mechanical DNA delivery by ultrasonic cavitation. *Somat Cell Mol Genet* 2002; **27**: 115-134 [PMID: 12774945 DOI: 10.1023/A:]

15 **Xu Z**, Raghavan M, Hall TL, Chang CW, Mycek MA, Fowlkes JB, Cain CA. High speed imaging of bubble clouds generated in pulsed ultrasound cavitational therapy--histotripsy. *IEEE Trans Ultrason Ferroelectr Freq Control* 2007; **54**: 2091-2101 [PMID: 18019247 DOI: 10.1109/TUFFC.2007.504]

16 **Tachibana K**, Tachibana S. Transdermal delivery of insulin by ultrasonic vibration. *J Pharm Pharmacol* 1991; **43**: 270-271 [PMID: 1676740 DOI: 10.1111/j.2042-7158.1991.tb06681.x]

17 **Wang W**, Li W, Ma N, Steinhoff G. Non-viral gene delivery methods. *Curr Pharm Biotechnol* 2013; **14**: 46-60 [PMID: 23437936]

18 **Unger EC**, Hersh E, Vannan M, Matsunaga TO, McCreery T. Local drug and gene delivery through microbubbles. *Prog Cardiovasc Dis* 2001; **44**: 45-54 [PMID: 11533926 DOI: 10.1053/pcad.2001.26443]

19 **Tomizawa M**, Ebara M, Saisho H, Sakiyama S, Tagawa M. Irradiation with ultrasound of low output intensity increased chemosensitivity of subcutaneous solid tumors to an anticancer agent. *Cancer Lett* 2001; **173**: 31-35 [PMID: 11578806 DOI: 10.1016/S0304-3835(01)00687-5]

20 **Fechheimer M**, Boylan JF, Parker S, Sisken JE, Patel GL, Zimmer SG. Transfection of mammalian cells with plasmid DNA by scrape loading and sonication loading. *Proc Natl Acad Sci USA* 1987; **84**: 8463-8467 [PMID: 2446324 DOI: 10.1073/pnas.84.23.8463]

21 **Kim HJ**, Greenleaf JF, Kinnick RR, Bronk JT, Bolander ME. Ultrasound-mediated transfection of mammalian cells. *Hum Gene Ther* 1996; **7**: 1339-1346 [PMID: 8818721 DOI: 10.1089/hum.1996.7.11-1339]

22 **Tsunoda S**, Mazda O, Oda Y, Iida Y, Akabame S, Kishida T, Shin-Ya M, Asada H, Gojo S, Imanishi J, Matsubara H, Yoshikawa T. Sonoporation using microbubble BR14 promotes pDNA/siRNA transduction to murine heart. *Biochem Biophys Res Commun* 2005; **336**: 118-127 [PMID: 16125678 DOI: 10.1016/j.bbrc.2005.08.052]

23 **O'Brien WD**. Ultrasound-biophysics mechanisms. *Prog Biophys Mol Biol* 2007; **93**: 212-255 [PMID: 16934858 DOI: 10.1016/j.pbiomolbio.2006.07.010]

24 **Newman CM**, Bettinger T. Gene therapy progress and prospects: ultrasound for gene transfer. *Gene Ther* 2007; **14**: 465-475 [PMID: 17339881 DOI: 10.1038/sj.gt.3302925]

25 **Meltzer RS**. Food and Drug Administration ultrasound device regulation: the output display standard, the "mechanical index," and ultrasound safety. *J Am Soc Echocardiogr* 1996; **9**: 216-220 [PMID: 8849623 DOI: 10.1016/S0894-7317(96)90035-8]

26 **Forsberg F**, Shi WT, Merritt CR, Dai Q, Solcova M, Goldberg BB. On the usefulness of the mechanical index displayed on clinical ultrasound scanners for predicting contrast microbubble destruction. *J Ultrasound Med* 2005; **24**: 443-450 [PMID: 15784762]

27 **Wang G**, Zhuo Z, Xia H, Zhang Y, He Y, Tan W, Gao Y. Investigation into the impact of diagnostic ultrasound with microbubbles on the capillary permeability of rat hepatomas. *Ultrasound Med Biol* 2013; **39**: 628-637 [PMID: 23415284 DOI: 10.1016/j.ultrasmedbio.2012.11.004]

28 **Zhou Y**, Yang K, Cui J, Ye JY, Deng CX. Controlled permeation of cell membrane by single bubble acoustic cavitation. *J Control Release* 2012; **157**: 103-111 [PMID: 21945682 DOI: 10.1016/j.jconrel.2011.09.068]

29 **Carugo D**, Ankrett DN, Glynne-Jones P, Capretto L, Boltryk RJ, Zhang X, Townsend PA, Hill M. Contrast agent-free sonoporation: The use of an ultrasonic standing wave microfluidic system for the delivery of pharmaceutical agents. *Biomicrofluidics* 2011; **5**: 44108-4410815 [PMID: 22662060 DOI: 10.1063/1.3660352]

30 **Sirsi S**, Borden M. Microbubble Compositions, Properties and Biomedical Applications. *Bubble Sci Eng Technol* 2009; **1**: 3-17 [PMID: 20574549 DOI: 10.1179/175889709X446507]

31 **Tachibana K**, Tachibana S. Albumin microbubble echocontrast material as an enhancer for ultrasound accelerated thrombolysis. *Circulation* 1995; **92**: 1148-1150 [PMID: 7648659 DOI: 10.1161/01.CIR.92.5.1148]

32 **Qiu Y**, Zhang C, Tu J, Zhang D. Microbubble-induced sonoporation involved in ultrasound-mediated DNA transfection in vitro at low acoustic pressures. *J Biomech* 2012; **45**: 1339-1345 [PMID: 22498312 DOI: 10.1016/j.jbiomech.2012.03.011]

33 **Kudo N**, Okada K, Yamamoto K. Sonoporation by single-shot pulsed ultrasound with microbubbles adjacent to cells. *Biophys J* 2009; **96**: 4866-4876 [PMID: 19527645 DOI: 10.1016/j.bpj.2009.02.072]

34 **Panje CM**, Wang DS, Pysz MA, Paulmurugan R, Ren Y, Tranquart F, Tian L, Willmann JK. Ultrasound-mediated gene delivery with cationic versus neutral microbubbles: effect of DNA and microbubble dose on in vivo transfection efficiency. *Theranostics* 2012; **2**: 1078-1091 [PMID: 23227124 DOI: 10.7150/thno.4240]

35 **Zheng X**, Ji P, Hu J. Sonoporation using microbubbles promotes lipofectamine-mediated siRNA transduction to rat retina. *Bosn J Basic Med Sci* 2011; **11**: 147-152 [PMID: 21875415]

36 **Li YH**, Jin LF, Du LF, Shi QS, Liu L, Jia X, Wu Y, Li F, Wang HH. Enhancing HSP70-ShRNA transfection in 22RV1 prostate cancer cells by combination of sonoporation, liposomes and HTERT/CMV chimeric promoter. *Int J Oncol* 2013; **43**: 151-158 [PMID: 23620085]

37 **Miller DL**, Dou C. Induction of apoptosis in sonoporation and ultrasonic gene transfer. *Ultrasound Med Biol* 2009; **35**: 144-154 [PMID: 18723272 DOI: 10.1016/j.ultrasmedbio.2008.06.007]

38 **Van Ruijssevelt L**, Smirnov P, Yudina A, Bouchaud V, Voisin P, Moonen C. Observations on the viability of C6-glioma cells after sonoporation with low-intensity ultrasound and microbubbles. *IEEE Trans Ultrason Ferroelectr Freq Control* 2013; **60**: 34-45 [PMID: 23287911 DOI: 10.1109/TUFFC.2013.2535]

39 **Zhong W**, Sit WH, Wan JM, Yu AC. Sonoporation induces apoptosis and cell cycle arrest in human promyelocytic leukemia cells. *Ultrasound Med Biol* 2011; **37**: 2149-2159 [PMID: 22033133 DOI: 10.1016/j.ultrasmedbio.2011.09.012]

40 **Zhong W**, Chen X, Jiang P, Wan JM, Qin P, Yu AC. Induction of endoplasmic reticulum stress by sonoporation: linkage to mitochondria-mediated apoptosis initiation. *Ultrasound Med Biol* 2013; **39**: 2382-2392 [PMID: 24063957 DOI: 10.1016/j.ultrasmedbio.2013.08.005]

41 **Chen X**, Wan JM, Yu AC. Sonoporation as a cellular stress: induction of morphological repression and developmental delays. *Ultrasound Med Biol* 2013; **39**: 1075-1086 [PMID: 23499345 DOI: 10.1016/j.ultrasmedbio.2013.01.008]

42 **Yeh CK**, Su SY. Effects of acoustic insonation parameters on ultrasound contrast agent destruction. *Ultrasound Med Biol* 2008; **34**: 1281-1291 [PMID: 18343019 DOI: 10.1016/j.ultrasmedbio.2007.12.020]

43 **Forsberg F**, Merton DA, Goldberg BB. In vivo destruction of ultrasound contrast microbubbles is independent of the mechanical index. *J Ultrasound Med* 2006; **25**: 143-144 [PMID: 16371568]

44 **Suzuki R**, Takizawa T, Negishi Y, Hagisawa K, Tanaka K, Sawamura K, Utoguchi N, Nishioka T, Maruyama K. Gene delivery by combination of novel liposomal bubbles with perfluoropropane and ultrasound. *J Control Release* 2007; **117**: 130-136 [PMID: 17113176 DOI: 10.1016/j.jconrel.2006.09.008]

45 **Suzuki R**, Namai E, Oda Y, Nishiie N, Otake S, Koshima R, Hirata K, Taira Y, Utoguchi N, Negishi Y, Nakagawa S, Maruyama K. Cancer gene therapy by IL-12 gene delivery using liposomal bubbles and tumoral ultrasound exposure. *J Control Release* 2010; **142**: 245-250 [PMID: 19883708 DOI: 10.1016/j.jconrel.2009.10.027]

46 **Miller DL**, Quddus J. Sonoporation of monolayer cells by diagnostic ultrasound activation of contrast-agent gas bodies. *Ultrasound Med Biol* 2000; **26**: 661-667 [PMID: 10856630 DOI: 10.1016/S0301-5629(99)00170-2]

47 **Tomizawa M**, Shinozaki F, Sugiyama T, Yamamoto S, Sueishi M, Yoshida T. Plasmid DNA introduced into cultured cells with diagnostic ultrasound. *Oncol Rep* 2012; **27**: 1360-1364 [PMID: 22266950]

48 **Tomizawa M**, Shinozaki F, Sugiyama T, Yamamoto S, Sueishi M, Yoshida T. Short interference RNA introduced into cultured cells with diagnostic ultrasound. *Oncol Rep* 2012; **27**: 65-68 [PMID: 22025318]

49 **Fujimoto T**, Tomizawa M, Yokosuka O. SiRNA of frizzled-9 suppresses proliferation and motility of hepatoma cells. *Int J Oncol* 2009; **35**: 861-866 [PMID: 19724923]

P- Reviewers: Ghatak S, Klein RL, Kiselev SL **S- Editor**: Wen LL
L- Editor: A **E- Editor**: Lu YJ

World Journal of Methodology

Online Submissions: http://www.wjgnet.com/esps/
bpgoffice@wjgnet.com
doi:10.5662/wjm.v3.i4.45

World J Methodol 2013 December 26; 3(4): 45-64
ISSN 2222-0682 (online)

An overview of translational (radio)pharmaceutical research related to certain oncological and non-oncological applications

Marlein Miranda Cona, Peter de Witte, Alfons Verbruggen, Yicheng Ni

Marlein Miranda Cona, Yicheng Ni, Department of Imaging and Pathology, Faculty of Medicine, Biomedical Sciences Group, KU Leuven, B-3000 Leuven, Belgium
Marlein Miranda Cona, Yicheng Ni, Molecular Small Animal Imaging Centre/MoSAIC, Faculty of Medicine, Biomedical Sciences Group, KU Leuven, B-3000 Leuven, Belgium
Peter de Witte, Alfons Verbruggen, Faculty of Pharmaceutical Sciences, Biomedical Sciences Group, KU Leuven, B-3000 Leuven, Belgium
Author contributions: Miranda Cona M and Ni Y contributed equally in writing the article and in reviewing the literature; Miranda Cona M, de Witte P, Verbruggen A and Ni Y participated in the revision for important intellectual content; Miranda Cona M, de Witte P, Verbruggen A and Ni Y approved the final version of submitted manuscript.
Supported by The KU Leuven Molecular Small Animal Imaging Center MoSAIC (KUL EF/05/08) and the center of excellence *in vivo* molecular imaging research; KU Leuven projects IOF-HB/08/009 and IOF-HB/12/018; the European Union (Asia-Link CfP 2006-EuropeAid/123738/C/ACT/Multi-Proposal No. 128-498/111); the National Natural Science Foundation of China, No. 81071828; and the Jiangsu Provincial Natural Science Foundation, No. BK2010594
Correspondence to: Yicheng Ni, MD, Professor of Medicine, PhD, Chief of Theragnostic Lab, Radiology Section, Department of Imaging and Pathology, University Hospitals, KU Leuven, Herestraat 49, B-3000 Leuven,
Belgium. yicheng.ni@med.kuleuven.be
Telephone: +32-16-330165 Fax: +32-16-343765
Received: September 4, 2013 Revised: October 3, 2013
Accepted: October 18, 2013
Published online: December 26, 2013

Abstract

Translational medicine pursues the conversion of scientific discovery into human health improvement. It aims to establish strategies for diagnosis and treatment of diseases. Cancer treatment is difficult. Radiopharmaceutical research has played an important role in multiple disciplines, particularly in translational oncology. Based on the natural phenomenon of necrosis avidity, OncoCiDia has emerged as a novel generic approach for treating solid malignancies. Under this systemic dual targeting strategy, a vascular disrupting agent first selectively causes massive tumor necrosis that is followed by iodine-131 labeled-hypericin (^{123}I-Hyp), a necrosis-avid compound that kills the residual cancer cells by crossfire effect of beta radiation. In this review, by emphasizing the potential clinical applicability of OncoCiDia, we summarize our research activities including optimization of radioiodinated hypericin Hyp preparations and recent studies on the biodistribution, dosimetry, pharmacokinetic and, chemical and radiochemical toxicities of the preparations. Myocardial infarction is a global health problem. Although cardiac scintigraphy using radioactive perfusion tracers is used in the assessment of myocardial viability, searching for diagnostic imaging agents with authentic necrosis avidity is pursued. Therefore, a comparative study on the biological profiles of the necrosis avid ^{123}I-Hyp and the commercially available ^{99m}Tc-Sestamibi was conducted and the results are demonstrated. Cholelithiasis or gallstone disease may cause gallbladder inflammation, infection and other severe complications. While studying the mechanisms underlying the necrosis avidity of Hyp and derivatives, their naturally occurring fluorophore property was exploited for targeting cholesterol as a main component of gallstones. The usefulness of Hyp as an optical imaging agent for cholelithiasis was studied and the results are presented. Multiple uses of automatic contrast injectors may reduce costs and save resources. However, cross-contaminations with blood-borne pathogens of infectious diseases may occur. We developed a radioactive method for safety evaluation of a new replaceable patient-delivery system. By mimicking pathogens with a radiotracer, we assessed the feasibility of using the system repeatedly without septic risks. This overview is deemed to be interesting to those involved

in the related fields for translational research.

Key words: Translational medical research; Cancer treatment; OncoCiDia; Vascular disrupting agent; Hypericin; Myocardial infarction; Gallstone; Transflux

Core tip: Translational medicine converts scientific discovery into clinical applications. Radiopharmacy has played a multidisciplinary role. Based on unique necrosis avidity, OncoCiDia presents a generic approach for management of cancers, on which recent results on its optimization are summarized. Myocardial infarction is a clinical problem. A comparative study between infarct avid iodine-131 labeled-hypericin and commercial ^{99m}Tc-Sestamibi is presented. Cholelithiasis may cause biliary complications. The usefulness of Hyp as an optical imaging agent for cholelithiasis is demonstrated. Multiple uses of automatic contrast injectors may reduce costs but can cause cross-contaminations. We developed a radioactive method for safety evaluation of a new replaceable patient-delivery system.

Miranda Cona M, de Witte P, Verbruggen A, Ni Y. An overview of translational (radio)pharmaceutical research related to certain oncological and non-oncological applications. *World J Methodol* 2013; 3(4): 45-64 Available from: URL: http://www.wjgnet.com/2222-0682/full/v3/i4/45.htm DOI: http://dx.doi.org/10.4329/wjm.v3.i4.45

INTRODUCTION

Translational medicine refers to the creativity of joining knowledge from "bench to bedside" or from laboratory experiments to clinical trials for producing new drugs, devices, diagnostic and therapeutic options for patients. Hence, translational research is identified as a crucial interface between basic science and clinical medicine. It intends to discover better ways to solve real practical problems enhancing human health and well-being. Another current trend in translational medical research is to hybrid diagnosis and therapy into a combined approach as newly termed a "theragnostic" modality.

In the area of cancer therapeutics, transforming basic research results into clinical practice is becoming increasingly important. Cancer is one of the leading causes of mortality worldwide and little progress has been achieved in treating most of the solid tumors, which could be resistant to common therapies. Based on necrosis-avidity, OncoCiDia is a generic and unconventional theragnostic strategy recently introduced as a complementary modality to improve cancer treatability[1,2]. Unlike other cancer therapies directly attacking multimutant and refractory cancer cells, OncoCiDia may selectively treat solid malignancies by massively necrotizing the tumors plus radioactively cleansing their microenvironments, meanwhile the tumors under treatment can be visualized by nuclear scintigraphy. Thus, a dedicated acronym OncoCiDia is created to portray this cancer (Onco) management approach with both tumoricidal (Ci) and diagnostic (Dia) effects. It consists of two sequential complementary treatments involving the intravenous application of a vascular disrupting agent (VDA) followed by systemic targeted radiotherapy (STR) using a potent necrosis-avid compound iodine-131 labeled-monoiodohypericin (^{131}I-Hyp). Furthermore, to make this novel anticancer strategy clinically applicable, optimizations of the procedures for labeling, purification and formulation of the radioiodinated hypericin (Hyp) have been performed and the outcomes are summarized and commented in this overview article. Results on biodistribution, dosimetry, pharmacokinetic and, chemical and radiochemical toxicities of OncoCiDia have been also presented, which hopefully may boost the advance of this strategy into the clinic.

Myocardial infarction constitutes a health problem with large morbidity, mortality and economic burden[3]. Nuclear imaging based on myocardial perfusion tracers, which distribute in proportion to the regional myocardial blood flow, has played an important role in the assessment of tissue viability[4,5]. However, the development of diagnostic imaging agents with authentic specific avidity for necrosis has been a desired goal due to the numerous utilities they may offer. In earlier studies, the necrosis avid ^{123}I-Hyp has shown its potential usefulness as a diagnostic cardiac agent due to its notable uptake in necrotic tissues[6,7]. In a more recent experiment, its biodistribution and targetability have been compared to those of the commercially available myocardial perfusion tracer ^{99m}Tc-Sestamibi and the results have been herein summarized.

Cholelithiasis is the medical term for gallstone disease. Gallstones are hard, rock-like collections, mainly from cholesterol and bile salts that build up in the gallbladder or bile duct. Eventually, they can cause gallbladder inflammation resulting in pain, jaundice, infection and other serious complications. Because the high affinity between cholesterol and the naturally occurring fluorophore hypericin has been reported[8,9], a preliminary *in vitro* study for assessing the potential suitability of Hyp as an optical diagnostic imaging agent in patients with gallstones was performed and the results are presented in this work.

Multiple uses of automatic contrast injection systems during imaging procedures can reduce costs and save resources. However potential outbreak associated with cross-contaminations with blood-borne pathogens of infectious diseases through the contrast medium may occur. The Transflux contrast delivery system is a simple tube delimited by two one-way valves intended to deliver contrast media from a reservoir to the patient and with the need to only change the tubing in direct contact with the patient blood. It incorporates a safety zone and a one-way valve in the patient line that allow the delivery system and the vein to be flushed and the blood reflux to be prevented. By mimicking microbial pathogens

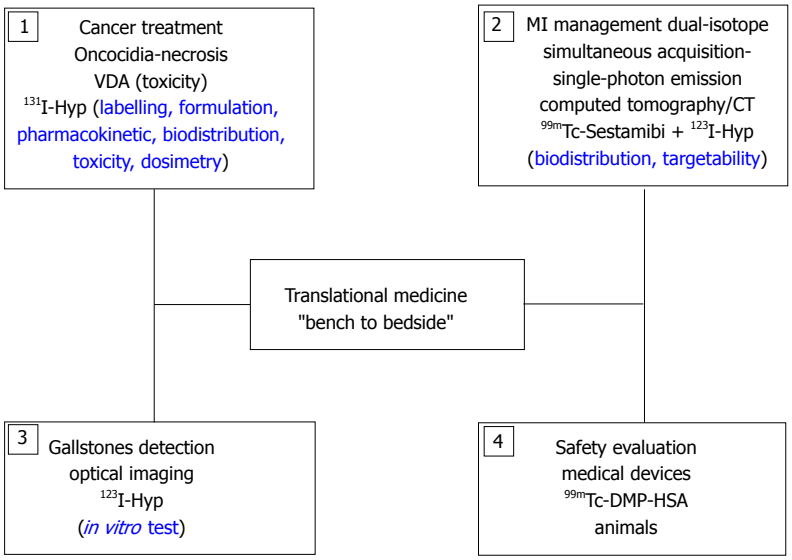

Figure 1 Schematic structure of the translational research activities covered by the overview article. ^{99m}Tc-sestamibi: Technetium-99m labeled-hexakis (2-methoxyisobutylisonitrile); ^{99m}TcDMP-HSA: Technetium-99m dimercaptopropionyl human serum albumin; $^{123/131}$I-Hyp: Iodine-123/iodine-131 labeled monoiodohypericin; MI: Myocardial infarction; VDA: Vascular disrupting agent.

with a particulate radiotracer, we developed a radioactive method for quantitative safety evaluation of this new replaceable patient-delivery system and the main findings are reported here.

This overview paper is in the framework of the full 4-year doctoral training, in which translational research has been attempted as a key component for resolving important problems in diverse medical fields (Figure 1).

APPLICATION OF TRANSLATIONAL RESEARCH IN THERAGNOSTIC ONCOLOGY

Background

Cancer is a complex group of malignant diseases influenced by genetic and environmental factors. Over the past decades, the incidence and prevalence of cancer have raised with an overall estimation of about 20 million new cases by 2030[10]. The costs associated with cancer diagnosis, therapy, and follow-up have drastically soared. Conventional therapies including surgery, chemotherapy and external beam radiotherapy are often ineffective for treating resistant and disseminated solid malignancies. Novel and cost-effective approaches, once available, are essential to improve cancer treatability and curability.

STR is a radiotherapy that makes use of systemically administered radioactive compounds for delivering lethal radiation doses to the tumor while preserving normal tissues. Several radioactive agents have been clinically used, for instance, radioiodine for thyroid cancer owing to its specific uptake by thyroid glandular tissues[11]; iodine-131 metaiodobenzylguanidine for treating pheochromocytoma[12] and neuroblastoma[13]; Metastron (strontium-89 chloride) as a palliative treatment in patients with bone metastases[14]; and radioactive microspheres for radioembolization of liver cancer[15]. Anti-CD20 monoclonal antibody (MoAb) conjugated to I-131 (tositumomab, Bexxar®)[16] or yttrium-90 (ibritumomab tiuxetan, Zevalin®)[17] for treating non-Hodgkins lymphoma, and somatostatin derivatives labeled with bound indium-111, lutetium-177 or yttrium-90 for neuroendocrine tumors (NETs)[18,19] are lately introduced, constituting a step forward in tumor specific targeting.

However, most of the above-mentioned cancer types represent a small proportion among the overall cancer cases. Malignant solid tumors, which represent the major cancer incidence worldwide, have been difficult to treat due to their histological diversity, disorganized angiogenesis and unpredictable mutations. Once carcinogenesis is established, tumor cells become resistant to therapies due to the multiple escape mechanisms facilitated by intrinsic mutations and/or overlapping molecular pathways. Even if a proper radioactive MoAb is chosen, in most of the cases, only small amounts of injected dose (0.001%-0.1% /g) could accumulate in the tumor[20]. Low absorbed doses (1500 cGy) are subsequently reached in cancer cells that are much lower than the usually required doses (5000 cGy) for getting therapeutic responses[21,22]. With somatostatin derivatives-based radiopharmaceuticals characterized by high affinity for distinct receptors overexpressed in the tumor, short-term accumulation in the tumor and retention in normal tissues have also been reported[23]. Therefore, necrosis as a generic alternative target has been utilized for potential theragnostic applications (Figure 2).

Tumor necrosis treatment

Rather than hitting cancer cells undergoing numerous mutations[24,25] that cause uncontrollable growth and escape from annihilation, leading to post-therapeutic cancer resistant clones[24], an innovative anticancer approach called tumor necrosis treatment (TNT) was introduced[26,27]. Since the proportion of dead tissue in fast-growing tumors can be more than 50% of the total cancer volume due to tumor vascular deformation or insufficient blood supply[28,29], necrosis could become a generic target in almost all solid tumors. TNT approach uses radiolabeled MoAbs that spare normal tissue and target naturally occurring intracellular antigens (a complex of double-stranded DNA and histone H1-antigens)

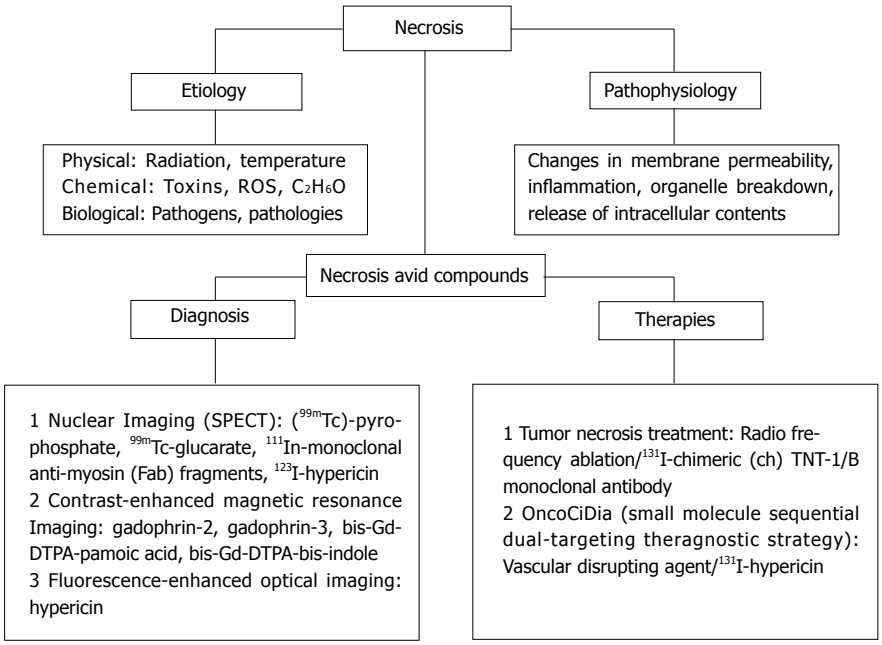

Figure 2 Flow diagram of the included research topics. ^{99m}Tc: Technetium-99m; ^{111}In: indium-111; ^{123}I: Iodine-123; ^{131}I: Iodine-131; C_2H_6O: Ethanol; DTPA: Diethylene triamine pentaacetic acid; Fab: Antigen-binding fragment; Gd: Gadolinium; ROS: Reactive oxygen species; SPECT: Single photon emission computed tomography; TNT: Tumor necrosis treatment.

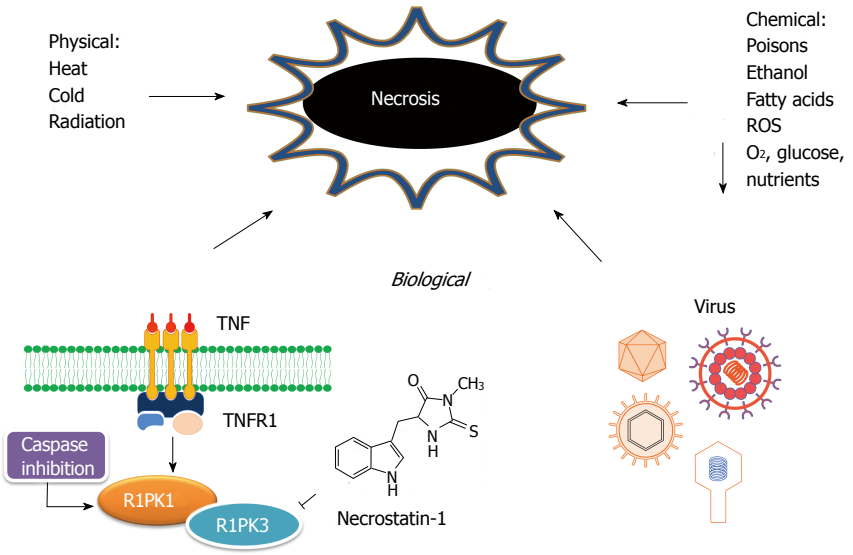

Figure 3 Schematic representation of the etiology of necrosis. ROS: Reactive oxygen species; TNT: Tumor necrosis treatment; RIPK1/3: Receptor-interacting protein kinase 1 and 3; TNFR1: Tumor-necrosis factor receptors 1.

present throughout tumor necrosis[30,31]. Unlike conventional STR, it is a crossfire-dose therapeutic modality, in which the radiation dose deposited to cancer cells only comes from radionuclides on surrounding necrosis.

Definition, etiology and pathophysiology of necrosis: The term of necrosis is originated from the Greek prefix "necros", meaning "dead". It constitutes an irreversible process or "no return" status in the cell life[32]. Cell death by necrosis has been historically stereotyped as an unregulated process[33]. Any severe lesions caused by physical stresses, toxins, infections or genetically programmed injuries if reaching a certain degree and receiving no intervention may alter physiological homeostasis, eventually leading to tissue or organ necrosis[34]. However, it turns increasingly evident that the multi-pathway cell-death program apoptosis may not be the only cellular mechanism involved in regulating cell death[35]. Programmed necrosis or necroptosis has emerged as a specialized biochemical mechanism that can be induced by different stimuli such as tumor-necrosis factor receptors (TNFR1, TNFR2)[36], inactivation of cysteine-aspartic acid proteases (caspase)[37] and caspase-8 mutations[38]. It becomes clear that necroptosis could be regulated by the kinase receptor-interacting protein 1 (RIPK1), which constitutes the molecular target of necrostatins, an emerging class of cytoprotective drugs inhibiting specifically necroptotic cells[37]. Recently, the kinase activity of RIPK3, a family member of RIPK1, has also been related to programmed necrosis[39] (Figure 3).

Necrosis is commonly believed to be a passive process since it involves no protein production, is not restrained by any homeostatic mechanisms, and includes almost negligible energy requirements. The necrotic cells can no longer retain the integrity of the cell or cytoorganelle membranes and perform inherent functions. Af-

ter losing the ability to maintain homeostasis, biological fluids from the blood cross the damaged cell membrane and enter the intracellular space, leading to organelles enlargement, production of toxins and activating enzymes associated to the degradation of cellular life molecules. The swollen organelles become nonfunctional, ceasing the synthesis of proteins and ATP. The mitochondrial swelling causes cytolysis and the debris is discharged into the surroundings, which triggers tissue inflammation regulated by small proteins-cytokines, reactive oxygen species and certain immune system cells[40]. The organism interprets the presence of the debris as signal of tissue injury and reacts to defend itself. In response, immune system cells migrate into the site of damage and combat the supposed invading microorganisms[40]. Dissociation of ribosomes from the endoplasmic reticulum and nucleus disintegration with chromatin condensation take place in turn[41]. The dead cells eventually fade away because of the combination of enzymatic denaturation and fragmentation process, followed by polymorphonuclear leukocyte phagocytosis of solid particles[42].

Preclinical studies and clinical trials on TNT: In a pioneer pre-clinical study conducted on a ME-180 human cervical carcinoma model with ^{131}I-labeled TNT-1 MoAb, Chen *et al*[31] proved the effective and preferential targeting of this radiotherapeutics within the tumor, which established the potential clinical usefulness of TNT. To date, about 200 patients have been treated with TNT worldwide. A phase I study of ^{131}I-chimeric(ch) TNT-1/B MoAb for the treatment of advanced colon cancer was performed. The infusion of ^{131}I-chTNT-1/B MoAb was well tolerated and showed no significant non-hematologic effects. Based on tumor cross-product response criteria, however, none of the patients exhibited complete or partial response[43]. Phase I and Ⅱ trials of convection-enhanced delivery of ^{131}I-chTNT-1/B MoAb were conducted on patients with high-grade adult gliomas, showing promising therapeutic outcomes[44]. Similar results were found in a pivotal study in patients with advanced lung cancer treated with ^{131}I-chTNT-1/B MoAB[45]. More recently, genetically engineered Fab' and F(ab') 2 constructs of chimeric TNT (chTNT)-3 antibody labeled with indium-111 were prepared and preclinically evaluated. The conjugates showed faster body clearance, better biodistribution but lower tumor uptake than the parental ^{111}In-labeled chTNT-3 in tumor-bearing mice[46].

To increase the amount of MoAb binding-necrotic sites in the tumor, necrosis-inducing treatments (NITs) such as radiofrequency ablation were also used as starting complementary techniques[47].

However, myelosuppression due to unfavorable pharmacokinetic properties of MoAbs constitutes an important dose limiting factor that prevents substantial improvement of TNT-based modality[43,44].

OncoCiDia

OncoCiDia, also known as small molecule sequential dual-targeting theragnostic strategy[1], is a novel anticancer approach with great potential for treating solid tumors. Relying on a soil-to-seeds concept, it offers a one-stop-shop for diagnostic imaging, treatment and follow-up[2]. Similar to the TNT approach, it is based on the natural phenomenon of necrosis. However, instead of using radioactive MoAb with large molecular size (150 kDa) and complex pharmacokinetics, it involves two small compounds (< 1 kDa) with pre-identified high and divert but complementary targetability. The intravenously (IV) administered VDA triggers selective tumor vascular shutdown and subsequent central necrosis. However, a viable rim of tumor cells in the periphery always exists as seeds for repopulation of cancer cells[48]. ^{131}I-Hyp is then IV injected, which preferentially localizes at the newly generated necrotic sites and acts as a cleansing shot to lethally irradiate residual tumor cells through a crossfire effect[2]. The small molecular size of ^{131}I-Hyp makes it possible to permeate fast through tissues and target less accessible sites throughout the solid tumor. This may overcome the initial barriers faced by the systemic delivery of MoAb, which limits diffusion from blood vessels and inhibits drug tumor penetration[21,49].

Vascular disrupting agents: Vascular disrupting agents (VDAs) are a novel category of potential anticancer drugs that induce tumor vascular shutdown by destroying the endothelium of tumor vasculature. It has been reported that blood vessels in tumors proliferate more rapidly than those in normal tissues[49]. Newly formed endothelial cells are more sensitive than mature ones that own a well-developed actin cytoskeleton and may retain the cell shape in spite of depolymerization of the tubulin cytoskeleton caused by the VDA[50]. After VDA administration, the occlusion of blood-supplying vessels and capillary sprouts obstructs oxygen and nutrient supply to the tumor cells, compromising cellular integrity and eventually leading to hemorrhagic tumor necrosis[51]. Different groups of VDAs have been developed, *e.g.,* tubulin-binding agents cause microtubule depolymerization by binding either the colchicine or vinblastine sites, whereas flavonoid derivatives selectively obstruct tumor-related vessels due to their indirect pharmacodynamic effects[51]. VDAs can be obtained from nature such as combretastatins (CA4P, OXi-4503, and AVE-8062), colchicines (ZD6126) and phenylahistin (NPI-2358), whilst others are synthetic compounds (DMXAA, MN-029 and EPC2407)[51].

Hyp: Hyp is a red-colored anthraquinone derivative (naphthodianthrone), which is one of the principal active compounds of the genus Hyp (Clusiaceae) comprising roughly 450 species worldwide[52]. Hyp was initially found in the dark glands of the flowering parts from Hyp perforatum L (St. John's Wort)[53], an aromatic, perennial plant. Hyp can be also obtained from fungi Dermocybe[54] or from endophytic fungi growing in different plant species[52]. However, the most commercially available Hyp

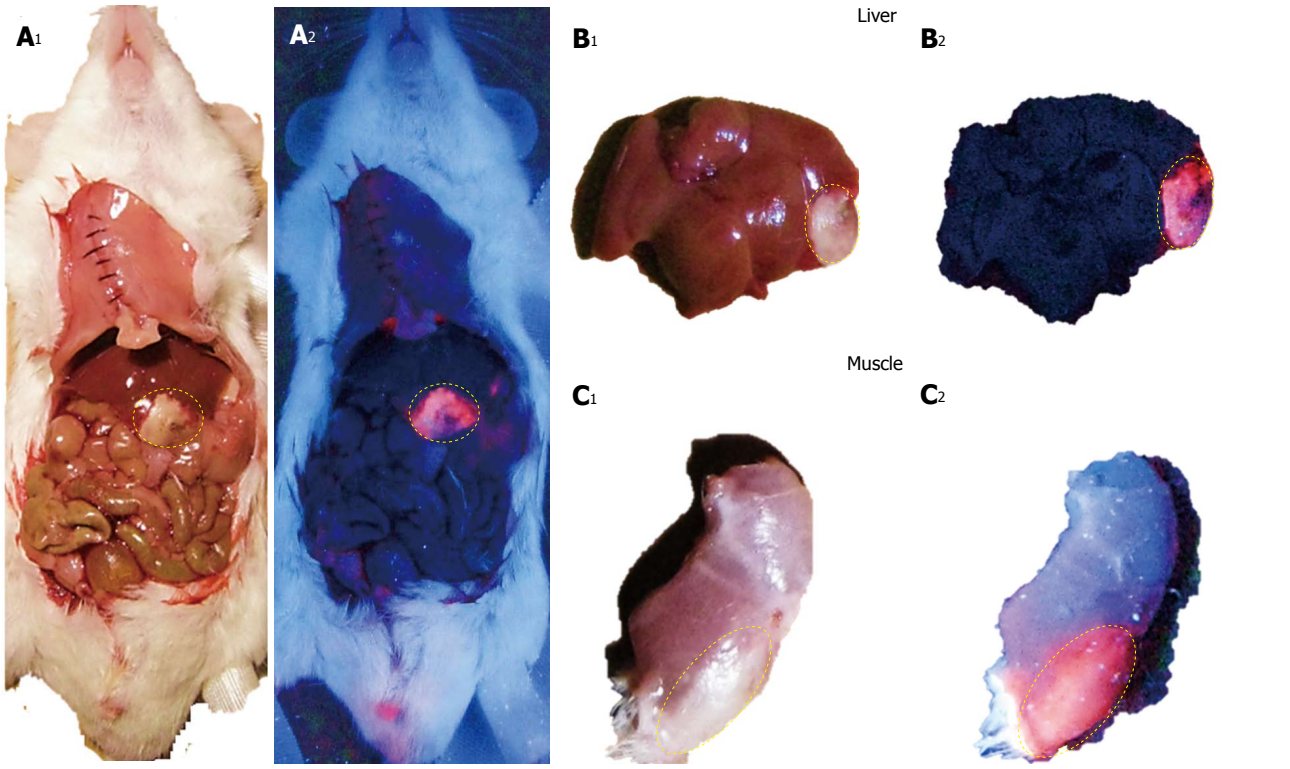

Figure 4 Macroscopic digital imaging of a mouse with acute ethanol-induced necrosis in the liver and muscle having received 5.0 mg/kg hypericin in DMSO/PEG400/water (25:60:15, v/v/v). Under normal tungsten light, viable liver, intestines and muscle show normal appearances whereas hepatic infarction and muscle necrosis appear as white cheesy tissue (A_1, B_1, C_1). With a UV light of 254 nm, a bright red fluorescence from liver (A_2, B_2) and muscle necrosis (C_2) but a lack of fluorescent signal from the liver (A_2, B_2), viable muscle (C_2) and other abdominal structures were observed (A_2). DMSO: Dimethyl sulfoxide; PEG400: Polyethylene glycol 400; UV: Ultraviolet.

compounds are synthesized.

Hyp has been considered a vinylogous carboxylic acid. Its deprotonations are likely at the phenolic hydroxyl groups at the peri- and bay-regions having different acidities. In aqueous system the bay- and peri-regions show estimated pKa values of 1.7 and 12.5[55], respectively. Hyp showed a non-planar conformation owing to the repelling interactions among the side chains of the aromatic skeleton[56]. The proximity of acidic and basic functional groups allows the formation of intramolecular hydrogen bonds, which influence the tautomeric equilibria and acid-base properties[55]. Hyp has 16 conceivable tautomers[57]. Among them, the most stable is the 7, 14-dioxoisomer[58]. Hyp dissolves in polar solvents over concentrations of 10^{-3} mol/L, producing red fluorescent solutions. It is soluble in Dimethyl sulfoxide (DMSO), ethanol, pyridine, methanol, acetone, butanone, ethyl acetate and aqueous alkaline solutions[59]. It has been found in soluble form under physiological conditions due to the complex formation with biological macromolecules, mainly low-density lipoprotein (LDL)[60].

Hyp is a natural product of pharmaceutical interest due to its ever-expanding anti-inflammatory[61], antiretroviral[62], antimicrobial[63], antitumor[64] and antidepressive[65] activities. Recently, it has been found with a highly selective affinity for necrosis[6,7] (Figure 4).

The mechanisms associated with the necrosis avidity of Hyp remain unknown and a number of hypotheses have been proposed. Hyp specifically accumulates in exposed sites of degraded life molecules in the necrotic cell debris[66]. Binding to LDL[60] and serum or interstitial albumins[67] have been put forward as potential interaction pathways. Hyp has also been found to show highly selective avidity for lipid components including cholesterol[8], phosphatidylserine and phosphatidylethanolamine[68] present in the cell membrane bilayer.

Iodine isotopes: Iodine-123 (^{123}I) is a halogen with a physical half-life of 13.1 h. It decays by electron capture to tellurium-123, emitting gamma radiation with a main energy of 159 kEV, which is exploitable for nuclear scintigraphy, biodistribution and radiodosimetry studies.

Iodine-131 (^{131}I) with a decay half-life of 8.02 d is the most common iodine radioisotope utilized in medical applications owing to its relatively easy availability and low cost. It decays by emission of beta minus electrons with a maximal energy of 606 kEV (89% abundance) and a tissue penetration of 0.6-2.0 mm[69] as well as 364 kEV gamma rays of 81% abundance. ^{131}I destroys tissue by short-range beta radiation, causing DNA damage and cell death to the cell that takes up the tracer by self-dose effect and to other cells up to several micrometers away by cross-fire effect.

Due to radioprotection reasons, ^{123}I is frequently used

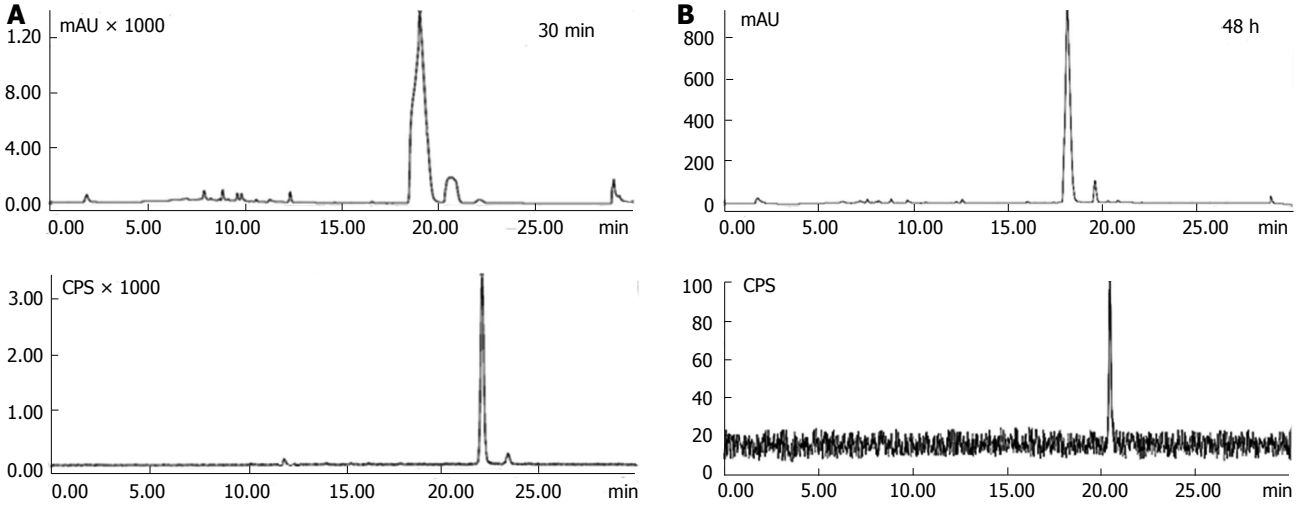

Figure 5 High performance liquid chromatographic analysis of the non-purified iodine-123 labeled hypericin with Ultraviolet (254 nm) and radiometric detection. A: Ultraviolet-chromatogram of the starting reagent hypericin (Hyp) with a retention time of 19.18 min (upper part) and radiochromatogram (lower part) of ^{123}I-Hyp eluting at 22.13 min with a mean radiochemical yield of 95.4%; B: High performance liquid chromatographic analysis of the non-purified ^{123}I-Hyp at 48 h after labeling. A single narrow peak coming out at 21.90 min (lower part) suggests the *in vitro* stability of ^{123}I-Hyp over time. CPS: Count per second.

as surrogate of ^{131}I for labeling optimization, biodistribution and dosimetry studies with the mutually interpretable outcomes.

Preparation of $^{123/131}$I -labeled-monoiodohypericin: Radioiodination *via* direct electrophilic substitution is a simple method based on *in situ* formation of positively charged iodine (I^+) using mild oxidants such as *N*-chloro para-toluenesulfonylamide (chloramine T), peracetic acid and 1,3,4,6-tetrachloro-3α, 6α-diphenyl glycoluril (Iodogen). The radioactive iodine atom in an oxidized form replaces a hydrogen atom of an activated aromatic ring. Since Hyp is a polycyclic aromatic quinone having hydroxyl substituents, it can be efficiently radioiodinated.

Two main methods for direct radiolabelling of Hyp with iodine isotopes have been described. Bormans *et al*[70] reported a radioiodination procedure of Hyp in ethanol using phosphoric acid and peracetic acid as oxidant for 30 min. On high performance liquid chromatography (HPLC), radiochemical yields ranging between 70%-97% were achieved[70]. Sun *et al*[71] described a simple method, in which Hyp in DMSO is labeled with $^{131/123}$I using iodogen as oxidant (either in a pre-coated tube or in powder form), at pH value between 6.5-7.5 for 2 to 10 min. Labeling yields higher than 99% were attained as indicated by paper chromatography (PC).

However, although PC is useful for the purpose of identification due to its convenience and simplicity, we investigated the method developed by Sun and Ni using HPLC. This technique provides high resolution and allows identifying and quantifying small amounts of substances. Labeling conditions were screened for varying reaction parameters such as Hyp mass, Hyp/iodogen molar ratio and reaction time. Stability over time of the radioactive Hyp was also checked. For radiochemical yield determination and purification, the effect of different mobile phases either in gradient or isocratic modes was studied on a quaternary HPLC system equipped with a Ultraviolet (UV) absorbance (254 nm) and radiometric detector. An XTerra® C18 column (4.6 mm × 150 mm, 5.0 μm) and a flow rate of 1.0 mL/min were used for radiochemical yield analysis. On the other hand, an XTerra® C18 semi-preparative column (10 mm × 250 mm, 10 μm) and a flow rate of 3.0 mL/min were set for purification. The peak areas of Hyp and radioiodinated Hyp were considered as response variables in this optimization test.

The preferred conditions for Hyp radioiodination were 2.0 mg Hyp in a molar ratio (Hyp: iodogen) of (3.4:1); 90/10, mL/L DMSO/50 mmol/L sodium phosphate buffer at pH 7.4 for 20 min. For radiochemical yield determination, a mobile phase consisting of acetonitrile/5 mmol/L ammonium acetate buffer pH 7.0 in gradient mode (0 min: 5:95 v/v, 25 min: 95:5 v/v, 30 min: 5:95 v/v) provided the best resolution between adjacent peaks. UV/radio-chromatograms showed unlabeled Hyp and iodine-123-labeled monoiodohypericin (^{123}I-Hyp) with t_R of 19.18 ± 0.15 min and 22.13 ± 0.05 min, respectively. Free iodide was not observed (Figure 5A). ^{123}I-Hyp was prepared with specific activity above 50 GBq/μmol in a radiochemical yield of 95.4% and remained stable over 48 h at room temperature (Figure 5B). As confirmed by mass spectrometry, the small differences between the labeling yield obtained by PC and HPLC were due to the concurrent formation of di-[(^{123}I) iodohypericin in low percentage (approximately 3%), which was detected together with mono-(^{123}I)] iodohypericin by PC.

After labeling, excessive reagents (unlabeled Hyp and iodogen) were removed by HPLC using acetonitrile/5 mmol/L ammonium acetate buffer at pH 7.0 as mobile phase in a gradient mode (0 min: 75:25, v/v, 5 min: 75:25, v/v, 30 min: 90:10, v/v). Good separation between Hyp

and radioiodinated Hyp peaks was achieved. ^{123}I-Hyp was obtained with a radiochemical purity above 99.0%. However, broad peaks with long retention times for Hyp and radioiodinated Hyp were typically observed during the purification process. It seems once radioiodinated Hyp is mixed with unlabeled Hyp in a total mass of about 2 mg, they might undergo partial retention in the HPLC system due to aggregate formation. Under physiological conditions, such aggregates may show reduced necrosis affinity and increased uptake in organs of the mononuclear phagocyte system (MPS), hampering the potential clinical usefulness of ^{131}I-Hyp for OncoCiDia.

Confronted problems: OncoCiDia has shown the best results using a mixture of radioiodinated Hyp/unlabeled Hyp[1]. To overcome the limitations related to the purification process, we recommended the clinical use of the non-purified radioiodinated Hyp, which is attained with high labeling yields (> 95%). However, conditions for Hyp radioiodination require excess of starting material at high concentrations of DMSO, which also dissolved the oxidizing agent iodogen. As a result, both reagents remain in the formulation of the non-HPLC purified radioiodinated Hyp, giving toxicity concerns. Moreover, the unlabeled Hyp present in the mixture is in a concentration range of 10^{-3} mol/L, in which it may aggregate in biocompatible aqueous formulations. Regarding $^{123/131}$I-Hyp, the incorporation of an iodine atom into a molecule can also result in a more lipophilic and less water soluble derivative[72]. Under these circumstances, a proper delivery system is essential for preventing aggregate formation and subsequently ensuring efficient targeting to necrotic tumor. Another potential issue arises with the co-injection of unlabeled Hyp which could influence $^{123/131}$I-Hyp on the biodistribution and targetability over time. Since the treatment of solid tumors requires the preferential delivery of a radiotherapeutic dose to the tumor while preventing normal tissues from undesired side effects[73], the dosimetry of this co-injection approach has to be estimated, as well. These above-mentioned problems have been assessed or addressed below.

Formulation: For $^{123/131}$I-Hyp/Hyp, the co-solvency approach seems to be a good alternative due to its rapidness and simplicity. In preclinical investigations, a formulation consisting of water/ polyethylene glycol (PEG 400) (80/20, v/v) has been reported[1]. Pure DMSO as solvent for the poorly water soluble $^{123/131}$I-Hyp/Hyp has also been used[74]. However, further optimizations are needed.

In a recent study, we tested several delivery systems for $^{123/131}$I-Hyp/Hyp using macroscopic and microscopic techniques and the results are summarized in Table 1[75]. Overall, formulations with a water content below 40% showed red fluorescent solutions without aggregate formation. In contrast, formulations containing around 70% water appeared as cloudy brownish solutions with reduced fluorescent properties. Animal studies confirmed the previous *in vitro* observations. For instance, when DMSO/PEG 400/water (25:60:15, v/v/v) was used as a vehicle, $^{123/131}$I-Hyp/Hyp showed low uptake in MPS organs, high necrosis affinity and striking tumoricidal effects days after OncoCiDia application. With $^{123/131}$I-Hyp/Hyp in DMSO/saline (20:80, v/v), instead, radioactivity accumulation in MPS organs but low uptake in necrotic tumor were found. Consequently, poor radiation dose was deposited in the tumor, leading to disease progression because of rapid repopulation of residual cancer cells at the tumor periphery after VDA attack[75].

However, earlier studies have reported that the common pharmaceutical solvents may have biological and pharmacological activity mainly when given undiluted[76-78]. Alternatively, the water-soluble sodium cholate (NaCh), a naturally occurring liver-produced surfactant with low toxicity, was assessed as a potential solubilizing agent for ^{123}I-Hyp/Hyp in an animal model of acute myocardial infarction (MI) (Cona *et al*[79]). The amphiphilic NaCh molecule with hydrophilic and hydrophobic sides of different solubility properties forms micelles, which act as emulsifier above the critical micellar concentration. Necrosis avidity of ^{123}I-Hyp/Hyp dissolved in a NaCh solution and its favorable biodistribution were demonstrated (Figure 6). The suitability of NaCh as a solubilizing agent of ^{123}I-Hyp for hotspot imaging of acute MI could be demonstrated (Cona *et al*[79]).

Biodistribution and dosimetry studies: Tissue distribution of ^{123}I-Hyp/Hyp was studied on animal models either of reperfused partial liver infarction (RPLI)[80] or ethanol-induced muscle necrosis. Dosimetric extrapolations of ^{131}I-Hyp from animals to humans were attempted using biodistribution data of ^{123}I-Hyp in RPLI animals in combination with Organ Level Internal Dose Assessment/Exponential Modeling software, microsphere model and human phantoms of both genders.

^{123}I-Hyp was accumulated at high concentrations in hepatic infarction and muscle necrosis but low uptake either in viable liver or muscle was detected (Figure 7), as previously reported[1,7,74,75]. Dosimetry studies revealed much higher (> 100 times) absorbed doses of ^{131}I-Hyp in hepatic infarction than in normal liver (Cona *et al*[79]). Based on this finding, such doses seem to be much higher than those estimated with other radiotherapeutics under investigation or currently used in clinic (Table 2)[31,81-88]. This corroborates the high affinity for tumor necrosis as well as the tumor shrinkage and growth delay previously observed in animals bearing different engrafts tumors after a single treatment with OncoCiDia (Figure 8)[1,75,89].

In biodistribution studies, ^{123}I-Hyp was cleared within 24 h with reduced blood pool radioactivity. Thyroid, the dose limiting organ for ^{131}I-labeled products, showed almost no radioactivity concentration due to the absence free iodide at earlier time points, suggesting *in vivo* stability of $^{123/131}$I-Hyp. However, an increased uptake in the gland was detected, starting at the second day after tracer administration. In the lungs, a persistent ^{123}I-Hyp uptake was found, leading to a moderately absorbed radiation

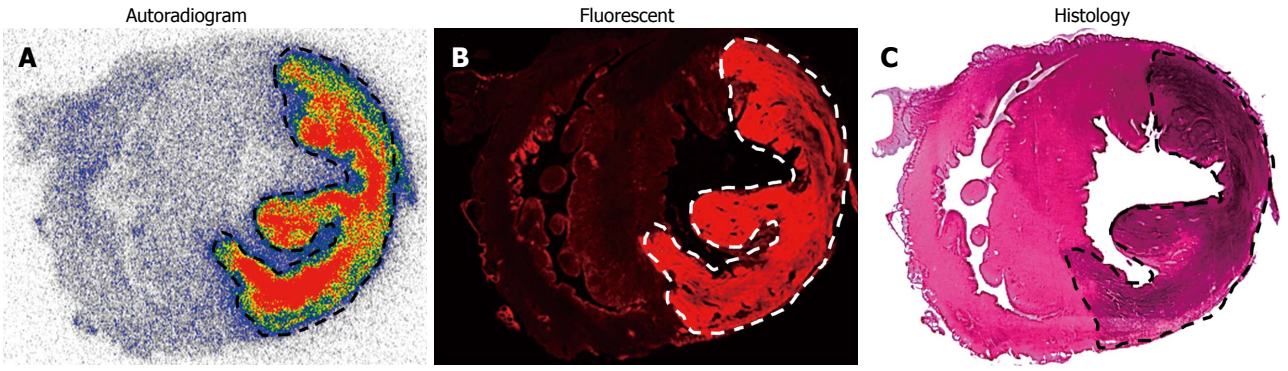

Figure 6 Post-mortem analysis of infarcts and viable heart tissues from rabbits with acute reperfused myocardial infarction having intravenously received iodine-123 labeled hypericin/hypericin dissolved in a 0.07 mol/L solution of the liver-produced surfactant sodium cholate. A: A typical autoradiogram of 50-μm-thick sections reveals higher tracer uptake in infarction than in viable myocardium. The color code bar indicates the coding scheme for the radioactivity; B: Microscopic images of 50-μm-thick sections confirm the selective affinity of the highly fluorescent iodine-123-labeled-hypericin/hypericin for acute myocardial infarction in contrast to the low fluorescent signal found in viable myocardium; C: The H and E-stained section corroborates the location of the viable myocardium tissue and the presence of myocardial necrosis characterized by scattered hemorrhage.

Table 1 Evaluation of physical properties of different formulations of ^{123}Hyp/Hyp examined by macroscopic digital imaging under white light and ultraviolet light (254 nm) and by microscopy over a corresponding drop in bright field and fluorescence illumination mode

Formulation	Macroscopic digital imaging	Microscopy
DMSO/saline (20/80, v/v)	Cloudy brownish solution, no fluorescence	Massive formation of aggregates reduced fluorescent intensity
DMSO/water (25/75, v/v)	Cloudy brownish solution, no fluorescence	Massive formation of aggregate reduced fluorescent intensity
DMSO/D10W (25/75, v/v)	Cloudy brownish solution, no fluorescence	Massive formation of aggregates reduced fluorescent intensity
DMSO/D20W (25/75, v/v)	Cloudy brownish solution, no fluorescence	Massive formation of aggregates reduced fluorescent intensity
DMSO/serum (25/75, v/v)	Cloudy brownish solution, moderate fluorescence signal	Massive formation of aggregates moderate fluorescent intensity
DMSO/PEG 400/water (25/60/15, v/v/v)	Bright red solution, highly fluorescent	No aggregates formation; strong, homogeneous fluorescence
EtOH/PEG 400/water (10/50/40, v/v/v)	Dark red solution, moderate fluorescence	Aggregate formation; moderate, heterogeneous fluorescence,
EtOH/PEG 400/water (10/60/30, v/v/v)	Red solution, minimum aggregation, high fluorescence	Some aggregates; strong, homogeneous fluorescence
PEG 400/water (60/40, v/v)	Red solution, high fluorescence	Some aggregates; strong, homogeneous fluorescence
PEG 400/water (70/30, v/v)	Bright red solution, highly fluorescent	Some aggregates; strong, homogeneous fluorescence
PVP-10000	Dark red solution, moderate fluorescence	Aggregate formation; reduced fluorescence intensity
PVP-29000	Dark red solution, moderate fluorescence	Aggregate formation; reduced fluorescence intensity
β-Cyclodextrins	Cloudy brownish solution, no fluorescence	Massive formation of aggregates reduced fluorescent intensity

DMSO: Dimethyl sulfoxide; D10W: 10% dextrose; D20W: 20% dextrose; EtOH: Ethanol; PEG 400: Polyethylene glycol 400; PVP: Polyvinylpyrrolidone.

dose of ^{131}I-Hyp. The highest levels of radioactivity were found in the intestines, which constitute the major elimination pathway of this radioactive compound. As a consequence, bowel structures received a high radiation dose, being identified as one of the dose limiting organs for OncoCiDia.

Effect of added Hyp on biodistribution and targetability of $^{123/131}$I-Hyp: In STR, it is known that the mass of the unlabelled (carrier) compound present in the final radioactive solution can be critical for high specific activities that are required for maximal radioactivity accumulation in the disease site. In a recent investigation for OncoCiDia, we proved that the co-injection of unlabelled Hyp positively affected the necrosis uptake of the radioiodinated Hyp in RPLI rats[90]. Although both preparations of ^{123}I-Hyp with micro- or Hyp-added dosing showed similar tissue distributions and major hepatobiliary excretion, it was found that the carrier-added ^{123}I-Hyp accumulated at higher concentrations in necrosis. Similarly, long retention into tumor necrosis for several weeks could characterize the carrier-added ^{131}I-Hyp (Figure 8 case 2), which explains the striking therapeutic effects observed in the previous experiments[1,75,89].

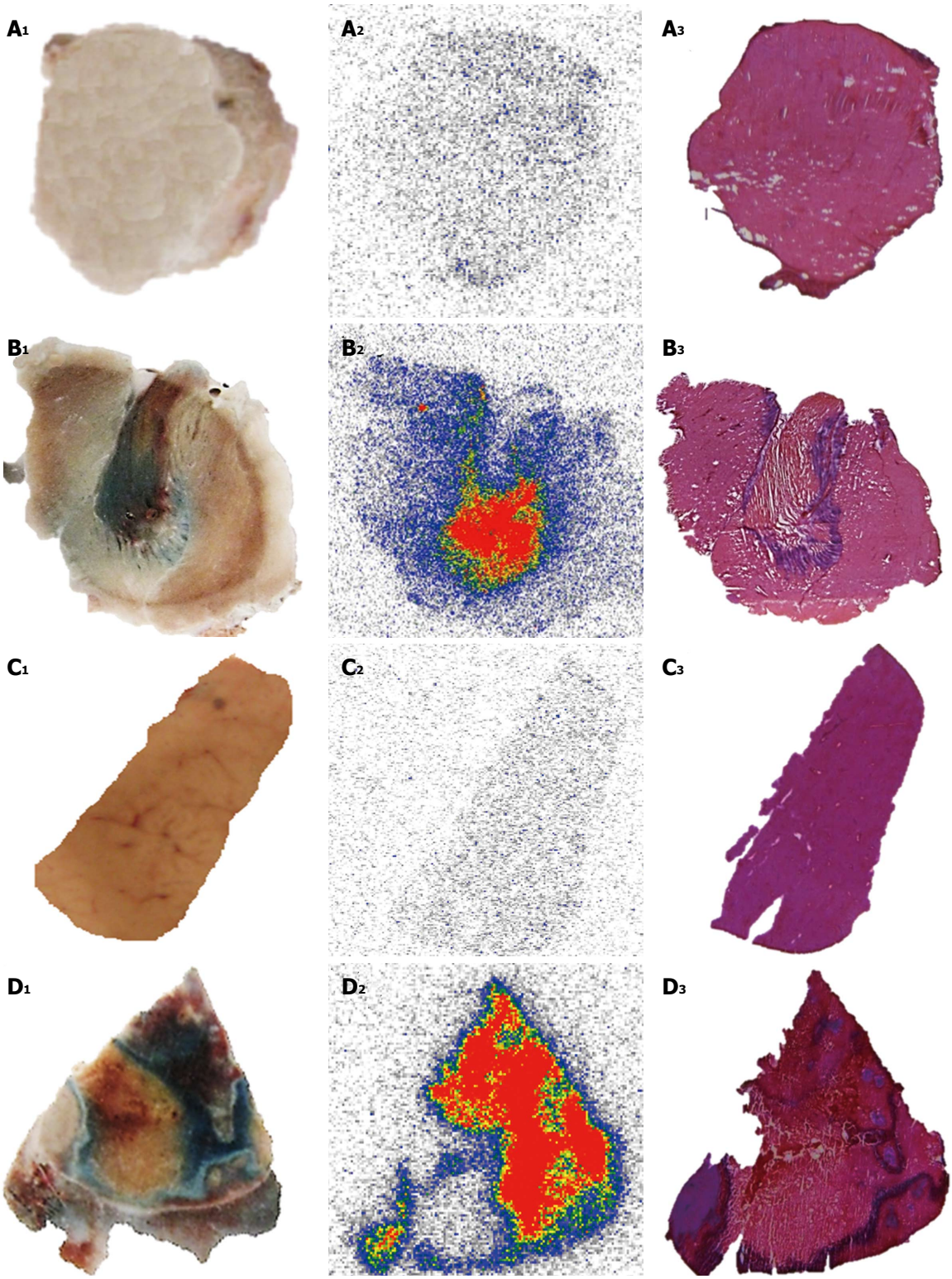

Figure 7 Post-mortem study of necrotic and viable tissues in the liver and muscle from animal models either of reperfused partial liver infarction or ethanol-induced muscle necrosis pre-injected with iodine-123 labeled hypericin/hypericin followed by 1% Evans blue solution. A, B: Muscle; C, D: Liver. The hepatic infarction (A_1) and necrotic muscle (B_1) retain Evans blue as blue hyper intense areas, with viable liver (C_1) and normal muscle (D_1) without staining. Autoradiograms of 50-μm-thick sections show high tracer uptake in hepatic infarction (A_2) and muscle necrosis (B_2) but low accumulation either in viable liver (C_2) or muscle (D_2). The color code bar represents the code for the radioactivity concentration. By histology, the presence of hepatic infarction (A_3) and muscle necrosis (B_3) and the location of the viable liver (C_3) and muscle (D_3) tissues are verified.

Toxicity studies: OncoCiDia is a two-step anticancer strategy involving different compounds with potential chemical and/or radiochemical toxicities, which have been investigated, and possible solutions are herein proposed.

Toxicity from VDAs can happen as a result of the ef-

Table 2 Dosimetry aspects of different anticancer therapeutic agents under pre-clinical and clinical investigation

Therapeutics	Dosimetry calculations	Species	Targeting tissue	Pathology	Dose to tumor (mGy/MBq)	Ref.
^{131}I-Hyp	OLINDA/EXM software	RPLI rats	Necrotic tissue	Solid tumors	276–93600	[79]
^{131}I-Labeled TNT-1 monoclonal antibody	Organ uptake-time integration by trapezoid method Whole body image analysis	Nude mice bearing ME-180 human cervical tumors	Histone fraction H1 in necrotic tissues	Cervical carcinoma cell	366–3610	[31]
^{131}I-m-iodobenzylguanidine (MIBG)	MicroPET/CT 124I-MIBG OLINDA/EXM software	Mice bearing A431 human epithelial carcinoma xenografts	Norepinephrine transporter	Neuroblastoma	97–380	[80]
^{131}I- labeled monoclonal antibody MN-14	MIRDOSE3 software	Nude mice with intraperitoneal LS174T tumors	Carcinoembryonic antigen	Peritoneal metastases of colorectal origin	-16200	[89]
^{131}I-tositumomab	SPECT/CT Imaging DPM Monte Carlo electron and photon transport program	Humans	CD20-positive B-cells	Refractory B-cell NHL	2.81 (mean)	[81]
^{177}Lu-DOTA-AE105	Organ uptake-time integration by trapezoid method Sphere model	Nude mice bearing colorectal HT-29 tumor	uPAR-positive HT-29 xenograft	Colorectal cancer	5.8	[82]
^{177}Lu-pertuzumab	Organ uptake-time integration by trapezoid method Sphere model	BALB/c (nu/nu) Mice with HER-2–overexpressing xenografts	HER-2 tyrosine kinase receptor	Breast cancer	-6900	[83]
^{186}Re-1-hydroxy- ethylidene-1,1 diphosphonic acid	MIRDOSE 3.1 software	Humans	Bone mineral metabolite	Skeletal metastases	23–34	[84]
^{90}Y-ibritumomab tiuxetan	PET/CT Imaging DPM ^{89}Zr-ibritumomab tiuxetan OLINDA/EXM software	Humans	CD20-positive B-cells	Relapsing NHL	8.6–28.6	[85]
^{90}Y- DOTA0-DPhe1-Tyr3-octreotide	SPECT/CT Imaging DPM ^{111}In-DOTA-TOC	Humans	Somatostatin receptor subtype 2	NETs	4-31 (mean 10)	[86]

CT: Computed tomography; DOTA: 1,4,7,10-tetraazacyclododecane-1,4,7,10-tetraacetic acid; ^{131}I: Iodine-131; ^{177}Lu: Lutetium-177; NETs: Neuroendocrine tumors; OLINDA/EXM: Organ level internal dose assessment/exponential modeling; PET: Positron emission tomography; ^{186}Re: Rhenium-186; RPLI: Reperfused partial liver infarction; SPECT: Single-photon emission computed tomography; TNT: Tumor necrosis treatment; DPM: Dose planning method; NHL: Non-Hodgkin lymphoma; DOTA-TOC: ^{90}Y- DOTA0-DPhe1-Tyr3-octreotide; ^{90}Y: Yttrium-90.

fect of VDAs either on tumor blood vessels or normal tissues. Lack of complete specificity for tumor-related vasculature or downstream effects induced by cytokines and other released factors can contribute to the toxic signs or effects. A distinctive transient and acute toxicity pattern with minor cumulative side effects such as tumor pain, nausea and vomiting, headaches, vision changes, symptoms associated to serotonin release, neuromotor abnormalities and cerebellar ataxia, acute hemodynamic disturbances, abdominal pain, hypertension, and tachycardia have been reported after VDA administration in clinical trials[91]. The degree and types of the side effects might differ among flavonoids and tubulin-binding agents[91].

So far, combretastatin A-4 phosphate (CA4P), a synthetic phosphorylated derivative of the natural product combretastatin A-4, is a tubulin-binding agent that has been most extensively used in OncoCiDia experiments. In preclinical studies, intravenous CA4P at a dose of 10 mg/kg has shown a complete and rapid vascular shutdown of the tumor with minimal effects at the well-perfused periphery[1,89]. However, some discrepancies have been noted in animal studies and clinical trials concerning the anticancer effect of VDAs[92]. According to the Food and Drug Administration-approved rules for the correct dose calculation[93], such a dose of 10 mg/kg in rodents would be equivalent to 60 mg/m^2 in humans. However, phase I clinical trials of CA4P have demonstrated a minimal objective tumor response by using similar doses of 52 to 68 mg/m^2[94]. The reason for this difference is not yet clear but could be caused by either miscalculations of the dose based on body surface area in mg/m^2 or due to inaccurate dose translation from animal (mg/kg) to humans (mg/m^2) in addition to the less likely interspecies differences. Based on our experiences, we believe that it may hamper the actual potentialities of VDAs for getting desired anticancer effects in human patients if the dose issues are not properly settled. To overcome the problem, an alternative option could be to increase the total injected dose of CA4P but in an approach of multiple small doses for preventing acute side effects[95]. Moreover, since cardiovascular toxicity seems to be with the most toxicity concerns for CA4P[96], pretreatments with high doses of intravenous diltiazem for preventing hypertension accompanied with amlodipine for secondary prophylaxis or nifedipine and atenolol for blocking tachycardia can be also applied[97,98]. Patients taking QT prolonging drugs, or with a history of significant cardiovascular disease, hypokalemia or hypomagnesemia should be handled with great caution[99].

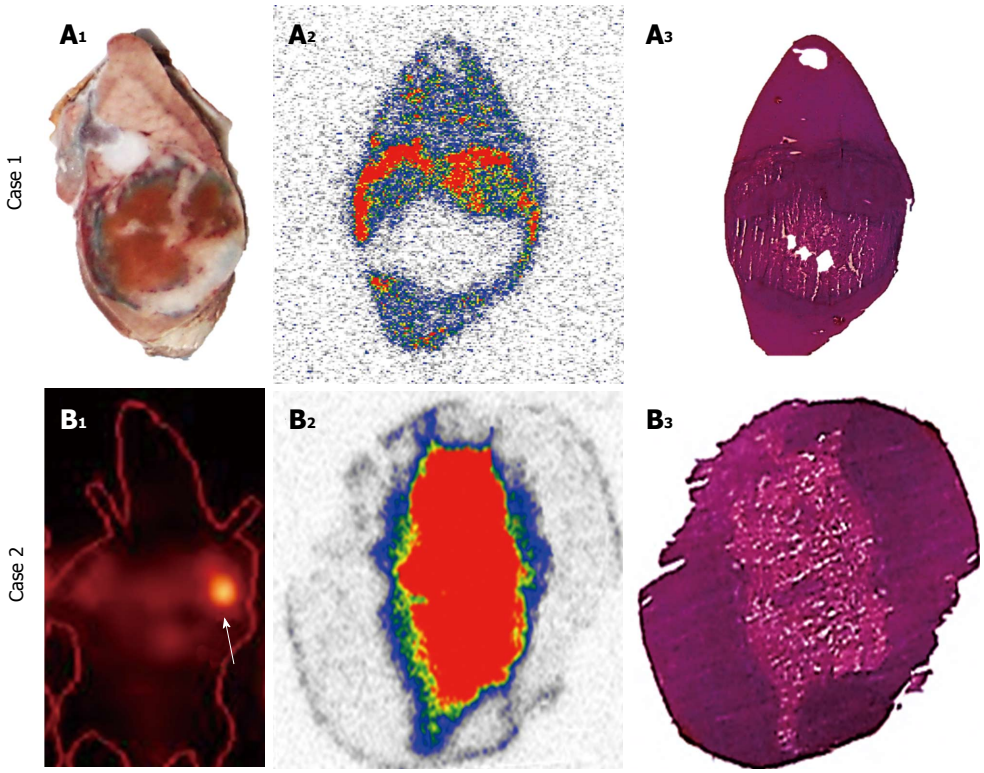

Figure 8 Difference in accumulation patterns of iodine-123/131 labeled hypericin/hypericin in tumor necrosis over time. Case 1: *Ex-vivo* analysis of necrotic tumors from rats with hepatic rhabdomyosarcoma (R1) in the first 24 h after the administration of iodine-123 labeled hypericin/hypericin (^{123}I-Hyp/Hyp) in DMSO/PEG 400/propylene glycol/water (25:25:25:25, v/v/v/v) followed by 1% Evans blue solution. At 24 h after ^{123}I-Hyp/Hyp injection, the tumor necrosis is perfectly outlined by the Evans blue as a blue rim, with viable tumor residues and normal liver with almost no staining (A_1). On the autoradiogram, a perfect match was seen between the high levels of ^{123}I-Hyp/Hyp accumulated in the ring (A_2) and the rim of Evans blue previously observed (A_1). Histology analysis confirms the regions of the liver, necrotic and viable tumors (A_3). Case 2: Single-photon emission computed tomography (SPECT), autoradiograms and histology in severe combined immunodeficiency mice bearing bilateral radiation-induced fibrosarcoma-1 subcutaneously having received combretastatin A-4 phosphate (CA4P) to induce tumor necrosis followed 24 h later by ^{131}I-Hyp/Hyp in DMSO/PEG 400/water (25:60:15, v/v/v). Twelve days after ^{131}I-Hyp/Hyp administration, SPECT detects a persistent intense high radioactivity mainly inside the tumor necrotic core (arrow). Autoradiography (B_2)[1] and histology (B_3) of the tumor after 30 d of tracer injection correspond well with the hotspot imaging on tumor (B_1). [1]The color code bar indicates the coding scheme for the radioactivity. DMSO: Dimethyl sulfoxide; PEG 400: Polyethylene glycol 400.

A study on plasma pharmacokinetics and cerebrospinal fluid penetration of Hyp in rhesus monkeys was conducted. Intravenous administration of 2 mg/kg Hyp was well tolerated. At a dose of 5 mg/kg, a transient severe photosensitivity rash was seen at 12 h that resolved within 12 d[100]. In a phase I study to evaluate the safety and antiretroviral activity of Hyp in thirty HIV-infected patients, weekly repeated IV doses of 0.25 or 0.5 mg/kg were tested. Eleven out of twenty-three patients developed severe cutaneous phototoxicity[101]. In patients with recurrent malignant glioma, a newly developed water soluble formulation of Hyp was IV given (0.1 mg/kg) for tumor visualization. Hyp application proved to be safe with no side effects[102]. Therefore, a low single dose of Hyp at < 0.2 mg/kg for OncoCiDia should be free of noticeable side effects.

I-131 has been used successfully for over 70 years to treat hyperthyroidism and papillary or follicular thyroid cancer and its proper therapeutic use is almost without side effects[103].

However, since accumulation of radioactive iodine was observed in the thyroid, potential damage to the gland could occur due to unnecessary radiation exposure. Therefore, patients undergoing OncoCiDia treatment should take a thyroid-blocking agent on a daily basis before, during and after radiopharmaceutical administration. Either Lugol's solution consisting of elemental iodine and potassium iodide in water or supersaturated potassium iodide solution or oral potassium iodide can be used for this purpose[104].

In a toxicity study with Hyp labeled with non-radioactive iodine (^{127}I), the animals tolerated well IV injections of 0.1 and 10 mg/kg without any signs of clinical toxicity or obvious side effects. The median lethal dose (LD_{50}) of 20.26 mg/kg for ^{127}I-Hyp was above 1000 times of the experimental chemical dose of ^{131}I-Hyp used in OncoCidia, suggesting a wide safety margin with insignificant chemotoxicity[105].

On the other hand, radiation toxic effects could be an issue for ^{131}I-Hyp. Experimental evidence indicated that persistent radioactivity retention mainly occurred in the intestines within few days after injection due to its hepatobiliary excretion[70,75,90]. The acute gastrointestinal syndrome is a main concern following irradiation of the intestinal tract[106]. In a recent study, we tested the suitability of using a newly designed catheter to reduce intestinal

retention of radioactivity after IV administration of ^{131}I-Hyp. Biodistribution and pharmacokinetics of radioiodinated Hyp were also investigated in animals with and without catheterization. In general, the total radioactivity accumulated in the intestines was dramatically reduced by ten times in those animals with catheter placement. Improved tissue biodistribution and kinetic parameters of ^{123}I-Hyp were also seen in cannulated animals. By using this approach, radiation overexposure because of prolonged excretion of ^{131}I-Hyp can be prevented in the future clinical practice[107].

A safety study of IV administered iodogen in DMSO was conducted in mice of both sexes. LD_{50} was determined with iodogen/DMSO doses ranging from 40.0 to 70.0 mg/kg. Toxicity at 30.0 mg/kg was tested for changes in behavior, body weight, and serum biochemistry over 14 d. Due to the toxicity concerns associated with the use of DMSO, a high dose of the solvent was also concurrently tested.

Good safety profile was demonstrated with iodogen in DMSO with LD_{50} values above 50.0 mg/kg and pure DMSO. No animal deaths, pathologies or clinical toxicities were recorded after 30.0 mg/kg iodogen in DMSO, which is 3000 times the dose intended for possible human applications[108].

Overall these data put forward a solid indication for the manageable and tolerable safety of OncoCiDia and potential upcoming clinically applicable formulations in terms of both radiotoxicity and chemotoxicity.

TRANSLATIONAL RESEARCH ON CARDIAC APPLICATIONS OF IODINATED HYPERICIN

Nuclear imaging for diagnosis of myocardial ischemia/infarction

Coronary heart disease, in which MI is a major component, represents the most common cause of death in the Western world. To assess myocardial viability, nuclear imaging uses radiolabelled compounds recognizing specific structures, receptors or antigens to scrutinize the molecular process under physiological conditions in a noninvasive manner. Several myocardial perfusion tracers for single photon emission computed tomography (SPECT) such as thallium-201 (^{201}Tl) and technetium-99m (^{99m}Tc) labeled agents (*e.g.*, sestamibi and tetrofosmin) are currently available in the clinic. They evenly distribute throughout the normal myocardium in proportion to the blood flow, depicting the dead/ischemic tissues as "black spot". However, the development of specific targeting agents with genuine necrosis affinity constitutes an important goal in the management of cardiac pathologies. They may allow early detection, delineation of the infarcted or ischemic area, patient follow-up over-time and evaluation of the response to revascularization therapies[109]. Other cardiovascular diseases related to cardiac cell death could be identified including diverse cardiomyopathy[110], myocardial inflammation, acute myocarditis[111]. Acute or chronic diffuse myocardial damage due to cardiac transplant rejection could also be detected[112].

Various "hot spot" imaging tracers have been exploited for the visualization of MI. Technetium (^{99m}Tc)-pyrophosphate accumulates in necrotic myocardium by targeting the calcium phosphate present in the mitochondria of infarcted or harshly damaged myocardium[113]. ^{99m}Tc-glucarate complex preferentially localizes into basic protein histones within denatured nuclei and subcellular organelles in the dead cardiomyocytes[114]. ^{111}In-labelled monoclonal anti-myosin Fab specifically recognizes the intracellular heavy chain of the exposed cardiac myosin of severely damaged cells[115]. Unfortunately, overestimation of the infarct size due to poor specificity for distinguishing ischemic and necrotic tissues[116,117], and reduced diagnostic accuracy and low target to background ratio on scintigraphic images because of the prompt dissociation of the tracer *in vivo* and short-term accumulation at the damage site[7] have been noticed.

^{123}I-Hyp as a complementary necrosis avid cardiac scintigraphic agent

By micro-single photon emission computed tomography (μSPECT), the potential usefulness of the necrosis avid ^{123}I-Hyp for detection and quantification of acute MI has been reported[118], which is essential for clinical management of ischemic heart disease. In a more recent study[119], ^{123}I-Hyp was compared with the commercial myocardial perfusion agent technetium-99m-labeled-hexakis (2-methoxyisobutylisonitrile) (^{99m}Tc-Sestamibi) in organ distribution and targetability in rabbits with acute MI using dual-isotope simultaneous acquisition-μSPECT/computed tomography and postmortem methods. ^{123}I-Hyp underwent hepatobiliary excretion whereas ^{99m}Tc-Sestamibi distribution was characterized by more rapid hepatorenal elimination. ^{99m}Tc-Sestamibi preferentially accumulated in the normal myocardium, whereas ^{123}I-Hyp confirmed to be a necrosis specific agent that allowed hot spot imaging of irreversibly damaged myocardium or acute MI. Therefore, ^{99m}Tc-Sestamibi and ^{123}I-Hyp can be considered as a pair of complementary tracers for DISA-SPECT/CT in nuclear cardiology[119].

A TRANSLATIONAL APPLICATION ELICITED FROM MECHANISM STUDY ON HYPERICIN

Gallstone basics and pathologies

Cholelithiasis refers to the presence of gallstones in the gallbladder. Although these supersaturated deposits of bile are initially formed within the gallbladder, they may distantly pass into other parts of the biliary tract, reaching the common bile duct, the cystic duct and the pancreatic duct. They can broadly vary in size and appear

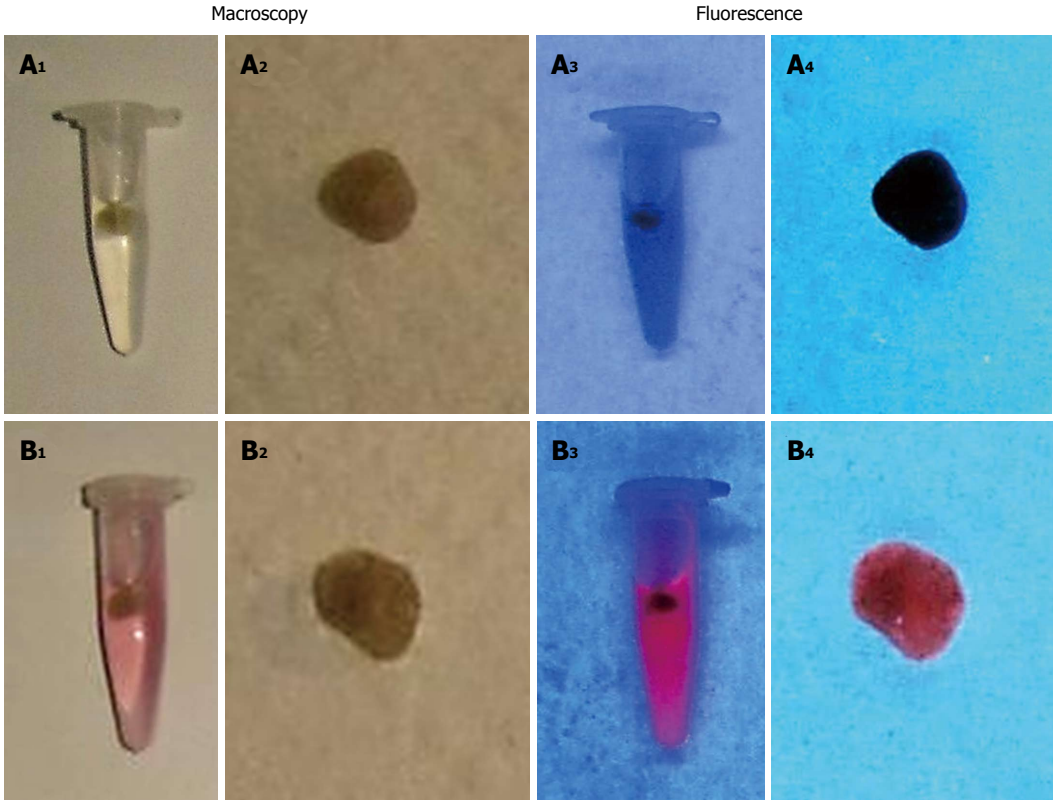

Figure 9 Macroscopic digital imaging of gallbladder stones which were extracted from patients. Stones previously incubated in DMSO/PEG400/water (25:60:15, v/v/v) for 72 h and set as control (A_1, A_2) lack of fluorescent properties (A_3, A_4). Stones treated for 72 h with a solution of Hyp in DMSO/PEG400/water (25:60:15, v/v/v) (B_1, B_2) reveals fluorescence (B_3, B_4) under the UV light of 254 nm. DMSO: Dimethyl sulfoxide; PEG 400: Polyethylene glycol 400; UV: Ultraviolet.

as a single stone or as an assortment of stones with different sizes. Gallstones generally come in three different types including cholesterol stones that represent about 80%, pigment stones composed of bilirubin, the yellow breakdown product of normal heme catabolism found in bile, and mixed stones. Gallstones in the gallbladder may cause acute cholecystitis[120], an inflammatory condition distinguished by bile retention leading to secondary infection by intestinal microorganisms, mainly Escherichia coli, Klebsiella, Enterobacter, and Bacteroides species[121]. Presence of gallstones in the biliary tract can produce obstruction of the bile ducts, leading to severe ascending cholangitis or pancreatitis, which can be life-threatening. Eventually, they can be very painful and may require surgical intervention to remove the gallbladder and/or stones.

Hypericin as an optical imaging agent for fluorescent detection of gallstones

Since Hyp is primarily excreted *via* bile and its interaction with cholesterols has been proved[8,9], the potential use of Hyp as an optical imaging agent for fluorescent detection of gallstones in the clinic was explored. Cholesterol, pigment and mixed gallstones were derived from cholecystectomy patients. *In vitro* studies were conducted by incubating the gallstones with Hyp solutions at increasing concentrations (0-0.01 mg/mL) either in solvent or bile. Under UV light at 254 nm wavelength, red fluorescence was seen on stones previously incubated with Hyp, but this was not observed on only solvent or bile-treated gallstones (Figure 9). The intensity of stone fluorescence depended on Hyp concentration. Although other techniques like ultrasonography or cholescintigraphy scan with ^{99m}Tc-hepatobiliary iminodiacetic acid can usually detect gallstones, the use of Hyp may aid fluorescent detection and removal of gallstones during open and/or endoscopic cholecystectomy and cholangiotomy. *In vivo* studies are needed to prove whether it is a vital and applicable approach.

SAFETY EVALUATION OF MEDICAL DEVICES USING RADIOPHARMACEUTICAL APPROACH

Potential contamination risk from multiple uses of a contrast injection pump

Multiple uses of automatic contrast injection systems for automatic delivery of contrast media during enhanced imaging procedures can reduce costs and save resources. However, cross-contaminations with blood-borne pathogens of infectious diseases may occur[122,123]. To avoid possible nosocomial outbreaks, the injection system including the power syringes, filling and injecting set and

the patient line has to be completely changed for each patient. However, this proves expensive and time consuming due to the wasted surplus contrast materials in the setup from each exam, the consumptions of disposable devices, and the long pauses for changing the entire setup per patient. To reduce material and costs, several institutions worldwide have been applying multiple usages of the syringes with automatic injectors for serial patients. Generally, these commercially available injection systems contain a special one-way-valve tube device. However, nosocomial outbreaks between patients are still a problem because of contamination of the injection system with blood-borne pathogen[124].

A radioactive method for assessing microbial safety of an infusion set

The purpose of this experiment was to develop a radioactive method for quantitative safety evaluation of a new replaceable patient-delivery system[125]. This system (Transflux™ Diepenbeek, Belgium) contains a safety zone composed by a tube and two one-way valves. It permits to flush the whole injector system and the vein but prevents blood reflux during contrast-enhanced imaging. This system is replaced for each new patient, whereas the power syringes need to be changed only once a day after multiple uses for a series of patients. It has been applied for years in many radiology units without any contaminative infections reported, which though has to be experimentally justified.

By mimicking pathogens with a diffusible radiotracer, we evaluated the feasibility of using this system repeatedly without septic risks. The experiment was performed by intravenous injection of ^{99m}Tc-dimercaptopropionyl-human serum albumin in rabbits previously connected *via* an endovenous catheter to an automatic contrast injection system. Protocols with normal saline and contrast agent plus saline loaded in the injection system were compared. By sampling and analyzing aliquots from the filling and injecting set, patient line and blood, it was checked if the radiotracer from the patient line in contact with animal blood was able to cross the safety zone and reach the power syringes.

Overall, with both protocols, radioactivity was found in blood and in patient line but in none of the samples from the filling-injecting set. This radioactive method appears accurate and reliable. The patient-delivery system proves safe and convenient, which is in line with the clinical experiences collected to date. By replacing the patient delivery system, cross-contamination risks can be avoided without changing the main part of injection system. This method can be applied for evaluation of similar devices before human use.

CONCLUSION

Translational medicine aims at identifying solutions to specific health problems. Different but important difficulties faced in cancer treatment, identification of cardiac infarction, detection of cholelithiasis and safety evaluation of medical devices might be considerably tackled by well-designed laboratory experiments.

OncoCiDia presents an unconventional but general approach based on the necrosis avidity for treating multifocal and multitype malignant tumors. It uses a combined sequence of a vascular disrupting agent for triggering massive tumor necrosis followed by the necrosis avid ^{131}I-Hyp to destroy remaining tumor cells. Some technical optimizations have been performed and herein demonstrated to assist in introducing OncoCiDia to the possible clinical practice. The feasible Hyp radioiodination with good radiochemical yields and a proper formulation for *in vivo* applications have been investigated and discussed. The favorable biodistribution, dosimetry and pharmacokinetic patterns as well as good *in vivo* tolerance and low toxicity of radioiodinated Hyp have been exhibited in animal experiments. In general, the genuine benefits of ^{131}I-Hyp distinguished by high and unprecedented long-term accumulation in tumor necrosis in the vicinity of cancer cells and its convenient clearance mechanism through bile without renal retention could noticeably impact on cancer theragnostic management or open doors for handling a wide diversity of cancers in future clinical practice.

Targeting necrosis may offer new opportunities for the management of cardiac pathologies. The clinical introduction of radioactive necrosis-specific agents like ^{123}I-Hyp might play a complementary role in detection and quantification of acute myocardial infarction. The combination of the genuine ^{123}I-Hyp necrosis avidity with the preferential uptake of the currently used commercial myocardial perfusion agent by normal myocardium might offer additional information in the clinical management of this life-threatening pathology.

On the other hand, the use of the fluorophore hypericin as an optical imaging agent with low *in vivo* toxicity could be an excellent diagnostic tool for the detection and removal of gallstones in patients suffering from such common clinical conditions.

Finally, the risk of accidental cross-contamination in medical devices can be minimized through safety evaluation studies based on the inherent sensitivity of radioactive methods in preclinical animal experiments.

REFERENCES

1 **Li J**, Sun Z, Zhang J, Shao H, Cona MM, Wang H, Marysael T, Chen F, Prinsen K, Zhou L, Huang D, Nuyts J, Yu J, Meng B, Bormans G, Fang Z, de Witte P, Li Y, Verbruggen A, Wang X, Mortelmans L, Xu K, Marchal G, Ni Y. A dual-targeting anticancer approach: soil and seed principle. *Radiology* 2011; **260**: 799-807 [PMID: 21712473 DOI: 10.1148/radiol.11102120]

2 **Aschylus.** OncoCidia. Available from: URL: http: //www.aeschylus-philanthropy.eu/index.php/b/project/oncocidia

3 **Roger VL.** Epidemiology of myocardial infarction. *Med Clin North Am* 2007; 91: 537–552 [DOI: 10.1016/j.mcna.2007.03.007]

4 **Bauer A**, Mehilli J, Barthel P, Müller A, Kastrati A, Ulm K, Schömig A, Malik M, Schmidt G. Impact of myocardial salvage assessed by (99m)Tc-sestamibi scintigraphy on car-

diac autonomic function in patients undergoing mechanical reperfusion therapy for acute myocardial infarction. *JACC Cardiovasc Imaging* 2009; **2**: 449-457 [PMID: 19580728 DOI: 10.1016/j.jcmg.2008.12.018]

5 **Lombardo A**, Rizzello V, Galiuto L, Natale L, Giordano A, Rebuzzi A, Loperfido F, Crea F, Maseri A. Assessment of resting perfusion defects in patients with acute myocardial infarction: comparison of myocardial contrast echocardiography, combined first-pass/delayed contrast-enhanced magnetic resonance imaging and 99mTC-sestamibi SPECT. *Int J Cardiovasc Imaging* 2006; **22**: 417-428 [PMID: 16496094 DOI: 10.1007/s10554-005-9045-8]

6 **Ni Y,** Bormans G, Marchal G, Verbruggen A. Tissue infarction and necrosis specific compounds (of hypericin derivatives). Available from: URL: http://www.google.com/patents/EP1651201B1

7 **Ni Y**, Huyghe D, Verbeke K, de Witte PA, Nuyts J, Mortelmans L, Chen F, Marchal G, Verbruggen AM, Bormans GM. First preclinical evaluation of mono-[123I]iodohypericin as a necrosis-avid tracer agent. *Eur J Nucl Med Mol Imaging* 2006; **33**: 595-601 [PMID: 16450141 DOI: 10.1007/s00259-005-0013-2]

8 **Ho YF**, Wu MH, Cheng BH, Chen YW, Shih MC. Lipid-mediated preferential localization of hypericin in lipid membranes. *Biochim Biophys Acta* 2009; **1788**: 1287-1295 [PMID: 19366588 DOI: 10.1016/j.bbamem.2009.01.017]

9 **Eriksson ESE,** Eriksson LA. The influence of cholesterol on the properties and permeability of hypericin derivatives in lipid membranes. J. *Chem Theory Comput* 2011; **7**: 560–574 [DOI: 10.1021/ct100528u]

10 **Cancer Research UK.** Cancer Worldwide - the global picture. Future trends. Available from: URL: http: //www.cancerresearchuk.org/cancer-info/cancerstats/world/cancer-worldwide-the-global-picture

11 **Luster M**, Clarke SE, Dietlein M, Lassmann M, Lind P, Oyen WJ, Tennvall J, Bombardieri E. Guidelines for radioiodine therapy of differentiated thyroid cancer. *Eur J Nucl Med Mol Imaging* 2008; **35**: 1941-1959 [PMID: 18670773 DOI: 10.1007/s00259-008-0883-1]

12 **Gedik GK**, Hoefnagel CA, Bais E, Olmos RA. 131I-MIBG therapy in metastatic phaeochromocytoma and paraganglioma. *Eur J Nucl Med Mol Imaging* 2008; **35**: 725-733 [PMID: 18071700 DOI: 10.1007/s00259-007-0652-6]

13 **Polishchuk AL**, Dubois SG, Haas-Kogan D, Hawkins R, Matthay KK. Response, survival, and toxicity after iodine-131-metaiodobenzylguanidine therapy for neuroblastoma in preadolescents, adolescents, and adults. *Cancer* 2011; **117**: 4286-4293 [PMID: 21387264 DOI: 10.1002/cncr.25987]

14 **McEwan AJ**, Amyotte GA, McGowan DG, MacGillivray JA, Porter AT. A retrospective analysis of the cost effectiveness of treatment with Metastron (89Sr-chloride) in patients with prostate cancer metastatic to bone. *Nucl Med Commun* 1994; **15**: 499-504 [PMID: 7970425]

15 **Rhee TK**, Lewandowski RJ, Liu DM, Mulcahy MF, Takahashi G, Hansen PD, Benson AB, Kennedy AS, Omary RA, Salem R. 90Y Radioembolization for metastatic neuroendocrine liver tumors: preliminary results from a multi-institutional experience. *Ann Surg* 2008; **247**: 1029-1035 [PMID: 18520231 DOI: 10.1097/SLA.0b013e3181728a45]

16 **Smith K**, Byer G, Morris CG, Kirwan JM, Lightsey J, Mendenhall NP, Hoppe BS, Lynch J, Olivier K. Outcomes of patients with non-Hodgkin's lymphoma treated with Bexxar with or without external-beam radiotherapy. *Int J Radiat Oncol Biol Phys* 2012; **82**: 1122-1127 [PMID: 21570217 DOI: 10.1016/j.ijrobp.2010.09.044]

17 **Micallef IN**. Ongoing trials with yttrium 90-labeled ibritumomab tiuxetan in patients with non-Hodgkin's lymphoma. *Clin Lymphoma* 2004; **5** Suppl 1: S27-S32 [PMID: 15498147]

18 **Virgolini I**, Traub T, Novotny C, Leimer M, Füger B, Li SR, Patri P, Pangerl T, Angelberger P, Raderer M, Burggasser G, Andreae F, Kurtaran A, Dudczak R. Experience with indium-111 and yttrium-90-labeled somatostatin analogs. *Curr Pharm Des* 2002; **8**: 1781-1807 [PMID: 12171531 DOI: 10.2174/1381612023393756]

19 **Kwekkeboom DJ**, Kam BL, van Essen M, Teunissen JJ, van Eijck CH, Valkema R, de Jong M, de Herder WW, Krenning EP. Somatostatin-receptor-based imaging and therapy of gastroenteropancreatic neuroendocrine tumors. *Endocr Relat Cancer* 2010; **17**: R53-R73 [PMID: 19995807 DOI: 10.1677/ERC-09-0078]

20 **Paganelli G**, Chinol M. Radioimmunotherapy: is avidin-biotin pretargeting the preferred choice among pretargeting methods? *Eur J Nucl Med Mol Imaging* 2003; **30**: 773-776 [PMID: 12557049 DOI: 10.1007/s00259-002-1090-0]

21 **Sharkey RM**. Radioimmunotherapy against the tumor vasculature: A new target? *J Nucl Med* 2006; **47**: 1070-1074 [PMID: 16818938]

22 **Govindan SV**, Goldenberg DM, Hansen HJ, Griffiths GL. Advances in the use of monoclonal antibodies in cancer radiotherapy. *Pharm Sci Technolo Today* 2000; **3**: 90-98 [PMID: 10707044 DOI: 10.1016/S1461-5347(00)00241-8]

23 **Ginj M**, Zhang H, Waser B, Cescato R, Wild D, Wang X, Erchegyi J, Rivier J, Mäcke HR, Reubi JC. Radiolabeled somatostatin receptor antagonists are preferable to agonists for in vivo peptide receptor targeting of tumors. *Proc Natl Acad Sci USA* 2006; **103**: 16436-16441 [PMID: 17056720 DOI: 10.1073/pnas.0607761103]

24 **Merlo LM**, Pepper JW, Reid BJ, Maley CC. Cancer as an evolutionary and ecological process. *Nat Rev Cancer* 2006; **6**: 924-935 [PMID: 17109012 DOI: 10.1038/nrc2013]

25 **Aggarwal BB**, Danda D, Gupta S, Gehlot P. Models for prevention and treatment of cancer: problems vs promises. *Biochem Pharmacol* 2009; **78**: 1083-1094 [PMID: 19481061 DOI: 10.1016/j.bcp.2009.05.027]

26 **Hornick JL**, Sharifi J, Khawli LA, Hu P, Biela BH, Mizokami MM, Yun A, Taylor CR, Epstein AL. A new chemically modified chimeric TNT-3 monoclonal antibody directed against DNA for the radioimmunotherapy of solid tumors. *Cancer Biother Radiopharm* 1998; **13**: 255-268 [PMID: 10850361]

27 **Epstein AL**, Chen FM, Taylor CR. A novel method for the detection of necrotic lesions in human cancers. *Cancer Res* 1988; **48**: 5842-5848 [PMID: 3048650]

28 **Charbit A**, Malaise EP, Tubiana M. Relation between the pathological nature and the growth rate of human tumors. *Eur J Cancer* 1971; **7**: 307-315 [PMID: 4328281 DOI: 10.1016/0014-2964(71)90073-9]

29 **Malaise EP**, Chavaudra N, Tubiana M. The relationship between growth rate, labelling index and histological type of human solid tumours. *Eur J Cancer* 1973; **9**: 305-312 [PMID: 4360278 DOI: 10.1016/0014-2964]

30 **Miller GK**, Naeve GS, Gaffar SA, Epstein AL. Immunologic and biochemical analysis of TNT-1 and TNT-2 monoclonal antibody binding to histones. *Hybridoma* 1993; **12**: 689-698 [PMID: 8288270 DOI: 10.1089/hyb.1993.12.689]

31 **Chen FM**, Taylor CR, Epstein AL. Tumor necrosis treatment of ME-180 human cervical carcinoma model with 131I-labeled TNT-1 monoclonal antibody. *Cancer Res* 1989; **49**: 4578-4585 [PMID: 2743341]

32 **Kanduc D**, Mittelman A, Serpico R, Sinigaglia E, Sinha AA, Natale C, Santacroce R, Di Corcia MG, Lucchese A, Dini L, Pani P, Santacroce S, Simone S, Bucci R, Farber E. Cell death: apoptosis versus necrosis (review). *Int J Oncol* 2002; **21**: 165-170 [PMID: 12063564]

33 **Kroemer G**, Galluzzi L, Vandenabeele P, Abrams J, Alnemri ES, Baehrecke EH, Blagosklonny MV, El-Deiry WS, Golstein P, Green DR, Hengartner M, Knight RA, Kumar S, Lipton SA, Malorni W, Nuñez G, Peter ME, Tschopp J, Yuan J, Piacentini M, Zhivotovsky B, Melino G. Classification of cell death: recommendations of the Nomenclature Committee on Cell Death 2009. *Cell Death Differ* 2009; **16**: 3-11 [PMID: 18846107 DOI: 10.1038/cdd.2008.150]

34 **Walker NI**, Harmon BV, Gobé GC, Kerr JF. Patterns of cell death. *Methods Achiev Exp Pathol* 1988; **13**: 18-54 [PMID: 3045494]

35 **Hitomi J**, Christofferson DE, Ng A, Yao J, Degterev A, Xavier RJ, Yuan J. Identification of a molecular signaling network that regulates a cellular necrotic cell death pathway. *Cell* 2008; **135**: 1311-1323 [PMID: 19109899 DOI: 10.1016/j.cell.2008.10.044]

36 **Wu W**, Liu P, Li J. Necroptosis: an emerging form of programmed cell death. *Crit Rev Oncol Hematol* 2012; **82**: 249-258 [PMID: 21962882 DOI: 10.1016/j.critrevonc.2011.08.004]

37 **Degterev A,** Huang Z, Boyce M, Li Y, Jagtap P, Mizushima N, Cuny GD, Mitchison TJ, Moskowitz MA, Yuan J. Chemical inhibitor of nonapoptotic cell death with therapeutic potential for ischemic brain injury. *Nat Chem Biol* 2005; **1**: 112-119 [DOI: 10.1038/nchembio711]

38 **Yu L**, Alva A, Su H, Dutt P, Freundt E, Welsh S, Baehrecke EH, Lenardo MJ. Regulation of an ATG7-beclin 1 program of autophagic cell death by caspase-8. *Science* 2004; **304**: 1500-1502 [PMID: 15131264 DOI: 10.1126/science.1096645]

39 **Cho YS**, Challa S, Moquin D, Genga R, Ray TD, Guildford M, Chan FK. Phosphorylation-driven assembly of the RIP1-RIP3 complex regulates programmed necrosis and virus-induced inflammation. *Cell* 2009; **137**: 1112-1123 [PMID: 19524513 DOI: 10.1016/j.cell.2009.05.037]

40 **Nanji AA**, Hiller-Sturmhöfel S. Apoptosis and necrosis: two types of cell death in alcoholic liver disease. *Alcohol Health Res World* 1997; **21**: 325-330 [PMID: 15706744]

41 **Ziegler U**, Groscurth P. Morphological features of cell death. *News Physiol Sci* 2004; **19**: 124-128 [PMID: 15143207 DOI: 10.1152/nips.01519.2004]

42 **Human pathology.** Available from: URL: http: //www.humpath.com/spip.php?article4548

43 **Street HH**, Goris ML, Fisher GA, Wessels BW, Cho C, Hernandez C, Zhu HJ, Zhang Y, Nangiana JS, Shan JS, Roberts K, Knox SJ. Phase I study of 131I-chimeric(ch) TNT-1/B monoclonal antibody for the treatment of advanced colon cancer. *Cancer Biother Radiopharm* 2006; **21**: 243-256 [PMID: 16918301 DOI: 10.1089/cbr.2006.21.243]

44 **Hdeib A**, Sloan AE. Convection-enhanced delivery of 131I-chTNT-1/B mAB for treatment of high-grade adult gliomas. *Expert Opin Biol Ther* 2011; **11**: 799-806 [PMID: 21521146 DOI: 10.1517/14712598.2011.579097]

45 **Chen S**, Yu L, Jiang C, Zhao Y, Sun D, Li S, Liao G, Chen Y, Fu Q, Tao Q, Ye D, Hu P, Khawli LA, Taylor CR, Epstein AL, Ju DW. Pivotal study of iodine-131-labeled chimeric tumor necrosis treatment radioimmunotherapy in patients with advanced lung cancer. *J Clin Oncol* 2005; **23**: 1538-1547 [PMID: 15735129 DOI: 10.1200/JCO.2005.06.108]

46 **Khawli LA**, Alauddin MM, Hu P, Epstein AL. Tumor targeting properties of indium-111 labeled genetically engineered Fab′ and F(ab′)2 constructs of chimeric tumor necrosis treatment (chTNT)-3 antibody. *Cancer Biother Radiopharm* 2003; **18**: 931-940 [PMID: 14969605 DOI: 10.1089/108497803322702897]

47 **Anderson PM,** Wiseman GA, Lewis BD, Charboneau W, Dunn WL, Carpenter SP, Chew T. A phase I safety and imaging study using radiofrequency ablation (RFA) followed by 131I-chTNT-1/B radioimmunotherapy adjuvant treatment of hepatic metastases. *Cancer Ther* 2003; **1**: 283-291

48 **Tozer GM**, Kanthou C, Baguley BC. Disrupting tumour blood vessels. *Nat Rev Cancer* 2005; **5**: 423-435 [PMID: 15928673 DOI: 10.1038/nrc1628]

49 **Chaplin DJ**, Hill SA. The development of combretastatin A4 phosphate as a vascular targeting agent. *Int J Radiat Oncol Biol Phys* 2002; **54**: 1491-1496 [PMID: 12459376 DOI: 10.1016/S0360-3016(02)03924-X]

50 **Chaplin DJ**, Dougherty GJ. Tumour vasculature as a target for cancer therapy. *Br J Cancer* 1999; **80** Suppl 1: 57-64 [PMID: 10466764]

51 **Siemann DW**, Bibby MC, Dark GG, Dicker AP, Eskens FA, Horsman MR, Marmé D, Lorusso PM. Differentiation and definition of vascular-targeted therapies. *Clin Cancer Res* 2005; **11**: 416-420 [PMID: 15701823]

52 **Karioti A**, Bilia AR. Hypericins as potential leads for new therapeutics. *Int J Mol Sci* 2010; **11**: 562-594 [PMID: 20386655 DOI: 10.3390/ijms11020562]

53 **Wolfender JL,** Queiroz EF, Hostettmann K. Photochemistry. In: Birkhäuser Verlag. St. John's Wort and its Active Principles in Depression and Anxiety. Basel, 2005: 5-19

54 **Dewick PM.** Aromatic Polyketides. Structural Modifications: Anthraquinones. In: Jonh Wiley & Sons Ltd. Medicinal natural products: a biosynthetic approach, 2nd ed. West Sussex, 2002: 63-71

55 **Leonhartsberger JG,** Falk H. The protonation and deprotonation equilibria of hypericin revisited. *Monatsh Chem* 2002; **133**: 167–172 [DOI: 10.1007/s706-002-8246-x]

56 **Etzlstorfer C,** Falk H, Müller N, Schmitzberger W, Wagner UG. Tautomerism and stereochemistry of hypericin: Force field, NMR, and X-ray crystallographic investigations. *Monatsh Chemie* 1993; **124**: 751-761 [DOI: 10.1007/BF00817311]

57 **Gutman I,** Marković Z, Solujić S, Sukdolak S. On the tautomers of hypericin. chemistry and materials science. *Monatshefte fur Chemie* 1998; **129**: 481-486 [DOI: 10.1007/PL00000105]

58 **Kapinus EI**, Falk H, Tran HTN. Spectroscopic investigation of the molecular structure of hypericin and its salts. *Monatshefte fuÈr Chemie* 1999; **130**: 623-635 [DOI: 10.1007/PL00010243]

59 **Bánó G**, Staničová J, Jancura D, Marek J, Bánó M, Uličný J, Strejčková A, Miškovský P. On the diffusion of hypericin in dimethylsulfoxide/water mixtures-the effect of aggregation. *J Phys Chem B* 2011; **115**: 2417-2423 [PMID: 21332112 DOI: 10.1021/jp109661c]

60 **Buriankova L**, Buzova D, Chorvat D, Sureau F, Brault D, Miskovský P, Jancura D. Kinetics of hypericin association with low-density lipoproteins. *Photochem Photobiol* 2011; **87**: 56-63 [PMID: 21114669 DOI: 10.1111/j.1751-1097.2010.00847.x]

61 **Sosa S**, Pace R, Bornancin A, Morazzoni P, Riva A, Tubaro A, Della Loggia R. Topical anti-inflammatory activity of extracts and compounds from Hypericum perforatum L. *J Pharm Pharmacol* 2007; **59**: 703-709 [PMID: 17524236 DOI: 10.1211/jpp.59.5.0011]

62 **Meruelo D**, Lavie G, Lavie D. Therapeutic agents with dramatic antiretroviral activity and little toxicity at effective doses: aromatic polycyclic diones hypericin and pseudohypericin. *Proc Natl Acad Sci USA* 1988; **85**: 5230-5234 [PMID: 2839837]

63 **Avato P**, Raffo F, Guglielmi G, Vitali C, Rosato A. Extracts from St John's Wort and their antimicrobial activity. *Phytother Res* 2004; **18**: 230-232 [PMID: 15103670 DOI: 10.1002/ptr.1430]

64 **Blank M**, Mandel M, Hazan S, Keisari Y, Lavie G. Anticancer activities of hypericin in the dark. *Photochem Photobiol* 2001; **74**: 120-125 [PMID: 11547544 DOI: 10.1562/0031-8655(2001)0740120AC]

65 **Linde K**, Ramirez G, Mulrow CD, Pauls A, Weidenhammer W, Melchart D. St John's wort for depression--an overview and meta-analysis of randomised clinical trials. *BMJ* 1996; **313**: 253-258 [PMID: 8704532 DOI: 10.1136/bmj.313.7052.253]

66 **Ni Y**, Bormans G, Chen F, Verbruggen A, Marchal G. Necrosis avid contrast agents: functional similarity versus structur-

al diversity. *Invest Radiol* 2005; **40**: 526-535 [PMID: 16024991]
67 **Miskovsky P**, Hritz J, Sanchez-Cortes S, Fabriciova G, Ulicny J, Chinsky L. Interaction of hypericin with serum albumins: surface-enhanced Raman spectroscopy, resonance Raman spectroscopy and molecular modeling study. *Photochem Photobiol* 2001; **74**: 172-183 [PMID: 11547551 DOI: 10.1562/0031-8655(2001)0740172IO]
68 **Song S**, Xiong C, Zhou M, Lu W, Huang Q, Ku G, Zhao J, Flores LG, Ni Y, Li C. Small-animal PET of tumor damage induced by photothermal ablation with 64Cu-bis-DOTA-hypericin. *J Nucl Med* 2011; **52**: 792-799 [PMID: 21498539 DOI: 10.2967/jnumed.110.086116]
69 **Loke KS**, Padhy AK, Ng DC, Goh AS, Divgi C. Dosimetric considerations in radioimmunotherapy and systemic radionuclide therapies: a review. *World J Nucl Med* 2011; **10**: 122-138 [PMID: 22144871 DOI: 10.4103/1450-1147.89780]
70 **Bormans G,** Huyghe D, Christiaen A, Verbeke K, de Groot T, Vanbilloen H, de Witte P, Verbruggen A. Preparation, analysis and biodistribution in mice of iodine-123 labeled derivatives of hypericin. *Journal of Labeled Compounds and Radiopharmaceuticals* 2004; **47**: 191–198 [DOI: 10.1002/jlcr.812]
71 **Sun ZP,** inventor. Iodogen method for preparation of radioiodinated Hypericin. Available from: URL: http://www.google.com/patents/CN101475461B?cl=zh
72 **Sihver W**, Bier D, Holschbach MH, Schulze A, Wutz W, Olsson RA, Coenen HH. Binding of tritiated and radioiodinated ZM241,385 to brain A2A adenosine receptors. *Nucl Med Biol* 2004; **31**: 173-177 [PMID: 15013482 DOI: 10.1016/j.nucmedbio.2003.10.007]
73 **Emami B**, Lyman J, Brown A, Coia L, Goitein M, Munzenrider JE, Shank B, Solin LJ, Wesson M. Tolerance of normal tissue to therapeutic irradiation. *Int J Radiat Oncol Biol Phys* 1991; **21**: 109-122 [PMID: 2032882 DOI: 10.1016/0360-3016(91)90171-Y]
74 **Li J**, Cona MM, Chen F, Feng Y, Zhou L, Yu J, Nuyts J, de Witte P, Zhang J, Himmelreich U, Verbruggen A, Ni Y. Exploring theranostic potentials of radioiodinated hypericin in rodent necrosis models. *Theranostics* 2012; **2**: 1010-1019 [PMID: 23139728 DOI: 10.7150/thno.4924]
75 **Cona MM,** Li J, Bauwens M, Feng Y, Sun Z, Zhang J, Chen F, Alpizar Y, Talavera K, de Witte P, Verbruggen A, Oyen R, Ni Y. Radioiodinated Hypericin: Its Biodistribution, Necrosis Avidity and Therapeutic Efficacy are Influenced by Formulation. *Pharm Res* 2013 Aug 9; Epub ahead of print [PMID: 23934256 DOI: 10.1007/s11095-013-1159-4]
76 **Laurent A**, Mottu F, Chapot R, Zhang JQ, Jordan O, Rüfenacht DA, Doelker E, Merland JJ. Cardiovascular effects of selected water-miscible solvents for pharmaceutical injections and embolization materials: a comparative hemodynamic study using a sheep model. *PDA J Pharm Sci Technol* 2007; **61**: 64-74 [PMID: 17479714]
77 **Reed KW**, Yalkowsky SH. Lysis of human red blood cells in the presence of various cosolvents. III. The relationship between hemolytic potential and structure. *J Parenter Sci Technol* 1987; **41**: 37-39 [PMID: 3559834]
78 **Conte G,** Di Blasi R, Giglio E, Parretta A, Pavel NV. Nuclear magnetic resonance and x-ray studies on micellar aggregates of sodium deoxycholate. *J Phys Chem* 1984; **88**: 5720–5724 [DOI: 10.1021/j150667a052]
79 **Miranda Cona M,** Feng YB, Jian Zhang, Yue Li, Verbruggen A, Oyen R, Ni Y. Sodium cholate, a solubilizing agent for the necrosis avid radioiodinated hypericin in rabbits with acute myocardial infarction. *Drug Delivery* 2014; (in press) [DOI: 10.3109/10717544.2013.873838]
80 **Miranda Cona M,** Koole M, Feng YB, Liu YW, Verbruggen A, Oyen R and Ni Y. Biodistribution and radiation dosimetry of radioiodinated hypericin as a cancer therapeutic. *International Journal of Oncology* 2014; 44 (in press) [DOI: 10.3892/ijo.2013.2217]
81 **Seo Y**, Gustafson WC, Dannoon SF, Nekritz EA, Lee CL, Murphy ST, VanBrocklin HF, Hernandez-Pampaloni M, Haas-Kogan DA, Weiss WA, Matthay KK. Tumor dosimetry using [124I]m-iodobenzylguanidine microPET/CT for [131I]m-iodobenzylguanidine treatment of neuroblastoma in a murine xenograft model. *Mol Imaging Biol* 2012; **14**: 735-742 [PMID: 22382618 DOI: 10.1007/s11307-012-0552-4]
82 **Koppe MJ**, Bleichrodt RP, Soede AC, Verhofstad AA, Goldenberg DM, Oyen WJ, Boerman OC. Biodistribution and therapeutic efficacy of (125/131)I-, (186)Re-, (88/90)Y-, or (177)Lu-labeled monoclonal antibody MN-14 to carcinoembryonic antigen in mice with small peritoneal metastases of colorectal origin. *J Nucl Med* 2004; **45**: 1224-1232 [PMID: 15235070]
83 **Kaminski MS**, Estes J, Zasadny KR, Francis IR, Ross CW, Tuck M, Regan D, Fisher S, Gutierrez J, Kroll S, Stagg R, Tidmarsh G, Wahl RL. Radioimmunotherapy with iodine (131)I tositumomab for relapsed or refractory B-cell non-Hodgkin lymphoma: updated results and long-term follow-up of the University of Michigan experience. *Blood* 2000; **96**: 1259-1266 [PMID: 10942366]
84 **Persson M**, Rasmussen P, Madsen J, Ploug M, Kjaer A. New peptide receptor radionuclide therapy of invasive cancer cells: in vivo studies using 177Lu-DOTA-AE105 targeting uPAR in human colorectal cancer xenografts. *Nucl Med Biol* 2012; **39**: 962-969 [PMID: 22739362 DOI: 10.1016/j.nucmedbio.2012.05.007]
85 **Persson M**, Gedda L, Lundqvist H, Tolmachev V, Nordgren H, Malmström PU, Carlsson J. [177Lu]pertuzumab: experimental therapy of HER-2-expressing xenografts. *Cancer Res* 2007; **67**: 326-331 [PMID: 17210714 DOI: 10.1158/0008-5472.CAN-06-2363]
86 **Argyrou M,** Valassi A, Andreou M, Lyra M. Dosimetry and therapeutic ratios for rhenium-186 HEDP. *ISRN Molecular Imaging* 2013; **2013**: 1-6 [DOI: 10.1155/2013/124603]
87 **Rizvi SN**, Visser OJ, Vosjan MJ, van Lingen A, Hoekstra OS, Zijlstra JM, Huijgens PC, van Dongen GA, Lubberink M. Biodistribution, radiation dosimetry and scouting of 90Y-ibritumomab tiuxetan therapy in patients with relapsed B-cell non-Hodgkin's lymphoma using 89Zr-ibritumomab tiuxetan and PET. *Eur J Nucl Med Mol Imaging* 2012; **39**: 512-520 [PMID: 22218876 DOI: 10.1007/s00259-011-2008-5]
88 **Cremonesi M,** Ferrari M, Bodei L, Tosi G, Paganelli G. Dosimetry in Peptide radionuclide receptor therapy: a review. *J Nucl Med* 2006; **47**: 1467-1475 [PMID: 16954555]
89 **Li J**, Cona MM, Chen F, Feng Y, Zhou L, Zhang G, Nuyts J, de Witte P, Zhang J, Yu J, Oyen R, Verbruggen A, Ni Y. Sequential systemic administrations of combretastatin A4 Phosphate and radioiodinated hypericin exert synergistic targeted theranostic effects with prolonged survival on SCID mice carrying bifocal tumor xenografts. *Theranostics* 2013; **3**: 127-137 [PMID: 23423247 DOI: 10.7150/thno.5790]
90 **Cona MM,** Li J, Feng Y, Chen F, Verbruggen A, de Witte P, Oyen R, Ni Y. Targetability and Biodistribution of Radioiodinated Hypericin: Comparison between microdosing and carrier-added preparations. *Anticancer Agents Med Chem* 2013 Aug 28; Epub ahead of print [PMID: 24102315]
91 **Hasani A**, Leighl N. Classification and toxicities of vascular disrupting agents. *Clin Lung Cancer* 2011; **12**: 18-25 [PMID: 21273175 DOI: 10.3816/CLC.2011.n.002]
92 **Felici A**, Verweij J, Sparreboom A. Dosing strategies for anticancer drugs: the good, the bad and body-surface area. *Eur J Cancer* 2002; **38**: 1677-1684 [PMID: 12175683 DOI: 10.1016/S0959-8049(02)00151-X]
93 **Reagan-Shaw S**, Nihal M, Ahmad N. Dose translation from animal to human studies revisited. *FASEB J* 2008; **22**: 659-661 [PMID: 17942826 DOI: 10.1096/fj.07-9574LSF]
94 **Ng QS**, Mandeville H, Goh V, Alonzi R, Milner J, Carnell D, Meer K, Padhani AR, Saunders MI, Hoskin PJ. Phase Ib trial of radiotherapy in combination with combretastatin-A4-phosphate in patients with non-small-cell lung cancer, prostate adenocarcinoma, and squamous cell carcinoma of the

head and neck. *Ann Oncol* 2012; **23**: 231-237 [PMID: 21765046 DOI: 10.1093/annonc/mdr332]
95 **Burke JM**, Miller JE. Evaluation of multiple low doses of copper oxide wire particles compared with levamisole for control of Haemonchus contortus in lambs. *Vet Parasitol* 2006; **139**: 145-149 [PMID: 16574324]
96 **Subbiah IM**, Lenihan DJ, Tsimberidou AM. Cardiovascular toxicity profiles of vascular-disrupting agents. *Oncologist* 2011; **16**: 1120-1130 [PMID: 21742963 DOI: 10.1634/theoncologist.2010-0432]
97 **Zweifel M,** Zweifel M, Jayson GC, Reed NS, Osborne R, Hassan B, Ledermann J, Shreeves G, Poupard L, Lu SP, Balkissoon J, Chaplin DJ, Rustin GJ. Phase II trial of combretastatin A4 phosphate, carboplatin, and paclitaxel in patients with platinum-resistant ovarian cancer. *Ann Oncol* 2011; **22**: 2036-2041 [PMID:21273348 DOI: 10.1093/annonc/mdq708]
98 **Gould S**, Westwood FR, Curwen JO, Ashton SE, Roberts DW, Lovick SC, Ryan AJ. Effect of pretreatment with atenolol and nifedipine on ZD6126-induced cardiac toxicity in rats. *J Natl Cancer Inst* 2007; **99**: 1724-1728 [PMID: 18000220 DOI: 10.1093/jnci/djm202]
99 **Rustin GJ**, Galbraith SM, Anderson H, Stratford M, Folkes LK, Sena L, Gumbrell L, Price PM. Phase I clinical trial of weekly combretastatin A4 phosphate: clinical and pharmacokinetic results. *J Clin Oncol* 2003; **21**: 2815-2822 [PMID: 12807934 DOI: 10.1200/JCO.2003.05.185]
100 **Fox E**, Murphy RF, McCully CL, Adamson PC. Plasma pharmacokinetics and cerebrospinal fluid penetration of hypericin in nonhuman primates. *Cancer Chemother Pharmacol* 2001; **47**: 41-44 [PMID: 11221960 DOI: 10.1007/s002800000188]
101 **Gulick RM**, McAuliffe V, Holden-Wiltse J, Crumpacker C, Liebes L, Stein DS, Meehan P, Hussey S, Forcht J, Valentine FT. Phase I studies of hypericin, the active compound in St. John's Wort, as an antiretroviral agent in HIV-infected adults. AIDS Clinical Trials Group Protocols 150 and 258. *Ann Intern Med* 1999; **130**: 510-514 [PMID: 10075619 DOI: 10.7326/0003-4819-130-6-199903160-00015]
102 **Ritz R**, Daniels R, Noell S, Feigl GC, Schmidt V, Bornemann A, Ramina K, Mayer D, Dietz K, Strauss WS, Tatagiba M. Hypericin for visualization of high grade gliomas: first clinical experience. *Eur J Surg Oncol* 2012; **38**: 352-360 [PMID: 22284346 DOI: 10.1016/j.ejso.2011.12.021]
103 **Shapiro B**. Optimization of radioiodine therapy of thyrotoxicosis: what have we learned after 50 years? *J Nucl Med* 1993; **34**: 1638-1641 [-PMID: 8410274]
104 **Cosgriff PS.** Thyroid blocking associated with I123- and I131 MIBG scans. Available from: URL: http: //www.nuclearmedicine.org.uk/thyroid/thyweb.pdf
105 **Li JJ**, Cona MM, Feng YB, Chen F, Zhang GZ, Fu XB, Himmelreich U, Oyen R, Verbruggen A, Ni YC. A single-dose toxicity study on non-radioactive iodinated hypericin for a targeted anticancer therapy in mice. *Acta Pharmacol Sin* 2012; **33**: 1549-1556 [PMID: 23103619 DOI: 10.1038/aps.2012.111]
106 **Van Landeghem L**, Blue RE, Dehmer JJ, Henning SJ, Helmrath MA, Lund PK. Localized intestinal radiation and liquid diet enhance survival and permit evaluation of long-term intestinal responses to high dose radiation in mice. *PLoS One* 2012; **7**: e51310 [PMID: 23236468 DOI: 10.1371/journal.pone.0051310]
107 **Cona MM,** Feng Y, Verbruggen A, Oyen R, Ni Y. Improved clearance of radioiodinated hypericin as a targeted anticancer agent by using a duodenal drainage catheter in rats. *Exp Biol Med* (Maywood) 2013 Oct 21; Epub ahead of print [PMID: 24146264]
108 **Cona MM**, Li J, Chen F, Feng Y, Alpizar YA, Vanstapel F, Talavera K, de Witte P, Verbruggen A, Sun Z, Oyen R, Ni Y. A safety study on single intravenous dose of tetrachloro-diphenyl glycoluril [iodogen] dissolved in dimethyl sulphoxide (DMSO). *Xenobiotica* 2013; **43**: 730-737 [PMID: 23294333 DOI: 10.3109/00498254.2012.756559]
109 **Ell PJ**, Langford R, Pearce P, Lui D, Elliott AT, Woolf N, Williams ES. 99mTc-imidodiphosphonate: a superior radiopharmaceutical for in vivo positive myocardial infarct imaging. I: Experimental data. *Br Heart J* 1978; **40**: 226-233 [PMID: 637975 DOI: 10.1136/hrt.40.3.226]
110 **Obrador D**, Ballester M, Carrió I, Augé JM, López CM, Bosch I, Martí V, Bordes R. Active myocardial damage without attending inflammatory response in dilated cardiomyopathy. *J Am Coll Cardiol* 1993; **21**: 1667-1671 [PMID: 8496535 DOI: 10.1016/0735-1097(93)90385-E]
111 **Dec GW**, Palacios I, Yasuda T, Fallon JT, Khaw BA, Strauss HW, Haber E. Antimyosin antibody cardiac imaging: its role in the diagnosis of myocarditis. *J Am Coll Cardiol* 1990; **16**: 97-104 [PMID: 2358612 DOI: 10.1016/0735-1097(90)90463-Y]
112 **Frist W**, Yasuda T, Segall G, Khaw BA, Strauss HW, Gold H, Stinson E, Oyer P, Baldwin J, Billingham M. Noninvasive detection of human cardiac transplant rejection with indium-111 antimyosin (Fab) imaging. *Circulation* 1987; **76**: V81-V85 [PMID: 3311460]
113 **Buja LM**, Tofe AJ, Kulkarni PV, Mukherjee A, Parkey RW, Francis MD, Bonte FJ, Willerson JT. Sites and mechanisms of localization of technetium-99m phosphorus radiopharmaceuticals in acute myocardial infarcts and other tissues. *J Clin Invest* 1977; **60**: 724-740 [PMID: 893676 DOI: 10.1172/JCI108825]
114 **Khaw BA**, Nakazawa A, O'Donnell SM, Pak KY, Narula J. Avidity of technetium 99m glucarate for the necrotic myocardium: in vivo and in vitro assessment. *J Nucl Cardiol* 1997; **4**: 283-290 [PMID: 9278874 DOI: 10.1016/S1071-3581(97)90105-7]
115 **Hiroe M**, Ohta Y, Fujita N, Nagata M, Toyozaki T, Kusakabe K, Sekiguchi M, Marumo F. Myocardial uptake of 111In monoclonal antimyosin Fab in detecting doxorubicin cardiotoxicity in rats. Morphological and hemodynamic findings. *Circulation* 1992; **86**: 1965-1972 [PMID: 1451268 DOI: 10.1161/01.CIR.86.6.1965]
116 **Bianco JA**, Kemper AJ, Taylor A, Lazewatsky J, Tow DE, Khuri SF. Technetium-99m(Sn2+)pyrophosphate in ischemic and infarcted dog myocardium in early stages of acute coronary occlusion: histochemical and tissue-counting comparisons. *J Nucl Med* 1983; **24**: 485-491 [PMID: 6854398]
117 **Khaw BA**, Strauss HW, Moore R, Fallon JT, Yasuda T, Gold HK, Haber E. Myocardial damage delineated by indium-111 antimyosin Fab and technetium-99m pyrophosphate. *J Nucl Med* 1987; **28**: 76-82 [PMID: 3025386]
118 **Fonge H**, Vunckx K, Wang H, Feng Y, Mortelmans L, Nuyts J, Bormans G, Verbruggen A, Ni Y. Non-invasive detection and quantification of acute myocardial infarction in rabbits using mono-[123I]iodohypericin microSPECT. *Eur Heart J* 2008; **29**: 260-269 [PMID: 18156139 DOI: 10.1093/eurheartj/ehm588]
119 **Cona MM**, Feng Y, Li Y, Chen F, Vunckx K, Zhou L, Van Slambrouck K, Rezaei A, Gheysens O, Nuyts J, Verbruggen A, Oyen R, Ni Y. Comparative study of iodine-123-labeled hypericin and 99mTc-labeled hexakis [2-methoxy isobutyl isonitrile] in a rabbit model of myocardial infarction. *J Cardiovasc Pharmacol* 2013; **62**: 304-311 [PMID: 23714775 DOI: 10.1097/FJC.0b013e31829b2c6b]
120 **Vorvick LJ,** Longstreth GF, Zieve D. Acute cholecystitis. *MedlinePlus* 2011. Available from: URL: http: //www.nlm.nih.gov/medlineplus/ency/article/000264.htm
121 **Csendes A**, Burdiles P, Maluenda F, Diaz JC, Csendes P, Mitru N. Simultaneous bacteriologic assessment of bile from gallbladder and common bile duct in control subjects and patients with gallstones and common duct stones. *Arch Surg* 1996; **131**: 389-394 [PMID: 8615724 DOI: 10.1001/archsurg.1996.01430160047008]
122 **Pañella H**, Rius C, Caylà JA. Transmission of hepatitis C virus during computed tomography scanning with contrast.

Emerg Infect Dis 2008; **14**: 333-336 [PMID: 18258135 DOI: 10.3201/eid1402.060763]

123 **Chen KT**, Chen CJ, Chang PY, Morse DL. A nosocomial outbreak of malaria associated with contaminated catheters and contrast medium of a computed tomographic scanner. *Infect Control Hosp Epidemiol* 1999; **20**: 22-25 [PMID: 9927261 DOI: 10.1086/501557]

124 **Cantin V**, Labadie R, Rhainds M, Simard FC. Intravenous contrast medium administration in computerized axial tomography at the CHUQ Medical Imaging Department. Centre hospitalier universitaire de Québec 2007. Available from: http://www.chuq.qc.ca/NR/rdonlyres/03BC97EF-5F04-4375-BC48-3852965A4EDD/0/R%C3%89SUM%C3%89substancedecontrasteVArevised_VF.pdf.Accessed%20Nov%2029,%202010

125 **Cona MM**, Bauwens M, Zheng Y, Coudyzer W, Li J, Feng Y, Wang H, Chen F, Verbruggen A, Oyen R, Ni Y. Study on the microbial safety of an infusion set for contrast-enhanced imaging. *Invest Radiol* 2012; **47**: 247-251 [PMID: 22353856 DOI: 10.1097/RLI.0b013e31823c0f87]

P- Reviewers: Guo ZS, Leitman IM **S- Editor**: Ma YJ
L- Editor: Wang TQ **E- Editor**: Wu HL

World Journal of Methodology

Online Submissions: http://www.wjgnet.com/esps/
bpgoffice@wjgnet.com
doi:10.5662/wjm.v3.i4.65

World J Methodol 2013 December 26; 3(4): 65-69
ISSN 2222-0682 (online)

MINIREVIEWS

Bone marrow cell-based regenerative therapy for liver cirrhosis

Takafumi Saito, Kyoko Tomita, Hiroaki Haga, Kazuo Okumoto, Yoshiyuki Ueno

Takafumi Saito, Kyoko Tomita, Hiroaki Haga, Kazuo Okumoto, Yoshiyuki Ueno, Department of Gastroenterology, Yamagata University School of Medicine, Yamagata 990-9585, Japan
Author contributions: Saito T, Tomita K, Haga H, Okumoto K and Ueno Y contributed equally to this paper.
Correspondence to: Takafumi Saito, MD, Associate Professor, Department of Gastroenterology, Yamagata University School of Medicine, 2-2-2 Iida-nishi, Yamagata 990-9585, Japan. tasaitoh@med.id.yamagata-u.ac.jp
Telephone: +81-23-6285309 Fax: +81-23-6285311
Received: September 25, 2013 Revised: November 6, 2013
Accepted: December 12, 2013
Published online: December 26, 2013

Abstract

Bone marrow cells are capable of differentiation into liver cells. Therefore, transplantation of bone marrow cells has considerable potential as a future therapy for regeneration of damaged liver tissue. Autologous bone marrow infusion therapy has been applied to patients with liver cirrhosis, and improvement of liver function parameters has been demonstrated. In this review, we summarize clinical trials of regenerative therapy using bone marrow cells for advanced liver diseases including cirrhosis, as well as topics pertaining to basic *in vitro* or *in vivo* approaches in order to outline the essentials of this novel treatment modality.

Key words: Bone marrow; Liver regeneration; Cirrhosis; Stem cell; Transplantation

Core tip: Bone marrow cells, which include multipotent progenitor cells, are capable of differentiation into liver cells. Autologous bone marrow infusion therapy has been applied to cirrhotic patients, and improvement of liver function parameters has been demonstrated. Although the efficacy of this treatment modality needs to be evaluated in more detail in a large number of patients, regenerative therapy using bone marrow cells for advanced liver diseases has considerable potential.

Saito T, Tomita K, Haga H, Okumoto K, Ueno Y. Bone marrow cell-based regenerative therapy for liver cirrhosis. *World J Methodol* 2013; 3(4): 65-69 Available from: URL: http://www.wjgnet.com/2222-0682/full/v3/i4/65.htm DOI: http://dx.doi.org/10.4329/wjm.v3.i4.65

INTRODUCTION

Bone marrow cells (BMCs) are capable of differentiating into liver cells[1-4] because they include stem cells known as multipotent adult progenitor cells[5,6]. These cells have been shown to produce albumin when cultured with hepatocyte growth factor (HGF)[7] and various liver-specific proteins, including albumin, when cultured with mature hepatocytes[8]. Using cells obtained with a negatively selective magnetic cell separation system for efficient sorting of rat BMCs enriched with stem cells, we have shown that BMCs differentiate into cells expressing liver-specific genes when cultured with mature hepatocytes or HGF[9]. As there is now much evidence indicating that BMCs can differentiate into cells resembling liver cells *in vitro*[6-11], the characteristics of such BMCs are of great interest in the context of liver-regenerative medicine[12-14].

Liver cirrhosis is the end stage of chronic liver disease, and is associated with many serious systemic complications resulting from both liver failure and portal hypertension. This condition has a poor prognosis and is difficult to treat. Therefore, development of an effective liver-regenerative therapy for liver cirrhosis is an urgent priority. Liver transplantation is the only curative remedy for cirrhotic patients, but is associated with many problems such as donor shortage, surgical complications,

rejection and high cost. As an alternative approach, regenerative cell therapy using stem cells is now attracting attention. Multipotent stem cells present in bone marrow are a particularly promising candidate for this purpose. In this review, we summarize clinical trials of liver-regenerative therapy using BMCs for advanced liver diseases including cirrhosis, as well as topics pertaining to basic *in vitro* or *in vivo* approaches in order to outline the essentials of this novel treatment modality.

MIGRATION AND ENGRAFTMENT OF TRANSPLANTED BMCs TO THE INJURED LIVER IN STUDIES USING ANIMAL MODELS

Although BMCs can show liver cell lineage differentiation *in vitro*, an understanding of the dynamics of transplanted BMCs *in vivo* is essential for the development of BMC-based regenerative therapy. In this context, two important issues need to be clarified: (1) How do transplanted BMCs migrate to and engraft in the liver? and (2) Is there a relationship between the degree of liver damage and the extent of migration of transplanted cells? A previous study using model rats with carbon tetrachloride (CCl_4)-induced liver injury has demonstrated that transplanted BMCs derived from transgenic rats expressing green fluorescent protein[15] in the spleen migrated to and remained in the periportal area of the recipient's damaged liver[16]. These transplanted cells expressed liver cell markers such as alpha-fetoprotein as well as Notch signaling markers for stem cells, suggesting that the BMCs retained in the recipient liver possess the potential to differentiate into liver cells.

Migration of transplanted BMCs to the liver after injection into the spleen has been compared in two models of liver injury induced by administration of CCl_4 and 2-acetylaminofluorene (2-AAF)[17], respectively, focusing particularly on differences in levels of liver mRNA for growth factors such as HGF and fibroblast growth factor (FGF), which have been shown to be responsible for efficient liver cell lineage differentiation of BMCs[9,18,19]. Interestingly, transplanted BMCs were found to engraft into CCl_4-induced injured liver characterized by submassive hepatic necrosis and induction of high levels of HGF and FGF, but not into liver damaged by 2-AAF[20]. A higher degree of HGF induction is characteristic of more severe liver damage[21,22]. These findings suggest that transplanted BMCs migrate more effectively to a liver with greater damage, and that this transplantation approach would be clinically promising for treatment of advanced liver diseases. However, further studies are needed to clarify the factors produced by both BMCs and hepatocytes that contribute to better differentiation of BMCs into liver cells *in vivo*, thus improving the effectiveness of BMC transplantation.

HUMORAL FACTORS BENEFICIAL FOR LIVER REGENERATION AFTER BMC TRANSPLANTATION

The degree of liver function and fibrosis, as well as survival rate, have been shown to improve significantly after BMC transplantation in animal models of severe liver injury[23,24]. With regard to the mechanisms of liver regeneration resulting from BMC transplantation, many of the physiological and regenerative roles of transplanted BMCs remain unclear. However, it can be said with certainty that humoral factors produced in the liver during the regenerative process after BMC transplantation have a crucial role in both improvement of liver fibrosis and liver cell lineage differentiation of stem cells originating from BMCs and hepatic epithelial stem cells.

Improvement of liver fibrosis results from fibrolysis through the proteolytic action of BMC-induced factors. In this context, matrix metalloproteinase (MMP) activity is particularly noteworthy[25]. Sakaida *et al*[23] showed that BMC transplantation ameliorated liver fibrosis in the CCl_4-induced liver-injury model, and that the fibrolytic change was attributable to MMP-9 secreted by BMCs that had migrated to fibrotic areas of the liver.

The liver cell lineage differentiation of BMCs occurs through the cooperative action of a variety of growth factors such as HGF or FGF induced in the injured liver[11,20,26]. Such differentiation may be accompanied by early elevation of the apolipoprotein A1 level in serum and liver[27]. Administration of FGF2 in combination with BMC transplantation synergistically ameliorates liver fibrosis in models of liver injury induced by CCl_4[28]. In addition, in severe liver injury where hepatocyte proliferation is strongly inhibited, hepatic stem cells such as oval cells are induced and show differentiation toward a liver cell lineage, thus leading to liver regeneration[29,30].

As BMC transplantation is successfully adaptable to cases of severe liver injury, it has been hypothesized that transplanted BMCs interact with hepatic epithelial stem cells and influence the subsequent proliferation and differentiation of stem cells. Studies of the interaction between BMCs and hepatic stem cells can provide new insight into the mechanisms of recovery from severe liver damage through liver regeneration after BMC transplantation. In this context, *in vitro* analysis using a system for co-culture of BMCs and an established epithelial hepatic stem cell line has been conducted. Haga *et al*[31] demonstrated that the expression of *FGF2* mRNA was upregulated in BMCs co-cultured with hepatic stem cells, and that expression of mRNAs for both albumin and tyrosine aminotransferase, representative of mature hepatic cells, became detectable in hepatic stem cells after culture with FGF2 protein. Thus, BMCs stimulate both proliferation and differentiation of hepatic stem cells into the hepatocyte lineage, and FGF2 is one of the factors produced by interaction with BMCs, which stimulates

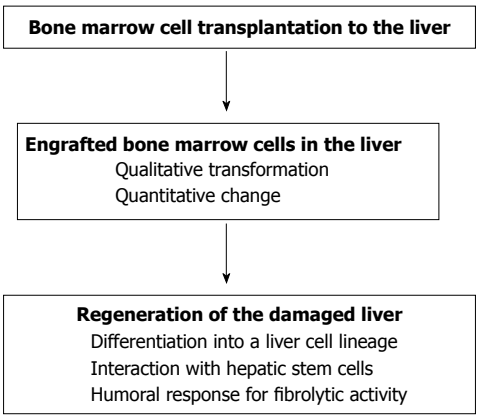

Figure 1 Putative action of transplanted bone marrow cells that include multipotent stem cells for regeneration of damaged liver.

such differentiation. Cross-talk between bone marrow stem cells and hepatic epithelial stem cells may underlie the process of liver regeneration, and this is an area of interest for future investigation. Figure 1 shows an overall representation of the putative action of transplanted BMCs in the regeneration of damaged liver.

CLINICAL TRIALS OF BMC TRANSPLANTATION FOR ADVANCED LIVER DISEASES

BMC transplantation has received increasing attention as a promising therapy for advanced and severe liver diseases such as cirrhosis. Clinical trials of BMC administration to patients with advanced liver diseases have been performed, and improvement of liver function parameters such as the serum level of albumin, Child-Pugh score or Model for Endstage Liver Disease score have been reported[32-40]. Another study has shown that intraportal administration of autologous $CD133^+$ BMCs and subsequent portal venous embolization of right liver segments resulted in a 2.5-fold increase in the mean proliferation rate of the left lateral segment, in comparison with controls not receiving BM transfusion[41]. These findings suggest that transplanted BMCs have a potential role in liver regeneration and proliferate in the recipient liver. Recently, autologous BMC transplantation - a technique named autologous BMC infusion (ABMi) therapy - has been applied to multi-center patients with liver cirrhosis due to hepatitis C[42], hepatitis B[43] and excess alcohol intake[44] using almost the same protocol, and a series of studies have demonstrated improvement of the serum albumin level, leading to improvement of the Child-Pugh score.

Although BMC administration for advanced liver diseases including cirrhosis is an attractive strategy in the field of cell therapy for liver regeneration, many concerns need to be addressed[45-47]. As *in vitro* and *in vivo* experiments have clearly shown, BMCs induce fibrolysis and show hepatocyte differentiation, and they may interact with hepatic epithelial stem cells to aid their differentiation into the hepatocyte lineage. However, it is still unclear how infused BMCs work to improve liver function in humans. A clinical trial of ABMi for patients with cirrhosis demonstrated that the number of AFP-positive cells increased significantly in the liver relative to the situation before ABMi[42]. In addition, ABMi appeared to induce hepatocyte proliferation in the liver, as expression of proliferating cell nuclear antigen, a marker of hepatocyte proliferation, was significantly increased after ABMi in comparison with the pretreatment situation. Although these findings suggest that transplanted BMCs have a potential role in liver regeneration and proliferate in the recipient liver, it remains unknown whether fully functional hepatocytes are induced by ABMi. The characteristics of stem cells present among BMCs that show hepatocyte differentiation require further elucidation.

The factors that determine the difference between effectiveness and non-effectiveness of ABMi are unclear. Collateral circulation resulting from the portal vein disorganization that characterizes liver cirrhosis may affect the flow and effective migration of infused BMCs to the liver, and thus migration of infused cells to the liver may partly depend on the portal venous pressure. In addition, the expression levels of cellular adhesion molecules associated with the attachment of infused cells to liver tissue may vary a great deal among patients. The long-term effectiveness of this therapy in terms of survival rate has not been demonstrated. These issues should be evaluated by a randomized controlled trial involving a large number of patients. Additionally, other issues that impact the efficacy of this therapy, *i.e.*, the long-term culture conditions optimal for stocking BMCs for repeated infusion, the optimal cell population to employ, the optimal number of cells to infuse, the effectiveness of repeated infusion and the optimal route for cell delivery need to be investigated further.

In conclusion, regenerative therapy using BMCs for advanced liver diseases including cirrhosis has considerable potential. Further studies are needed to develop a better method of BMC transplantation that can contribute to improvement of liver function and to clarify the long-term effectiveness of this therapy.

REFERENCES

1 **Petersen BE**, Bowen WC, Patrene KD, Mars WM, Sullivan AK, Murase N, Boggs SS, Greenberger JS, Goff JP. Bone marrow as a potential source of hepatic oval cells. *Science* 1999; **284**: 1168-1170 [PMID: 10325227 DOI: 10.1126/science.284.5417.1168]
2 **Alison MR**, Poulsom R, Jeffery R, Dhillon AP, Quaglia A, Jacob J, Novelli M, Prentice G, Williamson J, Wright NA. Hepatocytes from non-hepatic adult stem cells. *Nature* 2000; **406**: 257 [PMID: 10917519 DOI: 10.1038/35018642]
3 **Theise ND**, Badve S, Saxena R, Henegariu O, Sell S, Crawford JM, Krause DS. Derivation of hepatocytes from bone marrow cells in mice after radiation-induced myeloablation. *Hepatology* 2000; **31**: 235-240 [PMID: 10613752 DOI: 10.1002/hep.510310135]
4 **Theise ND**, Nimmakayalu M, Gardner R, Illei PB, Morgan G,

Teperman L, Henegariu O, Krause DS. Liver from bone marrow in humans. *Hepatology* 2000; **32**: 11-16 [PMID: 10869283 DOI: 10.1053/jhep.2000.9124]
5 **Jiang Y**, Jahagirdar BN, Reinhardt RL, Schwartz RE, Keene CD, Ortiz-Gonzalez XR, Reyes M, Lenvik T, Lund T, Blackstad M, Du J, Aldrich S, Lisberg A, Low WC, Largaespada DA, Verfaillie CM. Pluripotency of mesenchymal stem cells derived from adult marrow. *Nature* 2002; **418**: 41-49 [PMID: 12077603 DOI: 10.1038/nature00870]
6 **Schwartz RE**, Reyes M, Koodie L, Jiang Y, Blackstad M, Lund T, Lenvik T, Johnson S, Hu WS, Verfaillie CM. Multipotent adult progenitor cells from bone marrow differentiate into functional hepatocyte-like cells. *J Clin Invest* 2002; **109**: 1291-1302 [PMID: 12021244]
7 **Oh SH**, Miyazaki M, Kouchi H, Inoue Y, Sakaguchi M, Tsuji T, Shima N, Higashio K, Namba M. Hepatocyte growth factor induces differentiation of adult rat bone marrow cells into a hepatocyte lineage in vitro. *Biochem Biophys Res Commun* 2000; **279**: 500-504 [PMID: 11118315 DOI: 10.1006/bbrc.2000.3985]
8 **Avital I**, Inderbitzin D, Aoki T, Tyan DB, Cohen AH, Ferraresso C, Rozga J, Arnaout WS, Demetriou AA. Isolation, characterization, and transplantation of bone marrow-derived hepatocyte stem cells. *Biochem Biophys Res Commun* 2001; **288**: 156-164 [PMID: 11594767 DOI: 10.1006/bbrc.2001.5712]
9 **Okumoto K**, Saito T, Hattori E, Ito JI, Adachi T, Takeda T, Sugahara K, Watanabe H, Saito K, Togashi H, Kawata S. Differentiation of bone marrow cells into cells that express liver-specific genes in vitro: implication of the Notch signals in differentiation. *Biochem Biophys Res Commun* 2003; **304**: 691-695 [PMID: 12727209 DOI: 10.1016/S0006-291X(03)00637-5]
10 **Miyazaki M**, Akiyama I, Sakaguchi M, Nakashima E, Okada M, Kataoka K, Huh NH. Improved conditions to induce hepatocytes from rat bone marrow cells in culture. *Biochem Biophys Res Commun* 2002; **298**: 24-30 [PMID: 12379214 DOI: 10.1016/S0006-291X(02)02340-9]
11 **Okumoto K**, Saito T, Hattori E, Ito JI, Suzuki A, Misawa K, Ishii R, Karasawa T, Haga H, Sanjo M, Takeda T, Sugahara K, Saito K, Togashi H, Kawata S. Differentiation of rat bone marrow cells cultured on artificial basement membrane containing extracellular matrix into a liver cell lineage. *J Hepatol* 2005; **43**: 110-116 [PMID: 15893847 DOI: 10.1016/j.jhep.2005.01.037]
12 **Mitaka T**. Hepatic stem cells: from bone marrow cells to hepatocytes. *Biochem Biophys Res Commun* 2001; **281**: 1-5 [PMID: 11178951 DOI: 10.1006/bbrc.2001.4270]
13 **Faris RA**, Konkin T, Halpert G. Liver stem cells: a potential source of hepatocytes for the treatment of human liver disease. *Artif Organs* 2001; **25**: 513-521 [PMID: 11493271 DOI: 10.1046/j.1525-1594.2001.025007513.x]
14 **Forbes S**, Vig P, Poulsom R, Thomas H, Alison M. Hepatic stem cells. *J Pathol* 2002; **197**: 510-518 [PMID: 12115866 DOI: 10.1002/path.1163]
15 **Hakamata Y**, Tahara K, Uchida H, Sakuma Y, Nakamura M, Kume A, Murakami T, Takahashi M, Takahashi R, Hirabayashi M, Ueda M, Miyoshi I, Kasai N, Kobayashi E. Green fluorescent protein-transgenic rat: a tool for organ transplantation research. *Biochem Biophys Res Commun* 2001; **286**: 779-785 [PMID: 11520065 DOI: 10.1006/bbrc.2001.5452]
16 **Okumoto K**, Saito T, Hattori E, Ito JI, Suzuki A, Misawa K, Sanjyo M, Takeda T, Sugahara K, Saito K, Togashi H, Kawata S. Expression of Notch signalling markers in bone marrow cells that differentiate into a liver cell lineage in a rat transplant model. *Hepatol Res* 2005; **31**: 7-12 [PMID: 15652464 DOI: 10.1016/j.hepres.2004.11.005]
17 **Petersen BE**, Zajac VF, Michalopoulos GK. Hepatic oval cell activation in response to injury following chemically induced periportal or pericentral damage in rats. *Hepatology* 1998; **27**: 1030-1038 [PMID: 9537443 DOI: 10.1002/hep.510270419]
18 **Sekhon SS**, Tan X, Micsenyi A, Bowen WC, Monga SP. Fibroblast growth factor enriches the embryonic liver cultures for hepatic progenitors. *Am J Pathol* 2004; **164**: 2229-2240 [PMID: 15161655 DOI: 10.1016/S0002-9440(10)63779-0]
19 **Lange C**, Bassler P, Lioznov MV, Bruns H, Kluth D, Zander AR, Fiegel HC. Hepatocytic gene expression in cultured rat mesenchymal stem cells. *Transplant Proc* 2005; **37**: 276-279 [PMID: 15808618 DOI: 10.1016/j.transproceed.2004.11.087]
20 **Okumoto K**, Saito T, Haga H, Hattori E, Ishii R, Karasawa T, Suzuki A, Misawa K, Sanjo M, Ito JI, Sugahara K, Saito K, Togashi H, Kawata S. Characteristics of rat bone marrow cells differentiated into a liver cell lineage and dynamics of the transplanted cells in the injured liver. *J Gastroenterol* 2006; **41**: 62-69 [PMID: 16501859 DOI: 10.1007/s00535-005-1723-8]
21 **Tsubouchi H**, Kawakami S, Hirono S, Miyazaki H, Kimoto M, Arima T, Sekiyama K, Yoshiba M, Arakaki N, Daikuhara Y. Prediction of outcome in fulminant hepatic failure by serum human hepatocyte growth factor. *Lancet* 1992; **340**: 307 [PMID: 1353217 DOI: 10.1016/0140-6736(92)92396-W]
22 **Maher JJ**. Cell-specific expression of hepatocyte growth factor in liver. Upregulation in sinusoidal endothelial cells after carbon tetrachloride. *J Clin Invest* 1993; **91**: 2244-2252 [PMID: 7683700 DOI: 10.1172/JCI116451]
23 **Sakaida I**, Terai S, Yamamoto N, Aoyama K, Ishikawa T, Nishina H, Okita K. Transplantation of bone marrow cells reduces CCl4-induced liver fibrosis in mice. *Hepatology* 2004; **40**: 1304-1311 [PMID: 15565662 DOI: 10.1002/hep.20452]
24 **Terai S**, Sakaida I, Yamamoto N, Omori K, Watanabe T, Ohata S, Katada T, Miyamoto K, Shinoda K, Nishina H, Okita K. An in vivo model for monitoring trans-differentiation of bone marrow cells into functional hepatocytes. *J Biochem* 2003; **134**: 551-558 [PMID: 14607982 DOI: 10.1093/jb/mvg173]
25 **Haraguchi T**, Tani K, Koga M, Oda Y, Itamoto K, Yamamoto N, Terai S, Sakaida I, Nakazawa H, Taura Y. Matrix metalloproteinases (MMPs) activity in cultured canine bone marrow stromal cells (BMSCs). *J Vet Med Sci* 2012; **74**: 633-636 [PMID: 22167104 DOI: 10.1292/jvms.11-0395]
26 **Ishikawa T**, Terai S, Urata Y, Marumoto Y, Aoyama K, Sakaida I, Murata T, Nishina H, Shinoda K, Uchimura S, Hamamoto Y, Okita K. Fibroblast growth factor 2 facilitates the differentiation of transplanted bone marrow cells into hepatocytes. *Cell Tissue Res* 2006; **323**: 221-231 [PMID: 16228231 DOI: 10.1007/s00441-005-0077-0]
27 **Yokoyama Y**, Terai S, Ishikawa T, Aoyama K, Urata Y, Marumoto Y, Nishina H, Nakamura K, Okita K, Sakaida I. Proteomic analysis of serum marker proteins in recipient mice with liver cirrhosis after bone marrow cell transplantation. *Proteomics* 2006; **6**: 2564-2570 [PMID: 16548057 DOI: 10.1002/pmic.200500018]
28 **Ishikawa T**, Terai S, Urata Y, Marumoto Y, Aoyama K, Murata T, Mizunaga Y, Yamamoto N, Nishina H, Shinoda K, Sakaida I. Administration of fibroblast growth factor 2 in combination with bone marrow transplantation synergistically improves carbon-tetrachloride-induced liver fibrosis in mice. *Cell Tissue Res* 2007; **327**: 463-470 [PMID: 17093919 DOI: 10.1007/s00441-006-0334-x]
29 **Shiota G**, Kunisada T, Oyama K, Udagawa A, Nomi T, Tanaka K, Tsutsumi A, Isono M, Nakamura T, Hamada H, Sakatani T, Sell S, Sato K, Ito H, Kawasaki H. In vivo transfer of hepatocyte growth factor gene accelerates proliferation of hepatic oval cells in a 2-acetylaminofluorene/partial hepatectomy model in rats. *FEBS Lett* 2000; **470**: 325-330 [PMID: 10745090 DOI: 10.1016/S0014-5793(00)01337-5]
30 **Hu Z**, Evarts RP, Fujio K, Marsden ER, Thorgeirsson SS. Expression of hepatocyte growth factor and c-met genes during hepatic differentiation and liver development in the rat. *Am J Pathol* 1993; **142**: 1823-1830 [PMID: 8506951]
31 **Haga H**, Saito T, Okumoto K, Ugajin S, Sato C, Ishii R, Nishise Y, Ito J, Watanabe H, Saito K, Togashi H, Kawata S.

Enhanced expression of fibroblast growth factor 2 in bone marrow cells and its potential role in the differentiation of hepatic epithelial stem-like cells into the hepatocyte lineage. *Cell Tissue Res* 2011; **343**: 371-378 [PMID: 21152936 DOI: 10.1007/s00441-010-1093-2]

32 **Lyra AC**, Soares MB, da Silva LF, Fortes MF, Silva AG, Mota AC, Oliveira SA, Braga EL, de Carvalho WA, Genser B, dos Santos RR, Lyra LG. Feasibility and safety of autologous bone marrow mononuclear cell transplantation in patients with advanced chronic liver disease. *World J Gastroenterol* 2007; **13**: 1067-1073 [PMID: 17373741]

33 **Mohamadnejad M**, Namiri M, Bagheri M, Hashemi SM, Ghanaati H, Zare Mehrjardi N, Kazemi Ashtiani S, Malekzadeh R, Baharvand H. Phase 1 human trial of autologous bone marrow-hematopoietic stem cell transplantation in patients with decompensated cirrhosis. *World J Gastroenterol* 2007; **13**: 3359-3363 [PMID: 17659676]

34 **Gordon MY**, Levicar N, Pai M, Bachellier P, Dimarakis I, Al-Allaf F, M'Hamdi H, Thalji T, Welsh JP, Marley SB, Davies J, Dazzi F, Marelli-Berg F, Tait P, Playford R, Jiao L, Jensen S, Nicholls JP, Ayav A, Nohandani M, Farzaneh F, Gaken J, Dodge R, Alison M, Apperley JF, Lechler R, Habib NA. Characterization and clinical application of human CD34+ stem/progenitor cell populations mobilized into the blood by granulocyte colony-stimulating factor. *Stem Cells* 2006; **24**: 1822-1830 [PMID: 16556705]

35 **Pai M**, Zacharoulis D, Milicevic MN, Helmy S, Jiao LR, Levicar N, Tait P, Scott M, Marley SB, Jestice K, Glibetic M, Bansi D, Khan SA, Kyriakou D, Rountas C, Thillainayagam A, Nicholls JP, Jensen S, Apperley JF, Gordon MY, Habib NA. Autologous infusion of expanded mobilized adult bone marrow-derived CD34+ cells into patients with alcoholic liver cirrhosis. *Am J Gastroenterol* 2008; **103**: 1952-1958 [PMID: 18637092 DOI: 10.1111/j.1572-0241.2008.01993.x]

36 **Han Y**, Yan L, Han G, Zhou X, Hong L, Yin Z, Zhang X, Wang S, Wang J, Sun A, Liu Z, Xie H, Wu K, Ding J, Fan D. Controlled trials in hepatitis B virus-related decompensate liver cirrhosis: peripheral blood monocyte transplant versus granulocyte-colony-stimulating factor mobilization therapy. *Cytotherapy* 2008; **10**: 390-396 [PMID: 18574771 DOI: 10.1080/14653240802129901]

37 **Peng L**, Xie DY, Lin BL, Liu J, Zhu HP, Xie C, Zheng YB, Gao ZL. Autologous bone marrow mesenchymal stem cell transplantation in liver failure patients caused by hepatitis B: short-term and long-term outcomes. *Hepatology* 2011; **54**: 820-828 [PMID: 21608000 DOI: 10.1002/hep.24434]

38 **Mohamadnejad M**, Alimoghaddam K, Mohyeddin-Bonab M, Bagheri M, Bashtar M, Ghanaati H, Baharvand H, Ghavamzadeh A, Malekzadeh R. Phase 1 trial of autologous bone marrow mesenchymal stem cell transplantation in patients with decompensated liver cirrhosis. *Arch Iran Med* 2007; **10**: 459-466 [PMID: 17903050]

39 **Kharaziha P**, Hellström PM, Noorinayer B, Farzaneh F, Aghajani K, Jafari F, Telkabadi M, Atashi A, Honardoost M, Zali MR, Soleimani M. Improvement of liver function in liver cirrhosis patients after autologous mesenchymal stem cell injection: a phase I-II clinical trial. *Eur J Gastroenterol Hepatol* 2009; **21**: 1199-1205 [PMID: 19455046 DOI: 10.1097/MEG.0b013e32832a1f6c]

40 **Amer ME**, El-Sayed SZ, El-Kheir WA, Gabr H, Gomaa AA, El-Noomani N, Hegazy M. Clinical and laboratory evaluation of patients with end-stage liver cell failure injected with bone marrow-derived hepatocyte-like cells. *Eur J Gastroenterol Hepatol* 2011; **23**: 936-941 [PMID: 21900788 DOI: 10.1097/MEG.0b013e3283488b00]

41 **am Esch JS**, Knoefel WT, Klein M, Ghodsizad A, Fuerst G, Poll LW, Piechaczek C, Burchardt ER, Feifel N, Stoldt V, Stockschläder M, Stoecklein N, Tustas RY, Eisenberger CF, Peiper M, Häussinger D, Hosch SB. Portal application of autologous CD133+ bone marrow cells to the liver: a novel concept to support hepatic regeneration. *Stem Cells* 2005; **23**: 463-470 [PMID: 15790766]

42 **Terai S**, Ishikawa T, Omori K, Aoyama K, Marumoto Y, Urata Y, Yokoyama Y, Uchida K, Yamasaki T, Fujii Y, Okita K, Sakaida I. Improved liver function in patients with liver cirrhosis after autologous bone marrow cell infusion therapy. *Stem Cells* 2006; **24**: 2292-2298 [PMID: 16778155]

43 **Kim JK**, Park YN, Kim JS, Park MS, Paik YH, Seok JY, Chung YE, Kim HO, Kim KS, Ahn SH, Kim do Y, Kim MJ, Lee KS, Chon CY, Kim SJ, Terai S, Sakaida I, Han KH. Autologous bone marrow infusion activates the progenitor cell compartment in patients with advanced liver cirrhosis. *Cell Transplant* 2010; **19**: 1237-1246 [PMID: 20525430 DOI: 10.3727/096368910X506863]

44 **Saito T**, Okumoto K, Haga H, Nishise Y, Ishii R, Sato C, Watanabe H, Okada A, Ikeda M, Togashi H, Ishikawa T, Terai S, Sakaida I, Kawata S. Potential therapeutic application of intravenous autologous bone marrow infusion in patients with alcoholic liver cirrhosis. *Stem Cells Dev* 2011; **20**: 1503-1510 [PMID: 21417817 DOI: 10.1089/scd.2011.0074]

45 **Kallis YN**, Alison MR, Forbes SJ. Bone marrow stem cells and liver disease. *Gut* 2007; **56**: 716-724 [PMID: 17145739]

46 **Lorenzini S**, Andreone P. Stem cell therapy for human liver cirrhosis: a cautious analysis of the results. *Stem Cells* 2007; **25**: 2383-2384 [PMID: 17540855]

47 **Terai S**, Tanimoto H, Maeda M, Zaitsu J, Hisanaga T, Iwamoto T, Fujisawa K, Mizunaga Y, Matsumoto T, Urata Y, Marumoto Y, Hidaka I, Ishikawa T, Yokoyama Y, Aoyama K, Tsuchiya M, Takami T, Omori K, Yamamoto N, Segawa M, Uchida K, Yamasaki T, Okita K, Sakaida I. Timeline for development of autologous bone marrow infusion (ABMi) therapy and perspective for future stem cell therapy. *J Gastroenterol* 2012; **47**: 491-497 [PMID: 22488349 DOI: 10.1007/s00535-012-0580-5]

P- Reviewers: Akyuz U, Bayraktar Y, Invernizzi P
S- Editor: Gou SX **L- Editor**: A **E- Editor:** Lu YJ

百世登
Baishideng®

Published by **Baishideng Publishing Group Co., Limited**
Flat C, 23/F., Lucky Plaza, 315-321 Lockhart Road,
Wan Chai, Hong Kong, China
Fax: +852-65557188
Telephone: +852-31779906
E-mail: bpgoffice@wjgnet.com
http://www.wjgnet.com